THE ASTROPHYSICAL JOURNAL SUPPLEMENT SERIES, 86:5–93, 1993 May


# AN ATLAS OF ULTRAVIOLET SPECTRA OF STAR-FORMING GALAXIES

A. L. KINNEY, R. C. BOHLIN, AND D. CALZETTI
Space Telescope Science Institute, 3700 San Martin Drive, Baltimore, MD 21218
N. PANAGIA[1]
Space Telescope Science Institute, 3700 San Martin Drive, Baltimore, MD 21218; and Istituto di Astronomia, Università di Catania
AND
ROSEMARY F. G. WYSE[2]
Physics and Astronomy Department, Johns Hopkins University, Homewood Campus, Baltimore, MD 21218
*Received 1992 April 13; accepted 1992 September 21*

## ABSTRACT

An atlas of ultraviolet spectra of the central regions of 143 spiral, irregular, blue compact, Seyfert 2, and starburst galaxies is produced by combining 387 low-resolution spectra from the *IUE* data archives. The spectra have been extracted with an optimal algorithm and co-added to produce spectra with the best possible signal-to-noise ratio.

Our data support the picture proposed earlier on the basis of UV spectra from the *Orbiting Astronomical Observatory* and from the *Astronomical Netherlands Satellite* that spiral galaxies of later Hubble class have higher flux at the shortest UV wavelengths than do spiral galaxies of earlier Hubble class. A comparison of the UV spectra of low-ionization nuclear emission-line region (LINER) galaxies with the spectra of normal spiral galaxies shows that the UV continuum of LINERs is dominated by the galaxy continuum. In contrast, Seyfert 2 galaxies show a featureless blue continuum plus emission lines, with the UV spectrum of the host galaxy apparent only at the longest UV wavelengths. The starbursting, blue compact, and blue compact dwarf galaxies have UV continua that are flat or increasing toward short wavelengths, with a wide range in spectral index, going from $F_\lambda \propto \lambda^{0.26\pm0.14}$ to $F_\lambda \propto \lambda^{-1.85\pm0.06}$.

The spectral signature of dust with a wavelength dependence of the extinction such as is seen in the Milky Way is not apparent in these galaxies. The lack of an apparent dust feature (e.g., the 2200 Å bump) implies either that the extinction law is different or that any dust present in the galaxies is in the form of clumps and does not contribute to the flux, owing to the very high optical depth.

*Subject headings:* atlases — galaxies: ISM — galaxies: Seyfert — galaxies: spiral — galaxies: starburst — ultraviolet: galaxies

## 1. INTRODUCTION

We present a systematic study of the ultraviolet spectra of star-forming galaxies of different morphological type and activity class using a sample drawn from a uniformly reduced *IUE* data set. The spectra for a wide variety of galaxies, including normal spiral, low-ionization nuclear emission-line region (LINER), starburst, blue compact, blue compact dwarf, and Seyfert 2 galaxies, are presented, both in the form of spectral energy distributions, to demonstrate the overall characteristics according to morphology and activity class and in the form of absolute flux distributions, to better show the absorption and emission features of individual objects. Our data support the picture based on UV spectra of the *Orbiting Astronomical Observatory* (*OAO*) (Pence 1976) and of the *Astronomical Netherlands Satellite* (*ANS*) (Coleman, Wu, & Weedman 1980) that spiral galaxies of later Hubble class have more flux at the shortest UV wavelengths than do spiral galaxies of earlier Hubble class. With this atlas we aim to clarify the connection between morphological type, activity class based on optical spectra, and the ultraviolet ionizing continuum that often drives the activity observed in the optical. The *IUE* archives do not contain a complete, well-selected sample of galaxies, but rather contain a collection of the individual galaxies in which the scientific community has had the most interest. In spite of the fact that the sample is not particularly complete, the *IUE* archives contain a large number of galaxies, so that conclusions about UV spectral properties as a function of galaxy type can be made. However, acquisition of a well-defined sample of normal disk galaxies should be a high priority in the later years of *IUE*.

The object selection, data compilation, and reduction are described in § 2; digital distribution of the atlas is described in § 3; the spectral signatures of various contributors to the UV, such as the interstellar medium (ISM), early O and B stars, Wolf-Rayet stars, and later type stars, is discussed in § 4.1; the characteristics of the various types of galaxies and the impact of dust upon their spectra are discussed in § 4.2; and the individual objects and their UV spectra are discussed in § 4.3.

The ultraviolet spectra in this atlas will be analyzed in the context of a larger data set. Ground-based optical spectra are currently being obtained in an aperture matched to the size of the *IUE* aperture, so that wavelength coverage for the atlas

[1] Affiliated with the Astrophysics Division, Space Sciences Department of ESA.
[2] Alfred P. Sloan Foundation Fellow.

objects will eventually go from 1200 to 7800 Å. The UV spectra will be used to form template spectra of star-forming galaxies according to Hubble class and activity class. Template spectra will be used to predict the contribution to the diffuse UV background from star-forming galaxies. The template spectra will also be used to quantify UV colors of galaxies and to predict the optical colors of star-forming galaxies at high redshift ($z \approx 1$–2). A number of galaxies in the atlas are redshifted so that the region of the Ly$\alpha$ emission line can be observed. The observations of emission and absorption at Ly$\alpha$ will be analyzed in an attempt to understand the implications of our low-redshift star-forming galaxies for high-redshift star-forming galaxies.

## 2. THE DATA

The ultraviolet data are from the *IUE* archives and include spectra from the short-wavelength (SWP) and long-wavelength (LWR and LWP) cameras taken in the large ($10'' \times 20''$) aperture. The resolution is approximately 5 Å for the SWP and 8 Å for the LWR and LWP (see Turnrose & Thompson 1984 for a complete description of *IUE* data).

### 2.1. *Object Selection*

First a list of the positions of all spiral, irregular, and compact galaxies in the Catalogue of Principal Galaxies (Paturel et al. 1989, hereafter CPG) was produced. The CPG contains 73,000 galaxies and includes, among other catalogs, the Second Reference Catalogue of Bright Galaxies (de Vancouleurs, de Vaucouleurs, & Corwin 1976) and the Markarian lists of galaxies. Then a list of objects common to both the *IUE* archives and the CPG was produced, from which the Seyfert 1 galaxies present in the Véron-Cetty & Véron catalog (1986) were excluded, except for those low-luminosity objects found to have broad emission lines (called dwarf Seyfert 1 galaxies by Filippenko & Sargent 1985). Our initial list of galaxies was cross-referenced with the *IUE* archives object classes 80 and 82 (spiral and irregular galaxies) and cross-referenced with lists of starburst galaxies (Balzano 1983; Mazzarella & Balzano 1986), so that missing objects were added. The positions of the 240 candidate galaxies were then cross-referenced with the positions of objects ($\pm 5'$) in the *IUE* archives to produce a master list of ~780 low-dispersion spectra of galaxies.

The individual *IUE* spectra, observing scripts, and photowrites for this list were inspected to exclude spectra with incorrect pointings and to correct for errors in exposure time and other errors in the on-line archive. Of the ~780 low-dispersion *IUE* spectra of the galaxies, 387 spectra of 143 galaxies were selected for inclusion in the atlas. Their selection was based on their signal-to-noise ratio (see, e.g., Kinney et al. 1991b). Agreement was required between the catalog coordinates of a galaxy and the coordinates of the observation. Both observers' comments regarding offsets and publications by observers with information on offsets were taken into account to ensure that the center of the galaxy was within the *IUE* aperture. Aperture position is particularly important in producing a uniform data base, since many spectra have been taken with *IUE* of H II regions, supernova remnants, and other objects in the disks of galaxies, which we wish to exclude. The short- and long-wavelength spectra are plotted together in Figures 8–112 with *no normalization between the cameras.* The flux levels are generally well matched between the cameras, which is evidence that the center of the galaxy was contained in the large *IUE* aperture for all spectra co-added for a given object. We have compared our fluxes with those of Longo, Capaccioli, & Ceriello 1991, who report *IUE* fluxes for normal galaxies, and find that they agree to about 5%.

The list of atlas galaxies is given in Table 1 with the number of short-wavelength spectra (SW), the number of long-wavelength (LW) spectra, the galaxy name, the morphological type of the galaxy (where we used the simpler classification of those from the Revised Shapley-Ames Catalog [Sandage & Tammann 1987, hereafter RSA] and the NASA Extragalactic Database [NED]), the activity class of the galaxy, the heliocentric velocity, the photographic magnitude, the absolute magnitude (assuming $q_0 = \frac{1}{2}$ and $H_0 = 50$), the Galactic reddening (Burstein & Heiles 1982, 1984), the Galactic latitude and longitude, the right ascension and declination, and, finally, other names. For cross-reference, Table 2 lists the Messier objects that are included in the atlas, along with their positions and other names; and Table 3 lists Markarian objects and positions and other names.

### 2.2. *Extraction and Reduction*

In order to minimize the noise in the atlas spectra, the optimal extraction technique of Kinney, Bohlin, & Neill (1991c) is used to extract the spectra from the *IUE* line-by-line data files. This slit-weighted extraction can choose slit heights of either 9 or 15 lines, where the 9 or 15 is understood to be 18 or 30 lines in the more modern line-by-line files that have twice the number of lines in the file. Despite the optimal nature of our spectral extraction technique, the added noise in 15 lines seriously degrades the signal-to-noise ratio in the resultant spectra in many cases. Therefore, all spectra presented here are from 9 line optimal extractions. The loss of light in a 9 line slit is not large, as evidenced by the following facts: (*a*) An *IUE* slit of 9 lines corresponds to $19''.4$, or 91% of the $21''.4$ high *IUE* slit. (*b*) In the case of trailed spectra, 87% of the light is in the central 9 lines. (*c*) For one of the more extended galaxies, NGC 7590, the 9 line extraction includes 81% of the light of a 15 line extraction. In general, our current implementation of the optimal extraction algorithm for 15 lines tends to track some of the noise outside of the slit, which may produce an artificially large net signal, a falsely widened profile perpendicular to the dispersion, and excess noise in the result.

Changes of sensitivity over the decade of *IUE* observations are also taken into account (Bohlin & Grillmair 1988a, b), and the absolute calibration of Bohlin et al. (1990) is used. The spectra of galaxies observed multiple times are co-added by weighting with their relative statistical uncertainty (Kinney et al. 1991c) to produce spectra with the best possible signal-to-noise ratios.

### 2.3. *Methodology*

In an attempt to give an overview of the spectroscopic properties of the many classes of galaxies in this atlas, galaxies with short- and long-wavelength coverage and with relatively high signal-to-noise ratio are presented in Figures 1, 2, and 3, grouped by their activity class, ordered by observed slope, and

TABLE 1

ATLAS GALAXIES

| Fig. no. | SW | LW | Galaxy Name | Morph. Type | Activity Class | $v_H$ km s$^{-1}$ | $B_T$ | $M_B$ $H_o = 50$ | E(B-V) | l | b | $\alpha$(1950) (h-m-s) | $\delta$(1950) (d-m-s) | Other Names |
|---|---|---|---|---|---|---|---|---|---|---|---|---|---|---|
| 8 | 5 | 6 | NGC224 | Sb | | -297 | 4.38 | -21.61 | 0.08 | 121.2 | -21.6 | 00 40 00.0 | 41 00 06 | M31 |
| r2 | 1 | | IC1586 | | BCG | 5821* | 14.9p* | -20.53b | 0.02 | 121.7 | -40.5 | 00 45 17.0 | 22 06 07 | Mrk347 |
| 9 | 2 | | NGC262 | S0 | Sy 2 | 4507* | 13.90* | -20.78* | 0.06 | 122.3 | -30.9 | 00 46 04.4 | 31 41 00 | Mrk348 |
| 10 | 1 | | Haro15 | I | BCG | 6407* | 13.5 | -22.07b | 0.02 | 120.1 | -75.6 | 00 46 04.8 | -12 59 22 | Mrk960 |
| | 1 | 1 | ESO296-11 | Pair | | 5572* | 14.5* | -20.79* | 0.05 | 282.2 | -74.7 | 01 17 43.0 | -41 29 54 | MCG-07-03-016 |
| 11 | 1 | | Mrk357 | Pair? | SB nuc. | 15845* | 15.7 | -21.82c | 0.04 | 132.2 | -39.1 | 01 19 56.6 | 22 54 30 | |
| 12 | 3 | 1 | NGC598 | Scd | | -180 | 6.26 | -19.07 | 0.04 | 133.6 | -31.3 | 01 31 04.6 | 30 23 40 | M33 |
| r4 | 1 | | IC214 | pec., 2-nuc. | SB nuc. | 9061* | 14.7* | -22.07* | 0.03 | 157.8 | -52.0 | 02 11 28.8 | 04 56 33 | Mrk1027 |
| 13 | | 1 | NGC1023 | SB0 | | 661 | 10.36 | -21.17 | 0.06 | 145.0 | -19.1 | 02 37 15.8 | 38 50 55 | UGC2154 |
| 14 | 12 | 10 | NGC1068 | Sb | Sy 2 | 1131 | 9.55 | -22.93 | 0.01 | 172.1 | -51.9 | 02 40 06.5 | -00 13 32 | M77 |
| 15 | 1 | 2 | NGC1097 | SBbc | Hs+Lin | 1319 | 10.16 | -22.30 | 0.02 | 226.9 | -64.7 | 02 44 11.0 | -30 28 54 | UGCA041 |
| 16 | 2 | | NGC1140 | Irr. Am. | BCG | 1509 | 12.85 | -20.36 | 0.03 | 188.3 | -56.3 | 02 52 07.0 | -10 13 43 | Mrk1063 |
| 17 | 1 | 1 | NGC1313 | SBdm | HII | 452 | 9.37 | -19.66 | 0.02 | 283.4 | -44.6 | 03 17 39.0 | -66 40 42 | ESO082-G011 |
| 18 | 1 | 1 | NGC1433 | SBab | | 1061 | 10.68 | -21.15 | 0.00 | 255.7 | -51.2 | 03 40 27.0 | -47 22 48 | ESO 249-G014 |
| 19 | 1 | 1 | NGC1510 | Am. pec. | BCDG | 989* | 13.47* | -17.66*o | 0.00 | 248.8 | -48.2 | 04 01 54.0 | -43 32 12 | MCG-07-09-006 |
| 20 | 1 | 1 | NGC1553 | S0 pec. | | 1236 | 10.42 | -21.26 | 0.00 | 265.6 | -43.7 | 04 15 05.0 | -55 54 12 | ESO 157-G017 |
| 21 | 4 | 3 | NGC1569 | Im | SB nuc. | -83 | 11.90 | -16.22 | 0.51 | 143.7 | 11.2 | 04 26 05.8 | 64 44 18 | UGC3056 |
| | 1 | | NGC1614 | SBb pec. | SB nuc. | 4778* | 13.63* | -21.58* | 0.05 | 204.4 | -34.4 | 04 31 35.5 | -08 40 42 | Mrk617 |
| 22 | 4 | 1 | NGC1672 | SAB(s)bc | SB+Sy | 1335 | 11.03 | -21.37 | 0.00 | 268.8 | -38.9 | 04 44 55.0 | -59 20 18 | ESO118-G043 |
| r5 | 2 | | NGC1667 | Sbc | Sy2 | 4585 | 12.75 | -22.54 | 0.05 | 204.1 | -30.1 | 04 46 11.0 | -06 24 24 | MCG-01-13-013 |
| 23 | 2 | 4 | NGC1705 | Irr. Am. | BCDG | 640 | 12.80 | -17.00 | 0.04 | 261.1 | -38.7 | 04 53 06.0 | -53 26 30 | ESO 158-G013 |
| r6 | 1 | | NGC1800 | IBm. Am. | HII | 723 | 13.10 | -17.3 | 0.00 | 234.4 | -35.1 | 05 04 33.0 | -32 01 12 | MCG-05-13-004 |
| 24 | 1 | 1 | UGC3838 | Im | BCG | 3060* | 14.3p* | -20.09* | 0.02 | 142.6 | 28.5 | 07 22 20.0 | 72 40 33 | Mrk7 |
| r2 | 1 | 1 | IC2184 | Cl. Irr. | BCG | 3605* | 14.0p* | -20.44* | 0.01 | 143.1 | 28.6 | 07 23 39.4 | 72 13 55 | Mrk8 |
| 25 | 1 | 1 | NGC2403 | Sc | | 131 | 8.89 | -19.47 | 0.04 | 150.6 | 29.2 | 07 32 05.5 | 65 42 40 | UGC3918 |
| | 1 | 1 | NGC2415 | Irr. pec. | BCG | 3784* | 12.78* | -21.76* | 0.04 | 184.1 | 24.0 | 07 33 39.5 | 35 21 15 | Haro 1 |
| r1 | 2 | | NGC2537 | Sc | BCDG | 441 | 12.35 | -18.13 | 0.04 | 173.8 | 33.0 | 08 09 42.5 | 46 08 32 | Mrk86 |
| 27 | 1 | | HolmbergII | Irr. | BCDG | 158* | 11.10* | -16.77m | 0.02 | 144.3 | 32.7 | 08 13 53.5 | 70 52 13 | DDO 50 |
| 28 | 3 | | UGC4483 | dIm IV | HII | 156* | 15.0p* | -12.89m | 0.03 | 145.0 | 34.4 | 08 32 01.3 | 69 57 20 | MCG+12-08-048 |
| 29 | | 1 | NGC2639 | Sa | Lin+Sy | 3187 | 12.65 | -22.18 | 0.03 | 168.9 | 38.2 | 08 40 03.1 | 50 23 08 | UGC4544 |
| 30 | 1 | 2 | NGC2681 | Sa | Lin | 715 | 11.09 | -20.48 | 0.02 | 167.3 | 39.7 | 08 49 58.0 | 51 30 14 | UGC4645 |
| 31 | 2 | 2 | NGC2782 | SAB(rs)a | SB nuc. | 2551 | 12.15 | -22.06 | 0.00 | 182.2 | 43.7 | 09 10 53.8 | 40 19 17 | UGC4862 |
| 32 | 1 | | MCG10-13-71 | | BCDG | 4230* | 15.6 | -19.07c | 0.03 | 155.6 | 41.3 | 09 12 53.5 | 59 58 53 | Mrk19 |
| 33 | 2 | | NGC2798 | SBa | SB nuc. | 1741 | 13.0 | -19.81 | 0.00 | 179.5 | 44.3 | 09 14 09.4 | 42 12 34 | UGC4905 |
| r1 | 1 | 1 | NGC2820A | I0 pec. | BCDG | 1534* | 15.4* | -17.57*o | 0.04 | 149.8 | 40.3 | 09 17 26.1 | 64 26 57 | Mrk108, IC2458 |
| 34 | 1 | 1 | NGC2841 | Sb | Lin | 637 | 10.17 | -21.53 | 0.00 | 166.9 | 44.1 | 09 18 34.9 | 51 11 19 | UGC4966 |
| 35 | 2 | 1 | NGC2903 | Sbc | Hs | 550 | 9.50 | -20.96 | 0.02 | 208.7 | 44.5 | 09 29 19.9 | 21 43 19 | UGC5079 |
| 36 | 7 | 3 | I Zw 18 | Irr. | BCDG | 756* | 16.28a | -15.07*a | 0.01 | 160.5 | 44.8 | 09 30 30.3 | 55 27 46 | Mrk116, UGCA166 |
| 37 | 1 | 1 | NGC2997 | Sc(s) | Hs | 1081 | 10.32 | -21.40 | 0.12 | 262.6 | 16.8 | 09 43 28.0 | -30 57 36 | UGCA181 |
| 38 | 3 | 5 | NGC3031 | Sb | Lin | -36 | 7.86 | -20.75 | 0.04 | 142.1 | 40.9 | 09 51 27.6 | 69 18 13 | M81 |
| 39 | 2 | 1 | NGC3049 | SBbc | SB nuc. | 1494* | 13.04p* | -19.42*o | 0.01 | 227.6 | 44.7 | 09 52 10.2 | 09 30 32 | Mrk710 |
| 40 | 3 | 2 | NGC3081 | SBa | Sy2 | 2413 | 12.68 | -20.67 | 0.03 | 259.0 | 25.0 | 09 57 10.0 | -22 35 06 | IC2529 |
| | 1 | | NGC3077 | I0 | | 7 | 10.64 | -17.2 | 0.05 | 141.9 | 41.7 | 09 59 21.9 | 68 58 33 | UGC5398 |
| r7 | 1 | 1 | UGC5408 | | BCDG | 2602* | 14.84* | -18.96*o | 0.00 | 152.7 | 46.8 | 10 00 22.0 | 59 40 50 | Mrk25 |
| 41 | 2 | 1 | NGC3125 | Irr. Am. | BCDG | 1110 | 13.12 | -18.2 | 0.07 | 365.3 | 20.6 | 10 04 19.0 | -29 41 30 | MCG-05-24-022 |
| 42 | 1 | | NGC3256 | Sb(s) pec. | SB nuc. | 2821 | 11.98 | -22.80 | 0.13 | 277.4 | 11.7 | 10 25 43.0 | -43 39 00 | MCG-07-022-010 |
| 43 | 1 | 2 | UGC5720 | Im | BCDG | 1461* | 13.17a | -19.02*o | 0.00 | 156.2 | 52.8 | 10 29 22.9 | 54 39 34 | Mrk33, Haro 2 |
| 44 | 3 | 1 | NGC3310 | SAB(r)bc | SB nuc. | 992 | 11.2 | -20.82 | 0.00 | 156.6 | 54.1 | 10 35 40.3 | 53 45 45 | UGC5786 |
| 45 | 1 | 1 | NGC3351 | SBb | Hs | 779 | 10.52 | -20.66 | 0.01 | 234.0 | 56.4 | 10 41 19.6 | 11 58 00 | M95 |
| 46 | 1 | 1 | NGC3353 | Im | BCDG | 995 | 13.2 | -18.5 | 0.00 | 152.3 | 53.4 | 10 42 16.5 | 56 13 23 | Mrk35, Haro 3 |
| 47 | 1 | 2 | NGC3393 | SBa | Sy2 | 3730* | 13.10p* | -21.59* | 0.08 | 270.7 | 29.9 | 10 46 00.0 | -24 53 48 | MCG-04-26-011 |
| 48 | 1 | | MCG9-18-32 | Scp | BCDG | 2447* | 15.0p* | -19.02*o | 0.00 | 156.7 | 56.0 | 10 46 03.8 | 52 35 50 | Mrk153 |
| r18 | 1 | | NGC3395 | Scdp | SB nuc. | 1628 | 12.4 | -20.58 | 0.00 | 192.9 | 63.1 | 10 47 02.6 | 33 14 44 | UGC5931 |
| r8 | 1 | | NGC3396 | IBm | SB nuc. | 1648 | 12.6 | -20.56 | 0.00 | 192.9 | 63.2 | 10 47 08.9 | 33 15 18 | UGC5935 |
| | 1 | | NGC3432 | Sc | | 616 | 11.73 | -19.50 | 0.00 | 184.8 | 63.2 | 10 49 42.9 | 36 53 09 | UGC5986 |
| 49 | 1 | 1 | 1050+04 | | BCG | 5780* | 14.7p* | -20.78* | 0.03 | 246.2 | 53.9 | 10 50 28.4 | 04 53 52 | Mrk1267 |
| 50 | 1 | 1 | NGC3448 | Irr. Am. | SB nuc. | 1357 | 12.15 | -20.2 | 0.00 | 153.1 | 55.4 | 10 51 38.4 | 54 34 23 | UGC6024 |
| 51 | 1 | 1 | NGC3504 | SABab | SB nuc. | 1535 | 11.8 | -21.11 | 0.01 | 204.6 | 66.0 | 11 00 28.1 | 28 14 35 | UGC6118 |
| 52 | 1 | | Mrk36 | Irr. | BCDG | 646* | 15.69a | -15.06*a | 0.00 | 201.8 | 66.5 | 11 02 15.6 | 29 24 34 | UGCA225 |
| | 2 | 1 | NGC3622 | S ? | | 1306* | 13.65* | -19.10*o | 0.00 | 135.8 | 47.5 | 11 17 10.3 | 67 30 53 | UGC6339 |
| 53 | 1 | 1 | NGC3660 | SBbc | Sy1/NELG | 3678* | 15.5 | -18.74c | 0.02 | 269.1 | 48.4 | 11 21 00.1 | -08 23 01 | Mrk1291 |
| r1 | 1 | | UGC6448 | pec. | BCDG | 991* | 14.66a | -17.34*o | 0.00 | 137.3 | 50.6 | 11 23 55.8 | 64 24 46 | Mrk170 |
| r1 | 1 | | UGC6456 | pec. | BCDG | -93* | 14.70a | -14.6m | 0.02 | 127.8 | 37.3 | 11 24 36.6 | 79 16 06 | VII Zw 403 |
| | 1 | 1 | NGC3682 | S0/a | | 1543* | 13.3* | -19.39*o | 0.00 | 135.3 | 48.5 | 11 24 46.1 | 66 51 56 | UGC6459 |

TABLE 1—*Continued*

| Fig. no. | SW | LW | Galaxy Name | Morph. Type | Activity Class | $v_H$ km s$^{-1}$ | $B_T$ | $M_B$ $H_o = 50$ | E(B-V) | l | b | $\alpha$ (1950) (h-m-s) | $\delta$ (1950) (d-m-s) | Other Names |
|---|---|---|---|---|---|---|---|---|---|---|---|---|---|---|
| 54 | 2 | 1 | NGC3690 | Sc pec. | SB nuc. | 2988 | 12.02 | -22.30 | 0.00 | 141.9 | 55.4 | 11 25 44.2 | 58 50 23 | Mrk171 |
| 55 | 2 | 1 | NGC3738 | Irr. IV | HII | 224 | 12.14 | -17.21 | 0.00 | 144.6 | 59.3 | 11 33 04.5 | 54 47 58 | UGC6565 |
| r19 | 1 | 1 | NGC3758 | S0, 2-nuc. | Sy1 & HII | 8912* | 15.2p* | -21.21* | 0.00 | 226.8 | 72.1 | 11 33 52.5 | 21 52 24 | Mrk739 |
| r17 | 1 | | MCG-1-30-33 | Sb | SB nuc. | 5167* | 14.5 | -20.52c | 0.01 | 273.7 | 55.3 | 11 44 11.4 | -03 33 54 | Arp248B |
| 56 | 1 | 1 | NGC3982 | Sbc | Sy2 | 1102 | 11.91 | -20.30 | 0.00 | 138.8 | 60.3 | 11 53 52.3 | 55 24 10 | UGC6918 |
| 57 | 2 | 1 | NGC3991 | Im | BCG | 3192* | 13.5* | -20.74* | 0.01 | 185.7 | 77.2 | 11 54 56.3 | 32 36 54 | UGC6933 |
| 58 | 1 | 1 | NGC3994 | Sc | Lin | 3096* | 13.3* | -20.81* | 0.01 | 185.9 | 77.2 | 11 55 02.3 | 32 33 23 | UGC6936 |
| 59 | 1 | 1 | NGC3995 | Sm | HII | 3353 | 12.8 | -21.93 | 0.01 | 185.8 | 77.3 | 11 55 10.3 | 32 34 24 | UGC6944 |
| 60 | 1 | | ESO572-34 | | HII | 1075* | 14.19p* | -17.44*o | 0.02 | 286.1 | 42.1 | 11 56 25.0 | -18 44 54 | POX 36 |
| 61 | | 1 | NGC4102 | Sb | Lin/HII | 865 | 12.3 | -19.80 | 0.00 | 138.1 | 63.1 | 12 03 51.6 | 52 59 23 | UGC7096 |
| 62 | 2 | 2 | NGC4111 | S0 | Lin | 791 | 11.75 | -19.33 | 0.00 | 149.5 | 71.7 | 12 04 31.0 | 43 20 37 | UGC7103 |
| 63 | 1 | 1 | NGC4194 | Sm pec. | BCG | 2506* | 13.01* | -20.71*o | 0.00 | 134.4 | 61.8 | 12 11 41.7 | 54 48 21 | Mrk201 |
| 64 | 2 | 1 | NGC4214 | IABm | SB nuc. | 291 | 10.22 | -18.79 | 0.00 | 160.3 | 78.1 | 12 13 08.0 | 36 36 22 | UGC7208 |
| 65 | 2 | 1 | NGC4258 | SBc | Lin | 463 | 8.95 | -22.05 | 0.00 | 138.3 | 68.8 | 12 16 29.7 | 47 34 51 | M106 |
| r9 | 1 | 2 | NGC4314 | SBa pec. | Lin | 883 | 11.35 | -19.80 | 0.02 | 187.7 | 83.1 | 12 20 02.0 | 30 10 25 | UGC7443 |
| 66 | 2 | 2 | NGC4321 | Sbc | Hs | 1568 | 10.11 | -21.91 | 0.01 | 271.1 | 76.9 | 12 20 23.2 | 16 06 00 | M100 |
| 67 | | 3 | NGC4350 | S0 | | 1184 | 11.88 | -19.82 | 0.01 | 270.1 | 77.8 | 12 21 25.1 | 16 58 21 | UGC7473 |
| 68 | 1 | 1 | NGC4382 | S0 pec. | | 739 | 10.10 | -21.60 | 0.01 | 267.7 | 79.2 | 12 22 53.2 | 18 28 03 | M85 |
| 69 | 1 | 1 | NGC4385 | SBab | SB nuc. | 2142 | 13.05 | -20.38 | 0.02 | 288.8 | 62.7 | 12 23 09.2 | 00 50 53 | Mrk52 |
| 70 | 3 | 1 | NGC4388 | Sab | Sy2 | 2487 | 11.83 | -21.05 | 0.03 | 279.1 | 74.3 | 12 23 14.8 | 12 56 18 | UGC7520 |
| 71 | 2 | | MCG8-23-35 | Sm pec. | BCDG | 281* | 14.84a | ... | 0.00 | 134.1 | 68.1 | 12 23 51.7 | 48 46 13 | Mrk209 |
| 72 | 2 | 1 | NGC4449 | IBm | HII | 207 | 9.85 | -18.84 | 0.00 | 136.8 | 72.4 | 12 25 45.9 | 44 22 16 | UGC7592 |
| 73 | 1 | 1 | NGC4500 | SBa | BCG | 3115* | 13.1* | -21.02* | 0.00 | 128.1 | 59.0 | 12 29 02.6 | 58 14 26 | Mrk213 |
| 74 | | 1 | NGC4569 | SABab | Lin | -261 | 10.23 | -22.31 | 0.02 | 288.5 | 75.6 | 12 34 18.7 | 13 26 18 | M90 |
| 75 | 2 | 3 | NGC4579 | Sab | Lin | 1805 | 10.56 | -21.69 | 0.04 | 290.4 | 74.4 | 12 35 12.6 | 12 05 40 | M58 |
| 76 | 1 | 1 | NGC4594 | Sa | Lin | 1089 | 9.28 | -22.81 | 0.03 | 298.5 | 51.1 | 12 37 24.2 | -11 20 59 | M104 |
| 77 | 1 | 1 | IC3639 | SBb | Sy 2 | 3309* | 13.01p* | -21.23* | 0.06 | 300.6 | 26.1 | 12 38 11.0 | -36 29 00 | TOL1238-364 |
| 78 | 1 | | UGC7905S | | BCG | 4875* | 14.1 | -21.29b | 0.00 | 125.3 | 62.2 | 12 41 32.4 | 55 10 08 | Mrk220 |
| 79 | 2 | 1 | NGC4670 | Am. | BCDG | 1076 | 13.05 | -19.01 | 0.00 | 212.7 | 88.6 | 12 42 49.8 | 27 23 58 | UGC7930 |
| 80 | 3 | 2 | NGC4736 | SAab, | Lin | 311 | 8.92 | -20.81 | 0.00 | 123.4 | 76.0 | 12 48 32.0 | 41 23 27 | M94 |
| 81 | 1 | 1 | NGC4748 | | Sy1 | 4110 | | | 0.00 | 303.2 | 49.5 | 12 49 35.1 | -13 08 34 | IRAS1249-131 |
| 82 | 2 | 1 | NGC4826 | Sb | Lin | 413 | 9.37 | -20.61 | 0.04 | 315.7 | 84.4 | 12 54 16.9 | 21 57 18 | M64 |
| 83 | 2 | 2 | MCG6-28-44 | | BCG | 13421* | 15.3* | -22.15* | 0.01 | 110.6 | 84.5 | 12 54 32.6 | 32 43 04 | Mrk54 |
| 84 | 2 | 2 | NGC4853 | S0 | BCDG | 7595* | 14.41* | -21.67* | 0.02 | 49.8 | 88.3 | 12 56 10.4 | 27 52 03 | II Zw 67 |
| 85 | 2 | 1 | NGC4861+ | Im | BCDG | 831 | 12.8 | -18.64 | 0.00 | 111.5 | 82.1 | 12 56 38.5 | 35 06 56 | Mrk59 |
| 86 | 1 | 1 | IC 3961 | Im | BCDG | 831 | 12.8 | -18.64 | 0.00 | 111.5 | 82.1 | 12 56 38.5 | 35 06 56 | Mrk59 |
| r9 | 1 | 1 | NGC5005 | Sb | Lin | 1022 | 10.64 | -21.78 | 0.00 | 101.6 | 79.2 | 13 08 38.6 | 37 19 23 | UGC8256 |
| r17 | ? | | UGC8315N | S | SB nuc. | 1143 | 15.2 | -16.60 | 0.00 | 102.8 | 77.1 | 13 11 53.5 | 39 24 41 | MCG+07-27-052 |
| 87 | 5 | 3 | NGC5102 | SA0 pec. | SB nuc. | 420 | 10.64 | -18.73 | 0.05 | 309.7 | 25.8 | 13 19 07.0 | -36 22 12 | MCG-06-29-031 |
| 88 | 1 | 1 | NGC5135 | SABb | Sy2 | 4157 | 12.94 | -22.55 | 0.06 | 311.7 | 32.5 | 13 22 57.0 | -29 34 24 | MCG-05-32-013 |
| 89 | 1 | | Mrk66 | | BCG | 6525* | 15.0 | -20.62c | 0.00 | 113.8 | 59.3 | 13 23 57.8 | 57 30 39 | MCG+10-19-072 |
| 90 | 1 | 1 | NGC5194 | Sbc | Lin | 464 | 8.98 | -21.60 | 0.00 | 104.9 | 68.6 | 13 27 45.8 | 47 27 12 | M51a |
| r3 | 1 | | Mrk789 | 2-nuc. | SB nuc. | 9593 | 14.5 | -21.91c | 0.00 | 335.9 | 71.3 | 13 29 55.4 | 11 21 43 | VIII Zw 323 |
| 91 | 1 | 1 | NGC5236 | SBc | SB nuc. | 520 | 8.51 | -21.12 | 0.03 | 314.6 | 32.0 | 13 34 11.0 | -29 36 48 | M83 |
| 92 | 1 | 1 | ESO383-44 | SAd | SB ring | 3963* | 14.09p* | -20.93* | 0.03 | 313.9 | 28.9 | 13 34 36.0 | -32 45 06 | MCG-05-32-052 |
| 93 | 1 | 1 | NGC5256 | 2-nuc. | Sy2+Lin | 8353* | 14.00p* | -22.24* | 0.00 | 102.7 | 67.0 | 13 36 15.0 | 48 31 48 | Mrk266a,b |
| 94 | 7 | 8 | NGC5253 | Im Am. | SB nuc. | 395 | 11.11 | -18.2 | 0.05 | 314.9 | 30.1 | 13 37 05.0 | -31 23 30 | HARO10 |
| | 1 | | 1350-00 | | | | 15.4 | | 0.02 | 334.1 | 59.2 | 13 50 10.8 | 00 22 37 | Um619 |
| 95 | 1 | 1 | UGC8850 | 2-nuc. | Sy 2 | 15230* | 14.4* | -22.94* | 0.01 | 5.8 | 72.7 | 13 53 39.8 | 18 36 40 | Mrk463 |
| 96 | 1 | | NGC5457 | Sc | HII | 251 | 8.18 | -21.51 | 0.00 | 102.0 | 59.8 | 14 01 26.6 | 54 35 25 | M101 |
| r10,r12 | 1 | 1 | NGC5506 | Sa pec. | Sy2 | 1815* | 12.79* | -20.50*o | 0.03 | 339.2 | 53.8 | 14 10 39.1 | -02 58 26 | Mrk1376 |
| r3 | 1 | | IC4395 | S | Sy 2 | 10946* | 14.67p* | -22.08* | 0.00 | 37.0 | 70.9 | 14 15 06.1 | 27 05 15 | Mrk673 |
| 97 | 1 | 1 | NGC5643 | SBc | Sy 2 | 1194 | 10.89 | -21.20 | 0.12 | 321.4 | 15.0 | 14 29 28.0 | -43 57 12 | MCG-07-30-003 |
| r11 | 1 | 1 | NGC5674 | SBb/Sc | Sy 2 | 7472* | 13.70p* | -22.31* | 0.02 | 355.9 | 57.4 | 14 31 22.3 | 05 40 43 | UGC9369 |
| 98 | 2 | 1 | Mrk477 | Comp. | Sy 2 | 11379* | 15.4p* | -21.39c | 0.00 | 93.0 | 56.8 | 14 39 03.0 | 53 42 53 | I Zw 92 |
| 99 | 1 | 1 | NGC5728 | SBb | Sy2 | 2970 | 12.1 | -22.47 | 0.09 | 337.3 | 38.1 | 14 39 37.2 | -17 02 30 | MCG-03-37-005 |
| 100 | 2 | 1 | UGC9560 | Irr. pec. | BCDG | 1213* | 14.83* | -17.95*o | 0.00 | 58.8 | 63.2 | 14 48 55.1 | 35 46 36 | Mrk829, II Zw 70 |
| r3 | 1 | 1 | NGC5860 | pair of Es | SB nuc. | 5398* | 14.20 | -21.01c | 0.01 | 71.3 | 58.5 | 15 04 44.3 | 42 49 53 | Mrk480S |
| r1 | 1 | | UGCA410 | dE | BCDG | 665* | 15.45* | -16.63*a | 0.01 | 87.8 | 49.0 | 15 35 48.4 | 55 25 34 | Mrk487 |
| 101 | 1 | 1 | NGC5996 | SBd | SB nuc. | 3304* | 13.2* | -21.46* | 0.02 | 29.5 | 48.6 | 15 44 37.8 | 18 01 38 | Mrk691 |
| 102 | 1 | 1 | NGC6052 | Cl. Irr. | SB nuc. | 4729 | 13.45 | -21.69 | 0.03 | 35.3 | 45.5 | 16 03 01.2 | 20 40 43 | Mrk297 |
| r3 | 1 | | NGC6090 | Sd pec., pair | SB nuc. | 8785* | 14.5 | -21.76c | 0.00 | 81.4 | 45.2 | 16 10 24.5 | 52 35 06 | Mrk496 |
| 103 | 1 | | NGC6217 | SBbc | SB nuc. | 1365 | 11.86 | -21.11 | 0.03 | 111.3 | 33.4 | 16 35 05.1 | 78 18 05 | UGC10470 |

TABLE 1—*Continued*

| Fig. no. | SW | LW | Galaxy Name | Morph. Type | Activity Class | $v_H$ km s$^{-1}$ | $B_T$ | $M_B$ $H_o = 50$ | E(B-V) | l | b | $\alpha$ (1950) (h-m-s) | $\delta$ (1950) (d-m-s) | Other Names |
|---|---|---|---|---|---|---|---|---|---|---|---|---|---|---|
| 104 | 1 | | Mrk499 | | BCG | 7710* | 14.9* | -21.12* | 0.00 | 75.2 | 40.0 | 16 47 02.6 | 48 47 44 | UGC10565 |
| r13 | 1 | 1 | NGC6221 | SABbc pec. | Sy2+SB | 1478 | 11.52 | -21.55 | | 329.7 | -9.6 | 16 48 26.0 | -59 08 00 | ESO 138-G003 |
| r14,r15 | 2 | 1 | NGC6764 | SBb | Lin/HII | 2416* | 12.56* | -21.46*o | 0.06 | 81.5 | 18.2 | 19 07 01.2 | 50 51 08 | UGC11407 |
| 105 | 6 | 4 | TOL1924-416 | | BCG | 2869* | 13.3* | -20.79*o | 0.07 | 356.9 | -24.1 | 19 24 29.0 | -41 40 36 | ESO 338-IG004 |
| r16 | 1 | | 1941-543 | Comp. pec. | HII | 5625* | 15.0* | -20.37* | 0.04 | 343.6 | -29.4 | 19 41 03.0 | -54 22 18 | ESO 185-IG013 |
| 106 | 1 | 1 | NGC7130 | Sa pec. | Sy2+SB nuc. | 4796 | 12.92 | -22.27 | 0.00 | 9.9 | -50.4 | 21 45 20.0 | -35 11 06 | IC5135 |
| 107 | 2 | 1 | NGC7250 | S/I | SB nuc.? | 1157* | 13.22* | -20.11*o | 0.15 | 94.0 | -13.5 | 22 16 08.7 | 40 18 41 | Mrk907 |
| r15 | 1 | | Mrk309 | | SB nuc. | 12636 | 15.3 | -22.32c | 0.05 | 91.3 | -30.8 | 22 50 09.9 | 24 27 54 | |
| 108 | 2 | 1 | NGC7496 | SBc | Sy2+HII | 1472 | 11.78 | -20.89 | 0.00 | 347.8 | -63.8 | 23 06 59.0 | -43 42 00 | ESO 291-G001 |
| 109 | 2 | 1 | NGC7552 | SBbc | SB nuc. | 1589 | 11.40 | -21.49 | 0.00 | 348.1 | -65.2 | 23 13 25.0 | -42 51 24 | IC5294 |
| r13 | 3 | 4 | NGC7582 | SBab | Sy2+SB | 1498 | 11.46 | -21.75 | 0.00 | 348.1 | -65.7 | 23 15 38.0 | -42 38 36 | ESO 291-G016 |
| r16 | 1 | 1 | NGC7590 | SAbc | Sy2 | 1509 | 12.20 | -20.78 | 0.00 | 348.2 | -65.8 | 23 16 10.0 | -42 30 42 | ESO 347-G033 |
| 110 | 1 | 1 | NGC7673 | Cl. Irr. | HII | 3401* | 13.17* | -21.47* | 0.04 | 99.2 | -35.4 | 23 25 11.8 | 23 18 51 | Mrk325 |
| 111 | 2 | 1 | NGC7714 | Sdm pec. | SB nuc. | 2799* | 13.00* | -21.24* | 0.04 | 88.2 | -55.6 | 23 33 41.0 | 01 52 42 | Mrk538 |
| | 1 | | Mrk542 | Comp. | | 7354* | 15.8p* | -20.04c | 0.02 | 93.1 | -61.8 | 23 54 25.8 | -02 21 41 | UM 191 |
| 112 | 1 | 1 | NGC7793 | SAd | HII | 217 | 9.65 | -18.85 | 0.00 | 4.5 | -77.2 | 23 55 15.0 | -32 52 06 | MCG-06-01-009 |

NOTES TO TABLE 1

The names, cross-identifications, coordinates, and some of the morphological types are taken first from RSA or from the literature, and otherwise come from the NASA Extragalactic Database (NED). The morphological type follows, where possible, the classical Hubble classification. Specific symbols are: Am. = amorphous, Comp. = compact, Cl. Irr. = clumpy irregular, 2-nuc. = presence of two nuclei. The reddening $E(B - V)$ from our Galaxy is from Burstein & Heiles 1984. The activity classification is as follows: BCG and BCDG are, respectively, blue compact galaxies and blue compact dwarf galaxies (where a blue compact galaxy is considered to be a dwarf if it has $M_B$ fainter than $-20$); Sy2 are Seyfert 2 galaxies; SB nuc. are galaxies experiencing a starburst in their nuclei; Hs are hot spot galaxies; Lin are LINERs; HII are galaxies with spectra typical of a H II region.

The criterion for defining the class is not based on physical considerations but comes from the literature, where the most widely accepted classification has been used for each galaxy. The first column gives the figure number for galaxies treated individually in this paper. If no figure number is given, a reference for the activity classification is given as listed below:

REFERENCES.—(r1) Thuan & Martin 1981 (BCDG). (r2) Gordon & Gottesman 1981 (BCG). (r3) Mazzarella & Balzano 1986 (Mrk). (r4) Kollatschny & Fricke 1986. (r5) Phillips, Charles, & Baldwin 1983. (r6) Lamb, et al. 1985. (r7) Zamorano & Rego 1986. (r8) Joseph et al. 1984. (r9) Keel 1983c. (r10) De Robertis & Osterbrock 1986. (r11) Huchra, Wyatt, & Davis 1982. (r12) Heckman et al. 1983. (r13) Moorwood & Oliva 1988. (r14) Heckman 1980. (r15) Osterbrock & Cohen 1982. (r16) Véron-Cetty & Véron 1986. (r17) Lamb, Bushouse, & Towns 1989. (r18) Keel et al. 1985. (r19) Netzer, Kollatschny, & Fricke 1987.

The recession velocity ($v_H$) and the apparent magnitude ($B_T$) are from the RSA when no marks are shown; $v_H$ is the helicoentric velocity, $B_T$ is the apparent magnitude in the $B_T$ system of the RC2, $M_B$ is the absolute magnitude calculated from an apparent magnitude corrected for Galactic and internal absorption and from a recession velocity reduced to the centroid of the Local Group (cf. RSA).

An asterisk following a value of $v_H$, $B_T$, or $M_B$ means the following: The values of $v_H$ and $B_T$ correspond to the heliocentric velocity and to the uncorrected apparent magnitude from the RC3; $v_H$ is the $V_{21}$ or the $V_{opt}$ when the first is not available (the difference between the two is in general small). The absolute magnitude $M_B$ is obtained from RC3 using the velocity reduced with respect to the Galactic standard of rest, $v_{GSR}$, the apparent magnitude corrected for Galactic and internal absorption, $B_T^0$, and assuming $H_0 = 50$ km s$^{-1}$ Mpc$^{-1}$. For recession velocities between 500 and 3000 km s$^{-1}$ $M_B$ has been calculated with the usual formula after checking that it is not near a cluster. For $v > 3000$ km s$^{-1}$ the formula has been applied without problem. Redshift corrections were applied for $v > 10{,}000$ km s$^{-1}$. For galaxies belonging to a cluster, $M_B$ has been obtained from $B_T^0$ (RC3), assuming as distance the distance of the cluster.

Other notation: p—when $B_T$ is not available from RC3, the photographic magnitude has been reported; o—marks galaxies with redshift in the range 500–3000 km s$^{-1}$, but not belonging to a cluster; m—this marks the distances calculated through the distance modulus; a—$B_T$ or corrections to derive $B_T^0$ have been taken from Thuan & Martin 1981; b—$B_T^0$ from Gordon & Gottesman 1981; c—galaxies for which $B_T$ or $v_H$ or both have been taken from NED (NASA Extragalactic Database), since they are not reported in RSA or in RC3; the same values have been used to calculate an approximate value for $M_B$. The symbol indicates also an approximate $M_B$ for galaxies with both $v_H$ and $B_T$ from RC3, but without the extinction-corrected $B_T^0$.

plotted in the rest frame. Figure 1 shows normal spiral galaxies and LINER galaxies; Figure 2 shows starburst galaxies; and Figure 3 shows blue compact, blue compact dwarf, and Seyfert 2 galaxies. As an aid to the interpretation of these plots, Figure 4 shows O and B stars, while Figure 5 displays A–M stars, all on the same scale. The spectra are from the stellar atlas of Fanelli et al. (1992) and are separated by luminosity class.

Table 4 lists the strengths of UV interstellar absorption lines in three lines of sight through our Galaxy. Table 5 lists the discrete features—absorption, emission, and P Cygni—present in the spectra of early-type stars. Table 6 lists the absorption features due to mid- to late-type stars. Table 7 lists emission lines from nebular regions. These contributors to UV flux are described in § 4.1.

Table 8 contains fluxes and an approximate radius for the object. The radius given is half of the largest diameter from NED. Note that some galaxies are extended, so that the *IUE* aperture contains only the bulge (for example, NGC 224, with a radius of 80′), while other galaxies are much smaller, so that the *IUE* aperture contains the entire galaxy disk (for example, NGC 4385, with a radius of 6″). Thus the fluxes in this table represent various portions of the bulge plus disk depending on

TABLE 2

MESSIER GALAXIES

| Galaxy Name | $\alpha$ (1950) | $\delta$ (1950) | Other Name |
|---|---|---|---|
| M31 ..... | $00^h40^m00^s.0$ | 41°00′06″ | NGC 224 |
| M33 ..... | 01 31 04.6 | 30 23 40 | NGC 598 |
| M51 ..... | 13 27 45.8 | 47 27 12 | NGC 5194 |
| M58 ..... | 12 35 12.6 | 12 05 40 | NGC 4579 |
| M64 ..... | 12 54 16.9 | 21 57 18 | NGC 4826 |
| M77 ..... | 02 40 06.5 | −00 13 32 | NGC 1068 |
| M81 ..... | 09 51 27.6 | 69 18 13 | NGC 3031 |
| M83 ..... | 13 34 11.0 | −29 36 48 | NGC 5236 |
| M85 ..... | 12 22 53.2 | 18 28 03 | NGC 4382 |
| M90 ..... | 12 34 18.7 | 13 26 18 | NGC 4569 |
| M94 ..... | 12 48 32.0 | 41 23 27 | NGC 4736 |
| M95 ..... | 10 41 19.6 | 11 58 00 | NGC 3351 |
| M100 ..... | 12 20 23.2 | 16 06 00 | NGC 4321 |
| M101 ..... | 14 01 26.6 | 54 35 25 | NGC 5457 |
| M104 ..... | 12 37 24.2 | −11 20 59 | NGC 4594 |
| M106 ..... | 12 16 29.7 | 47 34 51 | NGC 4258 |

the galaxy size. The average observed ultraviolet flux is given along with the variance in 100 Å regions, centered on the wavelengths 1482, 1913, 2373, and 2700 Å. The first three of these wave bands were chosen to correspond to the three different wavelengths where the UV extinction curve of the Galaxy [$A_\lambda/E(B-V)$; Seaton 1979] has the same value. These three flux values have been fitted to $F_\lambda = F_0\lambda^\beta$, and the results for the parameters are shown in Table 9, ordered by activity class. A slope that is based on regions with equal extinction is independent of extinction like that of the Milky Way, and is also correct when no extinction is present. Of course, the UV extinction in these galaxies may have a different wavelength dependence from that of our Galaxy, but our method produces a uniform estimate for the true intrinsic UV slope.

The distributions of slopes, $\beta$, are shown as histograms by activity class in Figure 6, with the median and variance shown on the top of each plot. The slopes of the four Seyfert 2 galaxies which are common to this atlas and the work of Kinney et al. (1991a, where slopes were measured by removing the emission lines and fitting a power law to the continuum) are found to agree to within 1 $\sigma$.

Given that many of the atlas galaxies have metallicities considerably lower than that of the solar neighborhood, we have also dereddened two galaxies using the Large Magellanic Cloud (LMC) extinction curve. Figure 7 demonstrates the dereddening of starburst galaxies using both a Galactic extinction curve and the LMC extinction curve.

The spectra are displayed individually in Figures 8–112 (at the end of this paper), ordered by right ascension. About 25% of the galaxy spectra have little spectral information because of their low signal-to-noise ratio; these galaxies have not been shown in the figures except in cases where the object itself is particularly interesting. (The entire data set, including objects extracted but not shown in this paper, will be available in digital form as described below.) The gross flux number (FN) is shown at the bottom of each plot as a solid line. The background flux number is shown at the bottom as a dotted line. Above the gross and background FN, 1 $\sigma$ is plotted as a percentage of the total flux. The spectrum itself is plotted in units of ergs cm$^{-2}$ s$^{-1}$ Å$^{-1}$. A horizontal bar is drawn at the top of the plot with the location of typical absorption and emission lines marked at the redshift of the galaxy. A bar is drawn beneath the spectrum to flag some typical strong absorption lines from our Galaxy. The wavelengths for the absorption lines from our Galaxy are from Morton, York, & Jenkins (1989); wavelengths for emission lines shown on the plots are from Ulrich (1980); wavelengths for absorption lines from the galaxies are

TABLE 3

MARKARIAN GALAXIES

| Galaxy Name | $\alpha$ (1950) | $\delta$ (1950) | Other Name |
|---|---|---|---|
| Mrk 7 ..... | $07^h22^m20^s.0$ | 72°40′33″ | UGC 3838 |
| Mrk 8 ..... | 07 23 39.4 | 72 13 55 | IC 2184 |
| Mrk 19 ..... | 09 12 53.5 | 59 58 53 | MCG 10-13-71 |
| Mrk 25 ..... | 10 00 22.0 | 59 40 50 | UGC 5408 |
| Mrk 33 ..... | 10 29 22.9 | 54 39 34 | UGC 5720, H2 |
| Mrk 35 ..... | 10 42 16.5 | 56 13 23 | NGC 3353, H3 |
| Mrk 36 ..... | 11 02 15.6 | 29 24 34 | UGC A225 |
| Mrk 52 ..... | 12 23 09.2 | 00 50 53 | NGC 4385 |
| Mrk 54 ..... | 12 54 32.6 | 32 43 04 | MCG 6-28-44 |
| Mrk 59 ..... | 12 56 38.5 | 35 06 56 | NGC 4861 |
| Mrk 66 ..... | 13 23 57.8 | 57 30 39 | MCG 10-19-072 |
| Mrk 86 ..... | 08 09 42.5 | 46 08 32 | NGC 2537 |
| Mrk 108 ..... | 09 17 26.1 | 64 26 57 | NGC 2820A |
| Mrk 116 ..... | 09 30 30.3 | 55 27 46 | UGC A166 |
| Mrk 153 ..... | 10 46 03.8 | 52 35 50 | MCG 9-18-32 |
| Mrk 170 ..... | 11 23 55.8 | 64 24 46 | UGC 6448 |
| Mrk 171 ..... | 11 25 44.2 | 58 50 23 | NGC 3690 |
| Mrk 201 ..... | 12 11 41.7 | 54 48 21 | NGC 4194 |
| Mrk 209 ..... | 12 23 51.7 | 48 46 13 | MCG 8-23-35 |
| Mrk 213 ..... | 12 29 02.6 | 58 14 26 | NGC 4500 |
| Mrk 220 ..... | 12 41 32.4 | 55 10 08 | UGC 7905 |
| Mrk 235 ..... | 23 25 11.8 | 23 18 51 | NGC 7673 |
| Mrk 266a ..... | 13 36 15.0 | 48 31 48 | Mrk 266a |
| Mrk 266b ..... | 13 36 15.0 | 48 31 54 | NGC 5256 |
| Mrk 297 ..... | 16 03 01.2 | 20 40 43 | NGC 6052 |
| Mrk 309 ..... | 22 50 09.9 | 24 27 54 | ... |
| Mrk 325 ..... | 23 25 11.8 | 23 18 51 | NGC 7673 |
| Mrk 347 ..... | 00 45 17.0 | 22 06 07 | IC 1586 |
| Mrk 348 ..... | 00 46 04.4 | 31 41 00 | NGC 262 |
| Mrk 357 ..... | 01 19 56.6 | 22 54 30 | ... |
| Mrk 463 ..... | 13 53 39.8 | 18 36 40 | UGC 8850 |
| Mrk 477 ..... | 14 39 03.0 | 53 42 53 | ... |
| Mrk 480S ..... | 15 04 44.3 | 42 49 53 | NGC 5860 |
| Mrk 487 ..... | 15 35 48.4 | 55 25 34 | UGC A410 |
| Mrk 496a ..... | 16 10 24.5 | 52 35 06 | NGC 6090 |
| Mrk 496b ..... | 16 10 24.5 | 52 35 08 | NGC 6090 |
| Mrk 499 ..... | 16 47 02.6 | 48 47 44 | UGC 10565 |
| Mrk 538 ..... | 23 33 41.0 | 01 52 42 | NGC 7714 |
| Mrk 542 ..... | 23 54 25.8 | −02 21 41 | |
| Mrk 617 ..... | 04 31 35.5 | −08 40 42 | NGC 1614 |
| Mrk 673 ..... | 14 15 06.1 | 27 05 15 | IC 4395 |
| Mrk 691 ..... | 15 44 37.8 | 18 01 38 | NGC 5996 |
| Mrk 710 ..... | 09 52 10.2 | 09 30 32 | NGC 3049 |
| Mrk 739 ..... | 11 33 52.5 | 21 52 24 | NGC 3758 |
| Mrk 789 ..... | 13 29 55.4 | 11 21 43 | VIII Zw 323 |
| Mrk 799 ..... | 13 59 08.5 | 59 34 16 | NGC 5430 |
| Mrk 829 ..... | 14 48 55.1 | 35 46 36 | UGC 9560 |
| Mrk 907 ..... | 22 16 08.7 | 40 18 41 | NGC 7250 |
| Mrk 960 ..... | 00 46 04.8 | −12 59 22 | Haro 15 |
| Mrk 1027 ..... | 02 11 28.8 | 04 56 33 | IC 214 |
| Mrk 1063 ..... | 02 52 07.0 | −10 13 43 | NGC 1140 |
| Mrk 1267 ..... | 10 50 28.4 | 04 53 52 | 1050+04 |
| Mrk 1291 ..... | 11 21 00.1 | −08 23 01 | NGC 3660 |
| Mrk 1376 ..... | 14 10 39.1 | −02 58 26 | NGC 5506 |

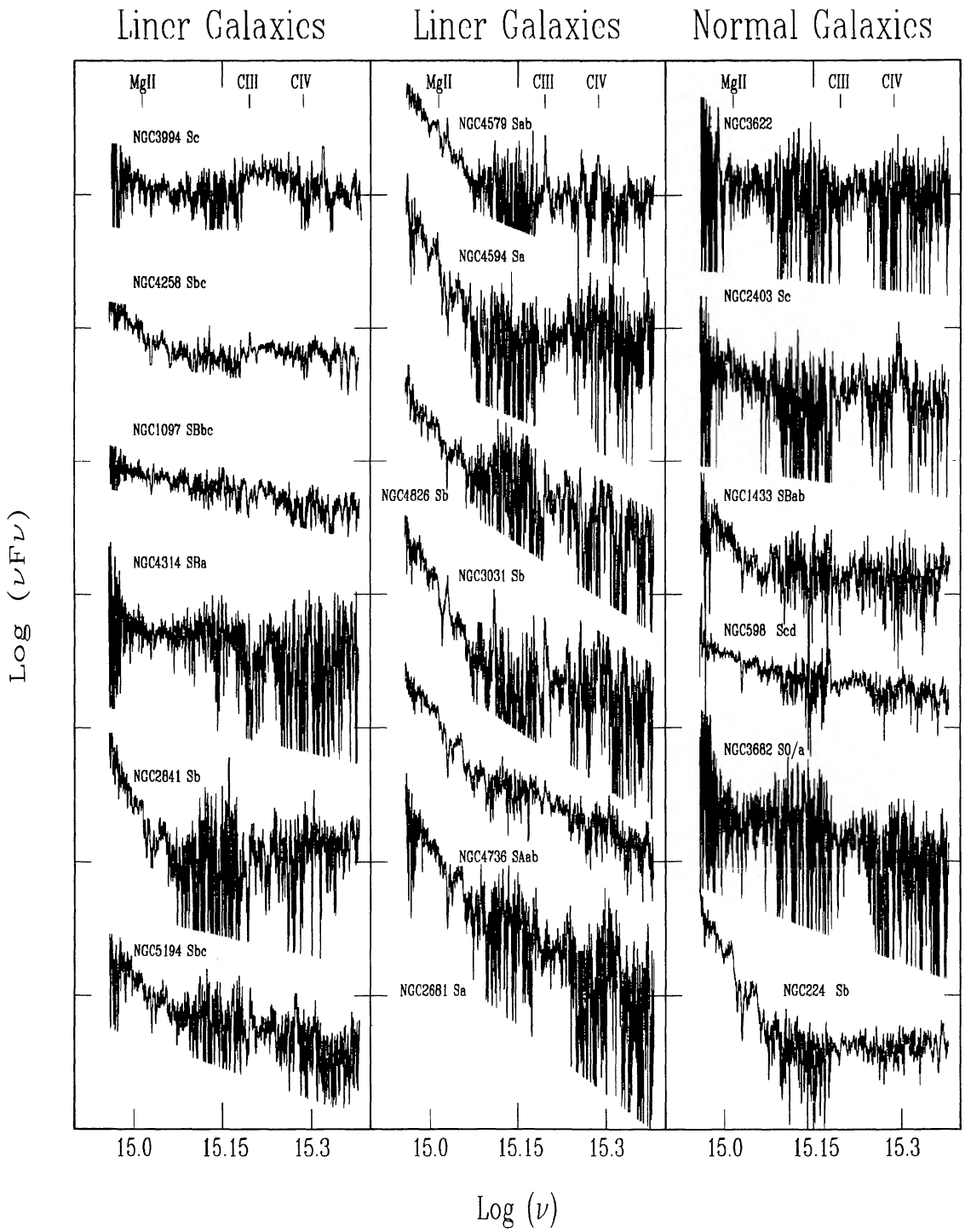


FIG. 1.—Spectral energy distribution of LINERs and normal spiral galaxies ordered by spectral slope. The units of the ordinate are ergs $cm^{-2}$ $s^{-1}$, while the units of the abscissa are Hz. The galaxies are displayed at their rest wavelengths, and the Mg II λ2800, C III] λ1909, and C IV λ1550 features are marked. No correction is made for extinction.

from Panek & Savage (1976), Nussbaumer et al. (1982), Heck et al. (1984), and Fanelli et al. (1987, 1990).

Figures 1–5 are in units of energy, log ($\nu F_\nu$), versus frequency, log $\nu$, while the plots of individual objects are in units of flux, $F_\lambda$, versus wavelength, λ. Slopes are quoted in $F_\lambda \propto \lambda^\beta$. Because spectral slope is commonly quoted as $F_\nu \propto \nu^\alpha$, we give the conversion between these three systems here:

$$F_\lambda \propto \lambda^\beta ,$$

$$F_\nu \propto \nu^\alpha = \nu^{-2-\beta} ,$$

$$\nu F_\nu \propto \nu^{-1-\beta} .$$

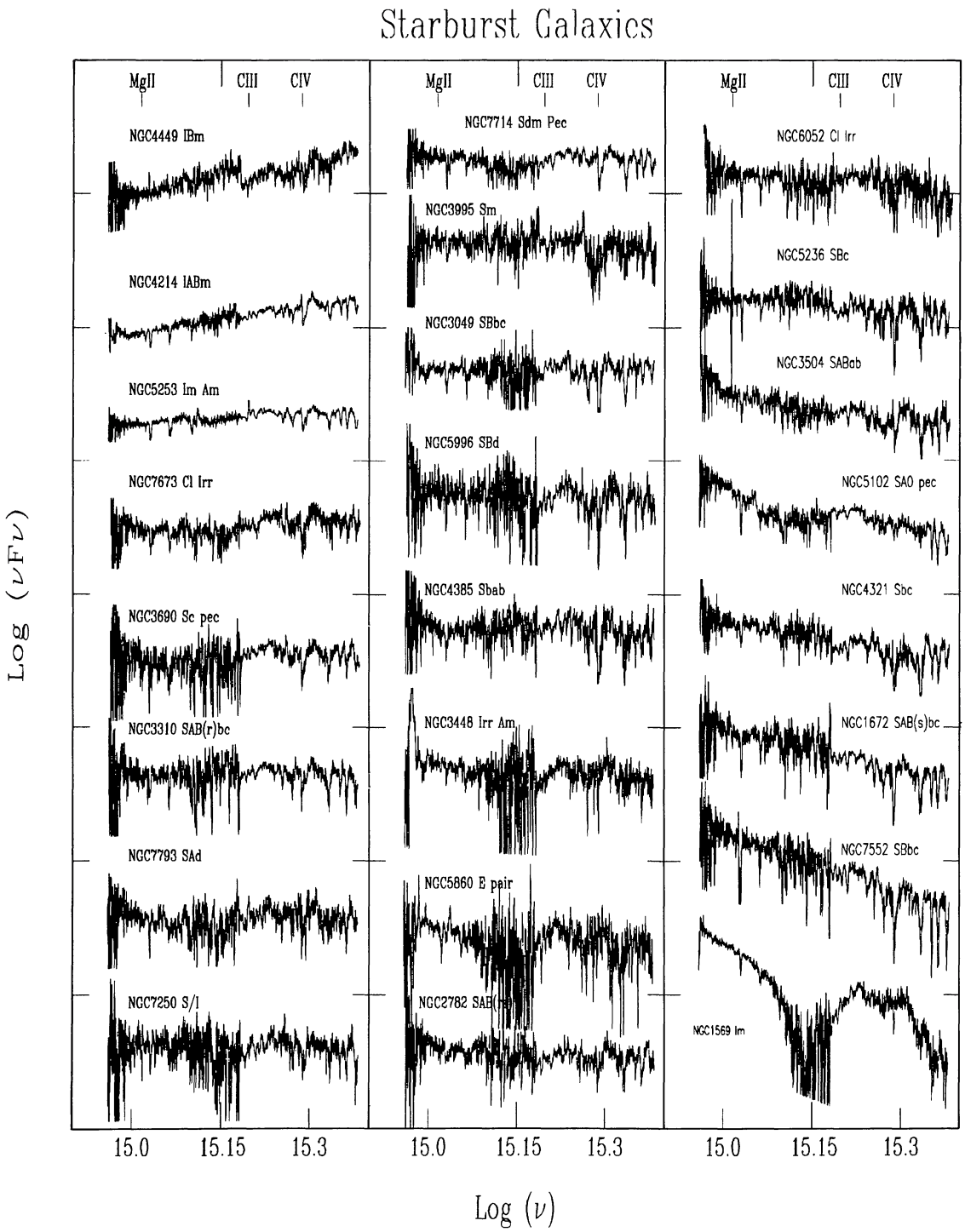


FIG. 2.—Spectral energy distribution of starburst galaxies, ordered by slope. The units of the ordinate are ergs $cm^{-2}$ $s^{-1}$, while the units of the abscissa are Hz.

A spectrum of approximately constant flux in $F_\lambda$ versus $\lambda$, i.e., with a slope of $\beta = 0$, has corresponding slopes of $F_\nu \propto \nu^{-2}$, and $\nu F_\nu \propto \nu^{-1}$. In discussions concerning slopes, "blue" is used as a relative term to refer to spectra that have strong flux at short UV wavelengths compared with the flux at long UV wavelengths. Likewise, "red" is used to refer to spectra that have weak flux at short UV wavelengths compared to the flux at long UV wavelengths. In this terminology, a UV slope of $\beta = 0$ ($\alpha = -2$) is redder than a slope of $\beta = -1$ ($\alpha = -1$).

## 3. DIGITAL DISTRIBUTION OF THE ATLAS

The atlas will be available to the astronomical community in digital form through several routes. The National Space

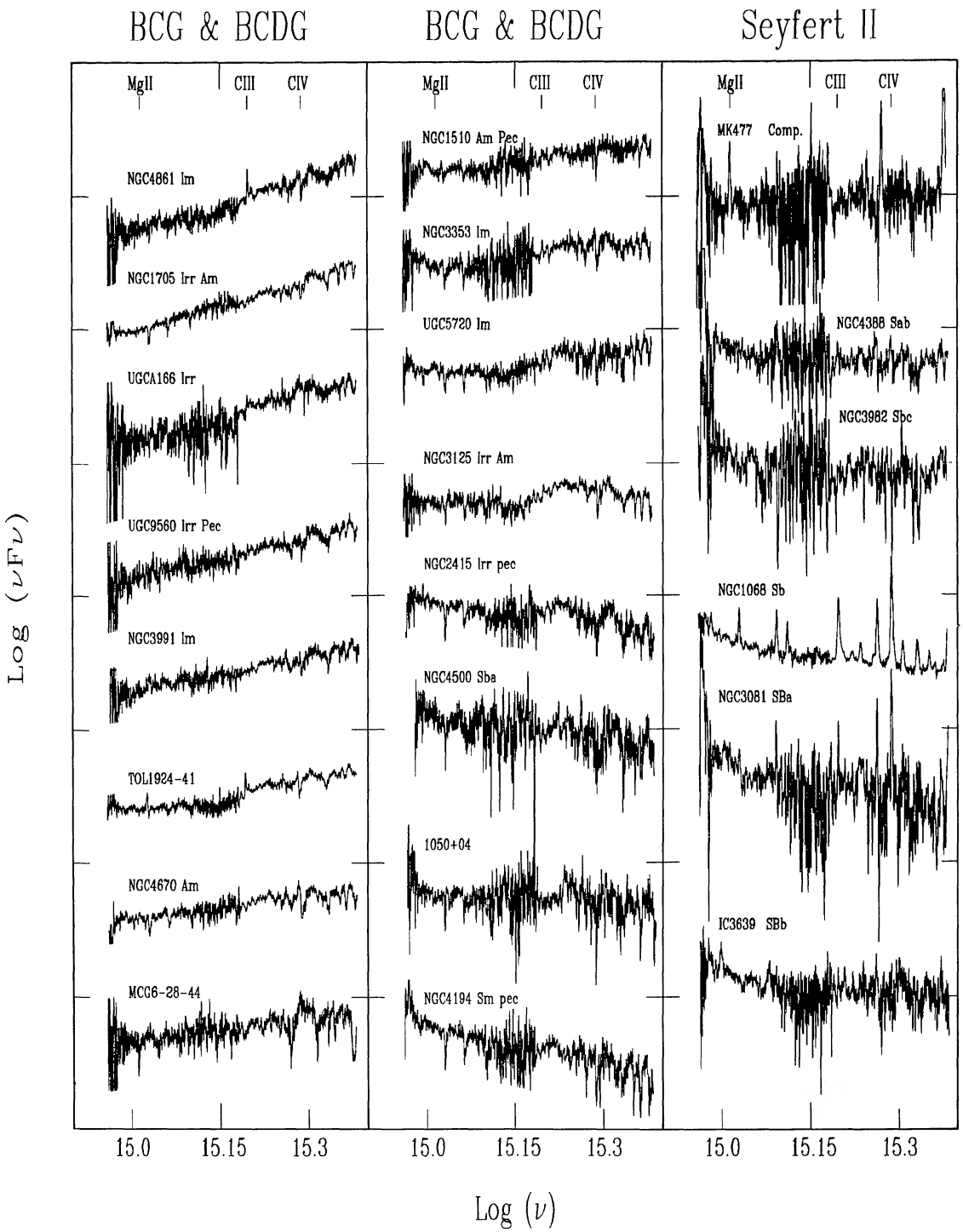


FIG. 3.—Spectral energy distribution of blue compact, blue compact dwarf, and Seyfert 2 galaxies, ordered by slope

Science Data Center (NSSDC) will contain the Atlas in their Astrophysics Data Catalogues (ADC). Requests can be directed to Requests, National Space Science Data Center, Code 933, Greenbelt, MD 20771. International requests can be directed to Requests, World Data Center A for Rockets and Satellites, Code 930.2, NASA/Goddard Space Flight Center, Greenbelt, MD 20771. Requests via electronic mail can be sent to the SPAN address NCF::Request or to the Internet address Request@nssdca.gsfc.nasa.gov. The tape format is the *IUE* format with character header and 16 bit integer data, except that the usual group of seven quantities (wavelength, data quality, gross, background, FN, $s^{-1}$, and flux) have been supplemented by an error array and an exposure time array. The fifth quantity is just FN on a standard *IUE* tape, and the correc-

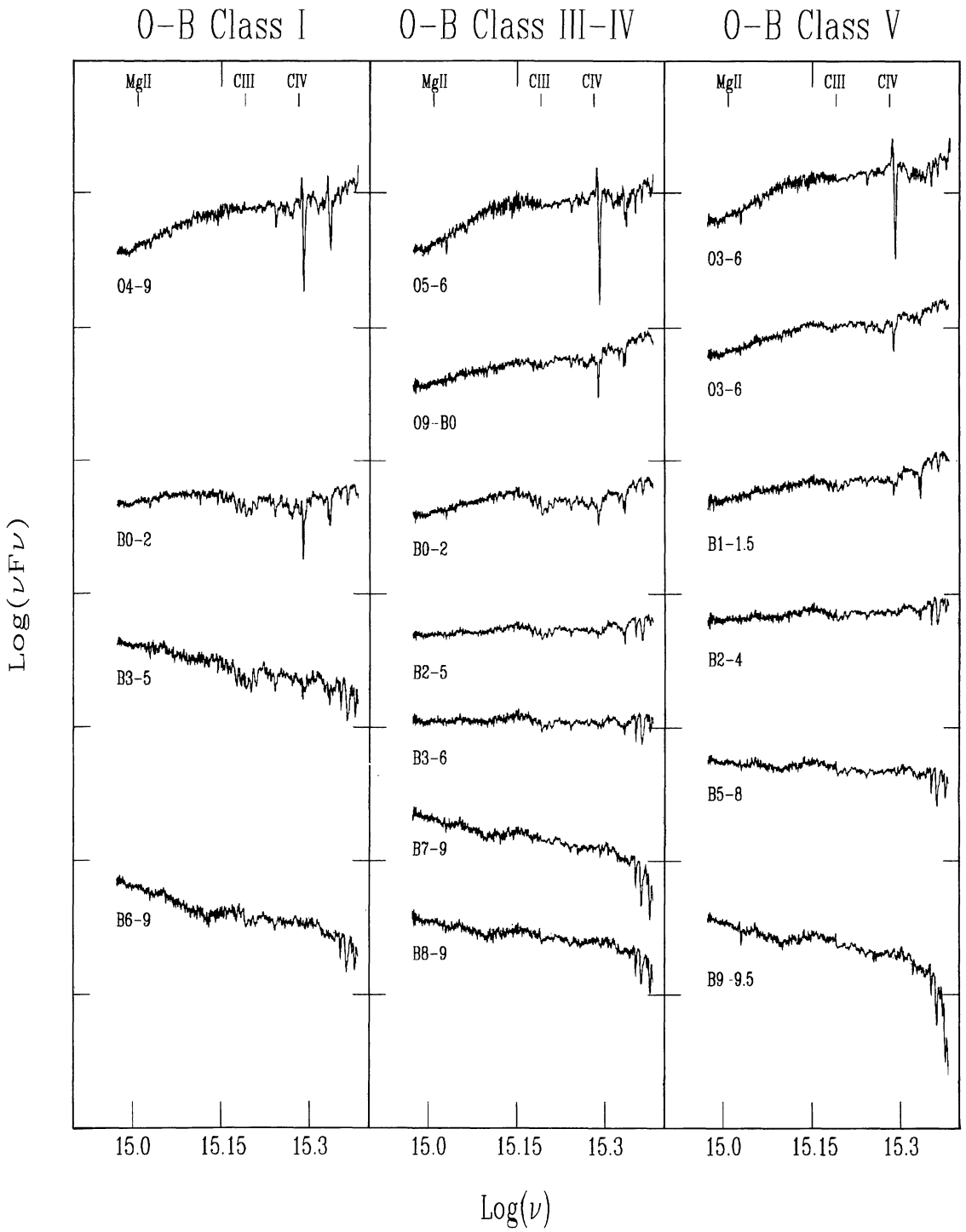


FIG. 4.—Spectral energy distribution of O and B stars from the Fanelli et al. (1992) atlas

tion for changing *IUE* sensitivity is applied to the flux array only. The on-line format is header and data, all in one ASCII file.

The atlas will also be available for a limited time via anonymous FTP at node stsci.edu (130.167.1.2). The data reside in the directory observer/catalogs/iue_galaxy_atlas. Eventually the atlas will be available via the Data Management Facility/ Data Archiving and Distribution System (DMF/DADS) at STScI. DMF/DADS does not now have the capability for on-line access to archived data but is expected to have such capability in the future.

## 4. DISCUSSION

### 4.1. *UV Absorption and Emission Signatures*

The absorption features in galaxy spectra can originate in the ISM of our Galaxy, in the ISM of the galaxy itself, or in the stellar atmospheres of stars contributing to the UV flux of the

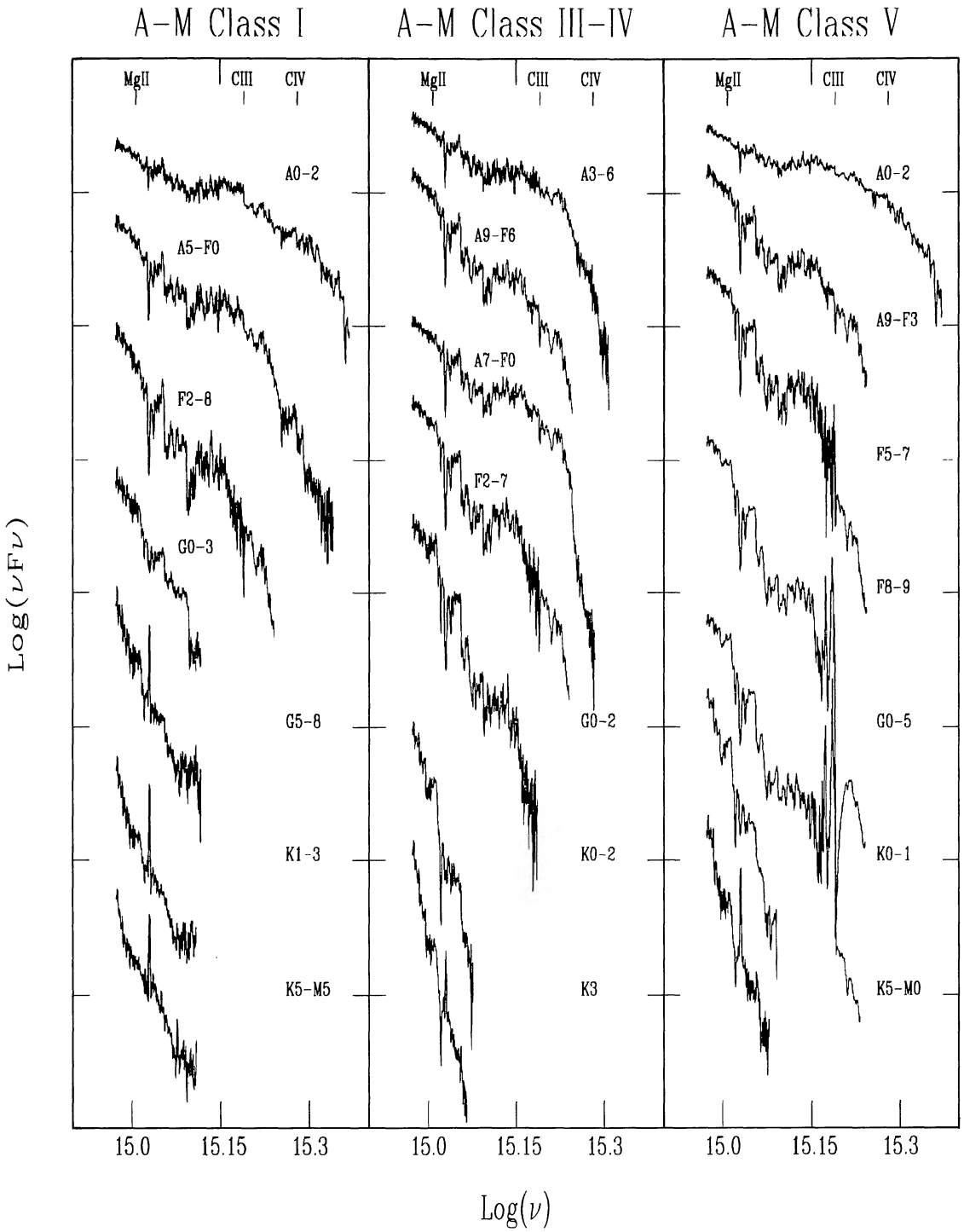


FIG. 5.—Spectral energy distribution of A–M stars from the Fanelli et al. (1992) atlas

galaxy. In addition to producing absorption lines, hot stars can produce emission lines and features with both emission and absorption (P Cygni profiles), and cool stars can produce absorption lines similar to those produced in the ISM. H II regions produce emission lines. Table 4 summarizes the equivalent widths of ISM absorption lines detected in several lines of sight through our Galaxy. Typical absorption lines, emission lines, and lines with P Cygni profile from early-type stars are summarized in Table 5. Typical absorption lines from late-type stars are summarized in Table 6. Typical emission lines from nebular regions are summarized in Table 7.

#### 4.1.1. *Interstellar Absorption Lines*

The diffuse medium associated with our own Galaxy absorbs both discrete and continuous radiation from external

TABLE 4

STRONGEST UV INTERSTELLAR ABSORPTION LINES

| λ (Å) | | | $W_\lambda$ (Å) | | |
|---|---|---|---|---|---|
| Average | Components | Ion | 3C 273 | SN 1987A | SN 1980K |
| 1192 | 1190.42, 1193.28 | Si II | 0.85 | ... | ... |
| 1200 | 1199.90 | N I | 0.85 | ... | ... |
| 1207 | 1206.51 | Si III | 0.50 | ... | ... |
| 1241 | 1238.81, 1242.80 | N V | 0.36 | ... | ... |
| 1252 | 1250.59, 1253.81 | S II | 0.35 | 0.39 | ... |
| 1260 | 1259.52, 1260.42 | Si II | 0.83 | >0.50 | ... |
| 1303 | 1302.08 | O I | 0.78 | >0.66 | ... |
| ... | 1304.40 | Si II | ... | ... | ... |
| 1335 | 1334.53 | C II | 0.75 | <1.64 | ... |
| ... | 1335.70 | C* II | ... | ... | ... |
| 1394 | 1393.76 | Si IV | 0.42 | 0.24 | ... |
| 1403 | 1402.77 | Si IV | 0.24 | 0.14 | ... |
| 1527 | 1526.72 | Si II | 0.51 | 0.58 | ... |
| 1549 | 1548.20, 1550.77 | C IV | 0.94 | 0.60 | ... |
| 1608 | 1608.45 | Fe II | 0.56 | 0.39 | ... |
| 1671 | 1670.91 | Al II | 0.54 | <0.60 | ... |
| 1855 | 1854.72 | Al III | 0.28 | 0.18 | ... |
| 1863 | 1862.78 | Al III | 0.18 | 0.10 | ... |
| 2344 | 2344.21 | Fe II | 0.73 | 0.75 | ... |
| 2374 | 2374.46 | Fe II | 0.61 | 0.53 | ... |
| 2383 | 2382.76 | Fe II | 0.83 | <0.96 | ... |
| 2577 | 2576.89 | Mn II | 0.34 | 0.22 | ... |
| 2586 | 2586.46 | Fe II | 0.80 | 0.73 | ... |
| 2594 | 2594.50 | Mn II | 0.28 | 0.20 | 1.6 |
| 2600 | 2600.18 | Fe II | 0.96 | 1.05 | 1.9 |
| 2796 | 2796.35 | Mg II | 1.13 | <1.27 | 3.7 |
| 2804 | 2803.53 | Mg II | 1.03 | <1.25 | 3.3 |
| 2853 | 2852.97 | Mg I | 0.39 | 0.53 | 1.6 |

NOTE.—Equivalent widths of the strongest UV interstellar lines in angstroms toward the quasar 3C 273 ($l = 290°$, $b = +64°$), SN 1987A in the LMC ($l = 280°$, $b = -33°$), and SN 1980K in NGC 6946 ($l = 96°$, $b = +12°$). See § 3.1 for references.

TABLE 5

MAIN DISCRETE FEATURES IN THE SPECTRA OF EARLY-TYPE STARS

| λ (Å) (1) | Ion (2) | O (3) | B (4) | WN (5) | WC (6) | References (7) |
|---|---|---|---|---|---|---|
| 1239, 1243 ..... | N V | p | ... | p | p | 1, 2 |
| 1255 ..... | Fe V | a | ... | ... | ... | 3 |
| 1300 ..... | Si III, Si II | a | a | ... | ... | 3 |
| 1333 ..... | Unidentified | a | ... | ... | ... | 3 |
| 1336 ..... | C II | ... | a | ... | ... | 3 |
| 1371 ..... | O V | a | ... | ... | ... | 3 |
| 1394, 1403 ..... | Si IV | p | p | p | p | 1, 2, 3 |
| 1428 ..... | C III | a | ... | e | e | 3 |
| 1453 ..... | Unidentified | a | ... | ... | ... | 3 |
| 1465 ..... | Unidentified | ... | a | ... | ... | 3 |
| 1486 ..... | N IV] | ... | ... | e | ... | 2 |
| 1548, 1551 ..... | C IV | p | a | p | e/p | 1, 2, 3 |
| 1600–1630 blend ..... | Fe III, Al III, N II | a | a | ... | ... | 1 |
| 1640 ..... | He II | a | ... | e/p | e/p | 1, 2 |
| 1719 ..... | N IV | p | a | p | e | 1, 2, 3 |
| 1907, 1909 ..... | C III] | ... | ... | ... | e | 2 |
| 2009, 2010 ..... | C III | ... | ... | ... | e | 2 |
| 2297 ..... | C III | ... | ... | ... | e | 2 |
| 2385 ..... | He II | ... | ... | e | e | 2 |
| 2511 ..... | He II | ... | ... | e | e | 2 |
| 2530 ..... | C IV | ... | ... | ... | e | 2 |
| 2733 ..... | He II | ... | ... | e | e | 2 |
| 2906 ..... | C IV | ... | ... | ... | e | 2 |

NOTE.—In cols. (3)–(6), a = absorption ($W_{eq} > 0$); e = emission ($W_{eq} < 0$); p = P Cygni profile ($W_{eq} \approx 0$).
REFERENCES.—(1) Panek & Savage 1976; (2) Nussbaumer et al. 1982; (3) Heck et al. 1984.

TABLE 6

MAIN DISCRETE FEATURES IN SPECTRA OF MID- TO LATE-TYPE STARS

| λ (Å) (1) | Ion (2) | A (3) | F (4) | G (5) | K (6) | References (7) |
|---|---|---|---|---|---|---|
| 1671 ..... | Al II | a | ... | ... | ... | 1 |
| 1855, 1863 ..... | Al III | a | ... | ... | ... | 1 |
| 2400 ..... | Fe II | ... | a | a | ... | 2 |
| 2600 ..... | Fe II | ... | a | a | ... | 2 |
| 2800 ..... | Mg II | ... | a | a | ... | 2 |
| 2852 ..... | Mg I | ... | ... | ... | a | 2 |
| 3000 ..... | Fe I | ... | ... | ... | a | 2 |

NOTE.—In cols. (3)–(6), a = absorption ($W_{eq} > 0$).

REFERENCES.—(1) Fanelli et al. 1987; (2) Fanelli et al. 1990.

galaxies. The dust component is responsible for the continuum absorption, which *reddens* the original spectrum. Allowance for this effect in the estimation of the true spectral slopes is discussed in § 2.2 and demonstrated in Figure 7. In addition, the interstellar gas is responsible for absorption at discrete wavelengths, both in the disk and in the halo of our Galaxy.

In general, interstellar (IS) absorption lines are narrow. In fact, with the exception of the Ly$\alpha$ line, their intrinsic width is much narrower than the *IUE* resolution in the low-dispersion mode ($\sim$1000 km s$^{-1}$). Therefore, only the strongest IS lines appear in the low-resolution spectra in this atlas. For example, if a full width at half-maximum of 7 Å is adopted for the SW camera, an absorption line with an intrinsic equivalent width of 0.5 Å will appear as a weak feature with a trough minimum of $\sim$7% of the continuum level. Such faint lines can be detected only in *IUE* spectra with much higher signal-to-noise ratios than those presented here.

Rather than resorting to theoretical models to estimate the lines and line strengths expected in the spectrum of extragalactic objects, Table 4 presents a compilation of the strongest IS absorption lines detected in the spectra of 3C 273 and SN 1987A, which are among the brightest extragalactic background sources.

For 3C 273 we have combined the results obtained with the *Hubble Space Telescope* (observed with the Faint Object Spectrograph [FOS] at a resolution of 1300 in the interval 1150–3300 Å, with a gap from 1600 to 1650 Å, by Bahcall et al. 1991; observed with the Goddard High Resolution Spectrograph (GHRS) at a resolution of 1500 in the interval 1175–1452 Å, and at a resolution of 15,000 in the intervals 1522–1556, 1775–1813, 2572–2617, and 2777–2821 Å by Morris et al. 1991) with the results obtained with *IUE* by co-adding 10 spectra taken with the SWP camera (1200–2000 Å) in the high-resolution mode (Burks et al. 1991).

The IS line intensities for the line of sight to SN 1987A are taken from the *IUE* high-dispersion observations of Blades et al. (1988a), including all components with velocities up to 80 km s$^{-1}$, which Blades et al. (1988b) have shown to be of Galactic origin.

The two lines of sight probe different parts of the disk, since their Galactic latitudes differ by 97° ($b_{3C\,273}$ = 64°, $b_{LMC}$ = −33°). The absorptions from both the low- and the high-ionization ions are stronger toward 3C 273 than toward the LMC, suggesting that there is a sizable asymmetry in the large-scale distribution of the absorbing gas relative to our Galactic plane. However, the equivalent widths of the few IS lines detected in the spectrum of SN 1980K in NGC 6946 ($b$ = 126°; Pettini et al. 1982) are about a factor of 3.4 higher than those toward 3C 273, i.e., approximately the ratio of their respective cosecant values (sin 64°/sin 12° = 4.3).

TABLE 7

MAIN EMISSION LINES FROM NEBULAR OBJECTS

| WAVELENGTH (Å) | ION | H II REGIONS | PNs | CRAB | SNR | | |
|---|---|---|---|---|---|---|---|
| | | | | | O-rich | N-rich | Cygnus Loop |
| 1239, 1243 ..... | N V | | x | | | | x |
| 1335, 1336 ..... | C II | | x | | | | x |
| 1394, 1403 ..... | Si IV | | x | | | | x |
| 1397–1407 ..... | O IV] | | x | | x | | x |
| 1483, 1487 ..... | N IV] | | x | | | x | x |
| 1548, 1550 ..... | C IV | | x | x | x | | x |
| 1640 ..... | He II | | x | x | | | x |
| 1658–1666 ..... | O III] | x | x | | x | | x |
| 1747–1754 ..... | N III] | x | x | | | x | x |
| 1882, 1892 ..... | Si III] | x | x | | | | x |
| 1907, 1909 ..... | C III] | x | x | x | | | x |
| 2325–2329 ..... | C II] | x | x | | x | | x |
| 2423, 2425 ..... | [Ne IV] | | x | | x | | x |
| 2470 ..... | [O II] | x | x | | | | x |
| 2733 ..... | He II | | x | | | | |
| 2796, 2803 ..... | Mg II | x | x | | x | | |
| 2837, 2838 ..... | C II | | x | | | | |
| 2837 ..... | O III | | x | | | | |
| 3023 ..... | O III | | x | | | | |
| 3043, 3047 ..... | O III | | x | | | | |
| 3133 ..... | O III | | x | | | | |

TABLE 8

OBSERVED FLUXES IN 100 Å BINS[a]

| Galaxy | Radius[b] | 1432-1532Å | 1863-1963Å | 2323-2423Å | 2650-2750Å |
|---|---|---|---|---|---|
| NGC224 | 80′00″ | 0.83 ± 0.14 | 0.61 ± 0.07 | 0.45 ± 0.17 | 1.09 ± 0.14 |
| IC1586 | | 0.59 ± 0.14 | 0.48 ± 0.05 | ... | ... |
| NGC262 | 33″ | 0.19 ± 0.13 | 0.23 ± 0.09 | ... | ... |
| HARO15 | 27″ | 2.11 ± 0.32 | 1.32 ± 0.11 | ... | ... |
| ESO296-11 | | 0.58 ± 0.22 | 0.28 ± 0.18 | 0.39 ± 0.21 | 0.33 ± 0.10 |
| MRK357 | | 1.36 ± 0.27 | 1.01 ± 0.07 | ... | ... |
| NGC598 | 35′24″ | 1.12 ± 0.17 | 0.88 ± 0.08 | 0.76 ± 0.15 | 0.91 ± 0.06 |
| IC214 | | 0.69 ± 0.21 | 0.44 ± 0.09 | ... | ... |
| NGC1023 | 4′33″ | ... | ... | 0.13 ± 0.10 | 0.29 ± 0.08 |
| NGC1068 | 3′33″ | 6.64 ± 1.06 | 7.53 ± 3.00 | 5.51 ± 1.54 | 4.79 ± 0.20 |
| NGC1097 | 24″ | 2.03 ± 0.38 | 1.89 ± 0.31 | 1.65 ± 0.21 | 1.75 ± 0.12 |
| NGC1140 | 51″ | 4.91 ± 0.51 | 3.02 ± 0.18 | ... | ... |
| NGC1313 | 4′33″ | 0.82 ± 0.17 | 0.53 ± 0.10 | 0.55 ± 0.13 | 0.57 ± 0.05 |
| NGC1433 | 3′15″ | 0.59 ± 0.23 | 0.42 ± 0.10 | 0.38 ± 0.14 | 0.40 ± 0.05 |
| NGC1510 | 39″ | 2.51 ± 0.23 | 1.60 ± 0.15 | 1.03 ± 0.13 | 0.95 ± 0.05 |
| NGC1553 | 2′15″ | 0.19 ± 0.13 | 0.15 ± 0.08 | 0.15 ± 0.11 | 0.40 ± 0.08 |
| NGC1569 | 1′48″ | 1.17 ± 0.16 | 0.81 ± 0.12 | 0.69 ± 0.13 | 1.33 ± 0.07 |
| NGC1614 | 39″ | 0.56 ± 0.22 | 0.43 ± 0.08 | ... | ... |
| NGC1672 | 3′18″ | 3.01 ± 0.31 | 2.77 ± 0.18 | 2.85 ± 0.67 | 2.90 ± 0.24 |
| NGC1667 | 54″ | 0.30 ± 0.18 | 0.26 ± 0.09 | ... | ... |
| NGC1705 | 57″ | 16.84 ± 1.49 | 8.46 ± 0.50 | 5.43 ± 0.42 | 4.08 ± 0.15 |
| NGC1800 | 60″ | 1.62 ± 0.49 | 0.94 ± 0.14 | ... | ... |
| UGC3838 | 24″ | 0.97 ± 0.20 | 0.62 ± 0.12 | 0.40 ± 0.21 | 0.39 ± 0.10 |
| IC2184 | | 0.63 ± 0.33 | 0.40 ± 0.12 | 0.35 ± 0.21 | 0.41 ± 0.10 |
| NGC2403 | 10′57″ | 0.44 ± 0.23 | 0.26 ± 0.07 | 0.19 ± 0.10 | 0.24 ± 0.05 |
| NGC2415 | 27″ | 2.50 ± 0.35 | 1.95 ± 0.26 | 1.44 ± 0.18 | 1.56 ± 0.08 |
| NGC2537 | 51″ | 0.91 ± 0.20 | 0.57 ± 0.08 | ... | ... |
| HolmbergII | 3′57″ | 1.56 ± 0.33 | 0.90 ± 0.17 | ... | ... |
| UGC4483 | 33″ | 0.71 ± 0.10 | 0.39 ± 0.07 | ... | ... |
| NGC2639 | 54″ | ... | ... | 0.13 ± 0.07 | 0.17 ± 0.04 |
| NGC2681 | 1′48″ | 0.36 ± 0.20 | 0.29 ± 0.07 | 0.32 ± 0.17 | 0.72 ± 0.08 |
| NGC2782 | 1′45″ | 2.24 ± 0.33 | 1.47 ± 0.16 | 1.40 ± 0.34 | 1.28 ± 0.10 |
| MCG10-13-71 | | 0.97 ± 0.18 | 0.64 ± 0.09 | ... | ... |
| NGC2798 | 1′18″ | 0.57 ± 0.21 | 0.51 ± 0.09 | ... | ... |
| NGC2820A | 15″ | 0.67 ± 0.18 | 0.45 ± 0.10 | 0.20 ± 0.10 | 0.15 ± 0.05 |
| NGC2841 | 4′03″ | 0.69 ± 0.27 | 0.39 ± 0.17 | 0.27 ± 0.17 | 0.42 ± 0.07 |
| NGC2903 | 6′18″ | 1.74 ± 0.29 | 1.81 ± 0.20 | 1.77 ± 0.28 | 2.25 ± 0.18 |
| IZW18 | | 1.55 ± 0.17 | 0.86 ± 0.10 | 0.46 ± 0.13 | 0.38 ± 0.06 |
| NGC2997 | 4′27″ | 0.59 ± 0.24 | 0.52 ± 0.10 | 0.63 ± 0.20 | 0.62 ± 0.08 |
| NGC3031 | 1327″ | 0.37 ± 0.23 | 0.35 ± 0.21 | 0.38 ± 0.27 | 0.56 ± 0.07 |
| NGC3049 | 1′06″ | 1.39 ± 0.19 | 1.00 ± 0.12 | 0.78 ± 0.15 | 0.73 ± 0.04 |
| NGC3081 | 1′03″ | 0.33 ± 0.19 | 0.31 ± 0.16 | 0.23 ± 0.10 | 0.22 ± 0.03 |
| NGC3077 | 2′42″ | 0.93 ± 0.29 | 0.60 ± 0.11 | ... | ... |
| UGC5408 | 15″ | 1.20 ± 0.28 | 0.75 ± 0.09 | ... | ... |
| NGC3125 | 33″ | 2.76 ± 0.29 | 1.89 ± 0.19 | 1.30 ± 0.17 | 1.20 ± 0.10 |
| NGC3256 | 1′54″ | 1.32 ± 0.25 | 1.29 ± 0.12 | ... | ... |
| UGC5720 | 30″ | 4.42 ± 0.59 | 2.95 ± 0.35 | 1.85 ± 0.17 | 1.74 ± 0.07 |
| NGC3310 | 1′33″ | 10.18 ± 1.29 | 7.45 ± 0.53 | 4.84 ± 1.62 | 5.07 ± 0.45 |
| NGC3351 | 3′42″ | 1.96 ± 0.40 | 2.03 ± 0.19 | 2.09 ± 0.33 | 2.23 ± 0.18 |
| NGC3353 | 39″ | 3.92 ± 0.46 | 2.47 ± 0.25 | 1.48 ± 0.37 | 1.40 ± 0.12 |
| NGC3393 | 1′06″ | 0.23 ± 0.15 | 0.30 ± 0.23 | 0.20 ± 0.12 | 0.21 ± 0.04 |
| MCG9-18-32 | 24″ | 3.23 ± 0.41 | 1.82 ± 0.18 | ... | ... |
| NGC3395 | 1′03″ | 1.34 ± 0.24 | 0.88 ± 0.13 | ... | ... |
| NGC3396 | 1′33″ | 0.49 ± 0.19 | 0.35 ± 0.09 | ... | ... |
| NGC3432 | 3′24″ | 0.78 ± 0.22 | 0.51 ± 0.09 | ... | ... |
| 1050+04 | 15″ | 0.93 ± 0.19 | 0.65 ± 0.10 | 0.53 ± 0.11 | 0.51 ± 0.06 |
| NGC3448 | 2′48″ | 1.03 ± 0.16 | 0.66 ± 0.09 | 0.57 ± 0.14 | 0.58 ± 0.05 |
| NGC3504 | 1′21″ | 2.75 ± 0.40 | 2.15 ± 0.18 | 1.86 ± 0.32 | 2.00 ± 0.18 |
| MRK36 | 9″ | 1.50 ± 0.31 | 0.93 ± 0.12 | ... | ... |
| NGC3622 | 36″ | 1.02 ± 0.46 | 0.63 ± 0.19 | 0.54 ± 0.34 | 0.59 ± 0.13 |
| NGC3660 | 1′21″ | 0.32 ± 0.21 | 0.24 ± 0.08 | 0.18 ± 0.07 | 0.23 ± 0.03 |
| UGC6448 | 30″ | 0.51 ± 0.22 | 0.28 ± 0.09 | ... | ... |
| UGC6456 | 42″ | 0.85 ± 0.27 | 0.62 ± 0.11 | ... | ... |
| NGC3682 | 51″ | 0.66 ± 0.38 | 0.57 ± 0.15 | 0.71 ± 0.39 | 0.62 ± 0.17 |
| NGC3690 | | 2.33 ± 0.27 | 1.68 ± 0.15 | 1.08 ± 0.31 | 1.02 ± 0.15 |
| NGC3738 | 1′15″ | 4.02 ± 0.46 | 2.37 ± 0.24 | 1.54 ± 0.21 | 1.32 ± 0.07 |
| NGC3758 | 15″ | 0.17 ± 0.15 | 0.36 ± 0.20 | 0.15 ± 0.09 | 0.23 ± 0.04 |
| MCG-1-30-33 | 45″ | 0.75 ± 0.17 | 0.53 ± 0.10 | ... | ... |
| NGC3982 | 1′09″ | 0.72 ± 0.21 | 0.51 ± 0.11 | 0.46 ± 0.28 | 0.50 ± 0.10 |
| NGC3991 | | 5.22 ± 0.47 | 3.00 ± 0.19 | 2.07 ± 0.26 | 1.71 ± 0.16 |
| NGC3994 | 30″ | 0.96 ± 0.22 | 0.97 ± 0.12 | 0.50 ± 0.10 | 0.52 ± 0.06 |
| NGC3995 | 1′24″ | 1.07 ± 0.21 | 0.90 ± 0.17 | 0.69 ± 0.11 | 0.65 ± 0.07 |
| ESO572-34 | 30″ | 2.22 ± 0.26 | 1.17 ± 0.12 | ... | ... |
| NGC4102 | 1′30″ | ... | ... | 0.12 ± 0.11 | 0.21 ± 0.04 |
| NGC4111 | 1′18″ | 0.15 ± 0.10 | 0.13 ± 0.05 | 0.15 ± 0.07 | 0.39 ± 0.05 |
| NGC4194 | 54″ | 1.58 ± 0.32 | 1.46 ± 0.16 | 1.24 ± 0.26 | 1.43 ± 0.10 |
| NGC4214 | 4′15″ | 10.34 ± 0.93 | 6.34 ± 0.39 | 4.34 ± 0.34 | 3.55 ± 0.12 |
| NGC4258 | 9′18″ | 2.28 ± 0.33 | 1.79 ± 0.20 | 1.16 ± 0.25 | 1.45 ± 0.13 |
| NGC4314 | 2′06″ | 0.96 ± 0.63 | 0.56 ± 0.31 | 0.76 ± 0.18 | 0.69 ± 0.07 |
| NGC4321 | 3′42″ | 1.91 ± 0.27 | 1.66 ± 0.11 | 1.72 ± 0.29 | 1.80 ± 0.12 |
| NGC4350 | 1′30″ | ... | ... | 0.13 ± 0.07 | 0.22 ± 0.03 |
| NGC4382 | 3′33″ | 0.17 ± 0.12 | 0.12 ± 0.07 | 0.28 ± 0.15 | 0.57 ± 0.10 |
| NGC4385 | 6″ | 1.56 ± 0.36 | 1.17 ± 0.11 | 0.85 ± 0.22 | 0.81 ± 0.08 |
| NGC4388 | 2′48″ | 0.62 ± 0.14 | 0.46 ± 0.09 | 0.46 ± 0.19 | 0.37 ± 0.05 |
| MCG8-23-35 | 24″ | 2.14 ± 0.25 | 1.44 ± 0.45 | ... | ... |
| NGC4449 | 3′06″ | 13.14 ± 2.14 | 7.09 ± 0.76 | 5.81 ± 0.91 | 4.46 ± 0.37 |
| NGC4500 | 48″ | 0.99 ± 0.28 | 0.79 ± 0.12 | 0.70 ± 0.23 | 0.70 ± 0.09 |
| NGC4569 | 4′45″ | ... | ... | 1.18 ± 0.21 | 1.41 ± 0.15 |
| NGC4579 | 2′57″ | 0.29 ± 0.11 | 0.33 ± 0.13 | 0.27 ± 0.08 | 0.35 ± 0.02 |
| NGC4594 | 4′21″ | 0.46 ± 0.27 | 0.28 ± 0.09 | 0.26 ± 0.15 | 0.49 ± 0.08 |
| IC3639 | 36″ | 1.06 ± 0.25 | 0.75 ± 0.14 | 0.56 ± 0.11 | 0.62 ± 0.05 |
| UGC7905S | 36″ | 1.51 ± 0.19 | 0.87 ± 0.08 | ... | ... |
| NGC4670 | 42″ | 6.39 ± 0.62 | 4.09 ± 0.29 | 2.81 ± 0.25 | 2.37 ± 0.12 |
| NGC4736 | 5′36″ | 0.98 ± 0.23 | 1.26 ± 0.17 | 1.13 ± 0.23 | 2.20 ± 0.24 |
| NGC4748 | | 1.01 ± 0.28 | 0.92 ± 0.25 | 0.54 ± 0.16 | 0.54 ± 0.05 |
| NGC4826 | 5′00″ | 0.41 ± 0.24 | 0.38 ± 0.18 | 0.51 ± 0.18 | 0.69 ± 0.07 |
| MCG6-28-44 | | 2.01 ± 0.36 | 1.13 ± 0.15 | 0.80 ± 0.14 | 0.71 ± 0.06 |
| NGC4853 | 24″ | 0.19 ± 0.12 | 0.18 ± 0.10 | 0.23 ± 0.10 | 0.25 ± 0.03 |
| NGC4861 | 2′00″ | 9.92 ± 0.98 | 5.47 ± 0.86 | 2.89 ± 0.37 | 2.45 ± 0.19 |
| IC3961 | 2′00″ | 8.85 ± 0.85 | 5.04 ± 0.67 | 3.34 ± 0.32 | 2.56 ± 0.20 |
| NGC5005 | 2′54″ | 0.32 ± 0.20 | 0.22 ± 0.12 | 0.28 ± 0.21 | 0.43 ± 0.07 |
| UGC8315N | | 0.44 ± 0.18 | 0.30 ± 0.07 | ... | ... |
| NGC5102 | 4′21″ | 2.47 ± 0.21 | 2.41 ± 0.12 | 1.55 ± 0.25 | 2.12 ± 0.19 |
| NGC5135 | 1′18″ | 0.96 ± 0.27 | 1.03 ± 0.17 | 0.80 ± 0.45 | 1.09 ± 0.24 |
| MRK66 | 12″ | 1.09 ± 0.18 | 0.61 ± 0.07 | ... | ... |
| NGC5194 | 5′36″ | 0.64 ± 0.24 | 0.64 ± 0.21 | 0.59 ± 0.22 | 0.73 ± 0.10 |
| MRK789 | 12″ | 0.35 ± 0.20 | 0.38 ± 0.07 | ... | ... |
| NGC5236 | 6′27″ | 23.43 ± 3.97 | 17.09 ± 1.22 | 16.43 ± 2.60 | 15.22 ± 1.24 |
| ESO383-44 | 42″ | 0.84 ± 0.30 | 0.67 ± 0.24 | 0.48 ± 0.14 | 0.44 ± 0.06 |
| NGC5256 | | 0.44 ± 0.20 | 0.36 ± 0.19 | 0.32 ± 0.14 | 0.29 ± 0.04 |
| NGC5253 | 2′30″ | 14.11 ± 1.10 | 10.58 ± 1.19 | 7.41 ± 0.77 | 6.54 ± 0.23 |
| 1350-00 | | 0.39 ± 0.20 | 0.19 ± 0.09 | ... | ... |
| UGC8850 | | 0.50 ± 0.21 | 0.47 ± 0.14 | 0.39 ± 0.08 | 0.32 ± 0.06 |
| NGC5457 | 14′24″ | 1.03 ± 0.21 | 0.75 ± 0.10 | ... | ... |
| NGC5506 | 1′24″ | 0.26 ± 0.19 | 0.17 ± 0.12 | 0.15 ± 0.11 | 0.13 ± 0.07 |
| IC4395 | 30″ | 0.41 ± 0.20 | 0.38 ± 0.07 | ... | ... |
| NGC5643 | 2′18″ | 0.28 ± 0.21 | 0.19 ± 0.18 | 0.12 ± 0.10 | 0.18 ± 0.03 |
| NGC5674 | 33″ | 0.32 ± 0.20 | 0.38 ± 0.31 | 0.24 ± 0.19 | 0.21 ± 0.08 |
| MRK477 | | 0.67 ± 0.18 | 0.56 ± 0.25 | 0.36 ± 0.12 | 0.33 ± 0.05 |
| NGC5728 | 1′33″ | 0.36 ± 0.18 | 0.28 ± 0.09 | 0.21 ± 0.11 | 0.27 ± 0.03 |
| UGC9560 | 21″ | 3.16 ± 0.31 | 1.78 ± 0.14 | 1.13 ± 0.16 | 0.91 ± 0.13 |
| NGC5860 | | 0.74 ± 0.21 | 0.50 ± 0.11 | 0.37 ± 0.11 | 0.46 ± 0.08 |
| UGCA410 | 9″ | 1.18 ± 0.35 | 0.76 ± 0.15 | ... | ... |
| NGC5996 | 51″ | 1.57 ± 0.35 | 1.01 ± 0.14 | 0.93 ± 0.25 | 0.86 ± 0.14 |
| NGC6052 | | 1.31 ± 0.28 | 1.08 ± 0.13 | 0.83 ± 0.16 | 0.83 ± 0.05 |
| NGC6090 | | 1.07 ± 0.34 | 0.87 ± 0.11 | ... | ... |
| NGC6217 | 1′30″ | 1.74 ± 0.21 | 1.55 ± 0.15 | ... | ... |
| MRK499 | 6″ | 1.06 ± 0.16 | 0.72 ± 0.07 | ... | ... |
| NGC6221 | 1′45″ | 0.25 ± 0.19 | 0.19 ± 0.08 | 0.21 ± 0.16 | 0.36 ± 0.09 |
| NGC6764 | 1′09″ | 0.45 ± 0.16 | 0.46 ± 0.07 | 0.49 ± 0.31 | 0.49 ± 0.12 |
| TOL1924-41 | 24″ | 3.81 ± 0.25 | 2.25 ± 0.33 | 1.41 ± 0.11 | 1.19 ± 0.05 |
| 1941-543 | 12″ | 0.92 ± 0.18 | 0.53 ± 0.07 | ... | ... |
| NGC7130 | 45″ | 0.86 ± 0.37 | 0.70 ± 0.19 | 0.67 ± 0.31 | 0.74 ± 0.15 |
| NGC7250 | 51″ | 1.27 ± 0.18 | 0.90 ± 0.13 | 0.76 ± 0.22 | 0.70 ± 0.10 |
| MRK309 | 15″ | 0.28 ± 0.20 | 0.31 ± 0.06 | ... | ... |
| NGC7496 | 45″ | 1.43 ± 0.21 | 1.06 ± 0.08 | 1.00 ± 0.14 | 0.87 ± 0.05 |
| NGC7552 | 1′42″ | 1.72 ± 0.28 | 1.91 ± 0.19 | 1.94 ± 0.56 | 2.32 ± 0.23 |
| NGC7582 | 2′30″ | 0.15 ± 0.10 | 0.22 ± 0.08 | 0.20 ± 0.12 | 0.29 ± 0.04 |
| NGC7590 | 1′21″ | 0.41 ± 0.19 | 0.42 ± 0.11 | 0.30 ± 0.13 | 0.30 ± 0.05 |
| NGC7673 | 39″ | 2.29 ± 0.37 | 1.52 ± 0.11 | 1.03 ± 0.16 | 1.00 ± 0.07 |
| NGC7714 | 57″ | 3.70 ± 0.41 | 2.55 ± 0.26 | 1.88 ± 0.27 | 2.00 ± 0.13 |
| MRK542 | 6″ | 0.72 ± 0.25 | 0.44 ± 0.10 | ... | ... |
| NGC7793 | 4′39″ | 1.31 ± 0.26 | 0.90 ± 0.14 | 0.58 ± 0.16 | 0.61 ± 0.09 |

[a] Fluxes are in units of $10^{-14}$ ergs cm$^{-2}$ s$^{-1}$ Å$^{-1}$.

[b] Radius is half the largest diameter for galaxy as given in NED.

TABLE 9

REDDENING-FREE SPECTRAL INDICES[a] LISTED BY ACTIVITY TYPE

| Galaxy | $\beta \pm \delta\beta$ | $\log(F_o) \pm \delta \log(F_o)$ |
|---|---|---|
| NORMAL | -0.82 ± 0.89 | |
| NGC224 | -1.26 ± 0.18 | -15.12 ± 0.13 |
| NGC598 | -0.82 ± 0.13 | -14.64 ± 0.10 |
| NGC1433 | -0.95 ± 0.28 | -15.04 ± 0.21 |
| NGC1553 | -0.58 ± 0.50 | -15.22 ± 0.36 |
| NGC2403 | -1.21 ± 0.35 | -15.46 ± 0.26 |
| NGC3682 | 0.14 ± 0.42 | -14.12 ± 0.30 |
| NGC4382 | 1.04 ± 0.47 | -14.00 ± 0.33 |
| LINER | 0.06 ± 0.93 | |
| NGC2681 | 0.17 ± 0.40 | -14.41 ± 0.29 |
| NGC2841 | -1.98 ± 0.37 | -15.81 ± 0.28 |
| NGC3031 | 0.07 ± 0.48 | -14.38 ± 0.35 |
| NGC3994 | -1.31 ± 0.16 | -15.00 ± 0.11 |
| NGC4111 | 0.20 ± 0.42 | -14.71 ± 0.30 |
| NGC4258 | -1.29 ± 0.14 | -14.70 ± 0.10 |
| NGC4314 | -0.07 ± 0.35 | -14.18 ± 0.23 |
| NGC4579 | 0.06 ± 0.28 | -14.49 ± 0.20 |
| NGC4594 | -1.23 ± 0.44 | -15.41 ± 0.32 |
| NGC4736 | 0.27 ± 0.17 | -13.74 ± 0.12 |
| NGC4826 | 0.79 ± 0.36 | -13.81 ± 0.24 |
| NGC5005 | -0.41 ± 0.49 | -14.88 ± 0.36 |
| NGC5194 | 0.08 ± 0.31 | -14.15 ± 0.23 |
| STARBURST | -1.25 ± 0.45 | |
| NGC1569 | -1.17 ± 0.13 | -14.91 ± 0.10 |
| NGC2782 | -1.25 ± 0.14 | -14.70 ± 0.10 |
| NGC3049 | -1.25 ± 0.11 | -14.89 ± 0.08 |
| NGC3310 | -1.35 ± 0.13 | -14.10 ± 0.10 |
| NGC3448 | -1.40 ± 0.15 | -15.16 ± 0.11 |
| NGC3504 | -0.93 ± 0.11 | -14.33 ± 0.08 |
| NGC3690 | -1.31 ± 0.11 | -14.71 ± 0.08 |
| NGC4214 | -1.85 ± 0.06 | -14.52 ± 0.05 |
| NGC4385 | -1.28 ± 0.16 | -14.85 ± 0.12 |
| NGC5102 | -0.57 ± 0.08 | -14.05 ± 0.06 |
| NGC5236 | -0.77 ± 0.13 | -13.30 ± 0.09 |
| ESO383-44 | -1.22 ± 0.27 | -15.06 ± 0.20 |
| NGC5253 | -1.32 ± 0.07 | -13.94 ± 0.06 |
| NGC5860 | -1.20 ± 0.26 | -15.13 ± 0.19 |
| NGC5996 | -1.52 ± 0.18 | -15.06 ± 0.13 |
| NGC6052 | -1.02 ± 0.16 | -14.70 ± 0.11 |
| NGC7250 | -1.28 ± 0.14 | -14.95 ± 0.11 |
| NGC7552 | 0.26 ± 0.14 | -13.54 ± 0.11 |
| NGC7714 | -1.49 ± 0.08 | -14.66 ± 0.06 |
| BCDG, BCG, HII | -1.75 ± 0.63 | |
| NGC1313 | -0.90 ± 0.17 | -14.87 ± 0.12 |
| NGC1510 | -1.89 ± 0.08 | -15.16 ± 0.06 |
| NGC1705 | -2.41 ± 0.06 | -14.79 ± 0.05 |
| UGC3838 | -1.62 ± 0.24 | -15.37 ± 0.18 |
| IC2184 | -1.20 ± 0.38 | -15.23 ± 0.28 |
| NGC2415 | -1.22 ± 0.10 | -14.59 ± 0.07 |
| NGC2820A | -2.04 ± 0.29 | -15.85 ± 0.22 |
| UGCA166 | -2.44 ± 0.13 | -15.83 ± 0.10 |
| NGC3125 | -1.56 ± 0.10 | -14.84 ± 0.07 |
| UGC5720 | -1.87 ± 0.09 | -14.88 ± 0.06 |
| NGC3353 | -1.90 ± 0.12 | -14.98 ± 0.09 |
| 1050+04 | -1.12 ± 0.18 | -14.98 ± 0.13 |
| NGC3738 | -2.03 ± 0.10 | -15.08 ± 0.07 |
| NGC3991 | -2.06 ± 0.07 | -14.99 ± 0.06 |
| NGC3995 | -0.89 ± 0.14 | -14.70 ± 0.11 |
| NGC4194 | -0.48 ± 0.15 | -14.18 ± 0.11 |
| NGC4449 | -1.75 ± 0.12 | -14.37 ± 0.09 |
| NGC4500 | -0.94 ± 0.21 | -14.77 ± 0.15 |
| NGC4670 | -1.74 ± 0.07 | -14.64 ± 0.05 |
| MCG6-28-44 | -1.62 ± 0.13 | -15.07 ± 0.09 |
| NGC4853 | 0.06 ± 0.40 | -14.66 ± 0.28 |
| NGC4861 | -2.57 ± 0.09 | -15.13 ± 0.07 |
| IC3961 | -2.06 ± 0.07 | -14.76 ± 0.06 |
| UGC9560 | -2.20 ± 0.09 | -15.33 ± 0.06 |
| TOL1924-41 | -2.10 ± 0.05 | -15.16 ± 0.04 |

TABLE 9—*Continued*

| Galaxy | $\beta \pm \delta\beta$ | $\log(F_o) \pm \delta \log(F_o)$ |
|---|---|---|
| BCDG, BCG, HII | | |
| NGC7673 | -1.75 ± 0.10 | -15.08 ± 0.08 |
| NGC7793 | -1.67 ± 0.18 | -15.26 ± 0.13 |
| HOTSPOT | | |
| NGC1097 | -0.45 ± 0.12 | -14.06 ± 0.09 |
| NGC2903 | 0.04 ± 0.13 | -13.72 ± 0.09 |
| NGC2997 | 0.21 ± 0.28 | -14.10 ± 0.20 |
| NGC3351 | 0.13 ± 0.14 | -13.60 ± 0.10 |
| NGC4321 | -0.32 ± 0.11 | -14.00 ± 0.08 |
| SEYFERT 2 | -0.76 ± 0.47 | |
| NGC1068 | -0.42 ± 0.14 | -13.52 ± 0.11 |
| NGC3081 | -0.64 ± 0.39 | -15.00 ± 0.28 |
| NGC3393 | -0.52 ± 0.48 | -15.02 ± 0.35 |
| NGC3982 | -1.09 ± 0.30 | -15.06 ± 0.22 |
| NGC4388 | -0.93 ± 0.22 | -14.98 ± 0.16 |
| IC3639 | -1.34 ± 0.17 | -15.08 ± 0.12 |
| NGC5135 | -0.16 ± 0.28 | -14.14 ± 0.21 |
| NGC5256 | -0.71 ± 0.34 | -14.94 ±0.25 |
| UGC8850 | -1.18 ± 0.28 | -15.24 ± 0.20 |
| NGC5506 | -0.97 ± 0.56 | -15.43 ± 0.41 |
| NGC5643 | -1.55 ± 0.58 | -15.85 ± 0.42 |
| NGC5674 | -0.12 ± 0.50 | -14.66 ± 0.37 |
| MK477 | -1.64 ± 0.28 | -15.51 ± 0.21 |
| NGC5728 | -0.76 ± 0.44 | -15.13 ± 0.32 |
| NGC7590 | -0.55 ± 0.35 | -14.80 ± 0.26 |
| Composite | -0.36 ± 0.83 | |
| NGC1672 | -0.24 ± 0.11 | -13.73 ± 0.08 |
| NGC3758 | -0.69 ± 0.49 | -14.98 ± 0.35 |
| NGC6221 | -0.51 ± 0.53 | -15.05 ± 0.39 |
| NGC6764 | 0.28 ± 0.38 | -14.14 ± 0.28 |
| NGC7130 | -0.78 ± 0.34 | -14.72 ± 0.24 |
| NGC7496 | -0.87 ± 0.10 | -14.58 ± 0.08 |
| NGC7582 | 0.61 ± 0.49 | -14.25 ± 0.36 |

[a] The full equation is $\log F_\lambda = \beta \log \lambda + \log f_0$. Slopes are based on 3 flux points which have equal contributions from Milky Way–type reddening, to minimize the effects of reddening on the slope determination. Only those galaxies with both short- and long-wavelength spectra are included. The $\beta \pm \delta\beta$ value reported adjacent to each activity class is the median value for the class. The conversion into $F_\nu \propto \nu^\alpha$ is given by $\alpha = -2 - \beta$.

Therefore, the spectra of most galaxies are probably affected by IS absorptions at least as strong as those measured for 3C 273 and SN 1987A. A cosecant law provides a rough estimate of the expected strength of low-ionization lines, which are produced predominantly in the Galactic disk, while those of highly ionized species are approximately independent of latitude. Since low Galactic latitude also means strong dust extinction in the 2200 Å absorption trough, deep interstellar absorption features should correlate with strong 2200 Å depressions in the spectrum of a galaxy.

The importance of knowing the strength of IS features is that sometimes they fall at the same wavelength as *stellar* absorption features. For example, the absorption lines which occur around 1300 and 1335 Å are produced in measurable strength by the ISM gas, where they are due to O I, Si II, and C II, but are also characteristic of O-type stellar spectra, where they are due to Si III and additional unidentified ions as discussed below (e.g., Heck et al. 1984). Even more confusing examples are provided by the absorptions of Si IV λ1400, C IV λ1550, and Mg II λ2800, which are strong features both for the interstellar medium and for some types of stars.

#### 4.1.2. *Early-Type Stars*

Early-type stars with spectral types B, O, and W-R (both WN and WC) are characterized by high temperatures ($T_{\rm eff} >$ 10,000 K), resulting in continuous flux distributions which increase in $F_\lambda$ toward shorter wavelengths. In practice, their slopes are essentially the same for all O and W-R types ($\beta \sim -2.5$), while the spectral energy distributions (SEDs) of later B and A stars become progressively flatter (see Figs. 4 and 5). As discussed further below, the evolutionary state of a hot star has no effect on its continuum slope, and there are short-lived phases of stellar evolution that pass through the O star region of the H-R diagram and that could, provided the luminosity were sufficient, contribute significantly to the *IUE* flux. We shall concentrate on massive hot stars for the present.

The main discrete spectral features seen in early-type stars are listed in Table 5, which has been compiled on the basis of the works by Panek & Savage (1976), based on *OAO 2* data, and Nussbaumer et al. (1982) and Heck et al. (1984), both based on low-dispersion *IUE* data (see also Walborn, Nichols-Bohlin, & Panek 1985 for high-dispersion *IUE* data). The

equivalent widths of these lines may be 10 Å or more, which is easily detectable in the spectrum of a galaxy, if many early-type stars are present. In the case of P Cygni lines, the *total* equivalent width is around zero, while the equivalent widths of their respective blue absorptions and red emissions may amount to several angstroms each.

Although a number of lines are common to the various spectral types, there are some characteristics that clearly distinguish the various types from each other:

1. Wolf-Rayet spectra are characterized by prominent lines of highly ionized ions which either display a "classical" P Cygni profile or appear essentially in emission. The detection of a strong P Cygni line of C IV is *not* clear evidence for a substantial population of W-R stars because O-type supergiants have similarly strong lines. On the other hand, characteristic emission of He II λ1640 does constitute a unique flag for the presence of W-R stars.
2. O-type stellar spectra contain lines of highly ionized ions. These lines either may be in absorption or may display a P Cygni profile, which is more prominent for supergiants because of their high rate of mass loss.
3. B-type stellar spectra are characterized by lines of lower ionization than those of O-type stars. The lines are generally in absorption, with the exception of the Si IV doublet, which displays a strong P Cygni profile in the case of supergiants.

In low-dispersion spectra such as the ones contained in this atlas, some of the stellar features may be confused with interstellar lines. There are instances in which the interstellar lines occur at the same wavelength and with a strength that is comparable to that of the stellar features, e.g., lines occurring around 1300 and 1335 Å, Si IV λ1400, and C IV λ1550.

As mentioned above, there exist several O star phases of stellar evolution, such as post-asymptotic giant branch

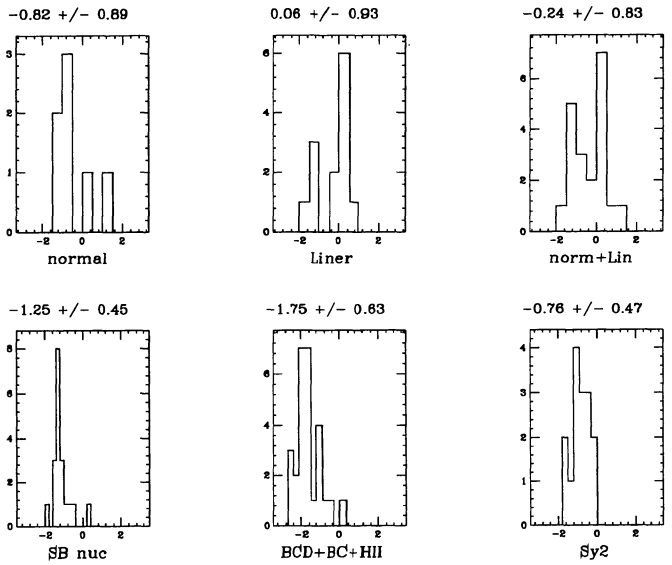


FIG. 6.—Histograms of spectral index $\beta$, where $F_\lambda \propto \lambda^\beta$. Galaxies are plotted according to their activity class, with the median value and the dispersion for each class shown above the respective histogram. Blue slopes are on the left; red slopes are on the right.

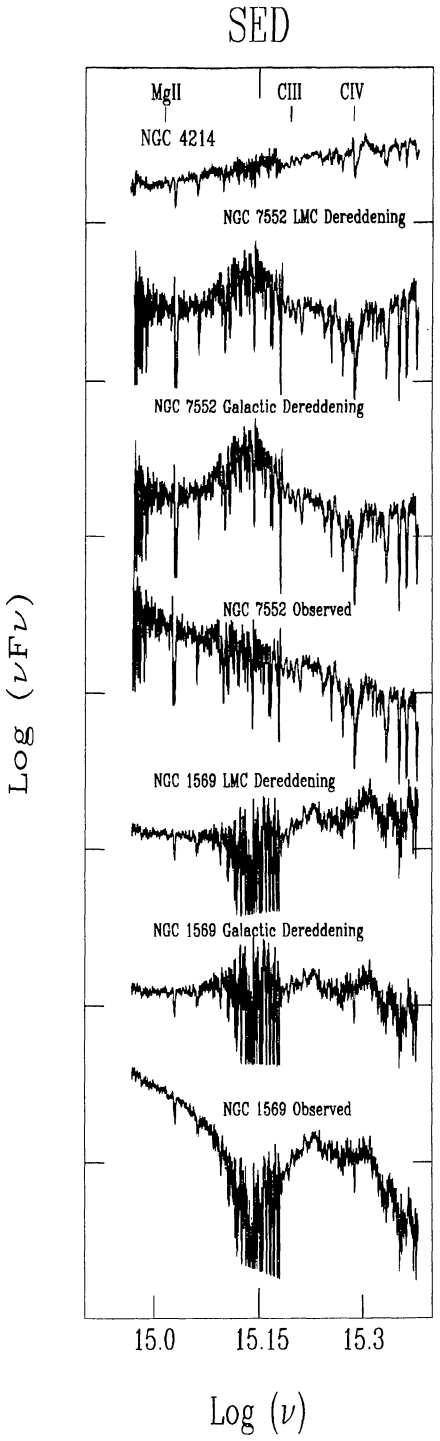


FIG. 7.—Spectral energy distributions of a galaxy at low Galactic latitude (NGC 1569), together with a red starburst (NGC 7552) and a blue starburst (NGC 4214). NGC 1569 and NGC 7552 are dereddened using both the Milky Way dereddening curve and the LMC dereddening curve. The dereddening results in a relatively smooth slope for the case of NGC 1569, while dereddening causes a broad emission feature in NGC 7552. Note that the Galactic latitude of NGC 7552 is −65°2.

(PAGB) stars which are on their way to becoming white dwarfs. These stars will have a UV continuum which increases toward shorter wavelengths just as do massive O stars. It has been shown (Barbaro & Olivi 1989) that this phase of stellar evolution could be very important in stellar populations which are both old (age greater than ~10 Gyr) and metal-rich (of greater than solar metallicity), characteristics believed to describe the dominant stellar population in elliptical galaxies and the bulges of spiral galaxies. It has been reported that the amplitude of the short-wavelength "rising branch" in the *IUE* spectra of elliptical galaxies correlates with metallicity, in such a way as to suggest that PAGB stars may be the source of the rising branch flux (Burstein et al. 1988). The bulge of M31, which is in the present sample, was also analyzed by Burstein et al. with this interpretation of the shortest *IUE* flux. See also Greggio & Renzini (1990) for a comprehensive discussion of hot phases of stellar evolution.

#### 4.1.3. *Mid- to Late-Type Stars*

Thermal emission from stars in the spectral range A–K dominates the UV emission of normal galaxies in the long-wavelength *IUE* camera. The continuum emission of A0 stars is practically flat ($F_\lambda \propto \lambda^0$) at wavelengths longer than 1600 Å, but the contribution at $\lambda < 2000$ Å becomes negligible for stars of type later than F3. Stars of spectral type G contribute only continuum emission longward of 2600 Å (Wu et al. 1991).

Lines from A–K stars are characterized by low ionization, which appear exclusively in absorption, with the lines of Fe and Mg being particularly strong. In later spectral types the strongest lines tend to be at the longer wavelengths. Burstein et al. (1988) attempted to remove the signatures of hotter stars from their *IUE* spectra of early-type (E and S0) galaxies and studied the strengths of the absorption lines in the resulting residual (after removal of hotter stars) spectra. They concluded that the strengths of the lines in the UV increased with those of optical absorption features such as $Mg_2$, which are believed to be a measure of the metallicity of the system. This trend will complicate the comparison between the stellar spectra obtained with *IUE* and the present galaxy sample, since the stellar templates are predominantly solar metallicity.

The most frequently observed cool star features in our atlas are listed in Table 6, along with the spectral type where the absorption-line equivalent width is the maximum. The list has been compiled on the basis of the study by Fanelli et al. (1987, 1990). The lines can be identified as having stellar origin when their equivalent width (EW) is larger than expected for IS absorption (see Table 4). Otherwise, the identification is ambiguous, since both the stars and the ISM contribute to the line.

Lines of Al II λ1671 appear in stars later than B8, while Al III λλ1855, 1863 increases in strength from B2 to mid-A (Fanelli et al. 1987). The blends of Fe II λ2400 and Fe II λ2600 reach a maximum value for dwarfs and giants of spectral type F9–G2. Fe I λ3000 originates from a quartet of lines and can be remarkably wide (~60 Å in stars of spectral type K). Fe I λ3000 arises predominantly from G5–K5 stars. Mg II λ2800 comes from a ground-state doublet transition and is the strongest for F8–G1 stars. The resonance transition Mg I λ2852 starts to appear in mid-A stars, reaching the maximum strength for K0–K3. Fanelli et al. (1990) have developed sophisticated spectral synthesis techniques which can determine the stellar mix from a galaxy spectrum.

#### 4.1.4. *Nebular Emission Lines*

Emission lines from "ordinary" ionized gas may arise from H II regions (here defined as the ionized regions around early-type, massive stars), planetary nebulae (PNs) (regions made of gas ejected and ionized by moderate-mass stars, which at the end of their evolution, in the transition from red giant to white dwarf, are bright and hot), and supernova remnants (both ejecta and interstellar gas swept by the ejecta, which are shock-heated and ionized).

In a typical late-type galaxy such as our own Galaxy, H II regions account for most of the nebular line emission. In fact, about 1% of the entire Galactic luminosity is produced by O- and B-type stars, and, since they are associated with massive clouds, most of their ionizing radiation goes into ionizing the surrounding gas. O- and B-type stars have effective temperatures definitely lower than 50,000 K and, therefore, the H II region gas is only moderately ionized; C, N, and O are no more than twice ionized, and He is never more than once ionized. Planetary nebulae and SNRs may display lines of highly ionized species, such as N V, C IV, He II, and Ne IV. On the other hand, their individual luminosity and their number density are far below that of H II regions, so that under "normal" conditions their contribution to the integrated spectrum may be orders of magnitude lower than that of H II regions.

Table 7 lists the most prominent lines that are observed in nebular objects. It is based mostly on the reviews of *IUE* data by Dufour (1987) for H II regions, Koeppen & Aller (1987) for PNs, and Blair & Panagia (1987) for SNRs. The actual list of the most prominent PN lines is from Feibelman et al. (1988). For SNRs we present four different cases, the first three referring to *young* remnants in which the emitting gas is mainly constituted by material ejected in the SN explosion. The last one corresponds to the Cygnus Loop, which is an *old* SNR and which is made mostly of swept-up material. The detailed information on SNR spectra is from Davidson et al. (1982) for the Crab Nebula, from Blair et al. (1984b) for O-rich SNRs, from R. A. Fesen (private communication cited in Blair & Panagia 1987) for Pup A as a prototype of N-rich SNRs, and from Raymond et al. (1980) for the Cygnus Loop.

In addition, one may expect emission lines originating from an "active nuclear region," in which a powerful nonthermal source (up to $10^{46}$ ergs $s^{-1}$) ionizes high-density gas and produces a high-excitation line spectrum (Kinney et al. 1991b).

### 4.2. *Characteristics of UV Spectra of Galaxies*

#### 4.2.1. *Normal Spiral Galaxies and LINERs*

The spectral energy distributions (SEDs) of normal galaxies and LINERs are shown in Figure 1. Although LINERs differentiate themselves from normal spiral galaxies in the optical by their low-ionization emission lines, the LINER spectra are dominated in the UV by the spectrum of the underlying galaxy, with little evidence of activity. Just as Heckman (1980) found no evidence in the optical for a featureless blue continuum, we find no evidence for it in the UV. Indeed, if the LINERs had been classified based on the UV spectra, most

would have been classified as normal spiral galaxies, since only a few (e.g., NGC 4579) show evidence of emission lines (see Reichert et al. 1992 for a detailed two-dimensional analysis of *IUE* spectra of the LINER NGC 3998). We are currently obtaining optical spectra to clarify the relation between galaxies with different levels of activity.

In Figure 1 the normal galaxies and the LINERs are ordered by slope, with the bluest on the top and the reddest on the bottom. The SEDs are not corrected for interstellar reddening. Although the galaxies do not strictly separate by Hubble class when ordered by slope, there is a tendency for the Sa and Sb galaxies to be redder than the Sc and Sd galaxies. For example, among the LINERs, the reddest galaxy is the Sa NGC 2681, while the bluest galaxy is the Sc NGC 3994. The normal spiral galaxies show a trend for early Hubble classes to have less flux at short wavelength than later Hubble types (cf. Coleman et al. 1980).

The earlier spiral galaxies show the SEDs and the spectral features of late A or early F stars in the long-wavelength camera. For example, the SAab galaxy NGC 4736 can be compared with the A and F stars in Figure 5. In the cases where cool star features can be clearly seen in the long-wavelength camera, the galaxies show an excess in short-wavelength flux relative to the cool star spectrum, which dominates the flux at long wavelength. Meanwhile, the later spiral galaxies (for example, NGC 598, Scd) show short-wavelength features which come from hot stars, as expected for galaxies with more active star formation. The massive hot star spectrum, which can be seen at the shortest wavelengths for the late-type spirals, dilutes the cool star signatures seen at longer wavelengths in the early-type galaxies.

The LINERs do not have significantly different slopes from the normal galaxies (see Fig. 6 and Table 9). Since LINERs are known to reside preferentially in spiral galaxies of early Hubble type (Heckman 1980), LINERs are expected to have redder slopes. In fact, the median value of Hubble types of the LINER galaxies present in the atlas is the same as the median value of Hubble type of the normal spiral galaxies, so the lack of a significant difference in slopes between the two is due to the distribution of Hubble types in the *IUE* archives and, therefore, our atlas.

#### 4.2.2. *Starburst, Blue Compact, and Blue Compact Dwarf Galaxies*

The active star formation of starbursting galaxies is evidenced by their blue spectra and their strong, hot star absorption features. Within the starburst galaxies, the slopes range from red (NGC 7552, $\beta = 0.26 \pm 0.14$) to blue (NGC 4214, $\beta = -1.85 \pm 0.06$). The spectral energy distributions (SEDs) of O and B stars with a range in luminosity class (Fanelli et al. 1992, Fig. 5) can be compared with the SEDs of the starburst galaxies as a way of performing a crude spectral synthesis. While the O and B stars have a range in slopes roughly comparable to the range in slopes of the starbursts and would serve as a natural explanation for the large range in UV slopes, the individual hot stars have very different absorption features from the starbursts, with different line ratios, different equivalent widths, and different lines present in the spectrum. Of course, one important factor is that the starbursts have a large range in metallicity, while the atlas of Fanelli et al. contains stars with metallicities typical of the solar neighborhood, being restricted to local stars.

The range in slopes of the starbursts may be due to internal dust extinction. However, the galaxies show little evidence of the type of extinction seen in our Galaxy. As an example, the extinction of the Milky Way is seen in Figure 2 for NGC 1569, with $b = 11°.2$, $E(B-V) = 0.51$ mag, and strong absorption at 2200 Å. The reddest starbursts, which might be expected to have the strongest extinction (for example, NGC 7552 and NGC 1672), show no absorption feature at 2200 Å. If dust is causing the dispersion in UV slope, that dust must have a different wavelength dependence than the dust in the Milky Way, as demonstrated in Figure 7. NGC 1569 is dereddened with the $E(B-V)$ value from Burstein & Heiles (1982), using both the average Galactic curve of Seaton (1979) and the LMC reddening curve of Fitzpatrick (1986). Both dereddenings produce a reasonable SED, although there is some deviation from the standard dereddening. For comparison, an attempt was made to deredden NGC 7552, a very red starburst galaxy, with both the Galaxy curve and the LMC curve, until it has the approximate slope of NGC 4214, a very blue starburst. In fact, the slope of the blue starburst cannot be produced by dereddening the red starburst with any known reddening law because of the excess of 2200 Å emission produced by these two dereddening laws. This demonstrates that the slope difference is difficult to explain with simple dereddening unless the extinction law is completely different from any measured to date.

The range in slopes may also be due to the range in hot star versus cool star populations present in the galaxy. If the galaxy is dominated by a recent burst of star formation after a period of quiescence, the slope may be very blue. But if the galaxy is a large, old spiral undergoing just another burst of star formation, there may be a substantive underlying population of cool stars to redden the spectrum.

One additional trait complicates any simple explanation of the dispersion in slopes: the red starburst galaxies (cf. NGC 1672 and NGC 7552) tend to have larger absorption-line equivalent widths at short wavelengths than the blue galaxies (cf. NGC 4214 and NGC 5253). The strength of the absorption lines in the spectrum of a galaxy is affected by the metallicity of the galaxy. Indeed, some optical features, less sensitive to other parameters such as temperature or gravity, are used as "metallicity indicators"—for example, $Mg_2$ (MgH + Mg $b$, 5156–5197 Å; Burstein et al. 1984). Generally, a lower metallicity content will correspond to lower equivalent widths. Thus I Zw 18 shows very weak absorption lines from early-type stars in its UV spectrum, although this galaxy has a large population of young massive stars: in fact, I Zw 18 is one of the lowest metallicity ($[O/H] = 0.02[O/H]_\odot$) blue compact galaxies known (see also § 4.1). We are currently collecting optical spectra in an *IUE*-sized aperture which will enable us to measure metallicity so as to determine the nature of the relation between UV slope and metallicity.

As a group, the blue compact galaxies and the blue compact dwarf galaxies are known to have lower metallicities than the starburst galaxies. Indeed, they have UV slopes that are bluer on average than the slope of the starburst galaxies. Thus, star-forming galaxies that are optically blue are also blue in the ultraviolet. (Note that this behavior contrasts with that of qui-

escent elliptical galaxies, where the galaxies which are redder optically tend to have bluer short-wavelength UV colors, as discussed by Burstein et al. 1988.)

#### 4.2.3. *Seyfert 2 Galaxies*

Seyfert 2 nuclei, which reside preferentially in early-type spiral galaxies, are redder in the UV than starburst or blue compact galaxies, and bluer than normal spirals and LINERs. In the optical, a Seyfert 2 spectrum is made up of an underlying galaxy continuum plus emission lines spanning a broad range of ionization, while in the UV the continuum is dominated by the featureless blue continuum plus emission lines (Kinney et al. 1991a). Of the Seyfert 2 galaxies with higher signal-to-noise ratios, shown in Figure 3, both NGC 3982 and NGC 3081 begin to be dominated by the host galaxy at the longest UV wavelengths. The implication is that there may be a sequence of active galactic nuclei ordered by the relative strengths of featureless blue continuum and the galaxy continuum.

Among the Seyfert 2 galaxies in Figure 3, NGC 1068 is more than 2 mag brighter than the others. The many emission lines of NGC 1068 presumably show what the spectra of the other galaxies would look like with higher signal-to-noise ratio. A significant percentage of the NGC 1068 flux at the shortest UV wavelengths is from the emission lines. Therefore, UV spectra of Seyfert 2 galaxies with lower signal-to-noise ratio will appear to have bluer continua than they actually have if their emission lines are not resolved. The method used to determine slope here is somewhat affected by this trend, because each of the three 100 Å wave bands used in the derivation of slope includes an emission line: N IV] λ1485 in the 1432–1532 Å region, C III] λ1909 in the 1863–1963 Å region, and C II] λ2326 in the 2323–2423 Å region. Of these emission lines, only C III] λ1909 has appreciable flux, and since C III] is in the center bin, the $F_0$ value in Table 9 (where $\log F_\lambda = \beta \log \lambda + \log F_0$) will be raised slightly, but the value for $\beta$ will not be greatly affected. Thus, the slopes here are in good agreement with those of Kinney et al. (1991a), who excluded all spectral regions with known emission lines and fitted the remaining continuum region to a power law.

#### 4.2.4. *The Role of Dust in the UV Spectra of Galaxies*

One surprising result of this compilation of galaxy spectra is that the spectral signature of dust is very rarely seen in galaxies, even when their spectra are intrinsically red, as with the red starburst galaxies. The only unambiguous 2200 Å dust feature seen in Figures 1, 2, and 3 is that in NGC 1569, which is expected because of its Galactic latitude of $b = 11°$ and corresponding $E(B - V)$ of 0.51. Although it is possible that the galaxies actually contain no dust, the most likely explanation for this apparent lack of dust intrinsic to the galaxies is that the dust is in clumps, so that dust rarely has an optical depth of around unity. Thus dust is like a "picket fence," either transparent or opaque (Heisler & Ostriker 1988). The effect of dust is not seen in the UV spectra except to lower the detected UV flux. We are currently observing the galaxies in the infrared in an aperture matched to the size of the aperture of *IUE*, and in follow-up work we also plan to look at *IRAS* fluxes to better understand the dust in these galaxies.

### 4.3. *Individual Objects*

*NGC 224 (M31, Andromeda); Sb.*—The UV spectrum of M31 is basically concave, with a minimum in flux at around 2000 Å and an increase in flux to both longer and shorter wavelengths. Absorption features of Si II, O I, Si III, and C II are present between 1200 and 1350 Å, as well as Mg II λ2800 (both Galactic and from M31) and Mg I λ2850.

M31 is the best example in the atlas of a spiral (Sb) galaxy with the center dominated by the bulge population (Burstein et al. 1988); the spectrum resembles that of an elliptical galaxy, but with a less prominent rising branch. Welsh (1982) observed the center of M31 with *IUE* and concluded that the rising branch did not come from young, metal-rich stars because of the weak absorption features of Si IV and C IV near 1300 Å. In the central region, Welsh also found that the blue stars are more centrally concentrated than are the metal-rich red giants, based on a comparison of the cross-dispersion profile in the UV with that in the optical. Deharveng et al. (1982) derived an upper limit for the star formation rate of $7.4 \times 10^{-5}$ $M_\odot$ yr$^{-1}$, by comparing the far-UV luminosity with the predictions of the steady state UV flux of Lequeux et al. (1981). The longer wavelength flux is presumably due to the main-sequence turnoff and is dominated by late F stars (see the stellar spectra in Fig. 5 for comparison).

*NGC 262 (Mrk 348); S0, Seyfert 2.*—The short-wavelength spectrum of Mrk 348 is flat ($F_\lambda \propto \lambda^0$) with strong emission lines. This Seyfert 2 nucleus resides in a face-on early-type (Sa) spiral, which has a companion, NGC 266 (Garcia-Vargas et al. 1989). Mrk 348 has been shown by Miller & Goodrich (1990) to have broad Seyfert 1 type emission lines in polarized flux, with a FWHM for Hα of ~7400 km s$^{-1}$. *IUE* data on Mrk 348 were first reported by Ferland & Osterbrock (1986), who found a value of $\alpha = -0.9$ for the UV spectral index, which is within the errors of the Kinney et al. (1991a) value of $\alpha = -1.4 \pm 0.5$ ($F_\nu \propto \nu^{-1.4 \pm .5}$). Kinney et al. (1991a) found that the number of recombination photons is larger than predicted from the number of ionizing photons, implying that the photoionizing continuum is obscured. Thus, Mrk 348 displays evidence of harboring a Seyfert 1 galaxy with broad Hα emission lines and with some of the ultraviolet continuum flux blocked from our line of sight.

*Haro 15 (Mrk 960); I, BCDG.*—The UV spectrum of Haro 15 is slowly rising from 2000 to 1200 Å, with strong absorption features indicating the presence of hot stars as discussed in § 4.1, and a moderate-strength intrinsic Lyα emission line. Fanelli, O'Connell, & Thuan (1988) found this metal-poor ($[O/H] \simeq 0.3[O/H]_{nx}$; Hunter & Gallagher 1986) bright blue compact dwarf galaxy (BCDG) to be undergoing intense star formation. From their spectral synthesis of the *IUE* spectrum they estimate that 3 $M_\odot$ yr$^{-1}$ of gas is being converted into massive ($M > 10\ M_\odot$) stars.

*Mrk 357; starburst.*—Balzano (1983) classifies Mrk 357 as a starburst galaxy, and indeed the spectrum shows a very strong C IV absorption feature. The region around Lyα is often contaminated by an artifact on the *IUE* camera (1280 Å), so there is some uncertainty in the strength of the Lyα emission line, although Lyα is considered an actual feature by Hartmann, Huchra, & Geller (1984). This comparatively distant ($z$ =

0.053) galaxy is observed with too poor a signal-to-noise ratio to detect many of the complex absorption features common to starburst galaxies. Mrk 357 appears stellar on the Palomar Sky Survey plates, so that it is sometimes incorrectly referred to as a QSO.

*NGC 598 (M33); Scd.*—The spectrum of the center of this nearby Scd galaxy is basically flat ($F_\lambda \propto \lambda^0$) across the entire *IUE* wave band. At shorter wavelengths the continuum is rich in absorption features from massive hot stars.

M33 is a bright galaxy in the X-ray band, and indeed its nucleus is the brightest X-ray source in the Local Group (Markert & Rallis 1983). An interpretation of the nucleus as a low-luminosity active nucleus has been suggested by Trinchieri, Fabbiano, & Peres (1988). Ciani, D'Odorico, & Benvenuti (1984) compared stellar synthesis models against the *IUE* spectrum of the center and found a best fit with a multigenerational model, with a young component of age $\sim 10^7$ yr and an old component with age $\sim 10^{10}$ yr superposed.

M33 has been very thoroughly studied in the UV; but most work concerns the properties of individual constituents of the galaxy, as opposed to the general stellar population of the central regions. The OB stars of M33 were studied by Massey, Hutchings, & Bianchi (1985); the M33 supernova remnants were studied by Blair, Kirshner, & Raymond (1984a); and the M33 Hubble-Sandage variables were studied by Humphreys et al. (1984). Surprisingly, only three short-wavelength spectra and one long-wavelength spectrum of the center of M33 are in the *IUE* archives.

*NGC 1023; SB0.*—The long-wavelength spectrum of NGC 1023 is apparently dominated by F and G stars. NGC 1023 is a normal SB0 galaxy in a group of 13 gravitationally bound galaxies (Tully 1980). Since NGC 1023 lies at Galactic latitude $b = 19°$, the strong absorption line of Mg II is very likely to be from our Galaxy. In contrast, Mg I is so strong that it is unlikely to be from just the Milky Way ISM, implying that there is an intrinsic Mg I component.

*NGC 1068 (M77); Sb, Seyfert 2.*—This spectrum has a flat ($F_\lambda \propto \lambda^{-0.4}$) continuum with emission lines of both low and high ionization. NGC 1068 is the nearest and brightest example of a Seyfert 2 galaxy. This highly studied Sb galaxy was observed by Antonucci & Miller (1985) in polarized light and found to harbor a Seyfert 1 nucleus (see Kinney et al. 1991a for a review).

Multiple *IUE* spectra were combined by Snijders, Netzer, & Boksenberg (1986), who found broad wings on the permitted emission lines and broad emission features of Fe II. Ferland & Osterbrock (1986) and Kinney et al. (1991a) found that the number of recombination photons measured was larger than would be predicted based on the number of photons available to ionize the gas. Thus the source of the UV continuum of NGC 1068 appears to be obscured from direct view.

*NGC 1097; SBbc, hot spot + LINER.*—This galaxy has been called a LINER by Keel (1983b) based on optical emission lines. The UV spectrum is flat with strong absorption features, which places the nucleus of NGC 1097 in the low activity range among the class of LINERs (cf. the emission lines of more active LINERs such as NGC 3031 or NGC 4579). NGC 1097 is a barred spiral with a ring of star formation surrounding the nucleus (a "hot spot" galaxy) at a radius of $\sim 10''$, or $\sim 1.5$ kpc, which is barely outside the *IUE* aperture. The ring emits in radio wavelengths, in the $^{12}$CO ($J = 1$–0) line, at 10 $\mu$m, and in H$\alpha$ (Phillips et al. 1984; Hummel, van der Hulst, & Keel 1987a; Gerin, Nakai, & Combes 1988). NGC 1097 also contains a weak, compact, flat-spectrum radio source at the center (Wolstencroft, Tully, & Perley 1984) and has two pairs of optical jets extending from the nucleus out to 90 kpc (see Lorre 1978 for spectacular images). Its large-scale morphology suggests dynamical disturbance, perhaps by interaction with the companion galaxy NGC 1097A.

*NGC 1140 (Mrk 1063); Irr Am, BCG.*—NGC 1140 is a blue irregular galaxy containing a large blob of ionized gas in its center, where the *IUE* aperture has been placed. Lamb, Hunter, & Gallagher (1986) have studied the *IUE* spectrum of this galaxy, which has a continuum slowly rising toward shorter wavelengths that is rich in absorption features. The above authors have also synthesized the spectrum, concluding that the galaxy has experienced a single burst of star formation starting about $3 \times 10^6$ yr ago and that its population is mainly constituted of main-sequence stars with masses $\lesssim 50\ M_\odot$, with a contribution from supergiants and, possibly, Wolf-Rayet stars.

*NGC 1313; SBdm,* H II.—The small apparent discontinuity between the short- and the long-wavelength spectra could be due to typical pointing errors of 1″–2″, or to the difficulty of extracting flux with high background (see Fig. 17). Marcelin & Gondoin (1983) map some of the many H II regions of NGC 1313 in the optical and show that they extend well outside the range of the *IUE* aperture. Although this object has been included in the Rosa, Joubert, & Benvenuti (1984) catalog of H II regions, the spectrum does not have the blue slope typical of H II regions.

*NGC 1433; SBab.*—This galaxy is classified as Seyfert-like by Véron-Cetty & Véron (1986) because of the presence of faint emission lines at optical wavelengths, with [N II] λ6583 stronger than H$\alpha$. The same classification does not appear obvious from the UV spectrum, which is that of a normal Sb galaxy. Absorption lines of C IV, Al III, Fe I, Fe II, Mg II reveal a complex contribution from a population with a range of stellar types. NGC 1433 is a nearly face-on, barred spiral galaxy, including three rings of enhanced blue color and active star formation (Buta 1983) which all lie outside the *IUE* aperture. The nuclear and the inner rings consist of two components: a blue, narrow one due to young associations and H II regions, and a broad, red component, composed of old stars (Buta 1986). Observations in the radio (Harnett 1987) show low-intensity nonthermal emission with a peak coincident with the optical nucleus.

*NGC 1510; Am pec, BCDG.*—NGC 1510 is a low-mass companion galaxy to the large barred spiral NGC 1512 and has complex central structures of size $\sim 10''$, which Eichendorf & Nieto (1984) call metal-poor H II regions with a strong A star component. The UV spectrum rises slowly toward shorter wavelengths and does have absorption features between 1850 and 2000 Å which are typical of A stars (see Fig. 5 for A star spectra).

*NGC 1553; S0 pec.*—The UV spectrum has weak flux below the main-sequence turnoff at $\sim 2400$ Å, which is typical of an older intermediate population present in quiescent S0 galaxies

(Gregg 1989). There is an increase in flux in the spectrum at wavelengths below 1400 Å (cf. Burstein et al. 1988 for analogous behavior among elliptical galaxies, the "rising branch"). This galaxy is at sufficiently high redshift ($z = 0.004$) that the intrinsic Mg II absorption feature is separated from the Galactic feature by 11 Å.

*NGC 1569; Im, starburst.*—NGC 1569 lies close to the plane of the Galaxy ($b = 11°.2$) and shows very strong Galactic dust extinction with a depression at 2200 Å and below 1475 Å. The very hot, bright nucleus of this galaxy resembles a superluminous, young star cluster (Arp & Sandage 1985). In the UV spectrum, only absorption features from our Galaxy can be seen (C IV λ1550, Fe II λλ2585, 2600, and Mg II λ2800, although the spectrum is noisy and other absorption features cannot be unambiguously excluded. NGC 1569 is a Magellanic irregular galaxy, which is said by Hunter et al. (1989b) to be undergoing active star formation and by Israel (1988) and Israel & van Driel (1990) to be past its burst of star formation by $10^7$ yr. Hunter et al. consider NGC 1569 a starburst on the basis of its population content (extreme Population I), as obtained from the study of optical and IR properties. Large uncertainties are expected in this analysis because of the high reddening of this galaxy [$E(B - V) = 0.56 \pm 0.10$ mag; Israel 1988]. Israel and Israel & van Driel conclude that NGC 1569 is recovering from star formation (poststarburst galaxy), based on UV and optical colors which show an OB star population deficient in very early O stars and based on analysis of the radio continuum, whose nonthermal part can be explained by a supernova rate decreasing in time (Israel & de Bruyn 1988).

*NGC 1672; SAB(s)bc, starburst + Seyfert.*—This galaxy has been classified variously as a LINER, a Seyfert 2, or a starburst galaxy (Diaz 1985, Mouri et al. 1989, Garcia-Vargas et al. 1990, respectively). Based on the UV spectrum, which is flat with no indication of a 2200 Å dust absorption feature, and with a rich collection of broad absorption lines, NGC 1672 is a starburst galaxy containing a wide range of ages represented in its stellar population. This late-type barred spiral has an elongated and amorphous structure centered on its nucleus (Sersic & Pastoriza 1965). NGC 1672 is both a radio source and an X-ray source (Fabbiano & Trinchieri 1987). Although its X-ray luminosity is comparable in intensity to that of most normal spirals, NGC 1672 probably hosts an X-ray pointlike source in its nucleus, unlike most normal spirals whose X-ray emission is due mainly to massive binaries. In addition, its X-ray emission appears extended (Fabbiano 1989).

*NGC 1705; Irr Am, BCDG.*—Lamb et al. (1985) suggest that this blue compact dwarf galaxy is either in a mild starburst phase or in a postburst phase. This irregular galaxy has a steep radial gradient in surface brightness. Its low metallicity resembles that of its neighbor, the LMC (Meurer et al. 1992). The strong emission lines observed in the optical spectrum and the strong absorption features in the UV spectrum of this galaxy are well accounted for by B0 and B1 stars of approximately 20 $M_\odot$, although this result does not exclude a contribution from stars of higher mass assuming a normal IMF (Lamb et al. 1985).

In a multi-wave-band study, Meurer et al. (1992) observe the presence of two stellar populations coexisting in the galaxy: an inner high surface brightness component, extending up to 500 pc from the center, and a low surface brightness one, up to 1.5 kpc. The dichotomy may originate from two bursts of star formation that arose at different times. Alternatively, the dichotomy may stem from a difference in the IMF, with the high brightness population being richer in high-mass stars. Hα imaging reveals the presence of a bipolar outflow of gas, likely to deplete the galaxy of a large amount of its gas supply.

NGC 1705 is a gas-rich BCG, and because of this, York et al. (1990) argue that the ISM contributes Si IV λ1400 and C IV λ1550 absorption lines comparable to the stellar contribution.

*UGC 3838 (VII Zw 153, Mrk 7); Im, BCG.*—This blue compact galaxy is a giant, clumpy irregular with a number of starbursting knots of exceptional intensity (Gordon & Gottesman 1981). UGC 3838 has bright clumps which are, on average, 100 times brighter in the optical than 30 Doradus and which have the typical absorption features of O and B stars indicative of the presence of supergiants (Benvenuti, Casini, & Heidmann 1982b). A feature is present at 2200 Å, which is narrower than the normal 2200 Å dust feature and is probably due to the high background and the low sensitivity of this region of the LWP camera.

Synthetic spectra (Benvenuti, Casini, & Heidmann 1982a) show that the UV continuum emission from the clumps of such galaxies is from a sum of stars ranging in spectral type from O to early B. Spectroscopic studies in the optical (Boesgaard, Edwards, & Heidmann 1982) show that the physical conditions such as temperature, electron density, and chemical abundances are typical of H II regions in normal spiral galaxies despite the exceptionally high luminosity of the clumps.

*NGC 2403; Sc.*—The flux of this galaxy is approximately constant through the ultraviolet region. This normal Sc galaxy of the M81 group is the prototypical flocculent spiral (Elmegreen 1981), based on the disjoint nature of its individual arms. NGC 2403 contains a large number of H II regions and OB associations that are similar in size and distribution to those in M33 and in the LMC (Hodge 1985). The more active star formation regions of NGC 2403 are not in the nucleus (Beckman et al. 1987), which appears quiescent.

*NGC 2415 (Haro 1); Irr pec, BCG.*—NGC 2415 is in a compact group, with three companions situated about 22′ (0.5 Mpc) north, but this galaxy shows no evidence of morphological disturbance (van der Burg 1985). This blue compact galaxy is slightly ellipsoidal, with an irregular core and irregular nebulosity (Gordon & Gottesmann 1981). NGC 2415 has a blue magnitude of $M_B = -21.0$ and a neutral hydrogen content of ~6% of the total mass of the galaxy (Gordon & Gottesmann 1981). Its far-infrared (FIR) luminosity is high [$\log (L_{\rm FIR}/L_\odot) \sim 11.1$; Iyengar, Rengarajan, & Verma 1985], probably owing to the presence of an intense burst of star formation and to the presence of dust. If dust is present as these authors suggest, it is either lacking in the 2200 Å feature seen in Milky Way reddening curves, or else the dust is possibly very clumped. The short-wavelength *IUE* spectrum has been discussed by Fanelli et al. (1988) and analyzed using spectral population synthesis. The UV spectrum is rich in absorption features and shows the presence of OB supergiants together with a composite population of O, B, and A stars. The spectral synthesis models suggest that star formation took place in discrete episodes rather than in continuous formation, with the last episode arising about 10 Myr ago.

*Holmberg II (VII Zw 223, Arp 268, DDO 50); Irr, BCDG.*—Holmberg II is a blue compact dwarf galaxy described by Zwicky (1971) as a large posteruptive blue irregular with compact core and many knots. It is a resolved galaxy in the M81–NGC 2403 group. With a distance of about 3 Mpc, it is one of the nearest condensations in the local supercluster (Sandage & Tammann 1975). Despite its location in a group, Holmberg II does not appear to be physically interacting (Davis & Seaquist 1983).

The UV emission of Holmberg II is dominated by a single giant H II region, where intense star formation is taking place. Indeed, the continuum of the UV spectrum is typical of an H II region (cf. Rosa et al. 1984). The spectrum shows possible nebular emission of C III] λ1909. The galaxy-wide star formation rate is lower than that typical of normal spiral galaxies and can be considered approximately constant over a Hubble time (Hunter & Gallagher 1985). Analysis of *IRAS* observations suggests that only a small amount of dust is present in Holmberg II, so that little hidden star formation can be present (Hunter et al. 1989a). Like most dwarf irregulars, the metallicity of Holmberg II is low compared to that of normal spiral galaxies and is intermediate between the metallicity of the LMC and that of the SMC (Hunter & Gallagher 1985).

*UGC 4483; dIm IV,* H II.—This dwarf galaxy is of relatively high surface brightness and belongs to the M81 group (Karachentseva, Karachentsev, & Borngen 1985). UGC 4483 is a possible companion of Holmberg II with an angular separation between them of $\simeq 1\overset{\circ}{.}7$ (Thuan & Seitzer 1979), corresponding to about 0.1 Mpc. Like most dwarf galaxies, the H I content of UGC 4483 is relatively high, with neutral hydrogen making up half the total mass of the galaxy (Thuan & Seitzer 1979; Huchtmeier & Richter 1988). The high short-wavelength UV flux of this galaxy is similar to that in Holmberg II and indicates star formation activity. However, there is no evidence of the absorption features typical of massive O and B stars from active star formation. Depressions in the UV continuum may indicate the presence of some weak absorption lines.

*NGC 2639; Sa, LINER + Seyfert.*—This early-type spiral galaxy (Sa) has a large bulge component with broad Hα emission and low-ionization emission lines, which lead Keel (1983b, 1984) to conclude that it is a composite of a LINER and a Seyfert galaxy. NGC 2639 is a radio-loud galaxy with an extended source. Condon et al. (1982) concluded from the extended nature of the radio emission that the emission process is thermal and related to star formation triggered by interaction with the companion A0843+49. When observed with higher resolution (VLBI), NGC 2639 is found to be one of the rare examples of a radio-emitting spiral galaxy with a VLBI core source (Hummel et al. 1982). Higher signal-to-noise ratio UV data would contribute significantly to understanding this intriguing galaxy.

*NGC 2681; Sa, LINER.*—Like other LINERs in the atlas, this early-type spiral galaxy (S0/a) shows little evidence for nuclear activity in the UV spectrum (Heckman 1980).

Although detected in the radio, no compact source has been seen (van der Kruit 1971; Condon 1987, Table 2). Analysis of the UV spectrum by Burstein et al. (1988) led to the conclusion that the galaxy has some residual star formation with major bursts about 1–2 Gyr ago.

*NGC 2782; SAB(rs)a, starburst.*—This starburst galaxy has a UV continuum and strong UV absorption lines which resemble those in the spectrum of the starburst prototype NGC 7714 (Kinney et al. 1984). The nucleus is a strong, extended (~1 kpc) radio source, whose emission is probably due to supernova remnants from the active star formation in the galaxy center. The star formation may be triggered by the anonymous companion (Condon et al. 1982). However, the source of the radio spectrum is controversial: Heckman et al. (1983) find a nonthermal component in addition, leading to the composite classification of LINER plus starburst. This idea is supported by Keel (1984), who notes the flatness of the radio spectrum. The high far-infrared luminosity and the strength of the CO emission support the scenario of an intense burst of star formation (Sanders & Mirabel 1985).

*MCG 10-13-71 (Mrk 19), Irr, BCDG.*—The optical spectrum of Mrk 19 shows the typical features of a giant H II region (Neugebauer et al. 1976) and is interpreted as reflecting a constant star formation rate since the start of the last burst about $6 \times 10^6$ yr ago (Dottori 1983). This galaxy is also defined as a "lazy" galaxy for its property of forming stars by intermittent short bursts (Kunth & Joubert 1985). The UV continuum is in agreement with the picture of an H II region (see Rosa et al. 1984), but the only visible absorption features are Si IV λ1400 and the blends for $\lambda > 1800$ Å. The paucity of absorption features may be due to the relatively low metallicity of the galaxy ($[O/H] \simeq 0.15[O/H]_\odot$; Kunth & Joubert 1985).

*NGC 2798; SBa, starburst.*—This barred spiral galaxy forms an interacting pair with NGC 2799. The gravitational interaction may be responsible for the strong burst of star formation present in the nucleus of the galaxy (Joseph, Wright, & Prestwich 1986), for the extended nuclear radio emission (Heckman et al. 1983), for the narrow optical emission lines, and for the powerful far-infrared luminosity (Armus, Heckman, & Miley 1990). The extended 10 and 20 μm emission is also in line with the above scenario (Joseph et al. 1986). The short-wavelength *IUE* spectrum of NGC 2798 has been studied by Joseph et al. (1986), and many details can be found in their paper. The *IUE* slit was centered on the peak of the 10 μm emission. The UV continuum is flat, as expected in a starburst (cf. NGC 7714), and there are C IV and Si IV absorption features, typical of massive O and early B stars.

*NGC 2841; Sb, LINER.*—This Sb galaxy is classified as a LINER by Heckman (1980) and Keel (1983a,b) on the basis of optical emission-line ratios and strengths. While Baldwin, Phillips, & Terlevich (1981) conclude that the ionizing mechanism is shock heating, Ferland & Netzer (1983) suggest that the mechanism is photoionization. A ring of enhanced star formation surrounding the nucleus is suggested by optical and near-IR data (Prieto et al. 1985). (The ring lies outside the *IUE* aperture.) No prominent emission features can be seen in the UV spectrum. However, NGC 2841 does show a clear rising branch, with flux increasing from 1800 to 1200 Å.

*NGC 2903; Sbc, hot spot.*—NGC 2903 contains active star formation within its hot spot knots and also throughout its entire nucleus (Bonatto, Bica, & Alloin 1989). The UV spectrum has deep, complex absorption features of a starburst galaxy, but with a slope increasing toward long wavelength. This slope, as well as the complex absorption features across the *entire IUE* wave band, indicates the presence of a mixture of early and late-type stars, which is consistent with the conclu-

sions of Oka et al. (1974) based on optical observations. Simons et al. (1988) note that the "patchy" appearance of the central regions in the $V$ band is due to a variation of internal extinction. The Mg II absorption feature is too strong to be due to Galactic absorption alone (see Table 4).

*I Zw 18 (UGCA 166, Mrk 116); Irr, BCDG.*—This blue compact dwarf galaxy is one of the most metal-poor galaxies known ([O/H] $\simeq 0.02$[O/H]$_\odot$; Dufour, Garnett, & Shields 1988). I Zw 18 has been described as the prototypical isolated extragalactic H II region that is most probably undergoing its first burst of star formation (Searle & Sargent 1970). There are two separate star-forming regions in this galaxy, surrounded by a 3 kpc envelope of H$\alpha$ emission (Dufour & Hester 1990). The UV spectrum of this super–metal-poor compact galaxy rises to the blue and contains weak low-ionization absorption features (Dufour et al. 1988).

*NGC 2997; Sc(s), hot spot.*—The nucleus of this "hot spot" galaxy has two parts, distinguished by their optical properties: a central red core, consisting of older stars and in a quiescent phase (no emission-line activity), and a blue annulus, consisting of a number of knots, whose emission spectrum identifies them as giant H II regions (Meaburn & Terret 1982). The radius of the ring is about 4″, and is included in the *IUE* slit (see Walsh et al. 1986). The UV spectrum is weak and noisy, and the only convincing features are the Si IV, C IV, and Mg II absorption lines. From population synthesis, the knots of NGC 2997 apparently consist of reddened O stars and less reddened B- and A-type stars (Walsh et al. 1986). The reddening is due to the obscuration induced by the clumpiness of the H II regions.

*NGC 3031 (M81); Sb, LINER.*—M81 is a nearby Sb galaxy, which has the low-ionization emission lines of a LINER (Heckman 1980) but also has the broad emission lines of a low-luminosity Seyfert 1 galaxy (Peimbert & Torres-Peimbert 1981). The galaxy contains a compact, powerful nuclear radio source (Condon et al. 1982; Kellermann et al. 1976). Keel et al. (1985) have found evidence that tidal interactions with companions increase the activity of the nucleus. M81 appears to be interacting with the other components of the M81 group, which show a common H I envelope (Condon et al. 1982).

The spectra of M81 include only those with the aperture centered on the galaxy (cf. Peimbert & Torres-Peimbert 1981; Ellis, Gondhalekar, & Efstathion 1982). The UV spectrum has been analyzed by Peimbert & Torres-Peimbert (1981) and by Ellis et al. (1982). The emission probably originates from two different regions: The narrow permitted lines and the forbidden lines, on the one hand, come from an extended region where gas is shock-heated by a central source or photoionized by a power-law spectrum. The broad permitted lines, on the other hand, originate in a small, compact central region. The line broadening is due to the motion of the gas around a very compact central object ($M \sim 10^7\ M_\odot$; Peimbert & Torres-Peimbert 1981; see also the detailed analysis of Filippenko & Sargent 1988). In spite of the presence of the typically broad Seyfert emission lines, such as Mg II λ2800, the UV continuum is that of a normal early-type spiral galaxy.

*NGC 3049 (Mrk 710); SBbc, starburst.*—This spiral galaxy belongs to the Virgo Cluster and is a starburst (Balzano 1983) that has also been called a W-R galaxy (a galaxy whose spectrum exhibits the emission from Wolf-Rayet stars) by Kunth & Schild (1986). Our UV spectrum does not show clear P Cygni profiles or He II emission, as would be expected if W-R stars were present. The near-IR emission has been attributed to a thermal source (Balzano & Weedman 1981). A discussion of the visible, UV, and far-infrared properties of Mrk 710, together with a population synthesis model, can be found in Mas-Hesse, Arnault, & Kunth (1989), who conclude that the present burst of star formation is probably only about 5 Myr old.

*NGC 3081; SBa, Seyfert 2.*—This early-type barred spiral galaxy has the same relative emission-line intensities and emission-line profiles as a Seyfert 2 galaxy, but with a much lower luminosity (Phillips, Charles, & Baldwin 1983). The UV spectrum (also studied by Durret & Bergeron 1986) shows the emission lines of high excitation and of low excitation typical of a Seyfert 2 galaxy, as well as the flat continuum ($F_\lambda \propto \lambda^0$).

*NGC 3125 (Tol 3), Irr Am, BCDG.*—This metal-poor, irregular amorphous galaxy is a dwarf undergoing strong star formation activity (Kunth & Sargent 1983; Gallagher & Hunter 1987; Kunth, Maurogordato, & Vigroux 1988). Recognized as a W-R galaxy in the optical, its population seems to be the result of periodic bursts of star formation followed by periods of quiescence (Kunth & Sargent 1981). The UV spectrum has a P Cygni profile of C IV λ1550, consistent with the picture of NGC 3125 as a W-R galaxy.

*NGC 3256; Sb(s) pec, starburst.*—This galaxy contains a very bright star-forming region spanning over 4 kpc and called by Joseph & Wright (1985) a "super-starburst." NGC 3256 is also ultraluminous in the infrared (Kawara, Nishida, & Gregory 1990). Tidal tails evident in the optical photographs of Joseph & Wright signal a merger. The short-wavelength UV spectrum shows a flux decreasing toward short wavelengths with very strong, deep absorption features. While the deep broad absorption features reveal the presence of young, hot stars, the overall slope is probably due to dust [$E(B-V) = 0.13$ mag].

*UGC 5720 (Haro 2, Mrk 33); Im, BCDG.*—This blue compact dwarf galaxy has gone through several bursts of star formation and possesses a large star formation region of size greater than 350 pc. The low metallicity resembles that of the LMC (Meurer, Cacciari, & Freeman 1990). The ultraviolet spectrum of UGC 5720 exhibits well-defined, strong absorption lines and a continuum that rises slowly toward short wavelengths (Fanelli et al. 1988). The stellar synthesis of Fanelli et al. indicates that the galaxy has gone through at least two earlier bursts of star formation, the most recent being not more than 20 Myr old.

*NGC 3310; SAB(r)bc, starburst.*—The central part of this bright peculiar galaxy has a complex morphology, with a ring of H II regions surrounding the nucleus (an H II region itself) at a radius of a few kiloparsecs, and with a "bow and arrow" structure in the northwest region (Walker & Chincarini 1967; Bertola & Sharp 1984). The galaxy has an extremely bright blue optical continuum (Telesco & Gatley 1984) and strong extended X-ray, UV, and radio emission of thermal origin (Fabbiano, Feigelson, & Zamorani 1982; van der Kruit & de Bruyn 1976). All these aspects, in addition to the intense optical emission lines (Heckman & Balick 1980) and the very high IR luminosity ($L_{IR} \simeq 3 \times 10^{10}\ L_\odot$; Telesco & Gatley 1984), place NGC 3310 among the most luminous star-forming galax-

ies. The most intense and youngest burst is taking place in the "jumbo" H II region, situated 15″ southwest of the nucleus (Telesco & Gatley 1984). The *IUE* spectrum is in perfect agreement with the picture of a starbursting galaxy: the rising continuum and the deep absorption lines are typical of OB associations.

*NGC 3351 (M95); SBb, hot spot.*—This is a typical ringed galaxy: a quiescent nucleus is surrounded by a ring of H II regions which appear as bluer knots where intense star formation is taking place. In particular, the ringlike structure of M95 has an external diameter of about 20″, around a redder nucleus of about 2″ (Alloin & Nieto 1982 and references therein). There are three major complexes of H II regions, whose high content of O stars gives a young age to the burst. Alloin & Nieto (1982) suggest that the burst is related to the existence of a radial inflow of the ring toward the nucleus, which might produce an accumulation of neutral gas on the inner Lindblad resonance, providing fuel for the star formation. The UV spectrum shows unusually strong C IV and Mg II absorption lines.

*NGC 3353 (Haro 3, Mrk 35); Im, BCDG.*—Haro 3 is a typical BCDG with a UV continuum rising toward short wavelengths and a spectrum rich in both low- and high-ionization absorption features. A complete discussion of the UV properties of this galaxy, in addition to a study of spectral synthesis, can be found in Fanelli et al. (1988). The main conclusions are that the stellar population is composed of main-sequence stars ranging from O3 to mid-A; the contribution from cool stars is negligible; there is no significant population of blue supergiants; the low-ionization absorption lines have stellar origin; due to the high star formation rate and limited gas supply, the star formation history is characterized by discrete star formation episodes.

*NGC 3393; SBa, Seyfert 2.*—This Seyfert 2 galaxy has a low-level continuum flux with some evidence of the underlying continuum of the SBa galaxy and with very strong, narrow emission lines typical of Seyfert 2 nuclei. A detailed analysis can be found in Diaz, Prieto, & Wamsteker (1988).

*MCG 9-18-32 (Mrk 153); Scp, BCDG.*—Mrk 153 is defined as a "lazy" galaxy by Kunth & Joubert (1985)—meaning that it is a blue emission-line galaxy forming stars by intermittent short bursts—and as a blue compact galaxy by Thuan & Martin (1981). The continuum rises steeply to short wavelengths with strong absorption features, suggesting the presence of massive, hot stars.

*1050+04 (Mrk 1267); BCG.*—The relatively large redshift of this galaxy separates intrinsic features from Galactic features. The spectrum of this BCG shows a rich and complex system of absorption lines, including those usually hidden by the geocoronal emission, i.e., Ly$\alpha$ $\lambda$1215 and N V $\lambda$1240. In addition, the intrinsic Fe II $\lambda$2600 and Mg II $\lambda$2800 lines are clearly distinguished from those due to Galactic absorption. The relatively flat continuum is a manifestation of the star-forming activity of the galaxy, and the presence of high-ionization absorption lines reveals that there are many early supergiants.

*NGC 3448, Irr Am, starburst.*—NGC 3448 is part of a tidally interacting binary with the dwarf spiral UGC 6016. This galaxy has been recognized as a starburst because of many properties; the radio brightness of this amorphous galaxy comes mainly from the nucleus, the spectrum is dominated by far-infrared emission, and the UV flux is typical of the presence of massive, hot stars (Noreau & Kronberg 1985a). The nuclear radio source has been resolved into a family of point sources similar to those seen in M82, which are most probably supernova remnants and are coincident with a dust lane in the center of the galaxy (Noreau & Kronberg 1985b, 1987). Bertola et al. (1984) conclude that the short-wavelength UV flux is due to early B stars.

*NGC 3504; SABab, starburst.*—Optical and radio data suggest that the galaxy has a composite nucleus, which shows both nonthermal activity and recent star formation (Keel 1984). The radio emission is due to the presence of a strong nuclear radio source in a region of about 1 kpc (Condon et al. 1982). The optical spectrum is dominated by the regions of active star formation (Keel 1984), which are possibly triggered by the companion NGC 3512, 50 kpc distant from the main galaxy (van Moorsel 1983).

The UV spectrum is rich in absorption lines, with the presence of a P Cygni profile for C IV, indicative of an evolved population of massive supergiants. The flat continuum and the rich absorption features resemble the spectrum of the prototype starburst galaxy NGC 7714.

*Mrk 36 (Haro 4), Irr, BCDG.*—This blue compact dwarf galaxy is faint and pointlike in the UV. Mrk 36 is probably young; although it is undergoing intense star formation, its dust content is exceptionally low, based on *IRAS* fluxes (Gondhalekar et al. 1986), suggesting that the stars may not be evolved enough to have built up the dust seen in normal galaxies. Indeed, the gas-to-dust ratio of this galaxy is greater than $10^5$ (Gondhalekar et al. 1986), which is two orders of magnitude above even that inferred for damped Ly$\alpha$ systems (Fall, Pei, & MacMahon 1989), purported to be proto–disk galaxies (Wolfe 1987).

The UV absorption lines are weak, probably because of the low metallicity. Only C IV $\lambda$1550 and the Fe blend around $\lambda \simeq$ 1620 Å are recognizable. The C III] $\lambda$1909 nebular emission line is also detected. The rising blue continuum is consistent with the star formation scenario.

*NGC 3660 (Mrk 1291); SBbc, mini-Seyfert 1, NELG.*—This galaxy is classified, on the basis of the optical spectrum, as between a Seyfert 1 and a narrow emission line galaxy (NELG) (Kollatschny et al. 1983). Nevertheless, the UV spectrum looks like that of a normal SBbc galaxy with no nonthermal activity. This galaxy, with $z = 0.012$, shows strong Ly$\alpha$ emission.

*NGC 3690 + IC 694; Sc pec, starburst.*—The *IUE* aperture contains both objects in this pair of "colliding or strongly interacting" galaxies (de Vaucouleurs, de Vaucouleurs, & Corwin 1976), the partner being IC 694. This system is the most representative example of intense and widespread star formation activity, presumably triggered by an interaction (Gehrz, Sramek, & Weedman 1983). It is a strong radio source (Condon et al. 1982), has a high infrared luminosity ($L_{IR} \simeq 5 \times 10^{11} L_{\odot}$; Carico et al. 1988), and has the most luminous optical emission lines of any non-Seyfert galaxy (Weedman 1972). All of these properties may be explained within a starburst model. The system has a complex morphology: three brightest regions can be identified in the optical, radio, and IR bands—region A (nucleus of IC 694), region B (nucleus of NGC 3690), and region C. All of them are starbursting (Gehrz et al. 1983). In

region A there is both a radio and an IR unresolved source, from which 60% of the far-infrared luminosity of the system originates (Joy et al. 1989). This source might be compact and may not be explainable with thermal processes (Gehrz et al. 1983). The remaining 40% of the far-infrared emission originates from a compact source in NGC 3690, probably the extranuclear region C (Joy et al. 1989). The absorption-line–rich UV spectrum confirms the intense thermal activity of NGC 3690. Because of the relatively high redshift of this galaxy ($z$ = 0.012), the Ly$\alpha$ absorption line is detected.

*NGC 3738; Irr IV,* H II.—NGC 3738 is a giant irregular galaxy with high-excitation emission lines, with a large fraction of its mass in the form of neutral hydrogen, and with moderately low metallicity. It has been called a normal H II galaxy by Phillips et al. (1983). Hunter & Gallagher (1986) conclude (following the prescription by Gallagher, Hunter, & Tutukov 1984) that the star formation rate has been constant in time. However, Tacconi & Young (1985) suggest that irregular galaxies form stars more efficiently than do spirals and, as a consequence, that the present star formation rate of NGC 3738 cannot be sustained for more than $10^8$ yr. The UV spectrum resembles those of H II regions (cf. Rosa et al. 1984) with emission dominated by massive, hot stars.

*NGC 3982; Sbc, Seyfert 2.*—This Sbc galaxy does not have any prominent emission lines in the UV, despite being classified as Seyfert 2-like by Phillips et al. (1983) based on the presence of high-excitation lines and low intrinsic luminosity in the optical. The UV continuum is dominated by the normal Sbc galaxy spectrum and shows evidence of absorption features.

*NGC 3991 (Haro 5); Im, BCG.*—This Magellanic irregular belongs to a multiple interacting system, which also includes NGC 3994 and NGC 3995. The gravitational interaction with the companions may trigger the activity of the galaxy (Keel et al. 1985). The optical spectrum shows that NGC 3991 resembles an H II galaxy, with a very blue nucleus (Keel et al. 1985). The BCG nature is supported by its low metallicity (see, e.g., Arnault et al. 1988, where the problem of nondetection of CO in BCGs is also treated) and by the characteristics of our UV spectrum, which according to Rosa et al. (1984) resembles an H II region. A higher level of activity is revealed in the radio, where the emission is comparable to that of a Seyfert galaxy (Seaquist & Bell 1968), and in the X-ray ($L_x = 2.5 \times 10^{41}$ ergs $s^{-1}$; Fabbiano et al. 1982). The authors attribute the X-ray emission to the intense star-forming activity. This spectrum with high signal-to-noise ratio shows absorption lines as well as emission in Ly$\alpha$ and He II.

*NGC 3994; Sc, LINER.*—This galaxy interacts with both NGC 3991 and NGC 3995. On the basis of the criteria given by Baldwin et al. (1981), NGC 3994 is classified as a LINER. It has a complex structure, with vigorous star formation going on in the ringlike outer arms (Keel et al. 1985). NGC 3994 also has a weak broad component of H$\alpha$ and is a radio source (Hummel et al. 1987b). In spite of the signs of activity in the optical and radio wave bands, the UV spectrum shows no evidence of emission lines, while the shape of the continuum resembles that of a normal Sc galaxy, with some additional continuum emission between 1500 and 1900 Å.

*NGC 3995; Sm,* H II.—The membership of this spiral galaxy in a multiple interacting system is considered the main cause of its enhanced H II region emission spectrum and very blue continuum in the visible (Kennicutt & Keel 1984). Despite the less than optimal signal-to-noise ratio, our UV spectrum is in agreement with the strong H II regions thought to be present in the galaxy. (The UV spectrum contains emission artifacts at 1280, 1290, and 1663 Å). Data in the radio (Hummel et al. 1987b) and in the X-ray (Fabbiano et al. 1982) also support the above picture. Although NGC 3391, NGC 3394, and NGC 3395 are all members of the same group, and are interacting, their response to the interaction must vary, since their spectra are all very different. Thus we are far from a good understanding of interaction-induced star formation.

*ESO 572–34;* H II.—The P Cygni profile of C IV and the broad absorption feature of Si IV indicate the presence of evolved, early-type massive stars, with temperatures hot enough to excite the forbidden nebular emission line C III] λ1909.

*NGC 4102; Sb, LINER* + H II.—NGC 4102 belongs to the Ursa Major galaxy group (Odenwald 1986). This Sb galaxy is a powerful far-infrared galaxy (FIRG) (Young et al. 1989), which appears as a supergiant H II region (Armus et al. 1990). Keel (1983b) classified this galaxy as a LINER because of the presence of optical low-ionization lines. NGC 4102 also has a strong nuclear radio source (Condon et al. 1982). Although the radio emission is attributed by Condon et al. to the supernova remnants associated with a strong burst of star formation, and the radio core is small enough to be included in the *IUE* aperture, the UV spectrum does not resemble that of a starburst galaxy. NGC 4102 appears to be a normal Sb galaxy with some evidence of a medium-age main-sequence turnoff.

*NGC 4111; S0, LINER.*—NGC 4111 is a normal S0 galaxy with an old stellar population (cf. Gregg 1989), showing Mg II and Fe absorption features longward of 2600 Å which are typical of F–G dwarfs. The short-wavelength spectrum is lacking a hot star component (Burstein et al. 1988). Although NGC 4111 has at least eight much fainter companions, they have no apparent effect on the galaxy itself (van der Burg 1985). NGC 4111 is classified as a LINER by Heckman (1980), but there is little evidence of nonthermal activity from the UV spectrum. NGC 4111 may be on the boundary between active and normal galaxies.

*NGC 4194 (Mrk 201); Sm pec, BCG.*—This BCG galaxy shows an unusually flat continuum (see Table 5). While the absorption features of Si IV and C IV (with a possible P Cygni profile of C IV) show the presence of a hot population of massive O and early B stars, the very flat spectrum suggests the presence of a cooler component of A stars. The depth of the Mg II λ2800 feature is greater than expected from our Galaxy and is probably due in part to intrinsic absorption in NGC 4194.

NGC 4194 is a BCG (Thuan & Martin 1981), a radio-loud galaxy (Heckman 1983), and a FIRG (Armus, Heckman, & Miley 1989). The activity is apparently powered by a central burst of star formation that is claimed to be driven by the merging of two galaxies, as evidenced in part by the tidal tail (Joseph & Wright 1985).

*NGC 4214; IABm, starburst.*—NGC 4214 is a metal-deficient blue Magellanic irregular galaxy. In the UV study by Huchra et al. (1983), who have carefully centered the *IUE* aperture on the optical center of the galaxy, the P Cygni profile

of C IV λ1550 was found to be consistent with the strong winds typical of O stars, which produce ~50% of the UV emission, while the absorption features at $\lambda < 1400$ Å show the presence of B stars. The galaxy has a complex physical structure, which can be optically resolved into H II regions and associations. The lack of evolved supergiants and Wolf-Rayet stars in the UV would seem to rule out a decreasing or constant star formation rate, suggesting instead a relatively recent burst of star formation, superposed upon an older population. However, note that Filippenko & Sargent (1991) find Wolf-Rayet features in some locations in NGC 4214. Hartmann, Geller, & Huchra (1986) conclude that the burst of star formation is the result of a merger or strong interaction with a companion. This consideration is based on the differences between the velocity fields of the gas and of the older stellar population of the galaxy.

*NGC 4258 (M106); SBc, LINER.*—This bright, barred spiral galaxy contains two anomalous arms of Hα emission in its inner regions, which also emit in the radio. The radio emission is nonthermal in origin and probably due to the ejection of matter or an explosive event in the nucleus, according to Krause, Beck, & Klein (1984). Based on the strengths and ratios of the optical emission lines, this galaxy has been classified as a LINER, approaching the Seyfert domain (Heckman 1980). The UV continuum does not manifest strong nuclear nonstellar emission. The blue rising branch of the UV, the broad, deep absorption features, and the nebular emission line of C III] λ1909 are all characteristic of H II regions. Ellis et al. (1982) find that NGC 4258 is dominated by B stars, with little contribution from O stars. Barbon, Capaccioli, & Longo (1984) suggest that the UV continuum can be explained by several bursts of star formation at different stages of their evolution. The short- and the long-wavelength spectra do not match up, most likely because the position angles of the 10″ × 20″ *IUE* aperture are not the same.

*NGC 4321; Sbc, hot spot.*—This is the largest spiral in the Virgo Cluster and is another example of a "hot spot" galaxy. The ring, about 13″ in radius, contains four distinct H II regions, where strong star formation is present (Pierce 1986; Arsenault et al. 1988). The UV spectra presented here are of two of these H II regions which are contained in the nuclear region of the galaxy, and have been studied by Panagia et al. (1980). They conclude that the absorption features are mostly due to the interstellar medium present in the halos and in the disks of both our Galaxy and NGC 4321.

*NGC 4350; S0.*—This normal early-type (S0) galaxy has a UV spectrum consistent with its Hubble type, as described in § 1. NGC 4350 belongs to the Virgo Cluster.

*NGC 4382 (M85); S0 pec.*—M85, a gas-poor galaxy of high surface brightness, belongs to the Virgo Cluster and forms a strongly interacting pair with NGC 4394 (Cutri & McAlary 1985). This interaction might explain its bluer visible color in comparison with typical S0 galaxies (Véron & Véron-Cetty 1985), interpreted as due to enhanced star formation in the disk as opposed to star formation in the nucleus. It is a radio-quiet galaxy with an X-ray/optical luminosity of about $1.3 \times 10^{-4}$ (Dressel & Wilson 1985), easily explained as the integrated contribution of low-mass binaries (Trinchieri, Fabbiano, & Canizares 1986). The UV spectrum of the nucleus of this normal galaxy has been studied and synthesized by Rocca-Volmerange & Guiderdoni (1987), who conclude that it has a dominant contribution from F and early G dwarf stars.

*NGC 4385 (Mrk 52); SBas, starburst.*—A large bibliography and an extensive discussion of the UV and optical properties of this galaxy are given in Durret & Tarrab (1988). To summarize, NGC 4385 is a starburst galaxy with plentiful H I and extended H II. It is a typical H II region galaxy, where the ionized gas is concentrated in a central region of a few kiloparsecs and many H II regions are distributed along the spiral arms. The presence of the Wolf-Rayet emission feature at 4650 Å, as well as the possible P Cygni profiles in N V and C IV in the UV, suggest the present of Wolf-Rayet stars. Population synthesis implies that the dominant contribution is given by WN7 and WC8.

*NGC 4388; Sab, Seyfert 2.*—This Seyfert 2 galaxy shows evidence that it harbors an obscured Seyfert 1 nucleus. Corbin, Baldwin, & Wilson (1988) and Pogge (1988) have reported high-ionization gas distributed in two cones, with apices at the nucleus, and extending above and below the disk. Shields & Filippenko (1988) detected broad Hα emission off the nucleus and suggested that this emission originates from an obscured Seyfert 1 broad-line region (BLR) which is reflected into our line of sight by dust in the interstellar medium. The *IUE* spectra were analyzed by Ferland & Osterbrock (1986) and by Kinney et al. (1991a). They both found a steep spectral slope and found that the number of recombination photons is much larger than predicted based on the strength of the ionizing continuum. Thus the UV source in NGC 4388 appears to be occulted from direct view.

*MCG 8-23-35 (Mrk 209); Sm pec, BCDG.*—Mrk 209 is a BCDG undergoing a burst of star formation (Thuan & Martin 1981). The UV spectrum rises toward shorter wavelengths, indicating the presence of hot stars, but lacks prominent features except for strong C III] λ1909 emission. The weakness of absorption features in an object thought to be undergoing star formation may be related to its low metallicity ($Z \sim 0.1\ Z_\odot$; Fanelli et al. 1988), while the strength of the strong C III] emission may be related to the high nebular temperature (Viallefond & Thuan 1983).

*NGC 4449; IBm,* H II.—NGC 4449 is a very blue Magellanic irregular galaxy, containing a large amount of gas, having a complex distribution of H II regions, and undergoing active star formation (Hunter 1982; Bothun 1986). Many of the UV observations of NGC 4449 are concerned with the off-nuclear H II regions (see, e.g., Rosa et al. 1984; Lamb et al. 1986) and with a peculiar supernova remnant (Blair et al. 1984b). Because of this, we have been especially careful to extract only the one short-wavelength and the one long-wavelength *IUE* spectra that were taken with the aperture placed on the galaxy center.

The time evolution of the star formation rate in NGC 4449 is thought to be constant, based on an analysis of the mass, blue luminosity, and the strength of Hα emission (Gallagher et al. 1984) and also based on the strength of the infrared emission (Thronson et al. 1987). From kinematical considerations, Hartmann et al. (1986) conclude that the strong star formation rate is due to a merger or interaction with the dwarf companion DDO 125. The poor match between the short- and the long-wavelength spectra is probably due to the placement of the aperture.

*NGC 4500; SBa, BCG.*—*IRAS* has revealed relatively intense far-infrared emission from this metal-deficient blue compact galaxy [$\log(L_{FIR}/L_{\odot}) = 10.40$; Deutsch & Willner 1987]. Mrk 213 has an intense UV luminosity (Gondhalekar et al. 1984), suggesting a recently triggered burst of star formation. Analysis of the combination of near-IR, visible, and UV observations shows that the burst is superposed on an underlying population of giants from an older population.

Our UV spectrum has a flat continuum with complex absorption features which are easily identified due to the galaxy's redshift. The only possible emission line is Ly$\alpha$; other features are probably due to *IUE* artifacts.

*NGC 4569 (M90); SABab, LINER.*—M90 belongs to the Virgo Cluster and, from properties of the optical emission lines, is classified as a LINER (Stauffer 1982; Keel 1983b). It is a strong emitter at 10 $\mu$m (Scoville et al. 1983), and its emission in the range 1–20 $\mu$m is dominated by dust and starlight, properties typical of normal galaxies (Willner et al. 1985). This object has Fe II absorption and unusually strong Mg II absorption.

*NGC 4579; Sab, LINER.*—NGC 4579 is a double radio source with a flat spectrum and an unresolved core (Hummel et al. 1987b). X-ray emission has also been detected, indicating the presence of a central, nonthermal source (Halpern & Steiner 1983). It has been classified as a LINER and as a dwarf Seyfert 1 (Stauffer 1982; Keel 1983b; Filippenko & Sargent 1985) based on the broad H$\alpha$ emission line. Its UV spectrum has been analyzed by Goodrich & Keel (1986), who found that the galaxy appears stellar in the UV. (The spectra of NGC 4579 presented in this atlas include additional spectra to those analyzed by Goodrich & Keel.) The UV spectrum contains both narrow and broad emission lines, unlike the other LINER in the atlas; this may be related to the fact that NGC 4579 has a double radio source with an unresolved, flat-spectrum radio core. Goodrich & Keel (1986) propose that its UV continuum is similar to the power law seen in Seyfert 2 galaxies, but our spectra suggest instead that the UV continuum is simply that of a spiral galaxy.

*NGC 4594 (M104); Sa, LINER.*—The Sombrero galaxy has in its nucleus both a very compact and strong nonthermal radio source (Shaffer & Marscher 1979; Condon et al. 1982) and a strong X-ray source (Halpern & Steiner 1983). The radio and X-ray emission may be related to the galaxy's activity as a LINER (Heckman 1980; Keel 1983a, b). However, in common with the other LINERs in this atlas, there are no emission lines in the UV. A search for a central massive object by Kormendy (1988) resulted in a velocity dispersion profile consistent with a mass of $M \sim 10^{8.5}$–$10^{9.5}\ M_{\odot}$. The lack of emission features in our UV spectrum indicates that the LINER activity is not strong, while the absorption lines (Mg II $\lambda$2800 and Fe I $\lambda\lambda$2868, 3025) and the shape of the continuum indicate the predominance of an old stellar population (Ellis et al. 1982).

*IC 3639; SBb, Seyfert 2.*—This nearby Seyfert 2 galaxy possesses a strong radio core embedded in diffuse emission, and has a very high surface brightness, so that it resembles NGC 1068, the prototype Seyfert 2 galaxy (Ulvestad & Wilson 1989). The narrow [O III] $\lambda$5007 emission line has a blue asymmetry similar to those seen in NLRGs (Heckman, Miley, & Green 1984), while no such asymmetry is seen in H$\beta$ (Fairall 1985). The UV spectrum is flat, with some weak emission lines (and an emission artifact at 1663 Å).

*UGC 7905S; BCG.*—UGC 7905S is a BCG in strong interaction with its companion UGC 7905N, and this is thought to have triggered the activity of the galaxy (Bushouse 1986). The short-wavelength UV spectrum is steeply rising to short wavelengths with a spurious emission feature at 1820 Å.

*NGC 4670; Am, BCDG.*—NGC 4670 is an amorphous, metal-deficient blue galaxy whose central regions have a spectrum typical of an H II region (Huchra et al. 1983). Its spectrum is very similar to that of NGC 4214, and the same considerations hold in this case, suggesting a relatively recent burst of star formation, with the young stars superposed on a much older population. As in NGC 4214, the *IUE* aperture has been carefully pointed to the optical center of the galaxy (Huchra et al. 1983).

*NGC 4736 (M94); SAab, LINER.*—This galaxy has an expanding ring of H II regions surrounding the nucleus. Studies of the H$\alpha$ emission from the ring (Buta 1988) and the discovery of many discrete compact radio sources similar to those found in M82 and NGC 253 (Duric & Dittmar 1988; Kronberg, Biermann, & Schwab 1985; Antonucci & Ulvestad 1988), explained as bremsstrahlung from H II regions and synchrotron radiation from supernova remnants, confirm that the ring is the site of intense star formation activity. The ring is 50″ from the nucleus, so that it falls outside the *IUE* aperture, and thus the galaxy does not appear as a starburst in the UV.

Studies of the nucleus show that this object is relatively blue and has an extremely high surface brightness (Keel & Weedman 1978). De Bruyn (1977) has reported an extended (5″) radio source centered on the nucleus. The anomalous strength of the CO bands is explained by Walker, Lebofsky, & Rieke (1988) as the result of a very powerful but not recent starburst. The presence of a high percentage of stars as early as A4–A7, as deduced by population synthesis models of the optical spectrum of NGC 4736, is consistent with the picture of past starbursting activity, although the weak lines and blue colors in the optical can be evidence also for a metal-poor population with a hot blue horizontal branch (Pritchet 1977). The presence of low-excitation emission lines led Heckman (1980) and Keel (1983a, b) to classify this galaxy as a LINER. The UV spectrum shows a forbidden emission line (C III] $\lambda$1909) and broad absorption features. The continuum is typical of an Sab galaxy.

*NGC 4748; Seyfert 1.*—IRAS 1249−131 is classified as a Seyfert 1 galaxy from its optical spectrum by Osterbrock & De Robertis (1985), de Grijp et al. (1985), and Carter (1984). It has been alternatively classified as a Seyfert 1.5 by Dahari & De Robertis (1988), on the basis of the scheme by Veilleux & Osterbrock (1987), and as a "narrow-line" Seyfert 1 by Goodrich (1989). Goodrich concluded that NGC 4748 is a Seyfert 1 with a small line-of-sight velocity dispersion in its BLR. The UV spectrum does indeed show emission lines (most notably C IV $\lambda$1550) narrower than those of a typical Seyfert 1 (Kinney et al. 1991b).

*NGC 4826 (M64); Sb, LINER.*—The "Black-Eye" galaxy has a complex emission structure with numerous H II regions and an irregular nuclear low-ionization zone (Keel 1983a). This galaxy is considered a LINER based on optical properties (Keel 1983b; Halpern & Steiner 1983). Like other LINERs,

the radio, X-ray, and far-infrared luminosities of NGC 4826 are typical of normal galaxies (Fabbiano, Gioia, & Trinchieri 1988). The UV spectrum is typical of an Sb galaxy but with a possible emission line of C III] λ1909).

*MCG 6-28-44 (Mrk 54), BCG.*—The strong UV continuum and the complex, broad absorption features suggest that this galaxy is a starburst (cf. Gondhalekar et al. 1984). The strong absorption line of Lyα can be observed because of the relatively high redshift. The nebular emission line [O III] + C II] is evident, while C III] cannot be detected, since its redshifted wavelength lies in the lowest sensitivity region of the *IUE* cameras.

*NGC 4853; S0, BCDG.*—This galaxy is a member of a group with 19 members which traces the central Coma region (Perea, 1986). The UV continuum of this BCDG is flat; the C IV line is the only identifiable absorption feature. The emission at 1940 Å is Si III].

*NGC 4861 + IC 3961 (Mrk 59); Im, BCDG.*—Mrk 59 (NGC 4861 + IC 3961) consists of a dwarf irregular (IC 3961) with a bright knot (NGC 4861) superposed on its southern part, the knot possibly being an H II region or an OB association (Huchra 1977). Our two spectra are taken with different pointings specifically targeting the bright knot (NGC 4861) and the center of the galaxy (IC 3961) separately. Note that Rosa et al. (1984) do not distinguish between the two pointings and refer to them both as NGC 4861. The UV spectrum of this BCDG (Thuan & Martin 1981; French 1980) shows the burst of star formation. The spectrum is dominated by hot stars, which produce a UV excess in the continuum and the strong absorption features which are the signature of O and B stars. The H II region is revealed by the strong C III] nebular emission line.

*NGC 5102; SA0 pec, starburst.*—This low-luminosity galaxy is very blue in the optical and has subsolar metal abundance (Bica & Alloin 1987; Bica 1988; Glass & Moorwood 1984). IR observations (Glass & Moorwood 1984) and population synthesis of the visible spectrum (Bica & Alloin 1987) suggest a burst of star formation, which occurred about $4 \times 10^8$ yr ago. A detailed analysis of the visible spectrum suggests an underlying metal-poor red (old) population; residual weak emission lines and a small H II region continuum contribution agree with the age of the burst (Bica 1988). The spectrum is flat with strong absorption lines typical of mid- to late-B stars.

*NGC 5135; SABb, Seyfert 2.*—NGC 5135 is a high-excitation emission-line galaxy belonging to a group of seven galaxies which are gravitationally bound and lie within 1 Mpc of one another. Tidal interactions may be causally related to the Seyfert 2 activity (Kollatschny & Fricke 1989). From X-ray and radio observations and from the luminosities of the optical emission lines, the nucleus of NGC 5135 has been called a mini–Seyfert 2 (Phillips et al. 1983; Thuan 1984). The UV spectrum shows a dual nature; several narrow emission lines are present, including Lyα, C IV λ1550, and He II λ1640, while absorption features of Si IV λλ1397, 1402 and He II λ1640 are also present. The luminosity of the Seyfert nucleus is sufficiently low that the underlying absorption features of the H II regions (contributing ~25% of the emission; Thuan 1984) are still detectable.

This galaxy has an anomalous ratio of Lyα/Hβ (~5), suggesting the presence of dust or an extinction law for NGC 5135 different from that of our Galaxy (Thuan 1984).

*Mrk 66; BCG.*—This blue compact, low-metallicity galaxy is redshifted enough that its Lyα emission is distinguishable from the geocoronal line. The strong UV continuum, rising to short wavelengths, and the C IV absorption line are typical signatures of massive stars, indicating that Mrk 66 is experiencing active star formation. The *IUE* spectrum of Mrk 66 has been studied by Hartmann et al. (1988), and further comments can be found in their paper.

*NGC 5194 (M51); Sbc, LINER.*—The Whirlpool Nebula forms an interacting system with its companion NGC 5195 (Keel et al. 1985). Heckman (1980) and Baldwin et al. (1981) have classified NGC 5194 as a transition galaxy between a LINER and a Seyfert galaxy because of the presence of broad wings in its optical emission lines. Studies of the radio emission of NGC 5194 show a complex structure of extranuclear bubbles, probably ejected from the nucleus (Ford et al. 1985). However, the composite nuclear activity in the radio does not have a counterpart in the X-ray (Palumbo et al. 1985). The X-ray emission is not concentrated in the nucleus but is extended over the galaxy disk. The X-ray emission is explained by Palumbo et al. (1985) as being due to evolved stellar systems such as X-ray binaries and old starbursts, or to gas outflowing from the nucleus. The UV spectrum does not show evidence of nonthermal activity; except for Si III and C III], there are no other detected emission lines. The presence of a strong absorption feature of Al III λ1857 and the shape of the continuum suggest that the dominant population is A–G stars (Ellis et al. 1982).

*NGC 5236 (M83); SBc, starburst.*—M83 is a nearby, bright southern galaxy which is almost face-on and which belongs to a class of galaxies with an "amorphous" nucleus (Sersic & Pastoriza 1965). M83 is undergoing a burst of star formation in the nucleus and in the spiral arms, possibly triggered by its companion NGC 5253 (Condon et al. 1982). Associated with the star formation is strong emission in the radio (Condon et al. 1982), in the infrared (Telesco & Houper 1980), and in the X-ray (Trinchieri, Fabbiano, & Palumbo 1985). The UV absorption lines, which have a strong similarity to those of NGC 7714, suggest that M83 is a starburst with an evolved population of supergiants, whose signature is the P Cygni profiles of Si IV λλ1397, 1402 and C IV λ1550 (Bohlin et al. 1983). A large number of supernovae have been observed in this galaxy (five since 1923, among which the one detected in the nucleus [1968L]) is a Type II supernova. The association of the Type II supernova with H II regions in the spiral arms and in the nucleus is in agreement with the general scenario of a starburst (Richter & Rosa 1984). Although the UV spectrum does not show a marked 2200 Å dust absorption, observation in optical wavelengths indicates a value for intrinsic $E(B-V) \simeq 0.3$ mag (Pastoriza 1975).

*ESO 383–44; SAd, starburst.*—ESO 383–44 is an Sd spiral with bright knots, which is a member of the IC 4296 group of galaxies (Dodd, Andrews, & Macgillivray 1986). This galaxy has a diffuse, extended H II region powered by OB associations which surrounds a more compact nucleus. The number of stars required compared with their lifetimes indicates intense star formation activity (Meaburn 1983). Although the UV spectrum is noisy, some features are present, such as absorp-

tion of redshifted C IV λ1550, the signature of a hot star population, and Si III emission. The unredshifted absorption lines probably come from our Galaxy.

*NGC 5256; Seyfert 2 + LINER.*—This peculiar galaxy contains two compact nuclei separated by about 4 kpc, thought to be the result of a merger. Both nuclei are included in the *IUE* aperture, and their contributions have been added in the final spectrum. The short-wavelength spectrum of NGC 5256 has been studied by Kollatschny & Fricke (1984). Emission lines of Lyα, C IV, and C III] can be identified in the short-wavelength spectrum, while Mg II can be recognized in the long-wavelength spectrum. The ratios between the emission lines in each of the two nuclei have led to the classification of nucleus **a** as a LINER and nucleus **b** as a Seyfert 2 galaxy.

The galaxy is characterized by a relatively high far-infrared emission [$\log (L_{\rm FIR}/L_\odot) \simeq 11.37$; Soifer et al. 1987], in agreement with the nonthermal activity of the nuclei and the widespread intense star formation across the structure.

Most of the radio emission is concentrated in three spots: two coincide with the two nuclei, while the third one is between the other two. Mazzarella et al. (1988) has tentatively explained this phenomenon as synchrotron emission due to the merging.

*NGC 5253 (Haro 10); Im Am, starburst.*—NGC 5253 is classified as an amorphous galaxy belonging to the NGC 5128 group (Sandage & Brucato 1979). The galaxy is undergoing violent star formation, which may be caused by interaction with the companion galaxy NGC 5236 (Moorwood & Glass 1982). The nucleus is dominated by emission from complex H II regions, as shown by a very blue continuum (Gonzalez-Riestra, Rego, & Zamorano 1987) and by hot star absorption lines in the UV which are typical of these regions (Perola & Tarenghi 1980). The small contribution from supernova remnants in the radio and X-ray, and the low ratio of red giants to supergiants as revealed in the IR, give an upper limit to the age of the present nuclear burst of $10^7$ yr and require that previous bursts must be much older than $10^8$ yr (Moorwood & Glass 1982). The very high signal-to-noise ratio UV spectrum of NGC 5253 shows complex absorption, even in Lyα, and emission lines of Wolf-Rayet stars (Ne IV] λ1486 and He II λ1640).

*UGC 8850 (Mrk 463); Seyfert 2.*—Extensive observations of this double nucleus galaxy in the optical, near-IR, and radio (Mazzarella et al. 1991) and in polarized light (Miller & Goodrich 1990), and studies of its featureless continuum in UV + optical and of its hydrogen lines (Kinney et al. 1991a), suggest that Mrk 463E is probably a dust-obscured Seyfert 1 nucleus. The presence of a large amount of dust surrounding Mrk 463E is also confirmed by the strong far-infrared luminosity of the galaxy [$\log (L_{\rm FIR}/L_\odot) = 11.77$; Sanders et al. 1988]. The nature of Mrk 463W is ambiguous; it could be either a Seyfert 2 nucleus or a powerful starburst.

The extended radio emission and the far-infrared luminosity may be enhanced by the merging process (Mazzarella et al. 1991), as manifested by the tidal tails and by the existence of a small difference in the recession velocity of the two nuclei ($\Delta v \sim 50$ km s$^{-1}$; Hutchings & Neff 1987). The two nuclei are separated by 3 kpc and are both included in the *IUE* slit.

*NGC 5457 (M101); Sc,* H II.—This face-on nearby Sc galaxy has a large angular size (~30′) and is the most luminous member of a rich group. NGC 5457 is tidally interacting with NGC 5474, NGC 5477, and Ho IV, resulting in a distortion of the H I distribution in its outer regions (Davies, Davidson, & Johnson 1980). The most striking X-ray features for this galaxy are in the disk, where several bright and distinct pointlike sources are found, while the nucleus shows only extended and not particularly strong emission. The disk sources are likely to be individual massive binary systems associated with H II regions and OB associations (Trinchieri, Fabbiano, & Romaine 1990). M101 is dominated in the UV by extreme Population I in the form of OB complexes (Hill, Bohlin, & Stecher 1984), which spread from its nucleus to the spiral arms, and of which 1264 have been identified (Hodge et al. 1990). The *IUE* spectrum shows a slowly rising blue continuum with deep absorption features, indicating star formation activity and a mixed stellar population from type O (C IV and Si IV absorption lines) through B (C IV, Si IV, and the lines for λ < 1350 Å) to mid-A (features for λ > 1750 Å).

*NGC 5643; SBc, Seyfert 2.*—The nucleus of this almost face-on barred spiral (Morris et al. 1985) shows high-excitation optical emission lines. These characteristics are suggestive of the nonthermal nuclear activity in Seyfert 2 galaxies. However, its luminosity is lower than that of a "classical" Seyfert 2, and thus it has been classified as a Seyfert 2–like galaxy by Phillips et al. (1983). It is also a strong nuclear radio emitter and an "extreme infrared" galaxy, that is, a galaxy for which the ratio between the IR (80 μm) emission and the *B*-band flux (per logarithmic frequency interval) is up to 250 (Antonucci & Olzewski 1985). The UV spectrum is noisy with very low signal-to-noise ratio in the short-wavelength region, but a few emission lines typical of Seyfert activity are clearly visible, such as C IV, C III], [Ne IV] λ 2424, and, marginally, Mg II.

*Mrk 477; Comp, Seyfert 2.*—Mrk 477 (I Zw 92) is a rare example of a Seyfert 2 galaxy that has displayed variability in the continuum (De Robertis 1987; Kinney et al. 1991a). A companion object lies 50″ from Mrk 477, with tidal tails extending between the two. The number of recombination photons agrees well with the number of photons available to ionize the gas (Kinney et al. 1991a), indicating that the ionizing source is not blocked from direct view. Remarkably, this object seems to have some traits of a Seyfert 1 galaxy, such as continuum variability and a direct view to the ionizing continuum, while at the same time showing characteristics of a Seyfert 2 galaxy, such as a lack of broad emission lines and a high $F_{[\rm O\ III]\ \lambda 5007}/F_\beta$ ratio. The UV continuum is flat with prominent emission lines typical of a Seyfert 2 galaxy.

*NGC 5728; SBb, Seyfert 2.*—Phillips et al. (1983) classified this barred spiral as a Seyfert 2 galaxy, but with emission line intensities lower than those of classical Seyfert 2 galaxies. Like many Seyfert 2 galaxies, NGC 5728 contains a central radio source (Wright 1974). As in NGC 5135, there is a suggestion that the ionization mechanism may be a composite, since there is a low-ionization gas ring around the nucleus whose line ratios indicate ionization by the hot stars contained in the ring (Schommer et al. 1988; Pogge 1989).

In the low signal-to-noise ratio *IUE* spectrum, the lack of absorption features does not allow any conclusions about the star-forming component. The shape of the continuum places NGC 5728 nearer to LINERs than to Seyfert 2 galaxies, with the spectrum of a typical Sb galaxy.

*UGC 9560 (II Zw 70, Mrk 829); Irr Pec, BCDG.*—The

interaction between UGC 9560 and UGC 9562 is probably the cause of the distortion in the spiral structure of the two galaxies (Cutri & McAlary 1985). In agreement with the hypothesis of the existence of a relation between gravitational interaction and abnormal activity, this galaxy shows enhanced emission both in the IR (Cutri & McAlary 1985; Young et al. 1989) and in the radio (Altschuler & Pantoja 1984). The radio emission is the combination of a thermal and a nonthermal component, probably due to a superposition of supernova remnants similar to those seen in M82 (Skillman & Klein 1988). The high signal-to-noise ratio UV spectrum in our atlas shows the usual characteristics of H II region emission, with a flux that is rising toward shorter wavelengths, absorption lines from high-ionization species, and the nebular emission line C III] λ1909 (cf. Rosa et al. 1984).

*NGC 5996 (Mrk 691); SBb, starburst.*—The UV spectrum of this starburst (classified as such by Balzano 1983 on the basis of optical data) is similar to the one of the prototype NGC 7714. Here also Si IV and C IV show P Cygni profiles, a signature of Wolf-Rayet stars. A high far-infrared luminosity confirms the presence of vigorous star formation (Deutsch & Willner 1987). This activity is possibly triggered by the strong interaction with the companion NGC 5994 (Bushouse 1987).

*NGC 6052 (Mrk 297); Cl Irr, starburst.*—NGC 6052 is the probable result of the collision of two galaxies, which might have produced the observed bursts of star formation in clumps in the center of the galaxy (Alloin & Duflot 1979). The *IUE* aperture includes "the central clump, about half of the next two strongest clumps," and a few minor knots (Benvenuti, Casini, & Heidmann 1979; see also Benvenuti et al. 1982a). The UV slope ($F_\lambda \propto \lambda^{-1}$), indicates that the clumps, which are the main contributors to the emitted light, are composed of stars of spectral type from O to A0. Absorption features are present which can be attributed to the galaxy because of their redshift.

*NGC 6217; SBbc, starburst.*—This optically normal galaxy has strong and extended IR emission, with $\log (L_{IR}/L_B) \simeq 1.4$ (Belfort, Mochkovitch, & Dennefeld 1987). However, a large burst of star formation coupled with a small extinction cannot be distinguished from weak star formation with high extinction on the basis of $L_{IR}/L_B$ alone. Other diagnostic tools suggest a current high level of star-forming activity in NGC 6217. VLA radio observations have shown the presence of both an unresolved nuclear source and extended emission (Vila et al. 1990). The extended radio emission has a complex structure concentrated in a few "condensations" and probably is thermal (Hummel, van der Hulst, & Dickey 1984). The similarity of its UV spectrum to that of NGC 7714, with a strong UV emission and the presence of deep absorption features (showing contributions from O to mid-A stars), is evidence of strong star formation activity.

*Mrk 499; BCG.*—This faint, blue compact galaxy shows a nearly stellar core with little visible nebulosity. The UV spectrum of Mrk 499 shows complex absorption features, including strong Lyα absorption as well as P Cygni lines of C IV. Hartmann et al. (1988) surmise that, since the expected stellar Lyα absorption equivalent widths should be much smaller than observed, the galaxy is likely to be surrounded by a substantial cloud of neutral hydrogen.

*Tol 1924−416; BCG.*—The central region of this BCDG is irregular and knotty, and unusually luminous for its type. Tol 1924−416 harbors an extremely blue $\sim 7 \times 10^6$ yr old starburst region plus extended systems of photoionized gas (Bergvall 1985). The UV spectrum is that of a typical starburst galaxy with the continuum rising toward short wavelengths. It is also rich in features: due to the relatively high redshift, Lyα λ1216 is visible; C IV λ1550 has a P Cygni profile; and there is an absorption feature around 1305 Å (Si II + O I) and nebular emission of C III] λ1909. The presence of Mg II λ2800 emission is unusual for a starbursting galaxy. The Mg II absorption at zero redshift is likely due to our Galaxy, consistent with the low Galactic latitude. The internal reddening is indeed $E(B-V) < 0.04$ mag (Iye, Ulrich, & Peimbert 1987). Carswell et al. (1980) have studied the *IUE* spectra of the galaxy, and additional considerations can be found in their paper, such as that the effective spectral type of the OB association ionizing the gas is O4. This galaxy has a low helium content. The gas-to-dust ratio of Tol 1924 − 416 is estimated by Gondhalekar et al. (1986) to be of order $6 \times 10^4$, which is two to three orders of magnitude higher than in large galaxies and about one order of magnitude larger than in high-redshift damped Lyα systems (Fall et al. 1989). Gondhalekar et al. suggest that the high gas-to-dust ratio simply reflects the lack of an evolved population, but this cannot explain the discrepancy between the value they obtain and that of the damped Lyα systems.

*NGC 7130; Sa pec, Seyfert 2 + starburst.*—NGC 7130 is an extremely luminous far-infrared source with a compact radio core (Norris et al. 1990). Both characteristics are related to the Seyfert activity. Thuan (1984) discusses the dual nature of the nucleus of this galaxy as seen in the *IUE* UV spectrum, with both broad absorption lines and blue continuum showing the presence of massive stars and star formation, and the Lyα emission line. Shields & Filippenko (1990) have confirmed the dual nature of the nucleus in optical and IR studies. NGC 7130 is similar to NGC 5135 in having both Seyfert 2 activity and a vigorous star-forming H II region.

*NGC 7250; S/I, starburst.*—This galaxy appears as a interacting double system (Markaryan et al. 1985). The presence of absorption lines typical of hot stars suggests that NGC 7250 has active star formation. However, it is difficult to distinguish absorption features due to the galaxy itself from those of the Milky Way. In addition, the *IUE* camera artifacts are evident here.

*NGC 7496; SBc, Seyfert 2 + H II.*—This barred spiral belongs to the Grus Cluster (Aaronson et al. 1981). It has a very bright nucleus with an intense UV continuum and fairly strong optical emission lines. The nucleus of the galaxy hosts both an H II region (the blue color is also due partly to early-type stars) and Seyfert 2 activity (Véron et al. 1981). It is also an extremely luminous far-infrared galaxy ($L_{FIR} \simeq 7.8 \times 10^{11}$ $L_\odot$), with a compact radio core (Norris et al. 1990). In the UV spectrum the H II region component dominates, with a rising continuum and deep absorption lines, the signature of hot stars. No emission lines are present in the UV.

*NGC 7552; SBbc, starburst.*—NGC 7552 is one of the components of the Grus quartet. The center shows the absorption features of early-type stars, presumably from a burst of recent star formation (Alloin & Kunth 1979). Spectral population synthesis by Bica (1988) indicates a population component younger than $5 \times 10^7$ yr and with solar metallicity. The UV

spectrum, in addition to having many absorption lines from young stars, is rising toward longer wavelengths and also has absorption features between 1850 and 2000 Å of Al II, Al III, Fe II, and Fe III—the latter two are both signs of a dominant A star population. The UV slope of this galaxy is one of the "reddest" of the starbursts, with $F_\lambda \propto \lambda^{+0.3}$. The complex optical spectrum of NGC 7552 has been attributed to the presence of three or four cycles of star formation (Dottori & Pastoriza 1986).

*NGC 7673 (Mrk 325); Cl Irr,* H II.—NGC 7673 is a clumpy irregular galaxy with many regions of star formation, four of which fall in the *IUE* aperture (Benvenuti et al. 1982a). This galaxy has a rich absorption spectrum, the relatively high redshift allowing easy identification. The C IV λ1550 absorption at rest wavelength is due to our Galaxy, but all other features are intrinsic, showing the presence of an early (OB) population in the clumps. The feature at 1670–1690 Å may be a blend of Al II and Fe II, indicating the presence of a stellar population later than B8. Also, the spectrum increases slowly toward shorter wavelengths, showing a nonnegligible contribution from stars later than B, although the OB stars dominate. Benvenuti et al. find that the UV luminosity of each clump is ~100 times that of 30 Doradus, indicating an enormous burst of star formation.

*NGC 7714 (Mrk 538); Sdm pec, starburst.*—NGC 7714 is the prototype starburst galaxy (Weedman et al. 1981). The P Cygni profiles of Si IV and C IV, whose absorption wings are blueshifted by 1000 and 500 km $s^{-1}$, respectively, manifest the presence of an evolved population of massive post–main-sequence stars (Leitherer & Lamers 1991). The burst of star formation is thought to be caused by interaction with the companion NGC 7715. The spectrum shows evidence of dust absorption at 2200 Å. It might be dust intrinsic to NGC 7714, since the extinction from our Galaxy (see Table 1) is not high enough to produce the observed 2200 Å feature.

*NGC 7793; SA(s)d,* H II.—NGC 7793 is a prototype Sd galaxy and the faintest of the five major members of the Sculptor group. As a typical late-type spiral, it is dominated by a disk component and has a much less dominant bulge component. The spectrum of the nucleus of this galaxy is dominated in the UV by the H II regions (see, for example, Rosa et al. 1984) and in the optical by relatively early-type and almost solar metallicity stars (B-A-F mixture; Diaz et al. 1982) coexisting with the older metal-poor population. The H II regions can be seen in the absorption features in the UV spectrum and the nebular C III] λ1909.

The authors acknowledge support from NASA grant NAG5-1675 and from the STScI Directors Research Fund. D. C. was supported by an ESA postdoctoral fellowship. We would like to thank Peter Challis for help in all aspects of this program, and Tania Ruiz for help with the individual objects. A. L. K. would like to thank K. Freeman and the Mount Stromlo Observatory for providing a pleasant and productive research environment. We would like to thank M. Rosa, J. Gallagher, P. Conti, R. R. J. Antonucci, R. Kennicutt, and K. Horne for useful discussions. We would like to thank the referee, A. V. Filippenko, for his thorough reading and detailed comments on this very long paper. This research has made use of the NASA/IPAC Extragalactic Database (NED), which is operated by the Jet Propulsion Laboratory, California Institute of Technology, under contract with NASA.

## REFERENCES

Aaronson, M., Dawe, J. A., Dickens, R. J., Mould, J. R., & Murray, J. B. 1981, MNRAS, 195, 1P
Alloin, D., & Duflot, R. 1979, A&A, 78, L5
Alloin, D., & Kunth, D. 1979, A&A, 71, 335
Alloin, D., & Nieto, J.-L. 1982, A&AS, 50, 491
Altschuler, D. L., & Pantoja, C. A. 1984, AJ, 89, 1531
Antonucci, R. R. J., & Miller, J. S. 1985, AJ, 297, 621
Antonucci, R. R. J., & Olzewski, E. W. 1985, AJ, 90, 2203
Antonucci, R. R. J., & Ulvestad, J. S. 1988, ApJ, 330, L97
Armus, L., Heckman, T. M., & Miley, G. K. 1989, ApJ, 347, 727
———. 1990, ApJ, 364, 471
Arnault, P., Casoli, F., Combes, F., & Kunth, D. 1988, A&A, 205, 41
Arp, H., & Sandage, A. 1985, AJ, 90, 1163
Arsenault, R., Boulesteix, J., Georgelin, Y., & Roy, J.-R. 1988, A&A, 200, 29
Bahcall, J. N., Jannuzi, B. T., Schneider, D. P., Hartig, G. F., Bohlin, R., & Junkkarinen, V. 1991, ApJ, 377, L5
Baldwin, J. A., Phillips, M. M., & Terlevich 1981, PASP, 93, 5
Balzano, V. A. 1983, ApJ, 268, 602
Balzano, V. A., & Weedman, D. W. 1981, ApJ, 243, 756
Barbaro, G., & Olivi, F. M. 1989, ApJ, 337, 125
Barbon, R., Capaccioli, M., & Longo, G. 1984, Mem. Soc. Astron. Italiana, 55, 429
Beckman, J., Ceper, J., Pueto, M., & Munoz Tanon, C. 1987, Rev. Mexicana Astron. Af., 14, 134
Belfort, P., Mochkovitch, R., & Dennefeld, M. 1987, A&A, 176, 1
Benvenuti, P., Casini, C., & Heidmann, J. 1979, Nature, 282, 272
———. 1982a, MNRAS, 198, 825
———. 1982b, Advances in Ultraviolet Astronomy: Four Years of *IUE* Research (NASA CP-2238), 156
Bergvall, N. 1985, A&A, 146, 269
Bertola, F., Casini, C., Bettoni, D., Galletta, G., Noreau, L., & Kronberg, P. P. 1984, AJ, 89, 350
Bertola, F., & Sharp, N. A. 1984, MNRAS, 207, 47
Bica, E. 1988, A&A, 195, 76
Bica, E., & Alloin, D. 1987, A&AS, 70, 281
Blades, J. C., Wheatley, J. M., Panagia, N., Grewing, M., Pettini, M., & Wamsteker, W. 1988a, ApJ, 334, 308
———. 1988b, ApJ, 332, L75
Blair, W. P., Kirshner, R. P., & Raymond, J. C. 1984a, BAAS, 16, 925
Blair, W. P., & Panagia, N. 1987, in Exploring the Universe with the *IUE* Satellite, ed. Y. Kondo (Dordrecht: Reidel), 549
Blair, W. P., Raymond, J. C., Fesen, R. A., & Gull, T. R. 1984b, ApJ, 279, 708
Boesgaard, A. M. Edwards, S., & Heidmann, J. 1982, ApJ, 252, 487
Bohlin, R. C., Cornett, R. H., Hill, J. K., Smith, A. M., & Stecher, T. P. 1983, ApJ, 274, L53
Bohlin, R. C., & Grillmair, C. J. 1988a, ApJS, 66, 209
———. 1988b, ApJS, 68, 487
Bohlin, R. C., Harris, A. W., Holm, A. V., & Gry, C. 1990, ApJS, 73, 413
Bonatto, C., Bica, E., & Alloin, D. 1989, A&A, 226, 23
Bothun, D. G. 1986, AJ, 91, 507
Burks, G. S., York, D. G., Blades, J. C., Bohlin, R. C., & Wamsteker, W. 1991, ApJ, 381, 55
Burstein, D., Bertola, F., Buson, L. M. Faber, S. M., & Lauer, T. R. 1988, ApJ, 328, 440
Burstein, D., Faber, S. M., Gaskell, C. M., & Krumm, N. 1984, ApJ, 287, 586
Burstein, D., & Heiles, C. 1982, AJ, 87, 1165
———. 1984, ApJS, 54, 33
Bushouse, H. A. 1986, AJ, 91, 255
———. 1987, ApJ, 320, 49

Buta, R. 1983, BAAS, 15, 659
———. 1986, ApJS, 61, 631
———. 1988, ApJS, 66, 233
Carico, D. P., Sanders, D. B., Soifer, B. T., Elias, J. H., Matthews, K., & Neugebauer, G. 1988, AJ, 95, 356
Carswell, R. F., Gondhalekar, P. M., Morgan, D., Nandy, K., & Wilson, R. 1980, in Proc. Second European *IUE* Conf. (ESA SP-157; Paris: ESA), 133
Carter, D. 1984, Astronomy Express, 1, 61
Ciani, A., D'Odorico, S., & Benvenuti, P. 1984, A&A, 137, 223
Coleman, G. D., Wu, C.-C., & Weedman, D. W. 1980, ApJS, 43, 393
Condon, J. J. 1987, ApJS, 65, 485
Condon, J. J., Condon, M. A., Grisler, G., & Puschell, J. J. 1982, ApJ, 252, 102
Corbin, M. R., Baldwin, J. A., & Wilson, A. S. 1988, ApJ, 334, 584
Cutri, R. M., & McAlary, C. W. 1985, ApJ, 296, 90
Dahari, O., & De Robertis, M. M. 1988, ApJS, 67, 247
Davidson, K., et al. 1982, ApJ, 253, 696
Davies, R. D., Davidson, G. P., & Johnson, S. C. 1980, MNRAS, 191, 253
Davis, L. E., & Seaquist, E. R. 1983, ApJS, 53, 269
de Bruyn, A. G. 1977, A&A, 54, 491
de Grijp, M. H. K., Miley, G. K., Lub, J., & de Jong, T. 1985, Nature, 314, 240
Deharveng, J. M., Joubert, M., Monnet, G., & Denar, J. 1982, A&A, 106, 16
De Robertis, M. M. 1987, ApJ, 316, 597
De Robertis, M. M., & Osterbrock, D. E. 1986, ApJ, 301, 727
Deutsch, L. K., & Willner, S. P. 1987, ApJS, 63, 803
de Vaucouleurs, G., de Vaucouleurs, A., & Corwin, H. G. 1976, Second Reference Catalogue of Bright Galaxies (Austin: Univ. Texas Press) (RC2)
Diaz, A. I. 1985, Ph.D. thesis, Univ. Sussex
Diaz, A. I., Pagel, B. E. J., Edmunds, M. G., & Phillips, M. M. 1982, MNRAS, 201, 49 P
Diaz, A. I., Prieto, M. A., & Wamsteker, W. 1988, A&A, 195, 53
Dodd, R. J., Andrews, F. P., & Macgillivray, H. T. 1986, Ap&SS, 122, 63
Dottori, H. A. 1983, Ap&SS, 90, 385
Dottori, H., & Pastoriza, M. 1986, Rev. Mexicana Astron. Af., 12, 119
Dressel, L. L., & Wilson, A. S. 1985, ApJ, 291, 668
Dufour, R. J. 1987, in Exploring the Universe with the *IUE* Satellite, ed. Y. Kondo (Dordrecht: Reidel), 577
Dufour, R. J., Garnett, D. R., & Shields, G. A. 1988, ApJ, 332, 752
Dufour, R. J., & Hester, J. J. 1990, ApJ, 350, 149
Duric, N., & Dittmar, M. R. 1988, ApJ, 332, L67
Durret, F., & Bergeron, J. 1986, A&A, 156, 51
Durret, F., & Tarrab, I. 1988, A&A, 205, 9
Eichendorf, W., & Nieto, J.-L. 1984, A&A, 132, 342
Ellis, R. S., Gondhalekar, P. M., & Efstathiou, G. 1982, MNRAS, 201, 223
Elmegreen, D. M. 1981, ApJS, 47, 229
Fabbiano, G. 1989, ARA&A, 27, 87
Fabbiano, G., Feigelson, E., & Zamorani, G. 1982, ApJ, 256, 397
Fabbiano, G., Gioia, I. M., & Trinchieri, G. 1988, ApJ, 324, 749
Fabbiano, G., & Trinchieri, G. 1987, ApJ, 315, 46
Fairall, A. P. 1985, Observatory, 105, 129
Fall, M. S., Pei, Y. C., & MacMahon, R. G. 1989, ApJ, 341, L5
Fanelli, M. N., O'Connell, R. W., Burstein, D., & Wu, C.-C. 1990, ApJ, 364, 272
———. 1992, ApJS, 82, 197
Fanelli, M. N., O'Connell, R. W., & Thuan, T. X. 1987, ApJ, 321, 768
———. 1988, ApJ, 334, 665
Feibelman, W. A., Oliversen, N. A., Nichols-Bohlin, J., & Barhart, M. P. 1988, *IUE* Spectral Atlas of Planetary Nebulae, Central Stars and Related Objects (NASA RP-1203)
Ferland, G. J., & Osterbrock, D. E. 1986, ApJ, 300, 658 (FO86)
Ferland, G. J., & Netzer, H. 1983, ApJ, 264, 105
Filippenko, A. V., & Sargent, W. L. W. 1985, ApJS, 57, 503
———. 1988, ApJ, 324, 134
Filippenko, A. V., & Sargent, W. L. W. 1991, IAU Symp. 143, Wolf-Rayet Stars and Interrelations with Other Massive Stars in Galaxies, eds. K. A. van der Hucht & B. Hydaat (Dordrecht: Kluwer), 655
Fitzpatrick, E. L. 1986, AJ, 92, 1068
Ford, H. C., Crane, P. C., Jacoby, G. H., Lawrie, D. G., & van der Hulst, J. M. 1985, ApJ, 293, 132
French, H. B. 1980, ApJ, 240, 41
Gallagher, J. S., III, & Hunter, D. A. 1987, AJ, 94, 43
Gallagher, J. S., III, Hunter, D. A., & Tutukov, A. V. 1984, ApJ, 284, 544
Garcia-Vargas, M. L., Diaz, A. I., Terlevich, R., & Terlevich, E. 1989, Ap&SS, 157, 125
———. 1990, Ap&SS, 171, 65
Gehrz, R. D., Sramek, R. A., & Weedman, D. W. 1983, ApJ, 267, 551
Gerin, M., Nakai, N., & Combes, F. 1988, A&A, 203, 44
Glass, I. S., & Moorwood, A. F. M. 1984, Observatory, 104, 231
Gondhalekar, P. M., Morgan, D. H., Dopita, M., & Ellis, R. S. 1986, MNRAS, 219, 505
Gondhalekar, P. M., Morgan, D. H., Dopita, M., & Phillips, A. P. 1984, MNRAS, 209, 59
Gonzalez-Riestra, R., Rego, M., & Zamorano, J. 1987, A&A, 186, 64
Goodrich, R. W. 1989, ApJ, 342, 224
Goodrich, R. W., & Keel, W. C. 1986, ApJ, 305, 148
Gordon, D., & Gottesmann, S. T. 1981, AJ, 86, 161
Gregg, M. D. 1989, ApJ, 337, 45
Greggio, L., & Renzini, A. 1990, ApJ, 364, 35
Halpern, J. P., & Steiner, J. E. 1983, ApJ, 269, L37
Harnett, J. I. 1987, MNRAS, 227, 887
Hartmann, L. W., Geller, M. J., & Huchra, P. J. 1986, AJ, 92, 1278
Hartmann, L. W., Huchra, J. P., & Geller, M. J. 1984, ApJ, 287, 487
Hartmann, L. W., Huchra, J. P., Geller, M. J., O'Brien, P., & Wilson, R. 1988, ApJ, 326, 101
Heck, A., Egret, D., Jaschek, M., & Jaschek, C. 1984, A&AS, 57, 213
Heckman, T. M. 1980, A&A, 87, 152
———. 1983, ApJ, 268, 628
Heckman, T. M., & Balick, B. 1980, A&A, 83, 100
Heckman, T. M., Miley, G. K., & Green, R. F. 1984, ApJ, 281, 525
Heckman, T. M., van Breugel, W., Miley, G. K., & Butcher, H. R. 1983, AJ, 88, 1077
Heisler, J., & Ostriker, J. P. 1988, ApJ, 325, 103
Hill, J. K., Bohlin, R. C., & Stecher, T. P. 1984, ApJ, 277, 542
Hodge, P. 1985, PASP, 97, 1065
Hodge, P. W., Gurwell, M., Goldader, J. D., & Kennicutt, R. C. 1990, ApJS, 73, 661
Huchra, J. P. 1977, ApJS, 35, 171
Huchra, J. P., Geller, M. J., Gallagher, J., Hunter, D., Hartmann, L., Fabbiano, G., & Aaronson, M. 1983, ApJ, 274, 125
Huchra, J. P., Wyatt, W. F., & Davis, M. 1982, AJ, 87, 1628
Huchtmeier, W. K., & Richter, O. G. 1988, A&A, 203, 237
Hummel, E., Fanti, C., Parma, P., & Schilizzi, R. T. 1982, A&A, 114, 400
Hummel, E., van der Hulst, J. M., & Dickey, J. M. 1984, A&A, 134, 207
Hummel, E., van der Hulst, J. M., & Keel, W. C. 1987a, A&A, 172, 32
Hummel, E., van der Hulst, J. M., Keel, W. C., & Kennicutt, R. C., Jr. 1987b, A&AS, 70, 517
Humphreys, R. M., Blaha, C., D'Odorico, S., Gull, T. R., & Benvenuti, P. 1984, ApJ, 278, 124
Hunter, D. A. 1982, ApJ, 260, 81
Hunter, D., & Gallagher, J. S., III. 1985, ApJS, 58, 533
———. 1986, PASP, 98, 5
Hunter, D., Gallagher, J. S., III, Rice, W. L., & Gillet, F. C. 1989a, ApJ, 336, 152
Hunter, D. A., Thronson, H. A., Casey, S., & Harper, D. A. 1989b, ApJ, 341, 697
Hutchings, J. B., & Neff, S. G. 1987, AJ, 97, 1306
Israel, F. P. 1988, A&A, 194, 24
Israel, F. P., & de Bruyn, A. G. 1988, A&A, 198, 109
Israel, F. P., & van Driel, W. 1990, A&A, 236, 323
Iye, M., Ulrich, M.-H., Peimbert, M. 1987, A&A, 186, 84
Iyengar, K. V. K., Rengarajan, T. N., & Verma, R. P. 1985, A&A, 148, 43
Joseph, R. D., Meikle, W. P. S., Robertson, N. A., & Wright, G. S. 1984, MNRAS, 209, 111
Joseph, R. D., & Wright, G. S. 1985, MNRAS, 214, 87
Joseph, R. D., Wright, G. S., & Prestwich, A. H. 1986, in Proc NASA, ESA, and SERC Int. Symp. (ESA SP-263; Paris; ESA), 597
Joy, M., Lester, D. F., Harvey, P. M., Telesco, C. M., Decher, R., Rickard, L. J., & Bushouse, H. 1989, ApJ, 339, 100

Karachentseva, V. E., Karachentsev, I. D., & Borngen, F. 1985, A&AS, 60, 213
Kawara, K., Nishida, M., & Gregory, B. 1990, ApJ, 352, 433
Keel, W. C. 1983a, ApJ, 268, 632
———. 1983b, ApJ, 269, 466
Keel, W. C. 1983c, ApJS, 52, 229
———. 1984, ApJ, 282, 75
Keel, W. C., Kennicutt, R. C., Jr., Hummel, E., & van der Hulst, J. M. 1985, AJ, 90, 708
Keel, W. C., & Weedman, D. W. 1978, AJ, 83, 1
Kellermann, K. I., Shaffer, D. B., Pauliny-Toth, I. I. K., Preuss, E., & Witzel, A. 1976, ApJ, 210, L121
Kennicutt, R. C., Jr., & Keel, W. C. 1984, ApJ, 279, L5
Kinney, A. L., Antonucci, R. R. J., Ward, M. J., Whittle, M., & Wilson, A. S. 1991a, ApJ, 377, 100
Kinney, A. L., Bohlin, R. C., Blades, J. C., & York, D. G. 1991b, ApJS, 75, 645
Kinney, A. L., Bohlin, R. C., & Neill, J. D. 1991c, PASP, 103, 665
Kinney, A. L., Bregman, J. N., Huggins, P. J., Glassgold, A. E., & Cohen, R. D. 1984, PASP, 96, 398
Koeppen, J., & Aller, L. H. 1987, in Exploring the Universe with the *IUE* Satellite, ed. Y. Kondo (Dordrecht: Reidel), 589
Kollatschny, W., Biermann, P., Fricke, K. J., Huchmeier, W., & Witzel, A. 1983, A&A, 119, 80
Kollatschny, W., & Fricke, K. J. 1984, A&A, 135, 171
———. 1986, IAU Symp. 121, Observational Evidences of Activity of Galaxies, ed. E. Khachikian, G. Melnick, & K. Fricke (Dordrecht; Reidel), 377
———. 1989, A&A, 219, 34
Kormendy, J. 1988, ApJ, 335, 40
Krause, M., Beck, R., & Klein, R. 1984, A&A, 138, 385
Kronberg, P. P., Biermann, P., & Schwab, F. R., 1985, ApJ, 291, 693
Kunth, D., & Joubert, M. 1985, A&A, 142, 411
Kunth, D., Maurogordato, S., & Vigroux, L. 1988, A&A, 204, 10
Kunth, D., & Sargent, W. L. W. 1981, A&A, 101, L5
———. 1983, ApJ, 273, 81
Kunth, D., & Schild, H. 1986, A&A, 169, 71
Lamb, S. A., Bushouse, H. A., & Towns, J. W. 1989, BAAS, 21, 1163
Lamb, S. A., Gallagher, J. S., Hjellming, M. S., & Hunter, D. A. 1985, ApJ, 291, 63
Lamb, S. A., Hunter, D. A., & Gallagher, J. S. 1986, in Star Formation in Galaxies, ed. J. C. Lonsdale Persson (NASA CP-2466), 259
Leitherer, C., & Lamers, H. J. G. L. M. 1991, ApJ, 373, 89
Lequeux, J., Maucherat-Joubert, M., Deharveng, J. M., & Kunth, D. 1981, A&A, 103, 305
Longo, G., Capaccioli, M., & Ceriello, A. 1991, A&AS, 90, 375
Lorre, J. J. 1978, ApJ, 222, L99
Marcelin, M., & Gondoin, P. 1983, A&AS, 51, 353
Markaryan, B. E., Erastova, L. K., Lipovetskii, V. A., Stepanyan, Dzh. A., & Shapovalova, A. I. 1985, Astrofizika, 22, 215
Markert, T. H., & Rallis, A. D. 1983, ApJ, 275, 571
Mas-Hesse, J. M., Arnault, P., & Kunth, D. 1989, Ap&SS, 157, 131
Massey, P., Hutchings, J. B., & Bianchi, L. 1985, AJ, 90, 2239
Mazzarella, J. M., & Balzano, V. A. 1986, ApJS, 62, 751
Mazzarella, J. M., Gaume, R. A., Aller, H. D., & Hughes, P. A., 1988, ApJ, 333, 168
Mazzarella, J. M., Gaume, R. A., Soifer, B. T., Graham, J. R., Neugebauer, G., Matthews, K. 1991, AJ, 102, 1241
Meaburn, J. 1983, A&A, 122, 111
Meaburn, I., & Terret, D. L. 1982, MNRAS, 200, 1
Meurer, G. R., Cacciari, C., & Freeman, K. C. 1990, AJ, 99, 1124
Meurer, G. R., Freeman, K. C., Dopita, M. A., & Cacciari, C. 1992, AJ, 103, 60
Miller, J. S., & Goodrich, R. W. 1990, ApJ, 355, 456
Moorwood, A. F., & Glass, I. S. 1982, A&A, 115, 84
Moorwood, A. F., & Oliva, E. 1988, A&A, 203, 278
Morris, S., Ward, M., Whitle, M., Wilson, A. S., & Taylor, K. 1985, MNRAS, 216, 193
Morris, S. L., Weymann, R. J., Savage, B. D., & Gilliland, R. L. 1991, ApJ, 377, L20
Morton, D. C., York, D. G., & Jenkins, E. B. 1989, ApJS, 68, 449
Mouri, H., Taniguchi, Y., Kawara, K., & Nishida, M. 1989, ApJ, 346, L73
Netzer, H., Kollatschny, W., & Fricke, K. J. 1987, A&A, 171, 61
Neugebauer, G., Becklin, E. E., Oke, J. B., & Searle, L. 1976, ApJ, 205, 29
Noreau, L., & Kronberg, P. P. 1985a, JRAS Canada, 79, 239
———. 1985b, BAAS, 17, 757
———. 1987, AJ, 93, 1045
Norris, R. P., Allen, D. A., Sramek, R. A., Kesteven, M. J., & Troup, E. R. 1990, ApJ, 359, 291
Nussbaumer, H., Schmutz, W., Smith, L. J., & Willis, A. J. 1982, A&AS, 47, 257
Odenwald, S. F. 1986, ApJ, 310, 86
Oka, S., Wakamatsu, K., Sakka, K., Nishida, M., & Jugaku, J. 1974, PASJ, 26, 289
Osterbrock, D. E., & Cohen, R. D. 1982, ApJ, 261, 64
Osterbrock, D. E., & De Robertis, M. M. 1985, PASP, 97, 1129
Palumbo, G. G. C., Fabbiano, G., Fransson, C., & Trinchieri, G. 1985, ApJ, 298, 259
Panagia, N., Vettolani, G., Palumbo, G. G. C., Benvenuti, P., & Macchetto, F. 1980, The Universe at Ultraviolet Wavelengths: First Two Years of *IUE* (NASA CP-2171), 725
Panek, R. J., & Savage, B. D. 1976, ApJ, 206, 167
Pastoriza, M. G. 1975, PASP, 33, 178
Paturel, G., Fouque, P., Bottinelli, L., & Gouguenheim, L. 1989, A&AS, 80, 299 (CPG)
Peimbert, M., & Torres-Peimbert, S. 1981, ApJ, 245, 845
Pence, W. 1976, ApJ, 203, 39
Perea, J., Moles, M., & del Olmo, A. 1986, MNRAS, 219, 511
Perola, G. C., & Tarenghi, M. 1980, in Proc. Second European *IUE* Conf. (ESA SP-157; Paris: ESA), 259
Pettini, M., et al. 1982, MNRAS, 199, 409
Phillips, M. M., Charles, P. A., & Baldwin, J. A. 1983, ApJ, 266, 485
Phillips, M. M., Pagel, B. E. J., Edmunds, M. G., & Diaz, A. I. 1984, MNRAS, 210, 701
Pierce, M. J. 1986, AJ, 92, 285
Pogge, R. W. 1988, ApJ, 332, 702
———. 1989, ApJ, 345, 730
Prieto, M., Battaner, E., Sanchez, C., & Beckman, J. 1985, A&A, 146, 297
Pritchet, C. 1977, ApJS, 35, 397
Raymond, J. C., Blac, J. H., Dupree, A. K., Hartmann, L., & Wolff, R. S. 1980, ApJ, 238, 881
Reichert, G. A., Branduardi-Raymont, G., Filippenko, A. V., Mason, K. O., Puchnarewicz, E. M., & Wu, C.-C. 1992, ApJ, 387, 536
Richter, O.-G., & Rosa, M. 1984, A&A, 140, L1
Rocca-Volmerange, B., & Guiderdoni, B. 1987, A&A, 175, 22
Rosa, M., Joubert, M., & Benvenuti, P. 1984, A&AS, 57, 361
Sandage, A., & Brucato, R. 1979, AJ, 84, 472
Sandage, A., & Tammann, G. 1975, ApJ, 196, 313
———. 1987, Revised Shapley-Ames Catalog of Bright Galaxies (Carnegie Inst. Washington Publ., No. 635) (RSA)
Sanders, D. B., & Mirabel, I. F. 1985, ApJ, 298, L31
Sanders, D. B., Soifer, B. T., Elias, J. H., Neugebauer, G., & Matthews, K. 1988, ApJ, 328, L35
Schommer, R. A., Caldwell, N., Wilson, A. S., Baldwin, J. A., Phillips, M. M., Williams, T. B., & Turtle, A. J. 1988, ApJ, 324, 154
Scoville, N. Z., Becklin, E. E., Young, J. S., & Capps, R. W. 1983, ApJ, 271, 512
Seaquist, E. R., & Bell, M. B. 1968, Nature, 219, 1032
Searle, L., & Sargent, W. L. 1970, ApJ, 162, L155
Seaton, M. J. 1979, MNRAS, 187, 73P
Sersic, J. L., & Pastoriza, M. G. 1965, PASP, 77, 287
Shaffer, D. B., & Marscher, A. P. 1979, ApJ, 233, L105
Shields, J. C., & Filippenko, A. V. 1988, ApJ, 332, L55
———. 1990, AJ, 100, 1034
Simons, D. A., DePoy, D. L., Becklin, E. E., Capps, R. W., Hodapp, K.-W., & Hall, N. B. 1988, ApJ, 335, 126
Skillman, E. D., & Klein, U. 1988, A&A, 199, 61
Snijders, M. A. J., Netzer, H., & Boksenberg, A. 1986, MNRAS, 222, 549
Soifer, B. T., Sanders, D. B., Madore, B. F., Neugebauer, G., Danielson, G. E., Elias, J. H., Lonsdale, C. J., & Rice, W. L. 1987, ApJ, 320, 238
Stauffer, J. S. 1982, ApJ, 262, 66
Tacconi, L. J., & Young, J. S. 1985, ApJ, 290, 602
Telesco, C. M., & Gatley, I. 1984, ApJ, 284, 557
Telesco, C. M., & Houper, D. A. 1980, ApJ, 235, 392
Thronson, H. A., Hunter, D. A., Telesco, C. M., Harper, D. A., & Decher, R. 1987, ApJ, 317, 180

Thuan, T. X. 1984, ApJ, 281, 126
Thuan, T. X., & Martin, G. E. 1981, ApJ, 247, 823
Thuan, T. X., & Seitzer, P. O. 1979, ApJ, 231, 327
Trinchieri, G., Fabbiano, G., & Canizares, C. R. 1986, ApJ, 310, 637
Trinchieri, G., Fabbiano, G., & Palumbo, G. G. C. 1985, ApJ, 290, 96
Trinchieri, G., Fabbiano, G., & Peres, G., 1988, ApJ, 325, 531
Trinchieri, G., Fabbiano, G., & Romaine, S. 1990, ApJ, 356, 110
Tully, R. B. 1980, ApJ, 237, 390
Turnrose, B. E., & Thompson, R. W. 1984, *International Ultraviolet Explorer* Image Processing Information Manual, Version 2.0
Ulrich, M.-H. 1980, MNRAS, 230, 121
Ulvestad, J. S., & Wilson, A. S. 1989, ApJ, 343, 659
van der Burg, G. 1985, A&AS, 62, 147
van der Kruit, P. C. 1971, A&A, 15, 110
van der Kruit, P. C., & de Bruyn, A. G. 1976, A&A, 48, 373
van Moorsel, G. A. 1983, A&AS, 54, 1
Veilleux, S., & Osterbrock, D. E. 1987, ApJS, 63, 295
Véron, P., Véron, M. P., Bergeron, J., & Zuidervijk, E. J. 1981, A&A, 97, 71
Véron, P., & Véron-Cetty, M.-P. 1985, A&A, 145, 433
Véron-Cetty, M.-P., & Véron, P. 1986, A&AS, 65, 291
Véron-Cetty, M.-P., & Véron, P. 1986, A&AS, 66, 335
Viallefond, F., & Thuan, T. X. 1983, ApJ, 269, 444
Vila, M. B., Pedlar, A., Davies, R. D., Hummel, E., & Axon, D. J. 1990, MNRAS, 242, 379
Walborn, N. R., Nichols-Bohlin, J., & Panek, R. J. 1985, *International Ultraviolet Explorer* Atlas of O-Type Spectra from 1200 to 1900 Å (NASA RP-1155)
Walker, C. E., Lebofsky, M. J., & Rieke, G. H. 1988, ApJ, 325, 687
Walker, M. F., & Chincarini, G. 1967, ApJ, 147, 416
Walsh, J. R., Nandy, K., Thompson, G. I., & Meaburn, J. 1986, MNRAS, 220, 453
Weedman, D. W. 1972, ApJ, 171, 5
Weedman, D. W., Feldman, F. R., Balzano, V. A., & Ramsey, L. W. 1981, ApJ, 248, 105
Welsh, G. A. 1982, ApJ, 259, 77
Willner, S. P., Elvis, M., Fabbiano, G., Lawrence, A., & Ward, M. J. 1985, ApJ, 299, 443
Wolfe, A. 1987, in QSO Absorption Lines: Probing the Universe, ed. J. C. Blades, D. A. Turnshek, & C. A. Norman (Cambridge: Cambridge Univ. Press)
Wolstencroft, R. D., Tully, R. B., & Perley, R. A. 1984, MNRAS, 207, 889
Wright, A. E. 1974, MNRAS, 67, 273
Wu, C.-C., Crenshaw, D. M., Blackwell, J. H. Jr., Wilson-Diaz, D., Schiffer, F. H., Burstein, D., Fanelli, M. N., & O'Connell, R. W. 1991, *IUE* Ultraviolet Spectral Atlas (NASA Newsletter No. 43)
York, D. G., Caulet, A., Rybski, P., Gallagher, J., Blades, J. C., Morton, D. C., & Wamsteker, W. 1990, ApJ, 351, 412
Young, J. S., Xie, S., Kenney, J. D. P., & Rice, W. L. 1989, ApJS, 70, 699
Zamorano, J., & Rego, M. 1986, A&A, 170, 31
Zwicky, F., & Zwicky, M. A. 1971, A Catalogue of Selected Compact Galaxies and of Post-eruptive Galaxies, ed. L. Speich (Guemligen: F. Zwicky)

(FIGS. 8–112 follow)

FIGS. 8–112.—Spectra of 105 of the 143 galaxies. The gross FN is shown at the bottom of each plot as a solid line; the background is a dotted line. Regions dropped from the co-addition due to contamination or saturation are the regions of lower FN in both the gross and the background. Above the gross and background FN, 1 $\sigma$ is plotted as a percentage of the total flux. Just above, absorption lines which are known to originate from our Galaxy are indicated. The spectrum itself is plotted in units of ergs $cm^{-2}\ s^{-1}\ \AA^{-1}$. A horizontal bar is drawn at the top of the plot with the location of typical features in both absorption and emission seen in star-forming galaxies. Camera artifacts are marked with an A.

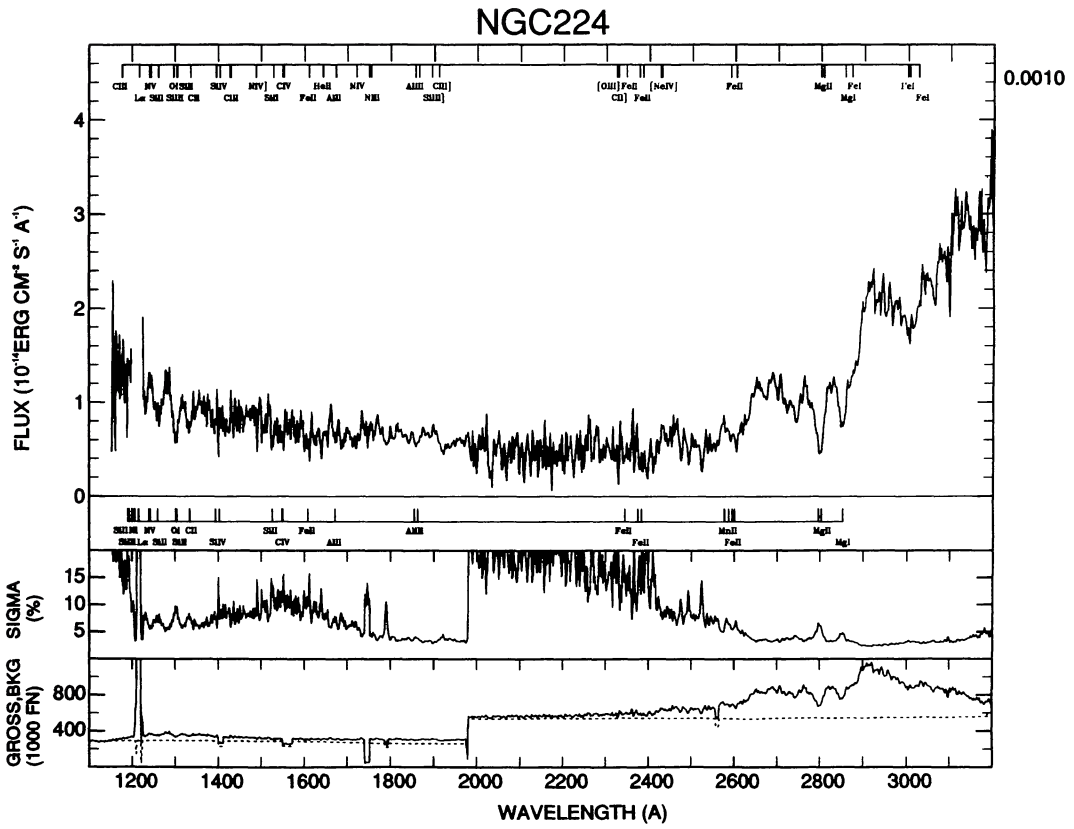


FIG. 8

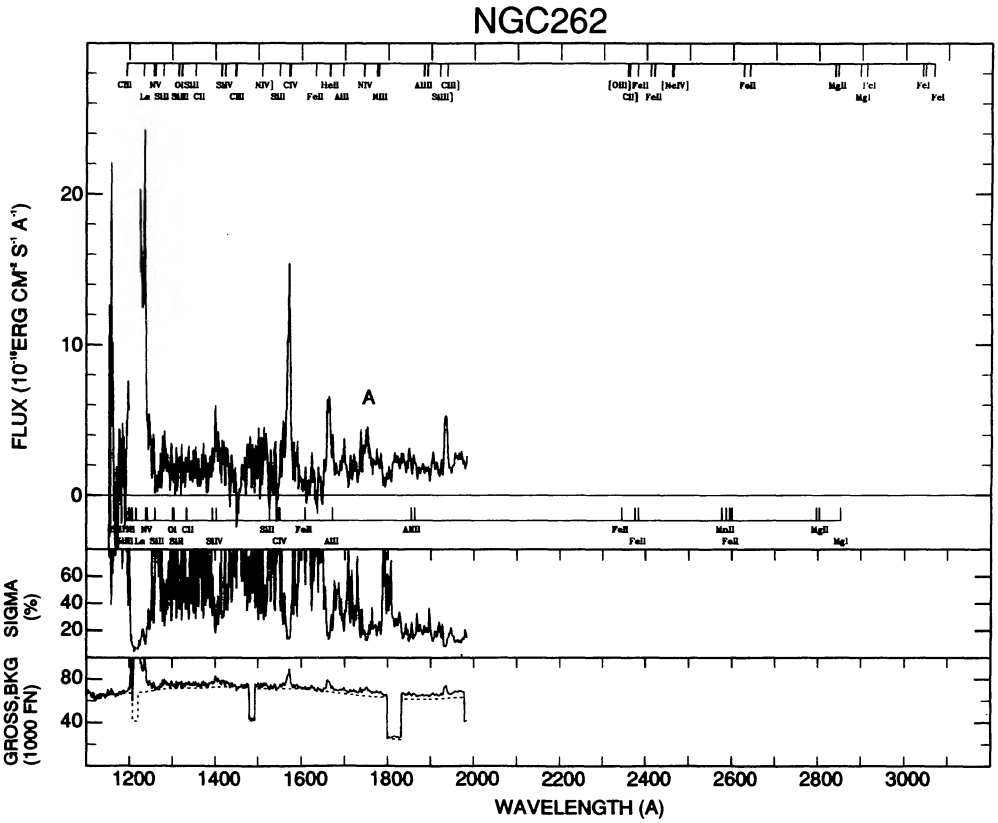


FIG. 9

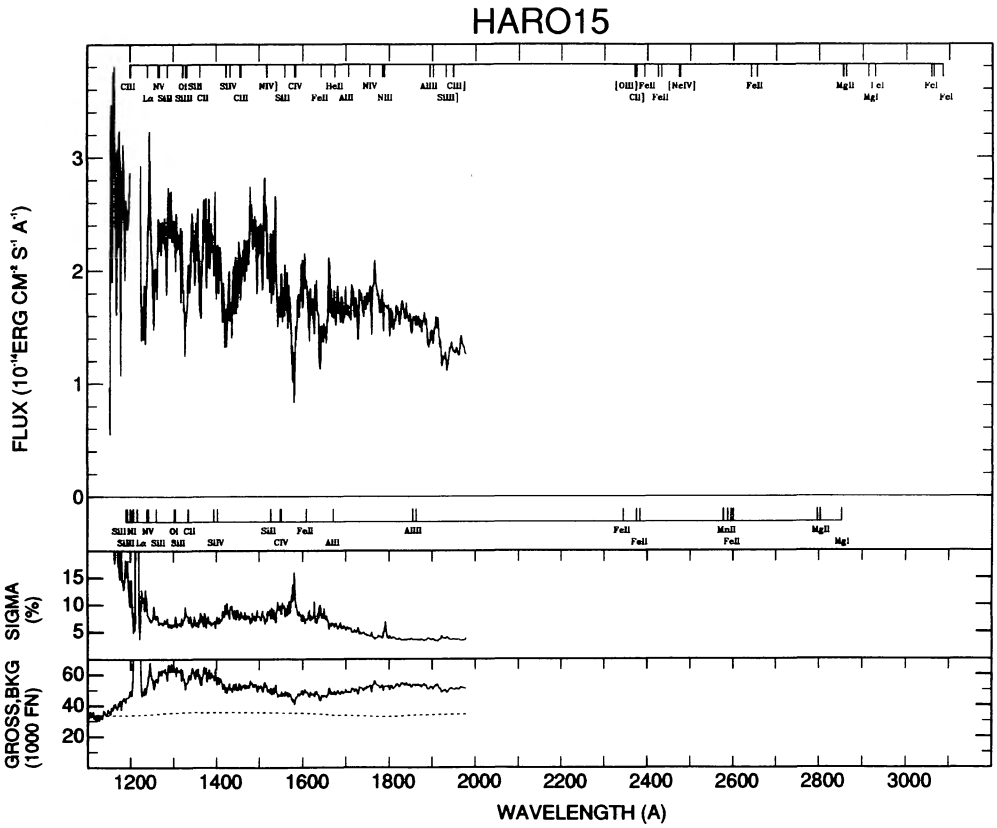


FIG. 10

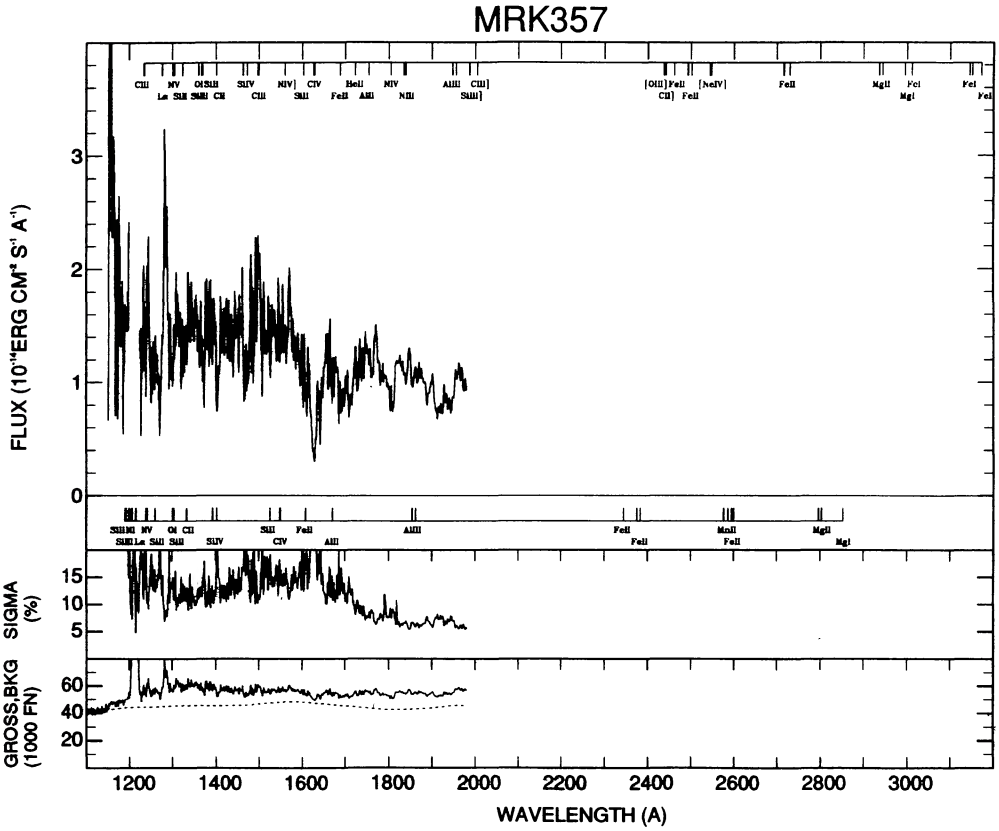


FIG. 11

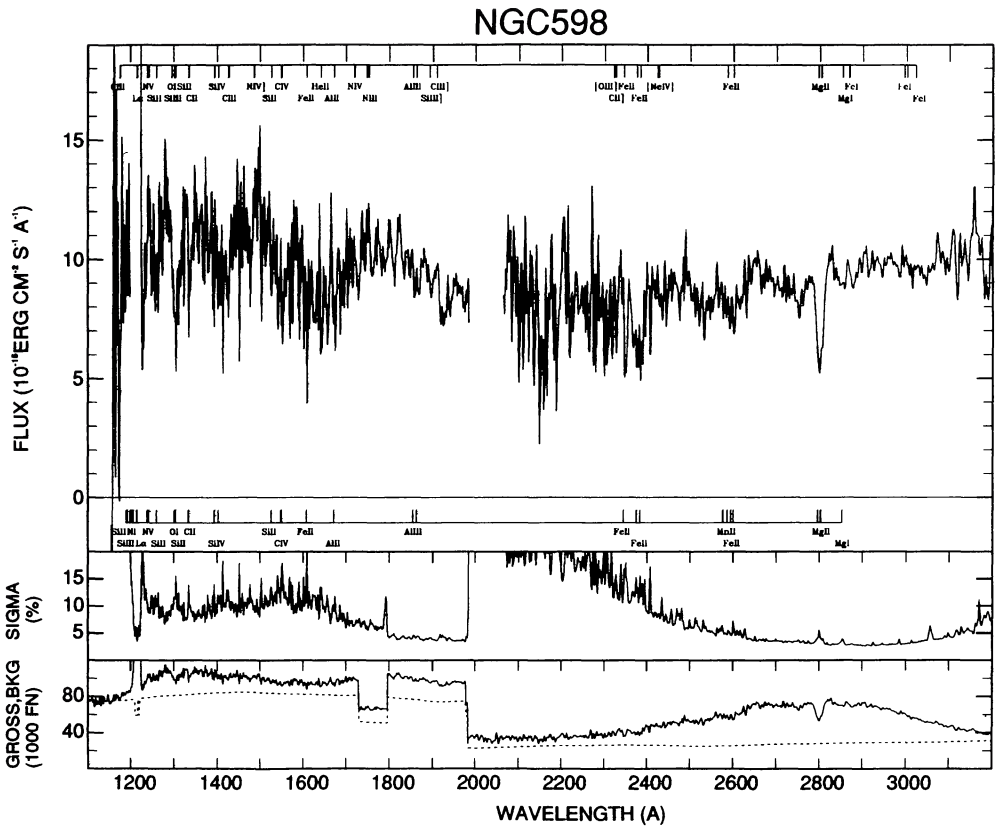


FIG. 12

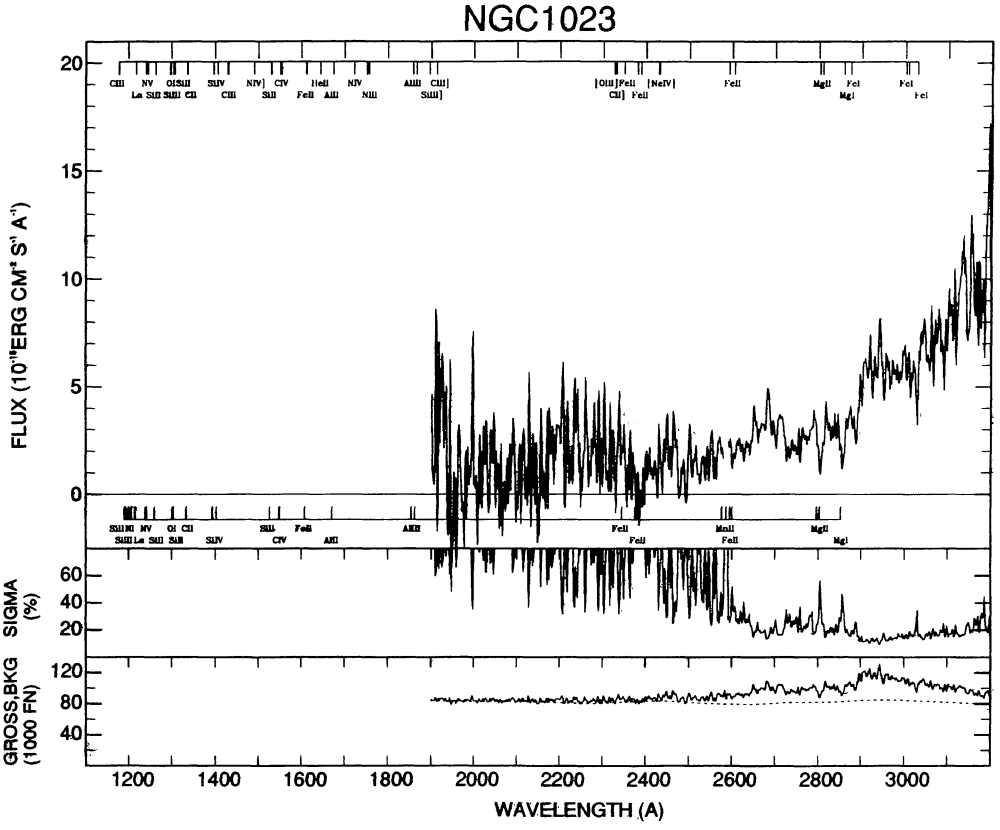


FIG. 13

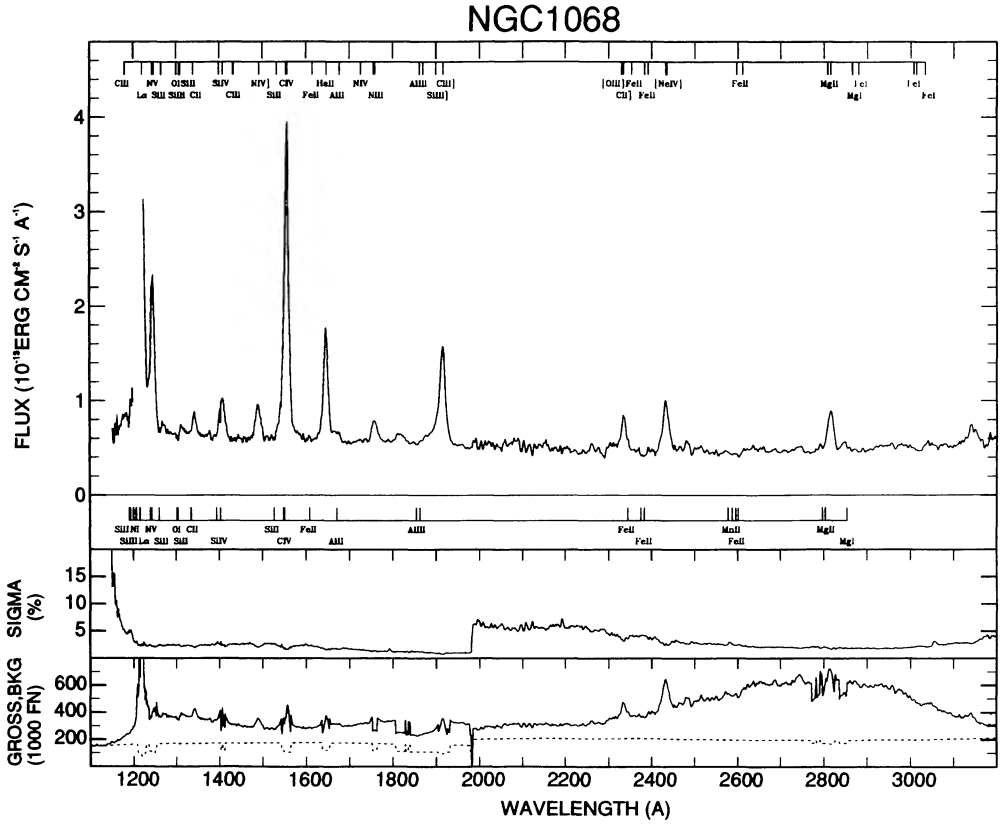


FIG. 14

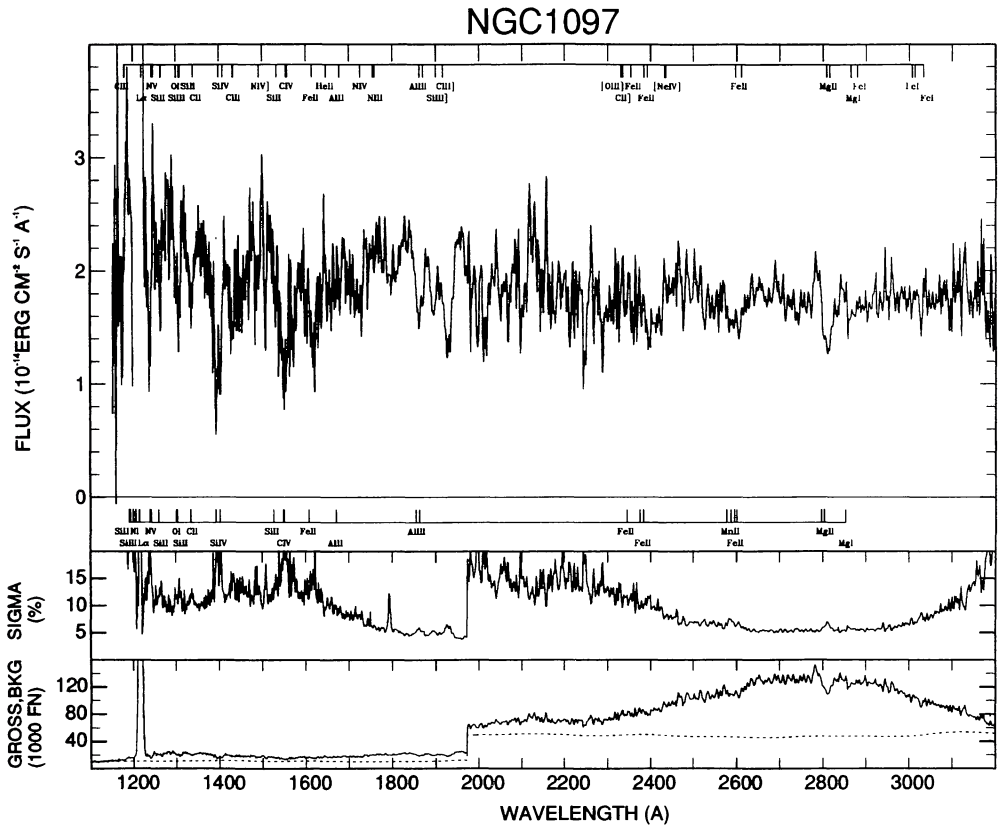


FIG. 15

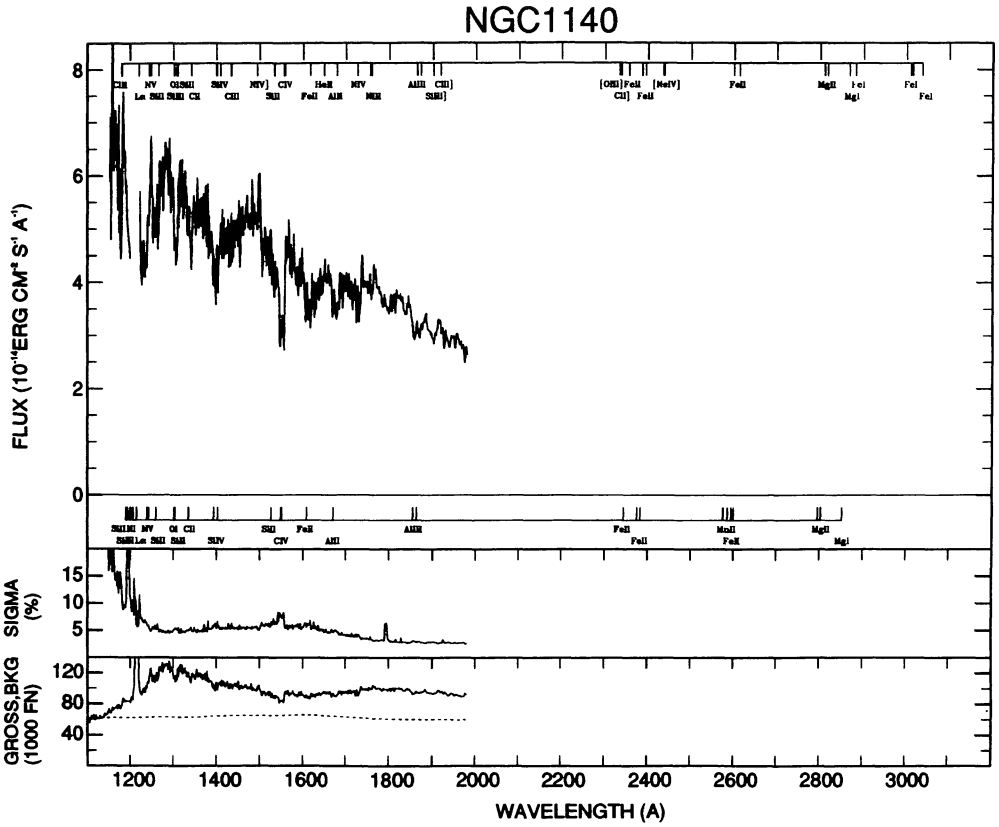


FIG. 16

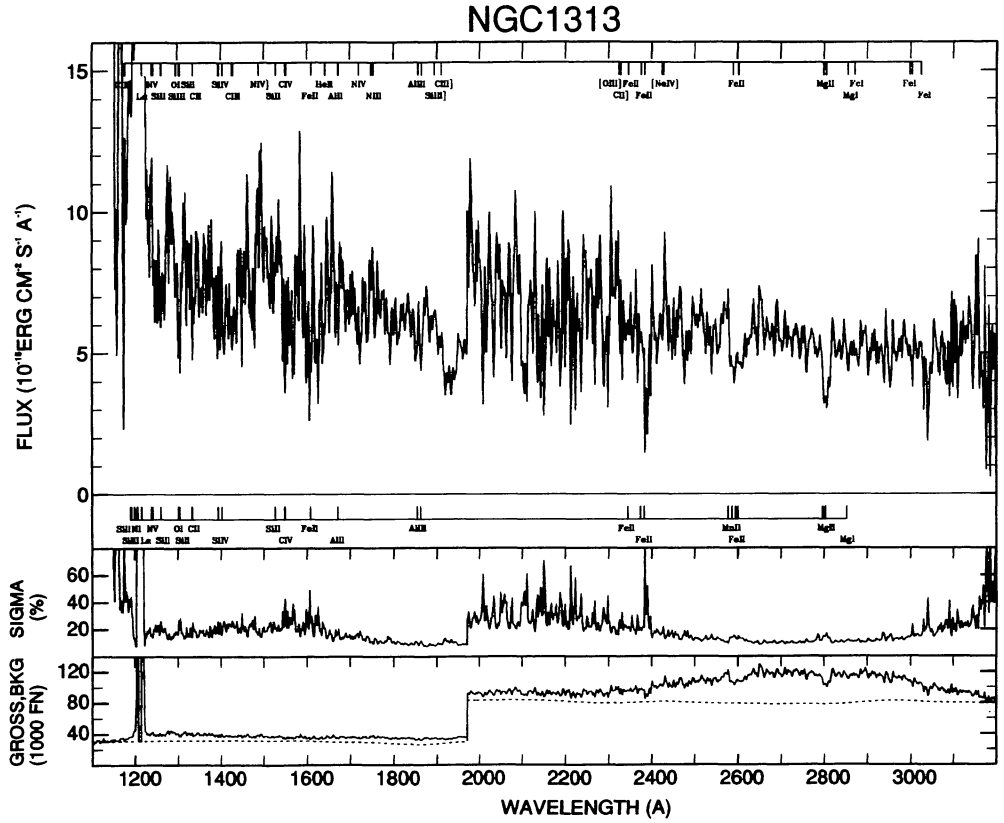


FIG. 17

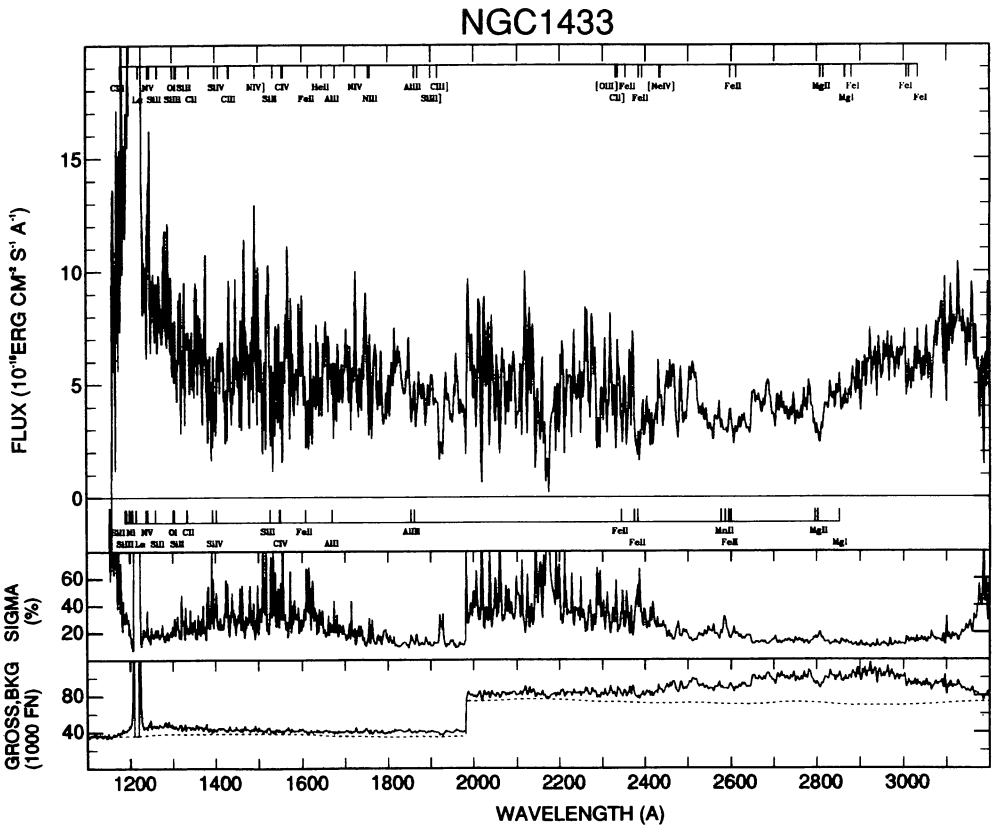


FIG. 18

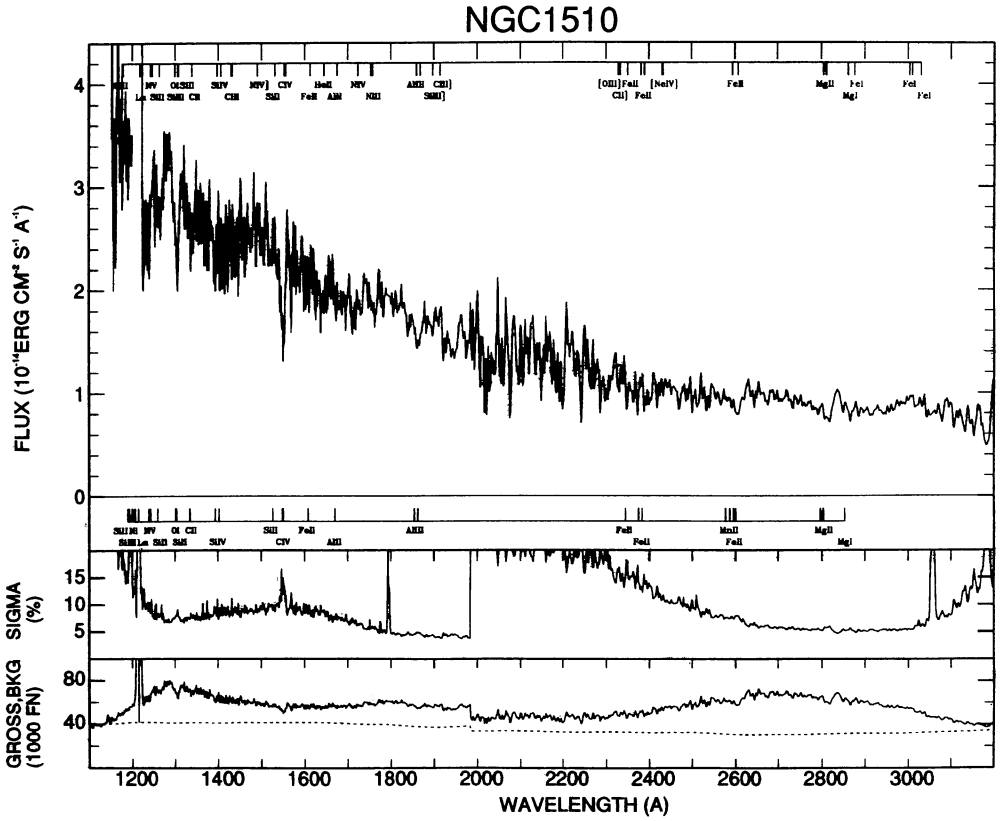


FIG. 19

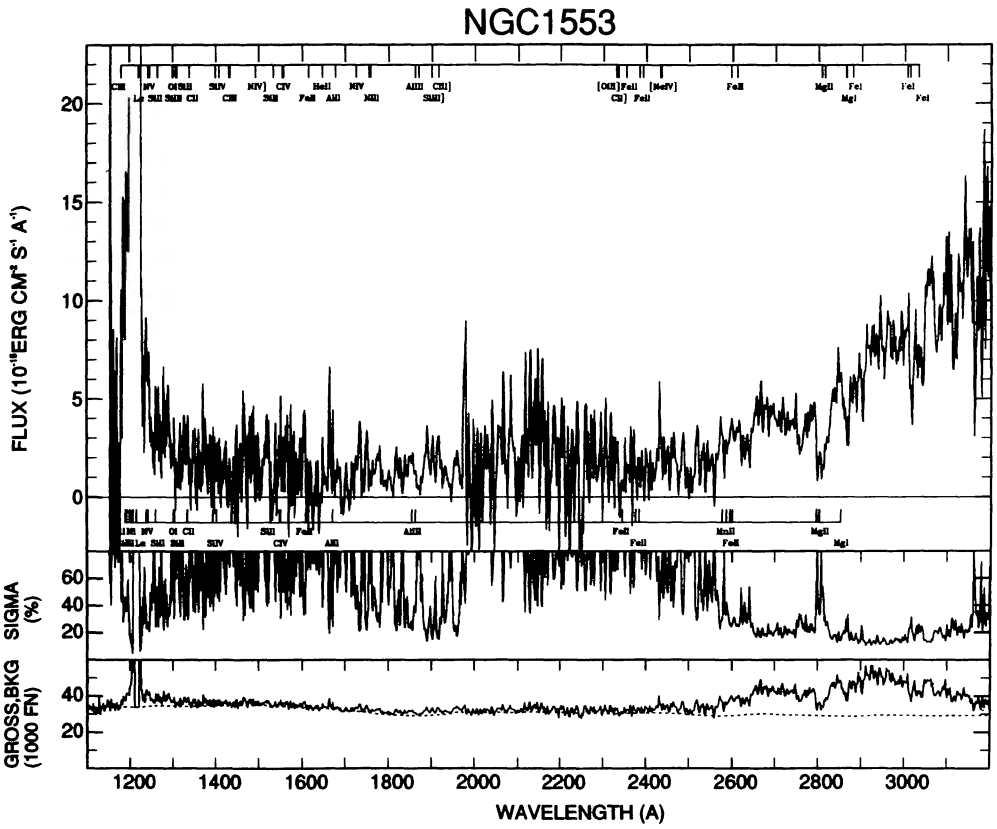


FIG. 20

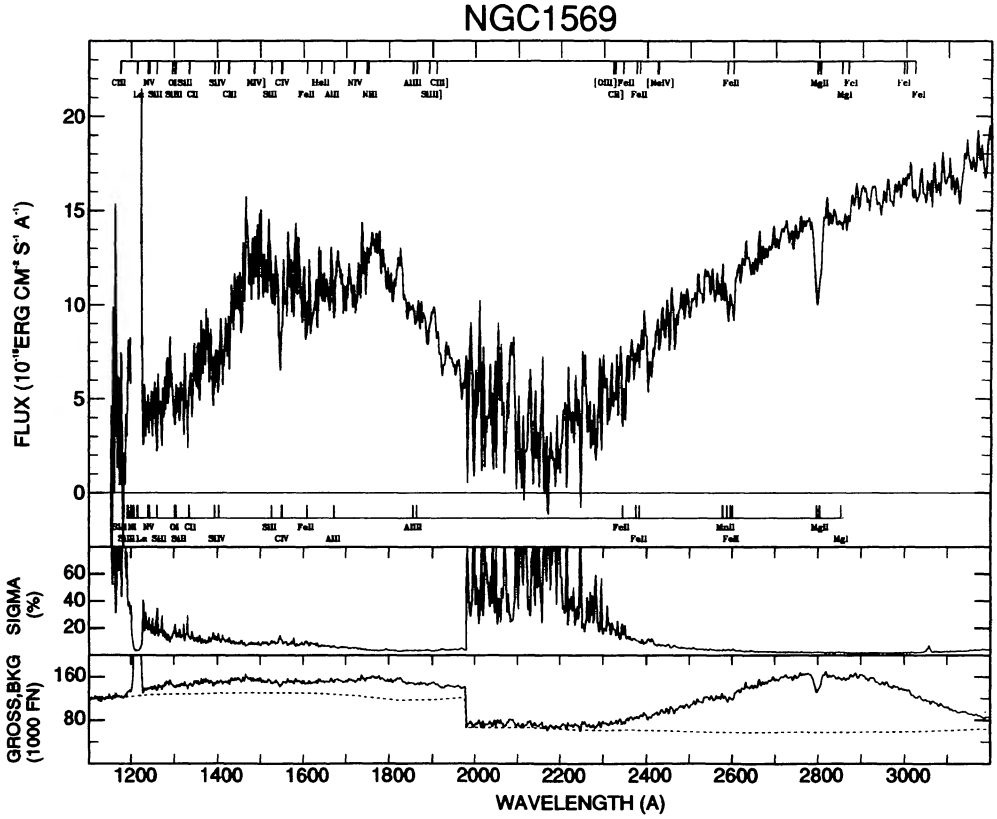


FIG. 21

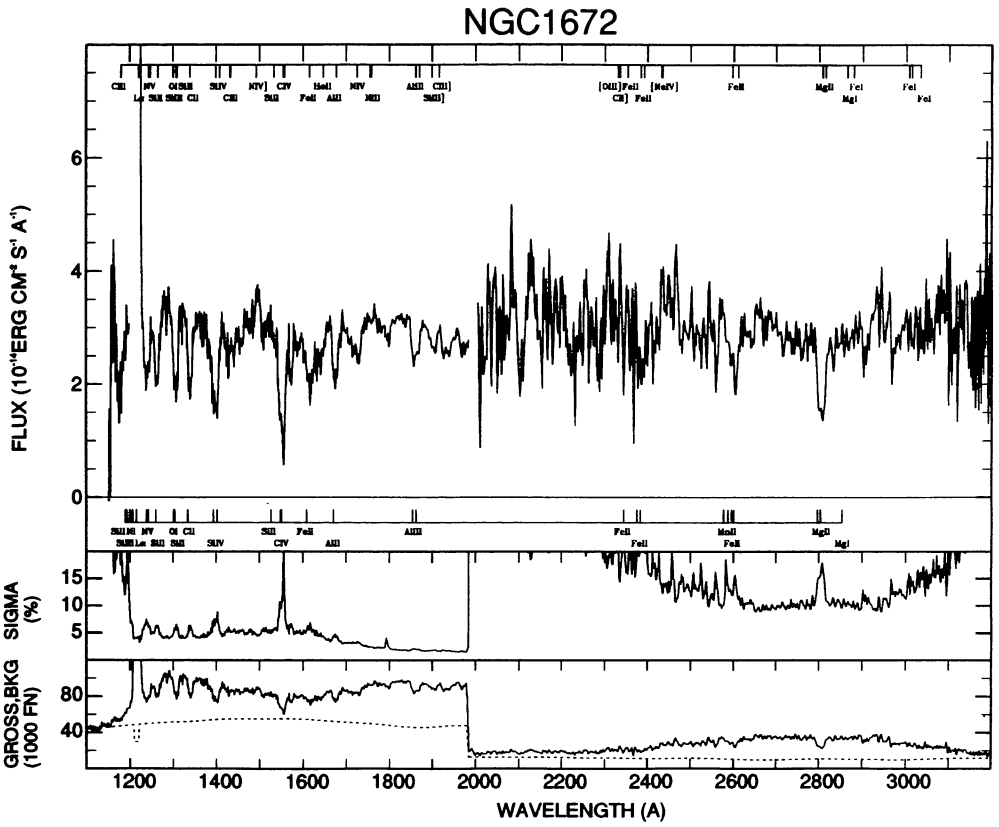


FIG. 22

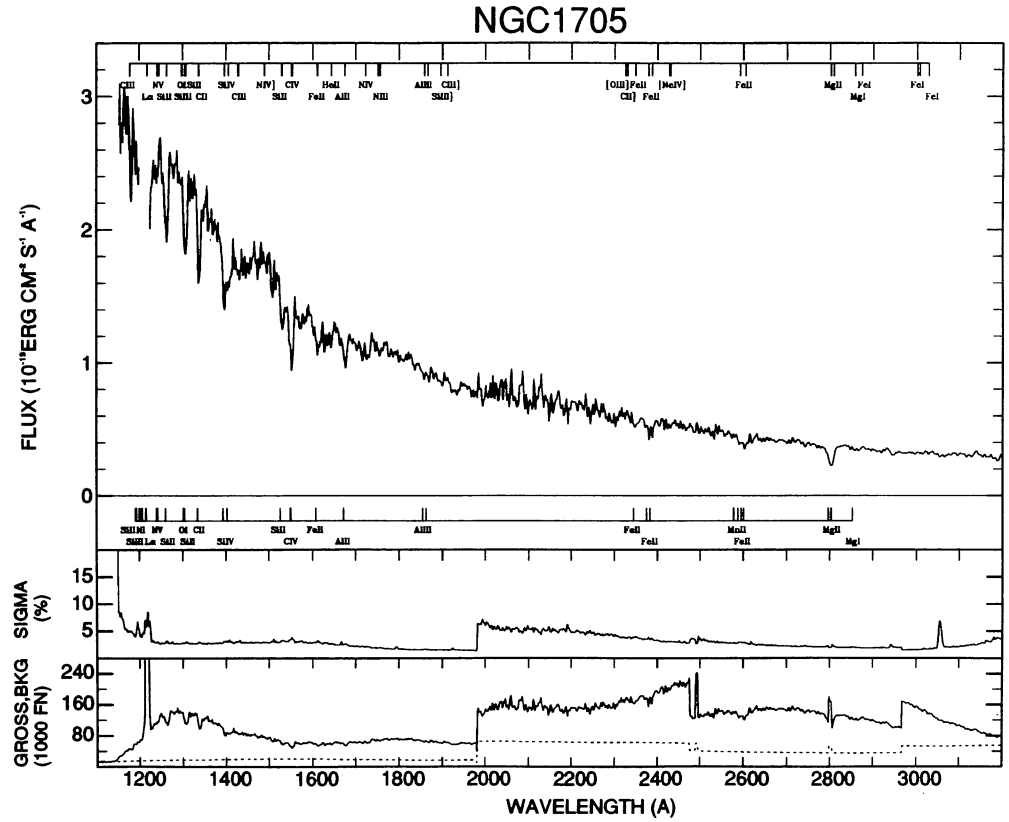


FIG. 23

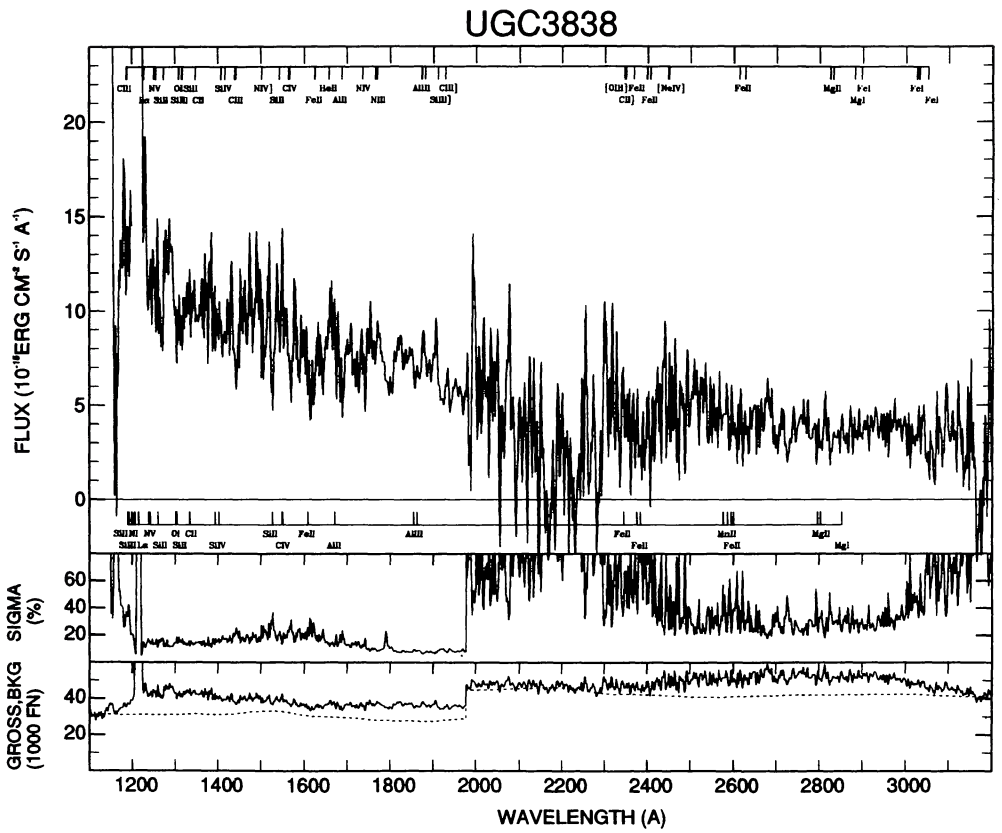


FIG. 24

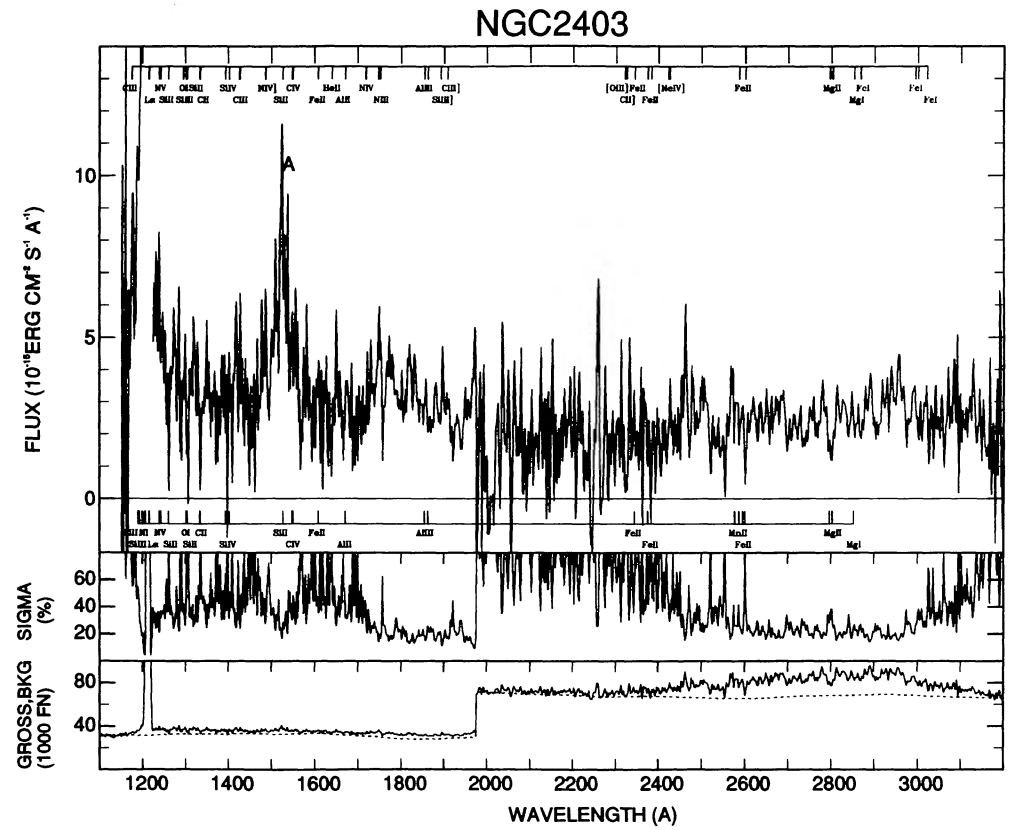


FIG. 25

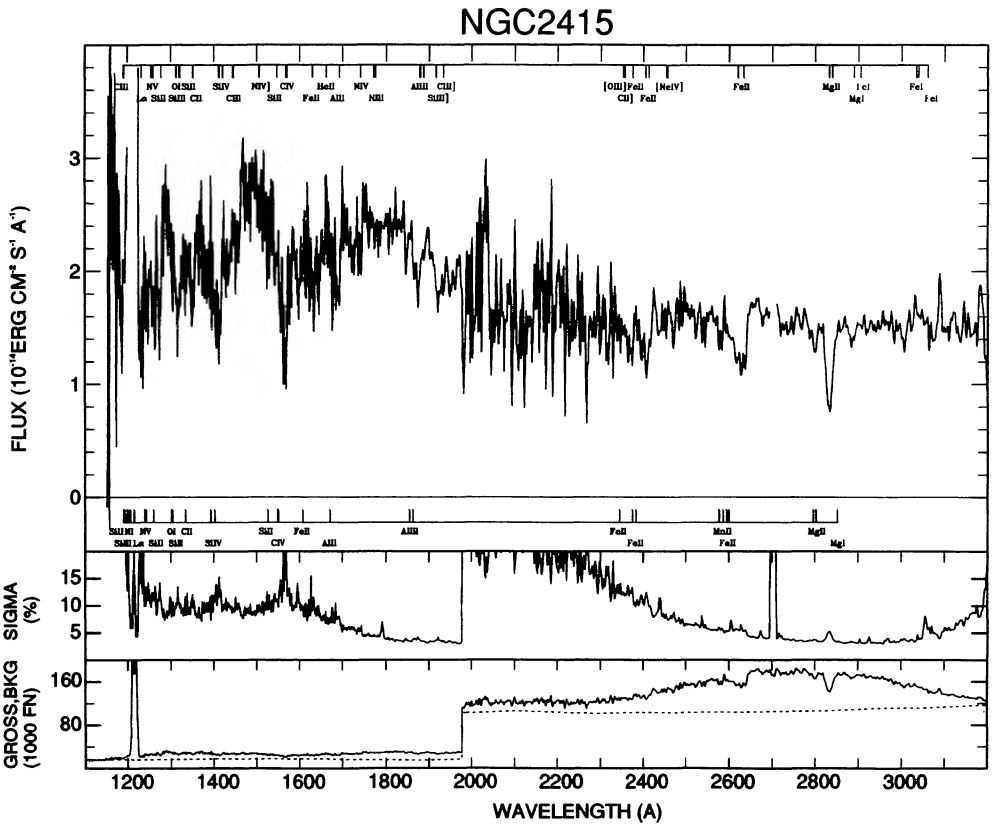


FIG. 26

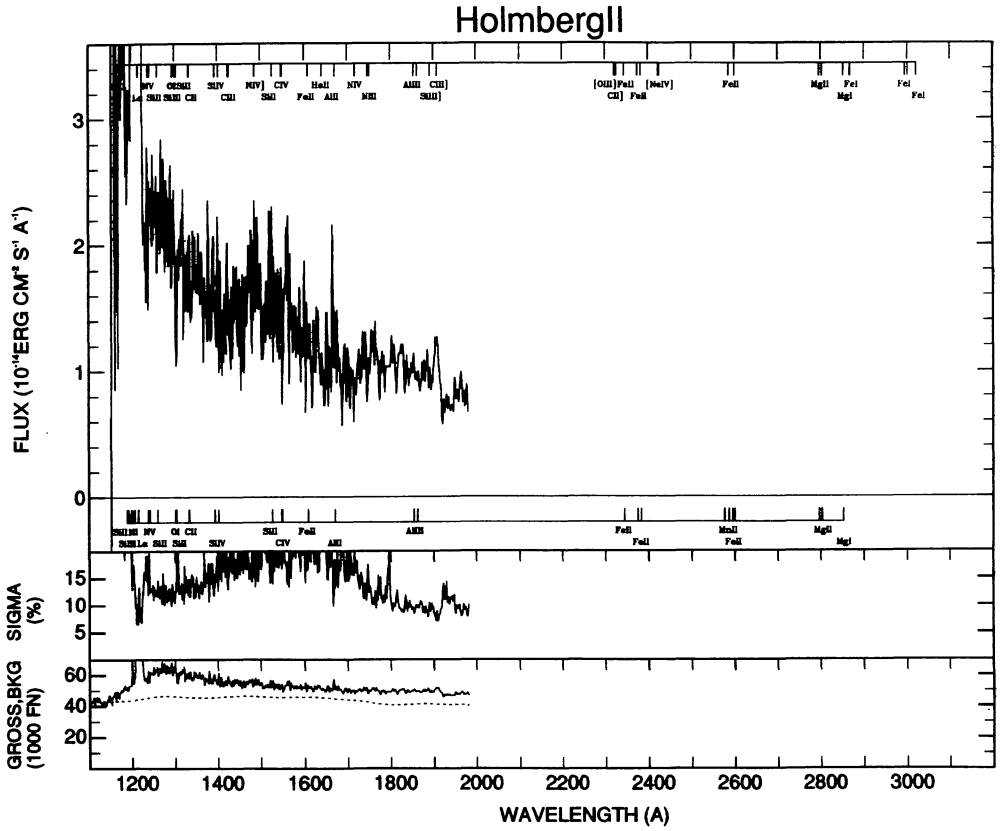


FIG. 27

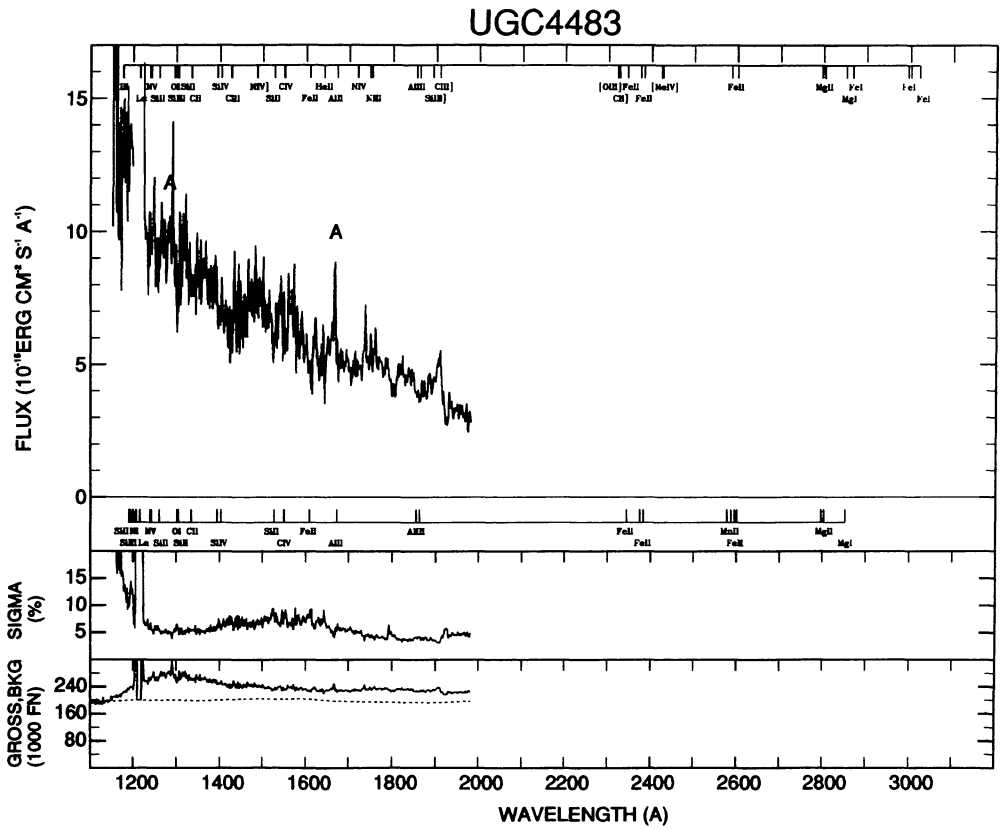


FIG. 28

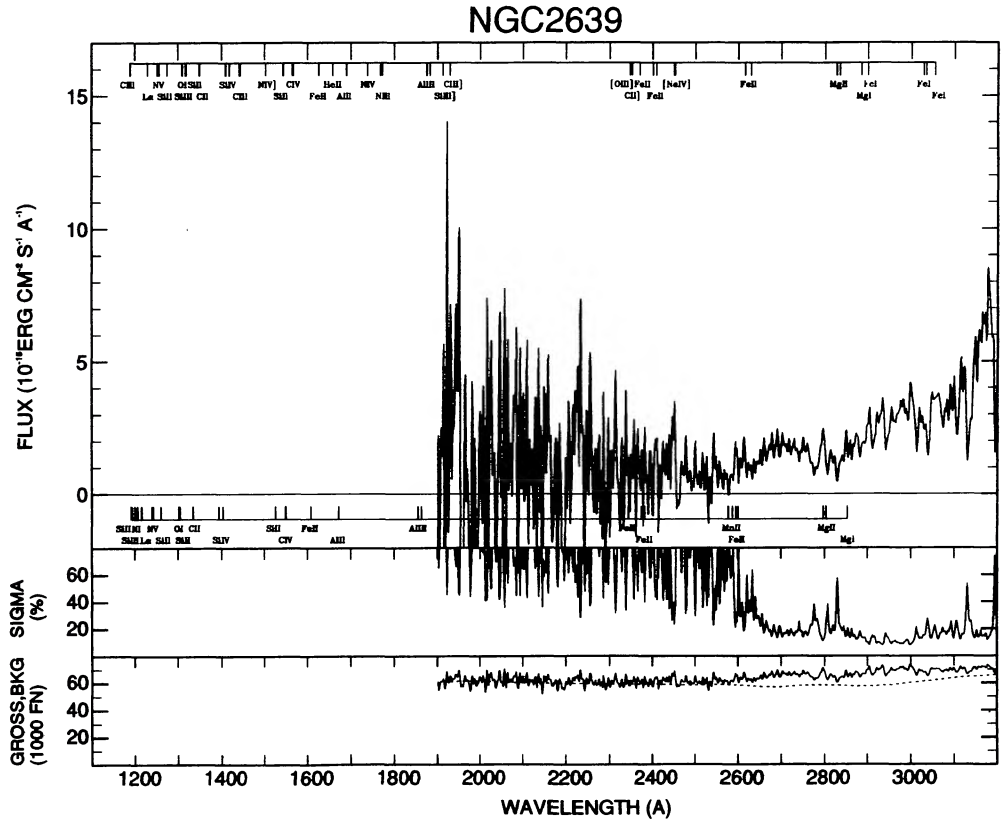


FIG. 29

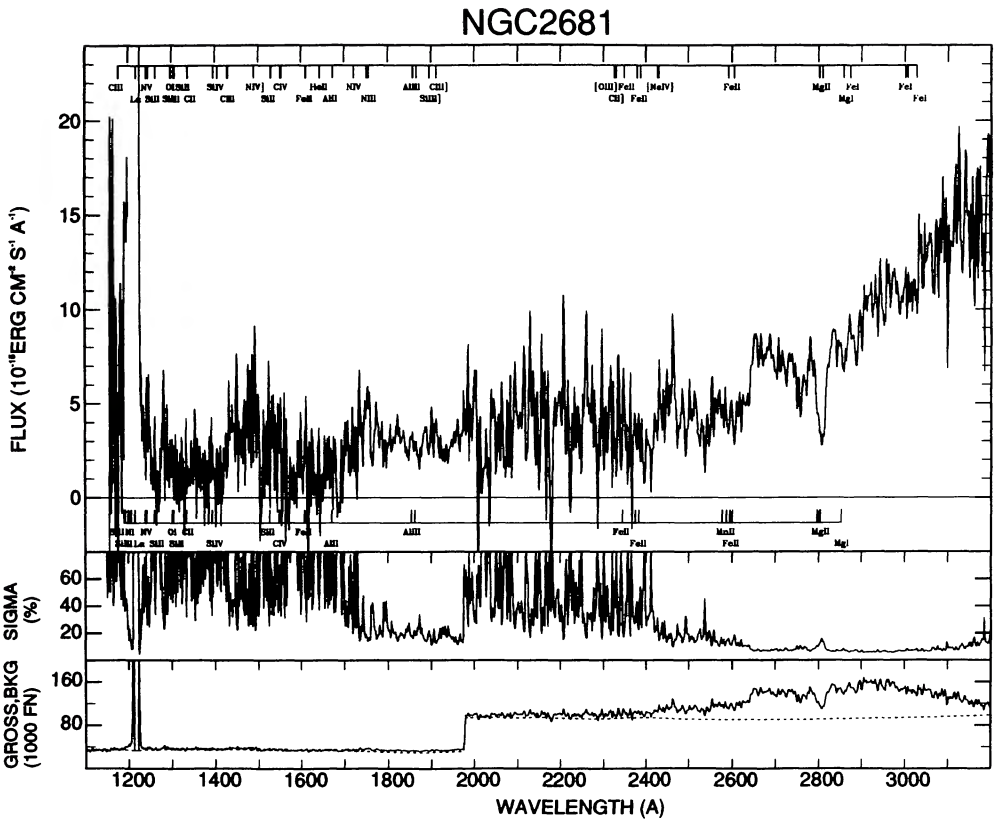


FIG. 30

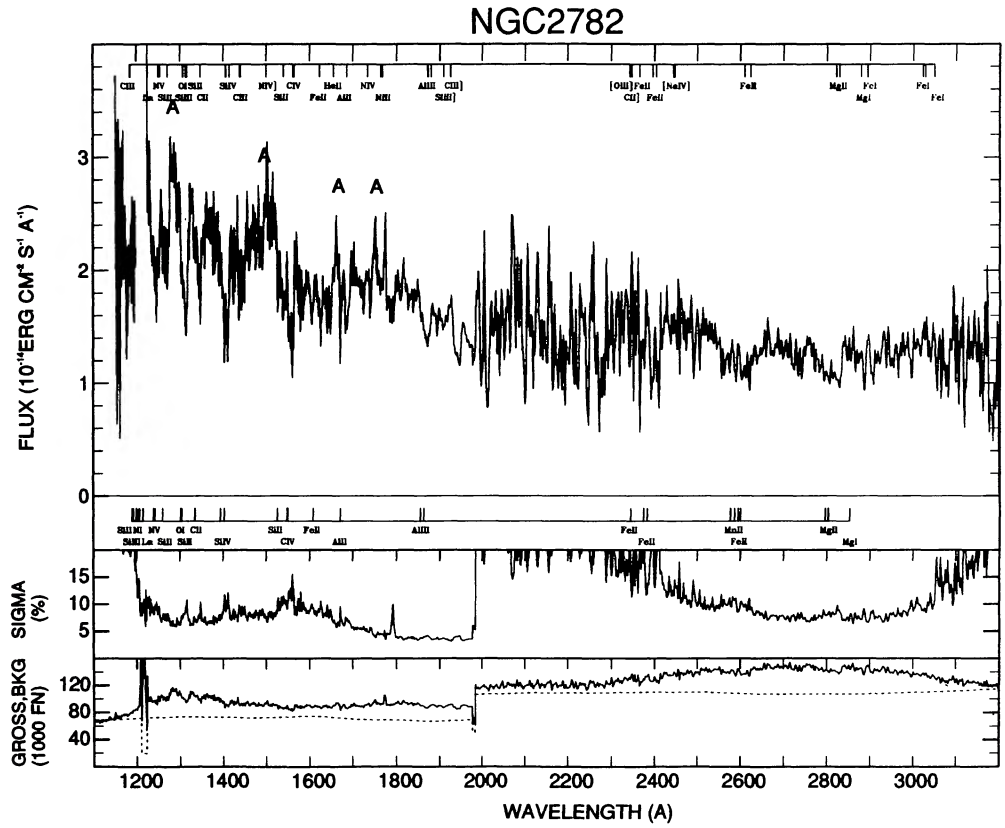


FIG. 31

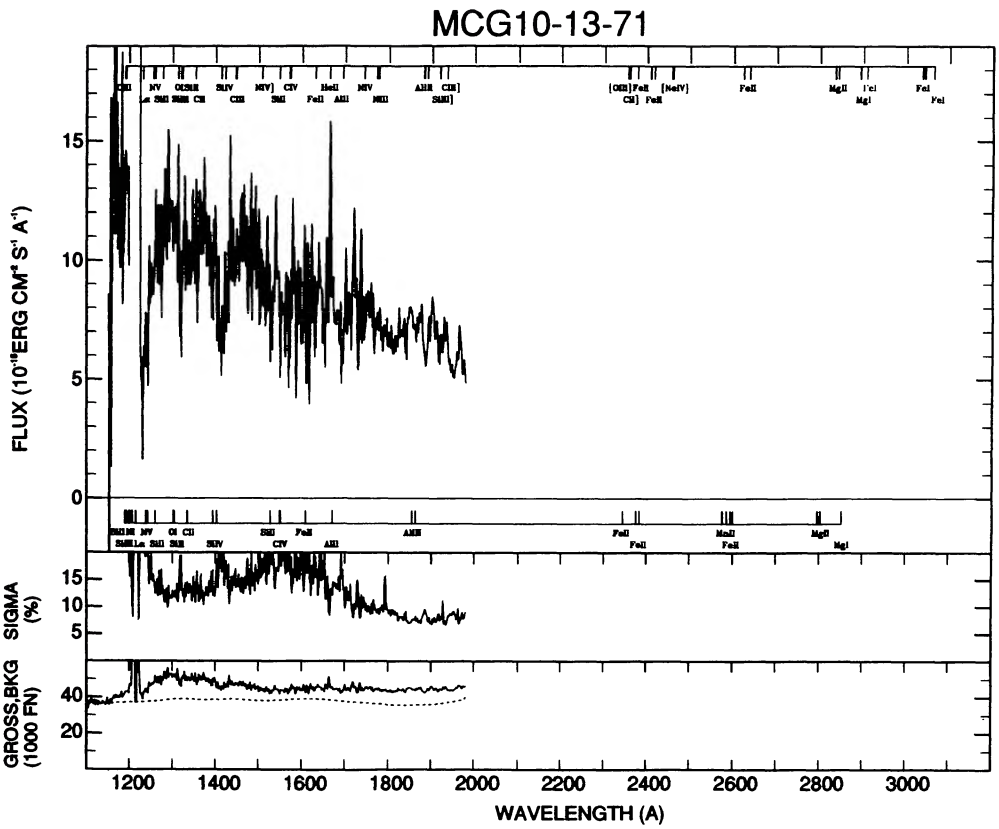


FIG. 32

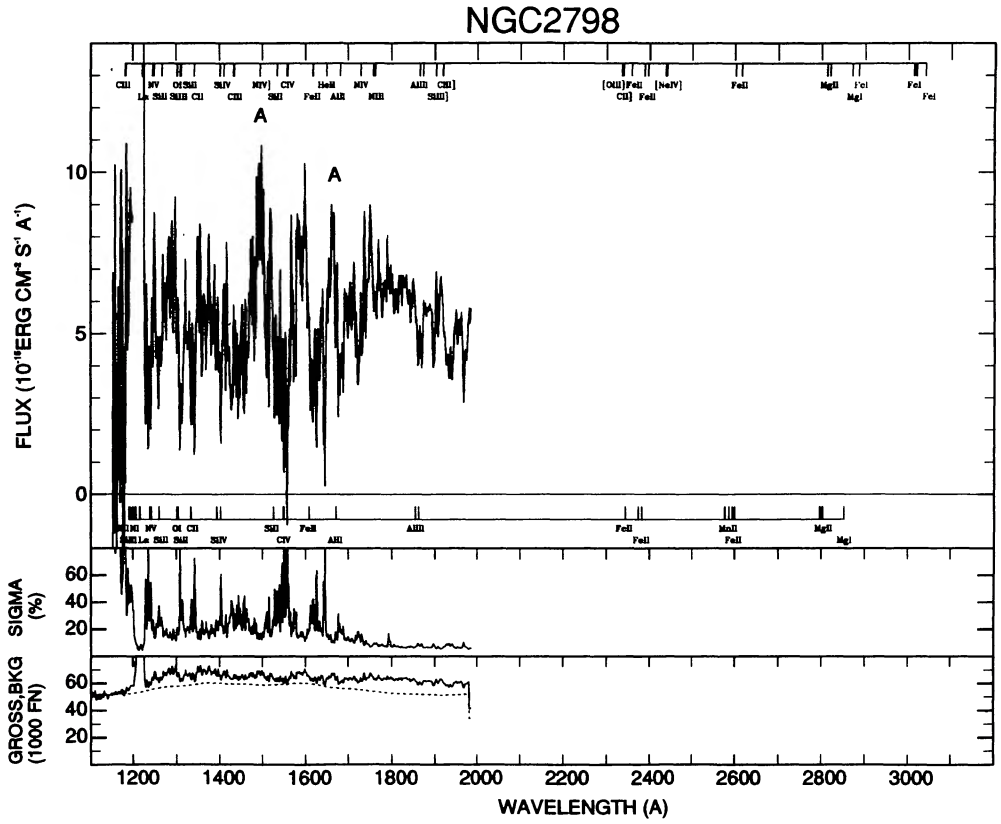


FIG. 33

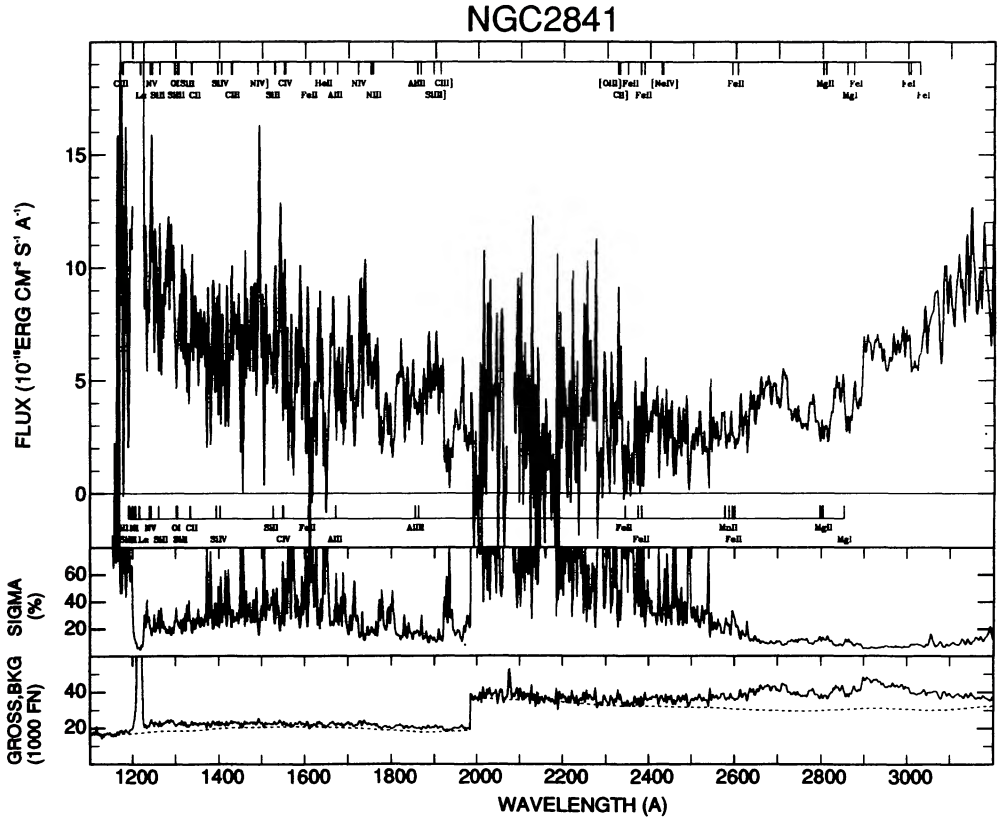


FIG. 34

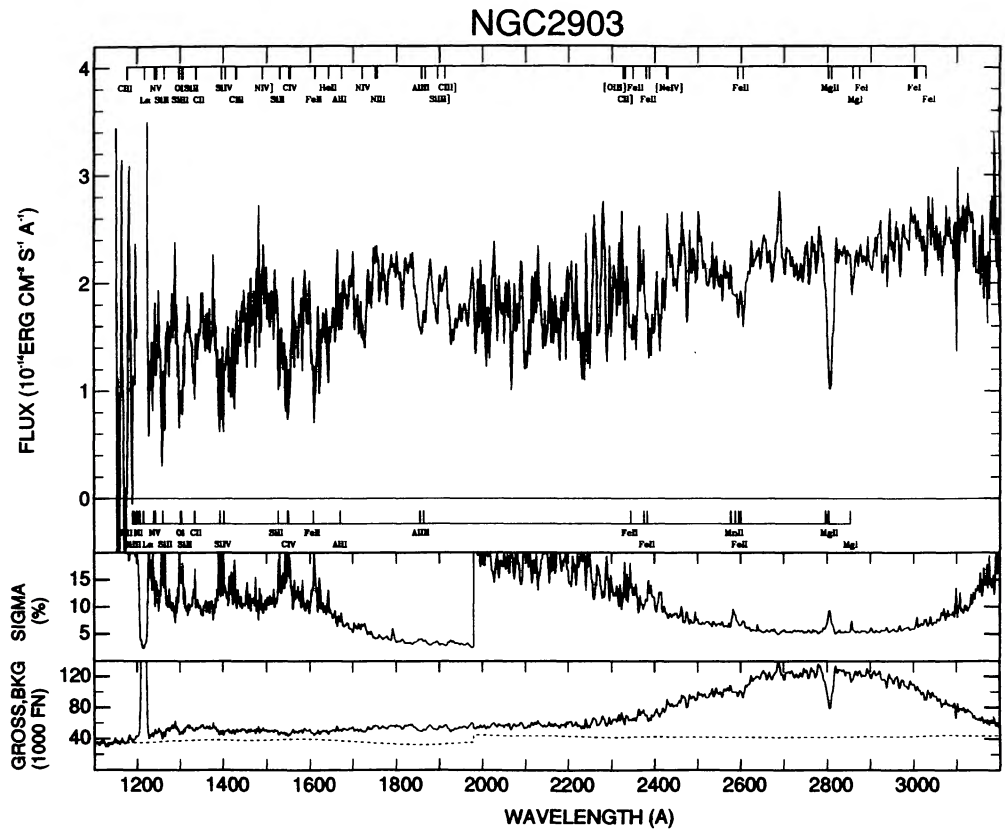


FIG. 35

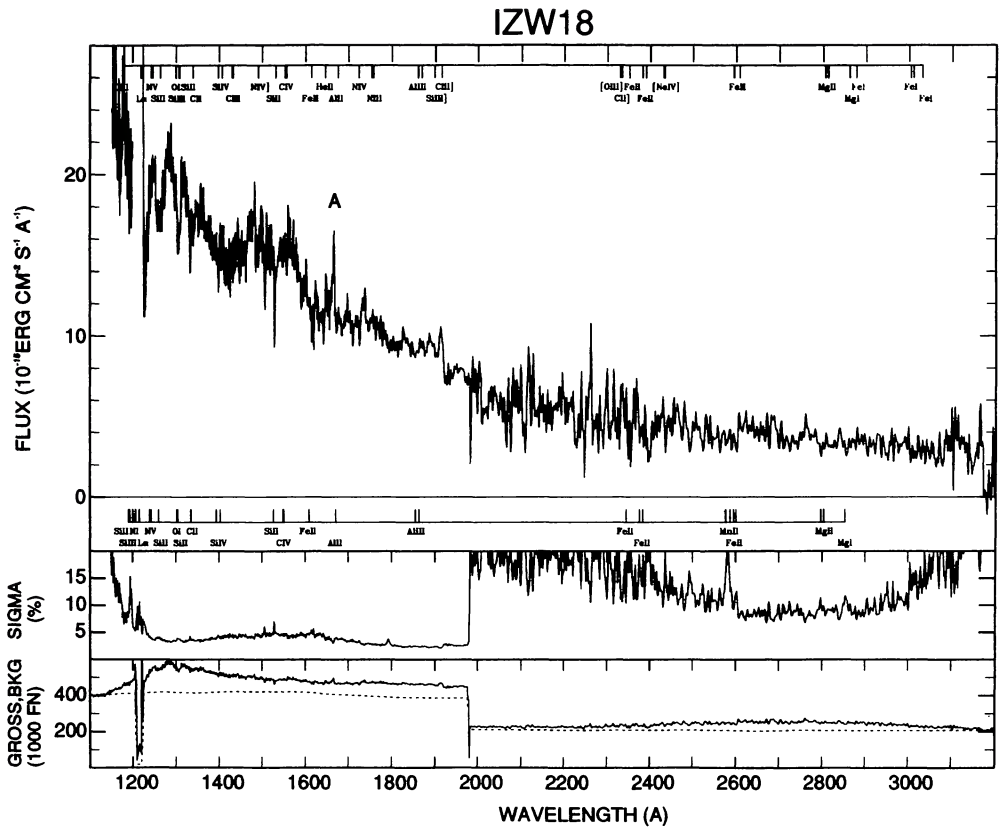


FIG. 36

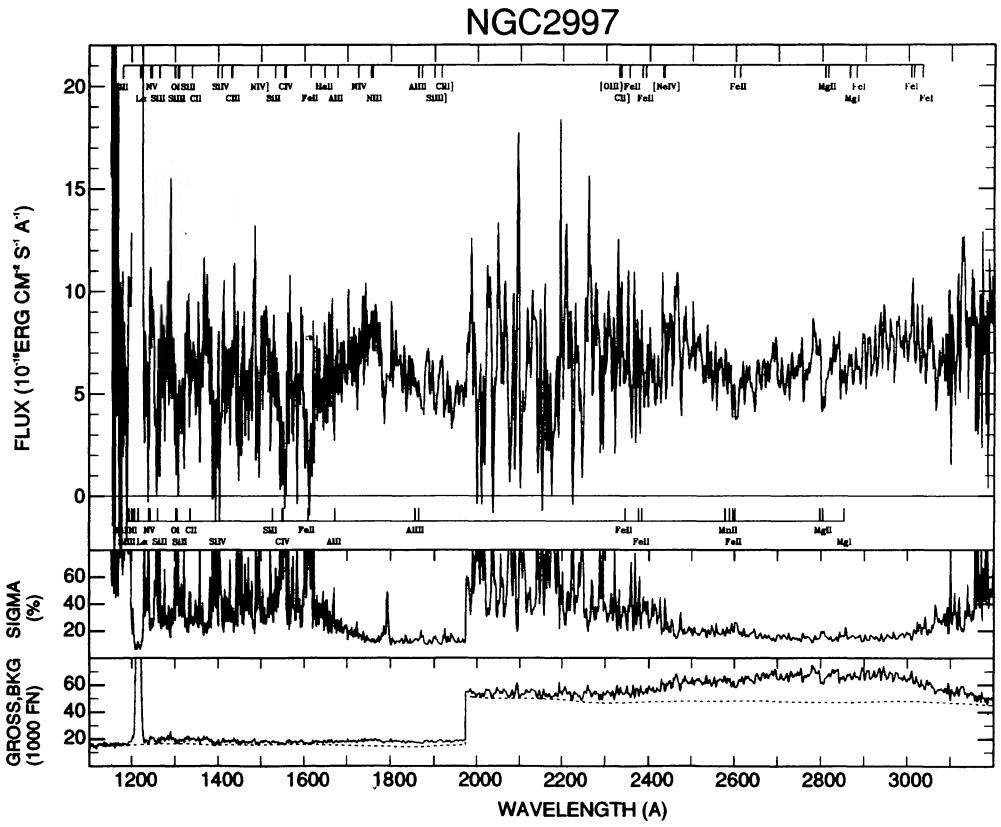


FIG. 37

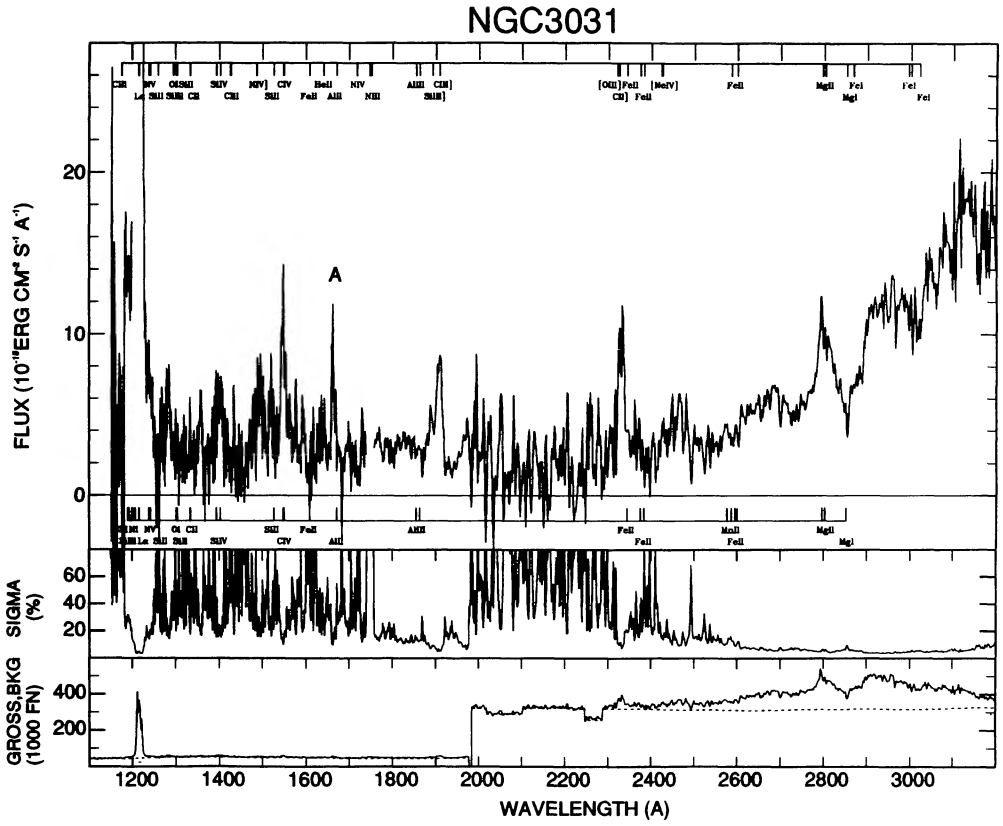


FIG. 38

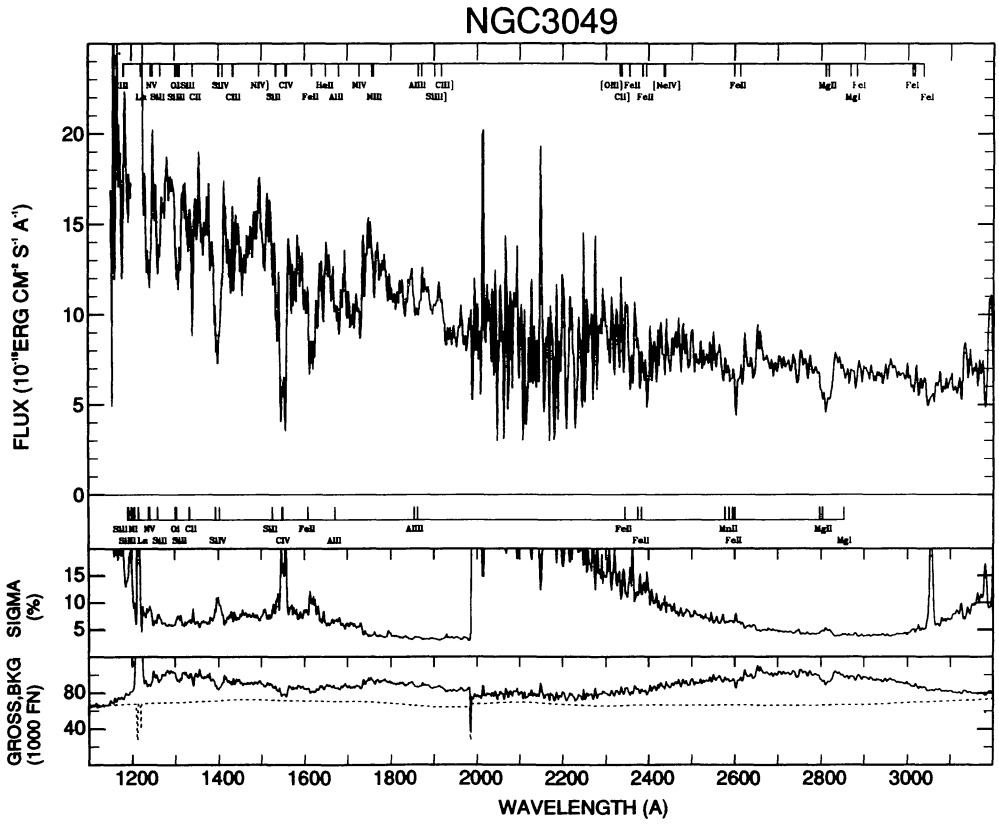


FIG. 39

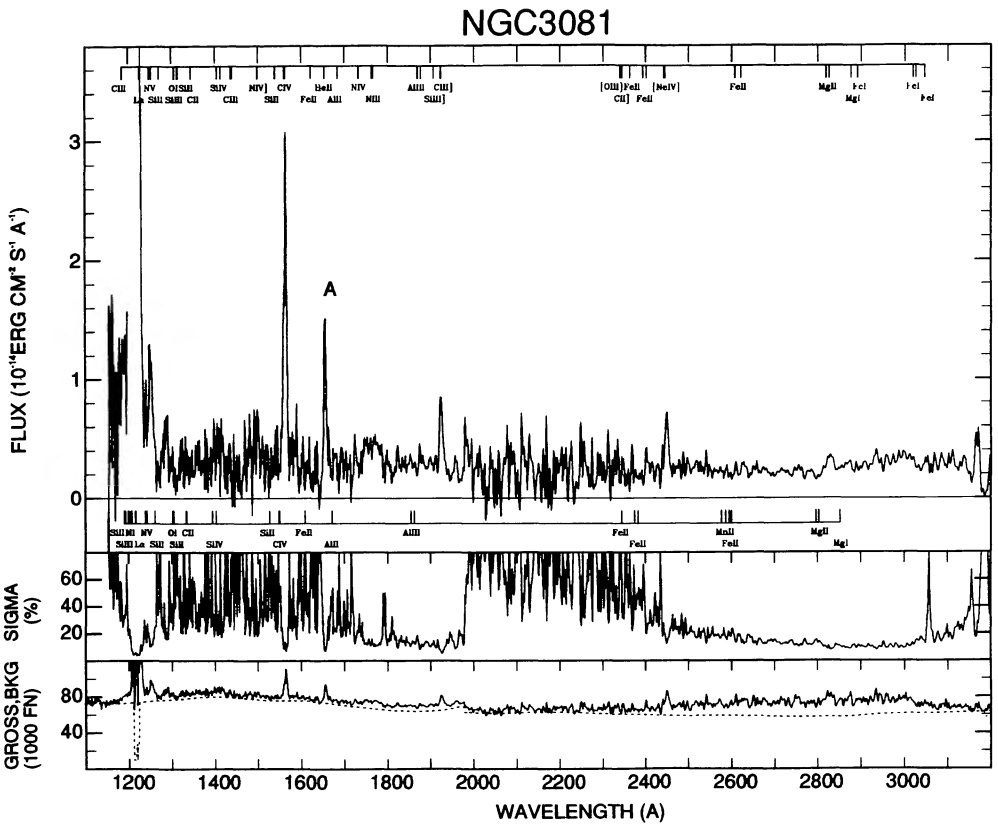


FIG. 40

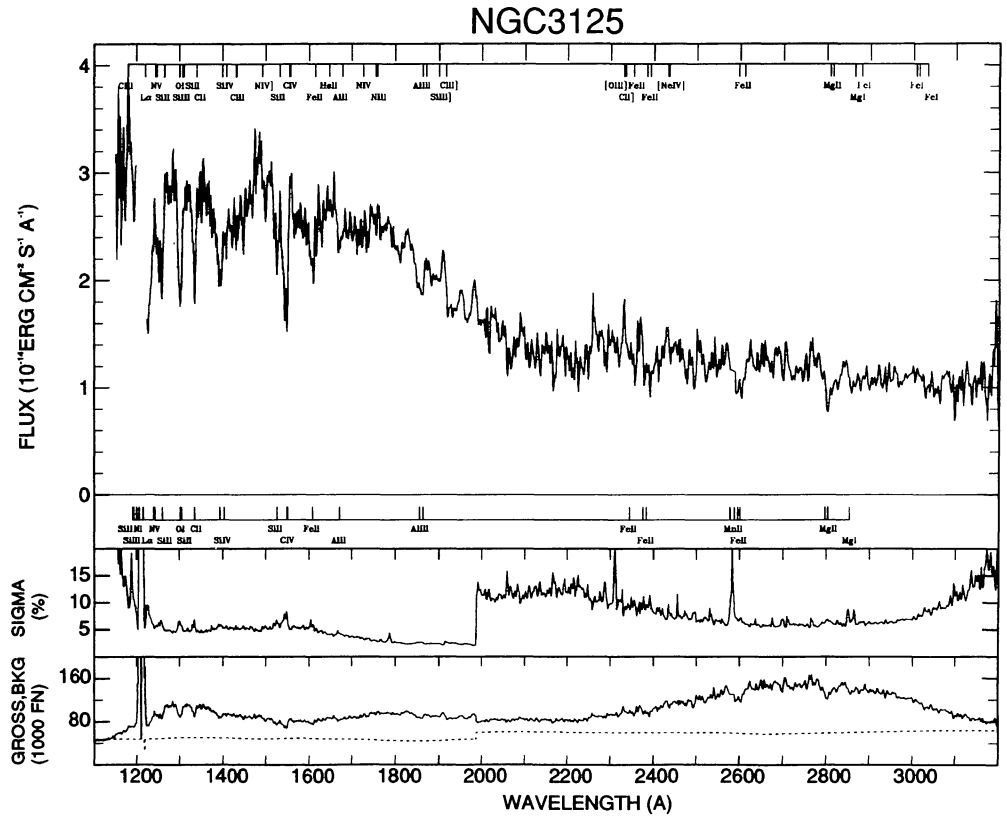


FIG. 41

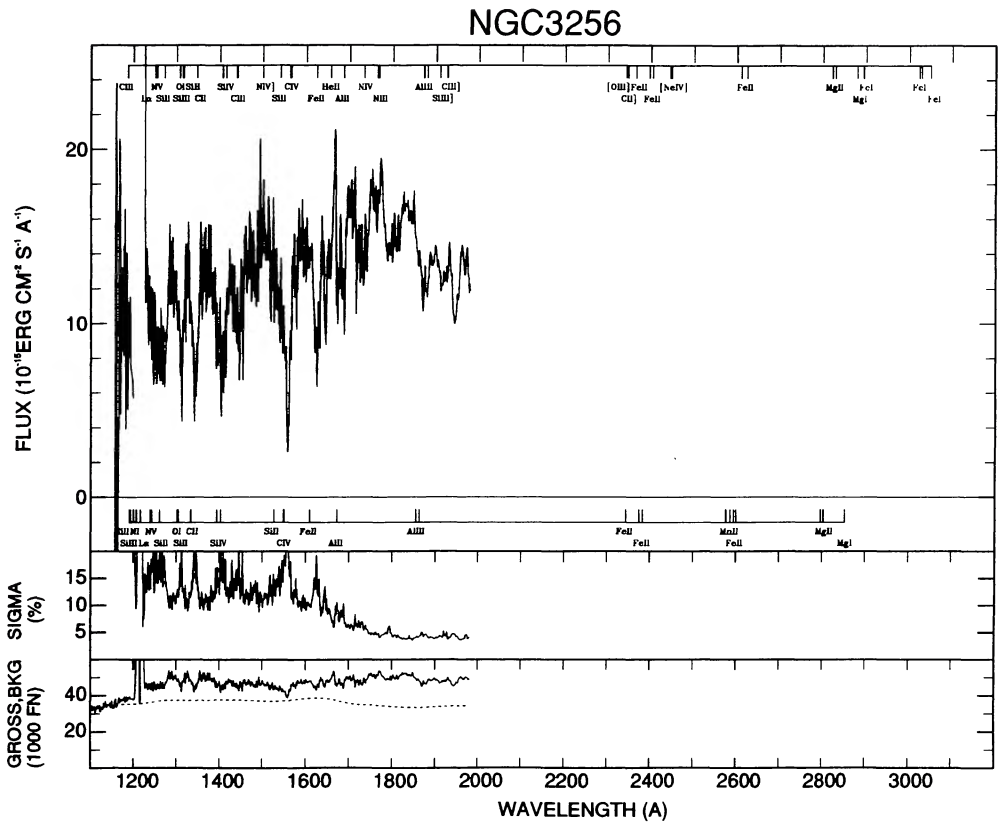


FIG. 42

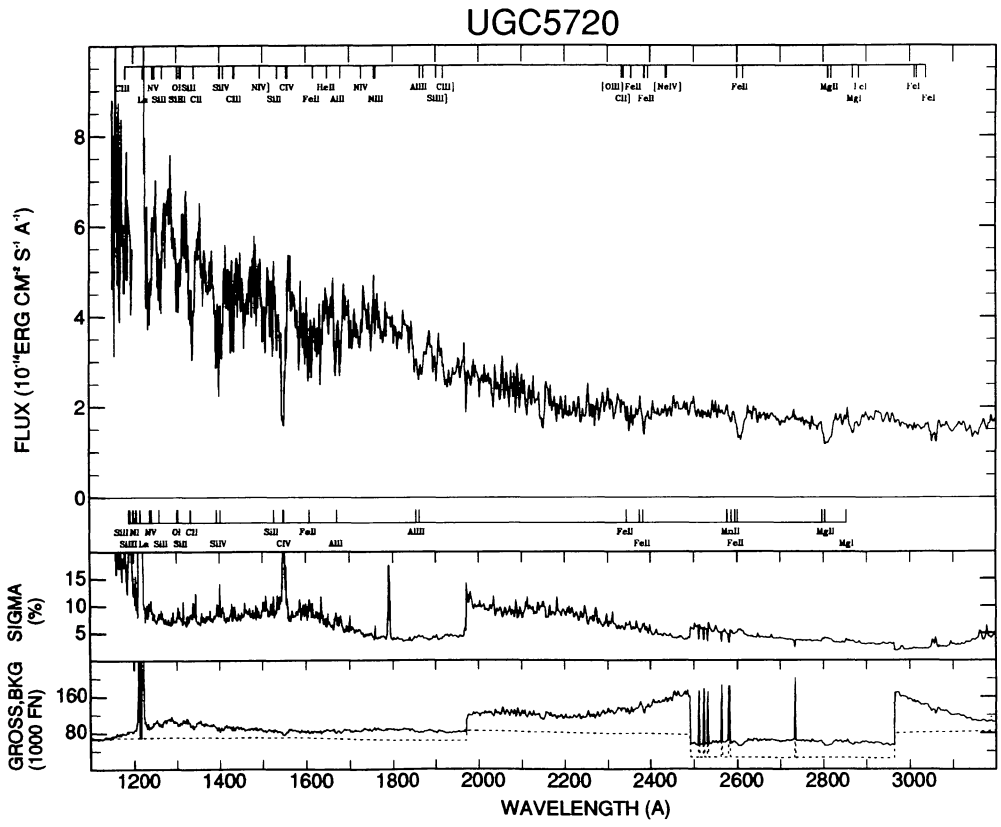


FIG. 43

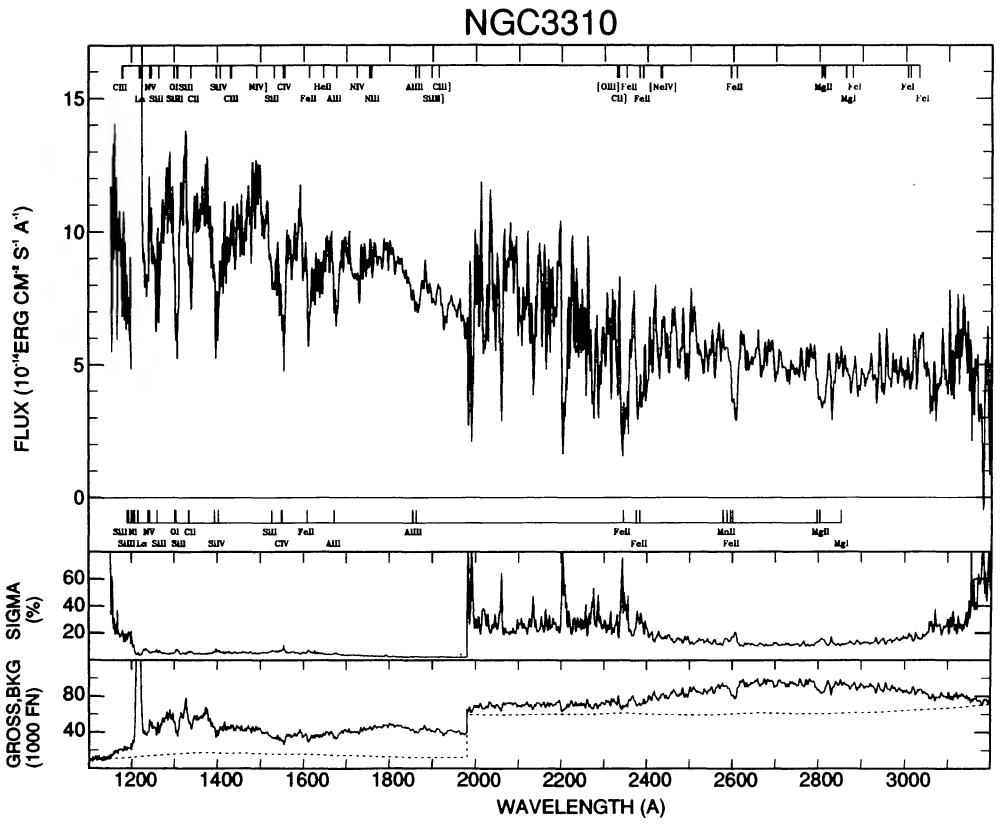


FIG. 44

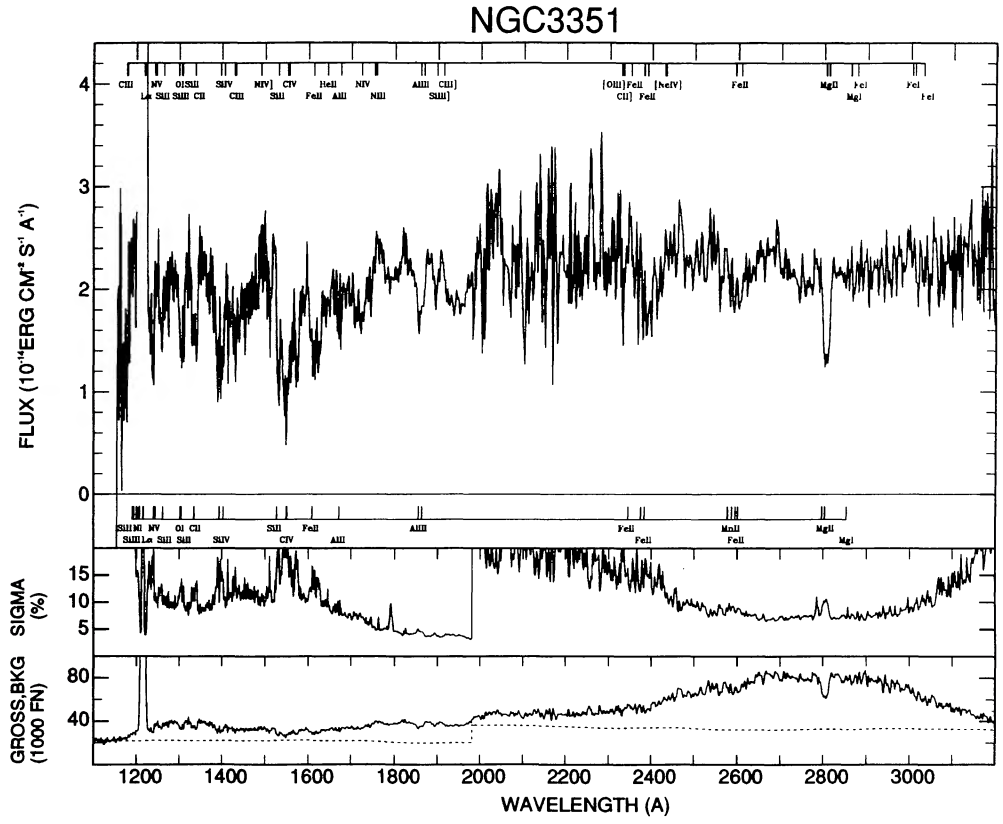


FIG. 45

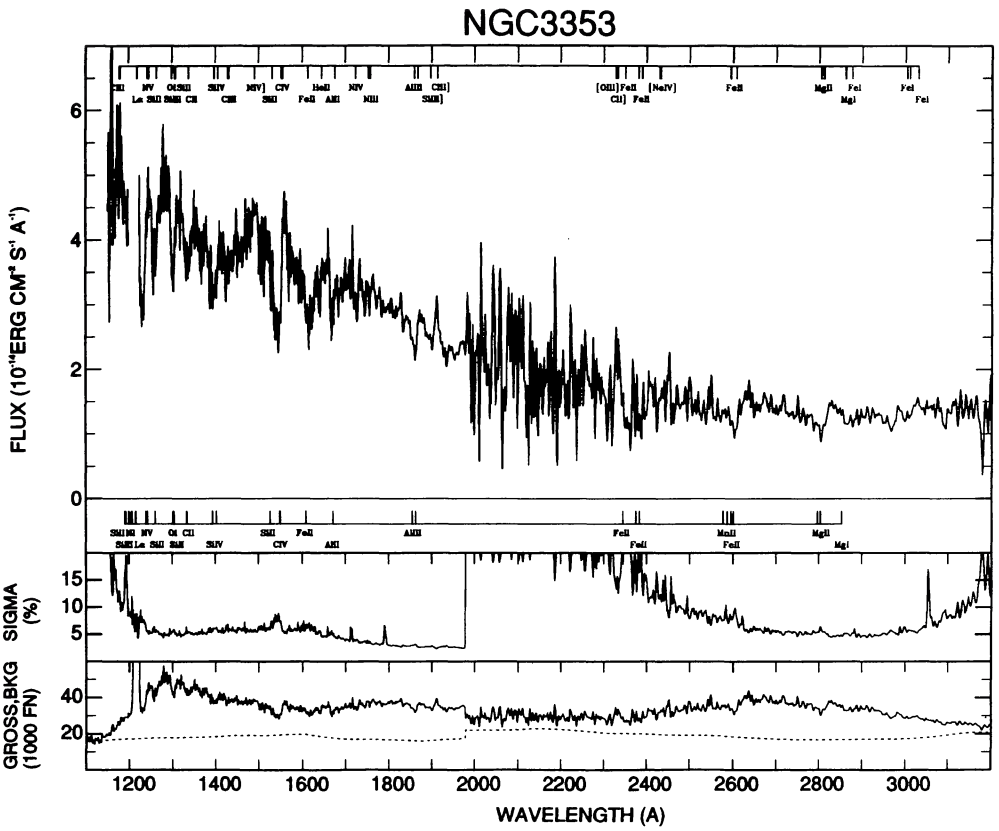


FIG. 46

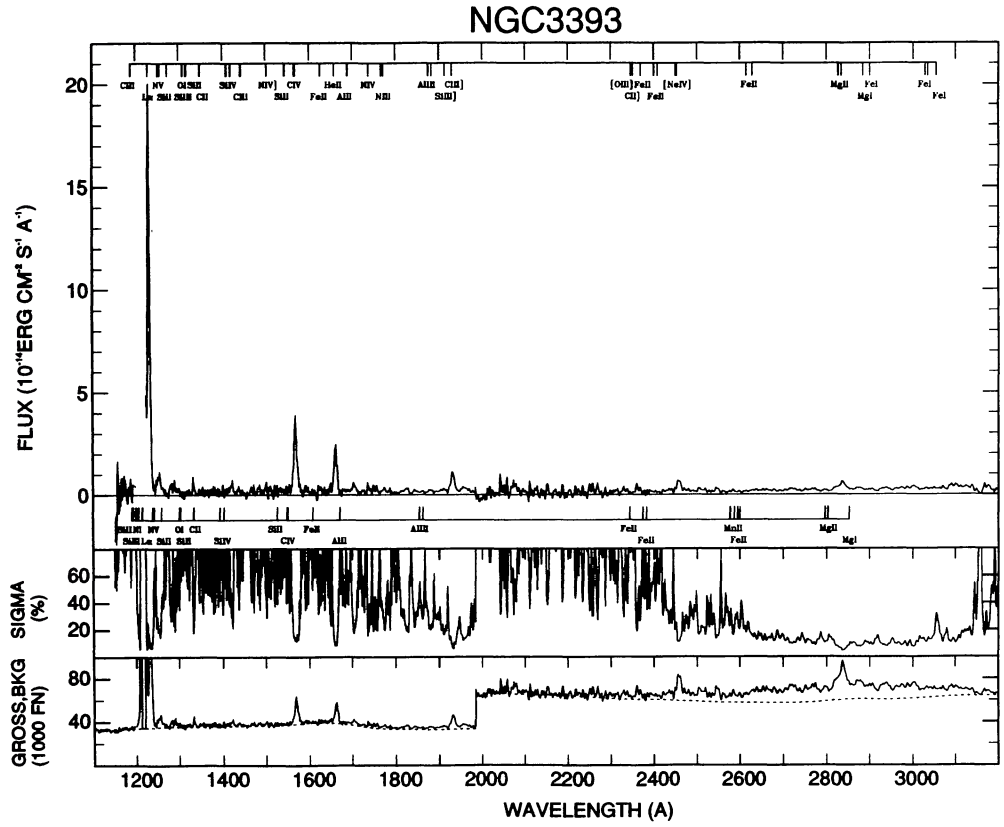


FIG. 47

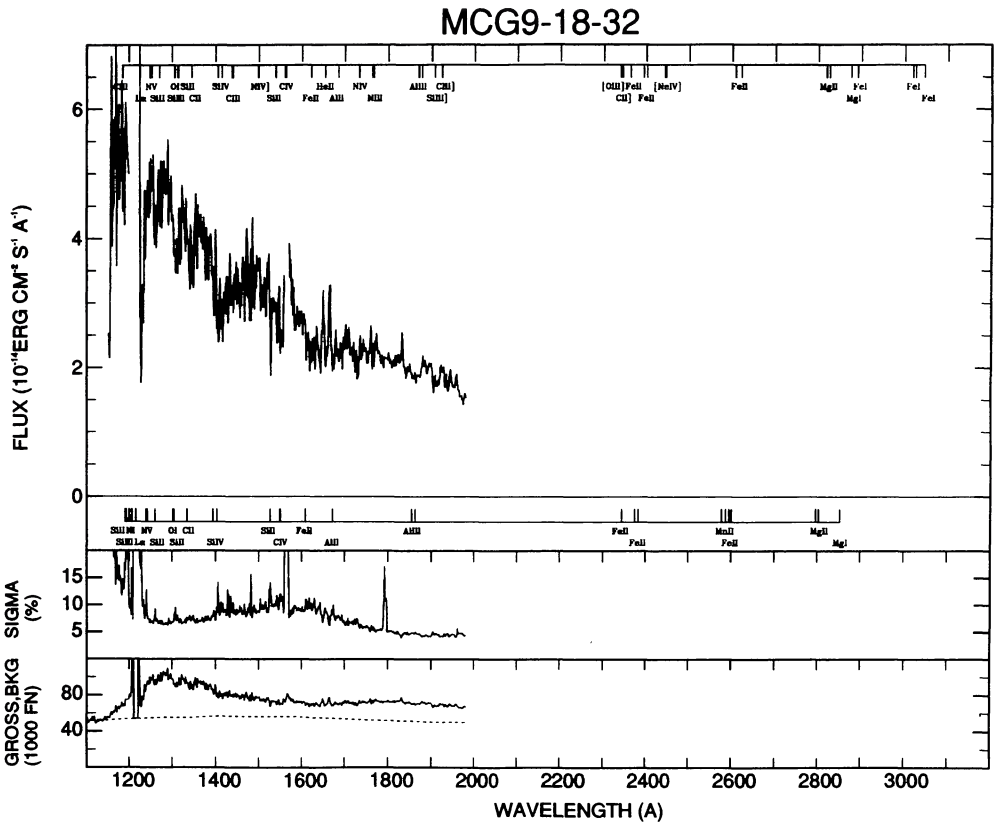


FIG. 48

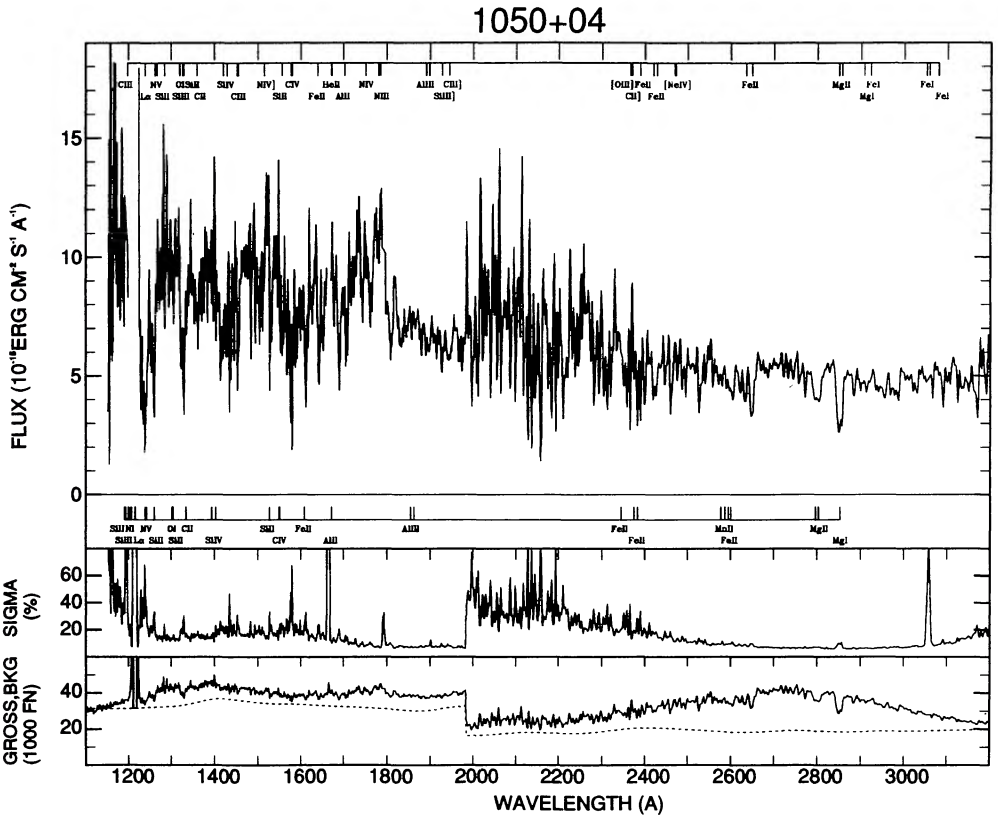


FIG. 49

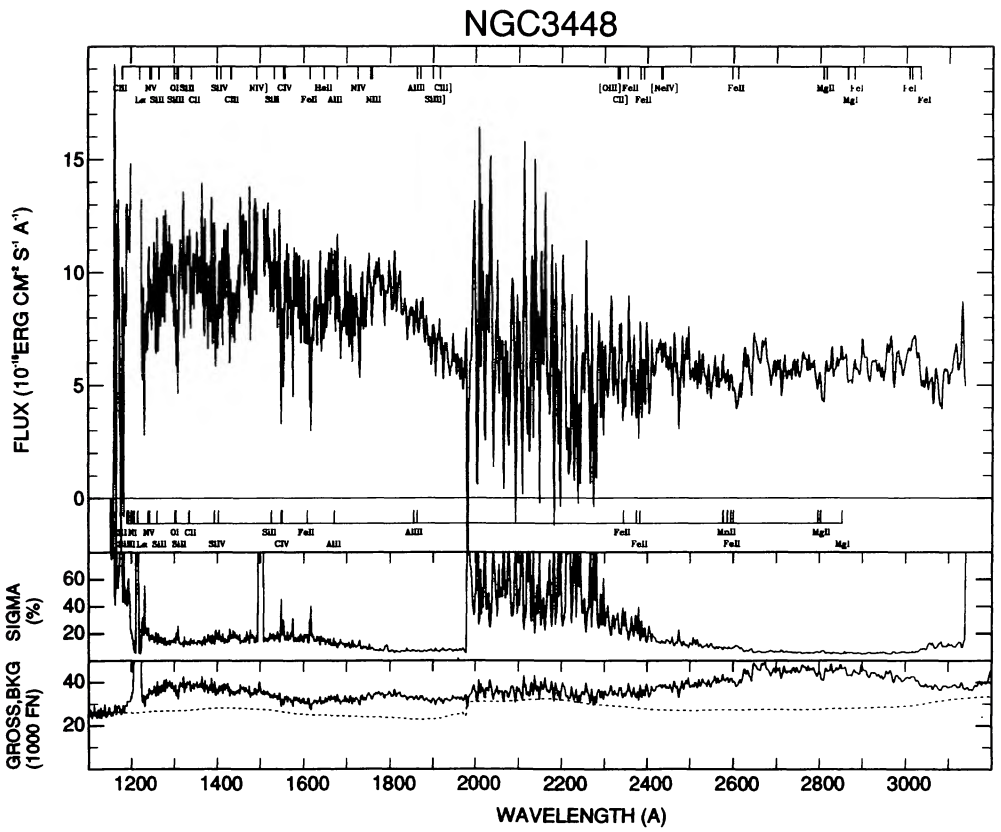


FIG. 50

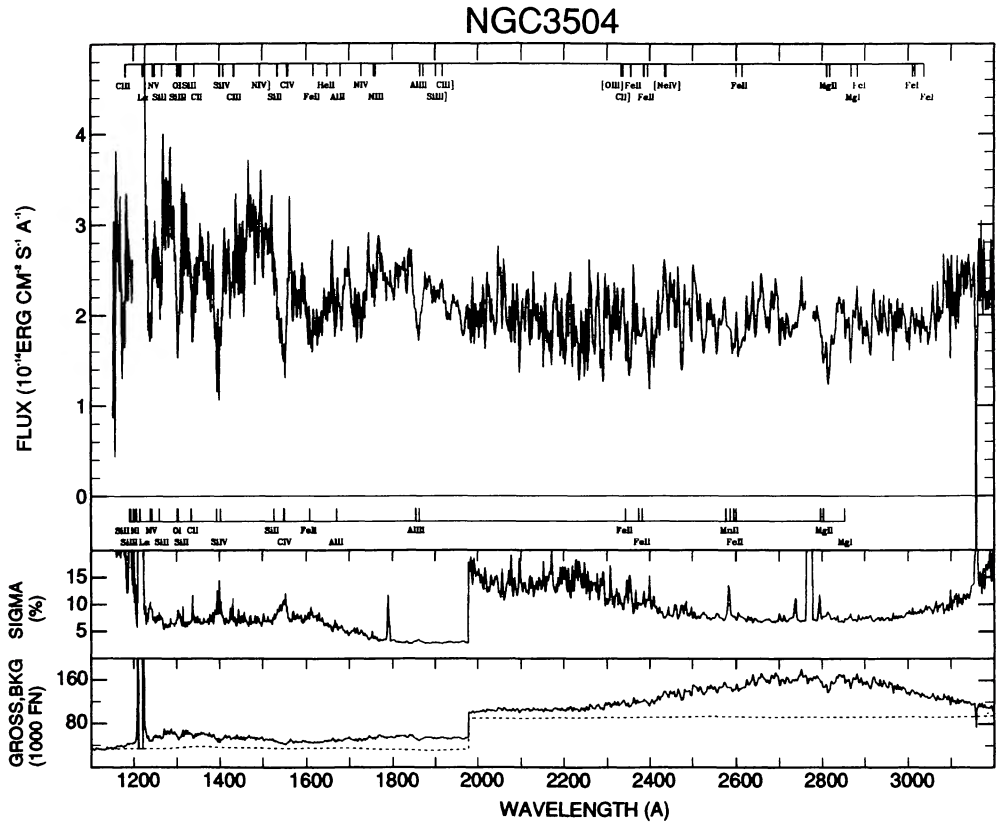


FIG. 51

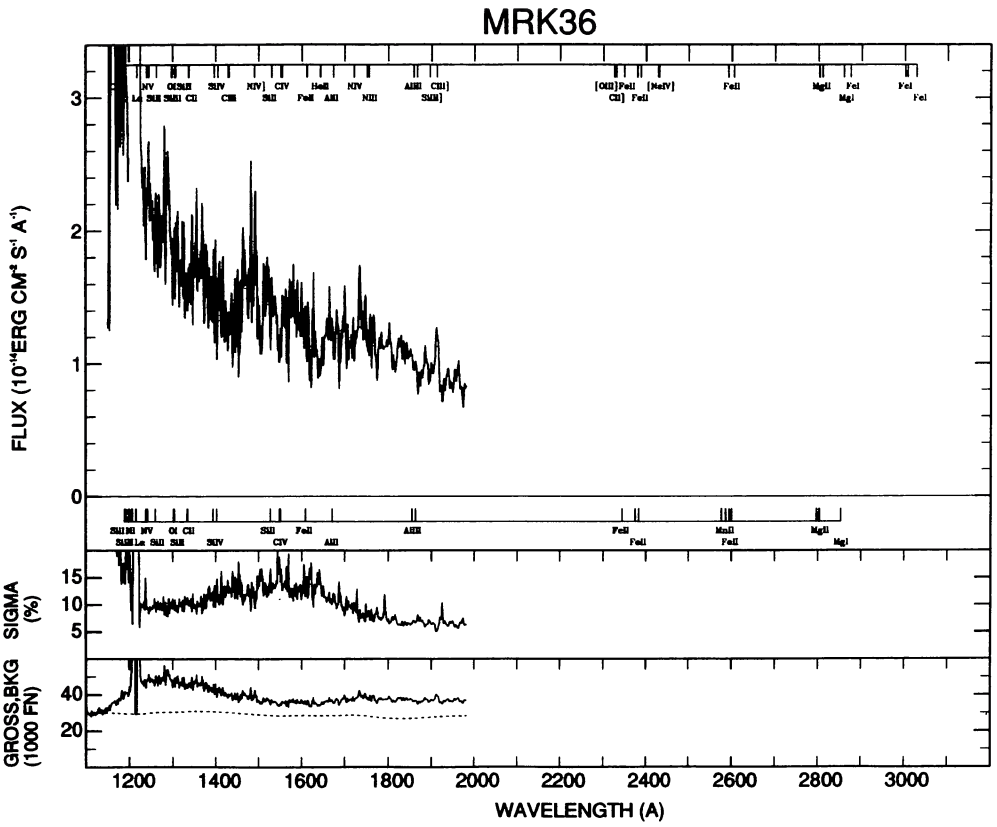


FIG. 52

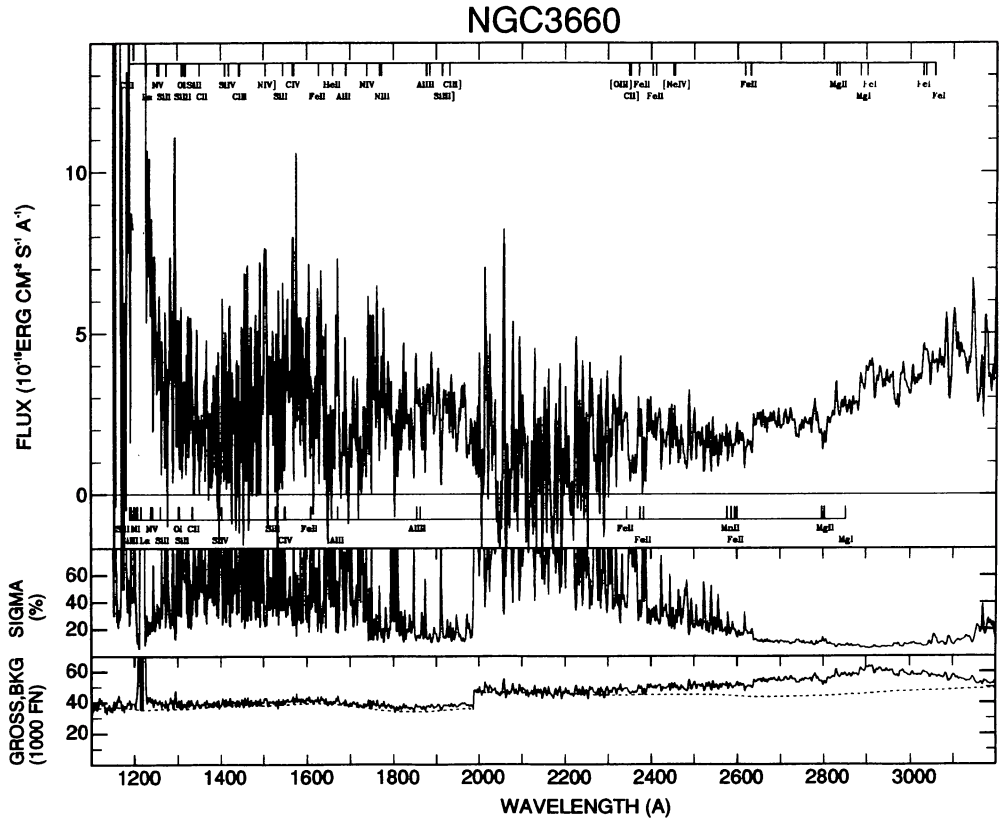


FIG. 53

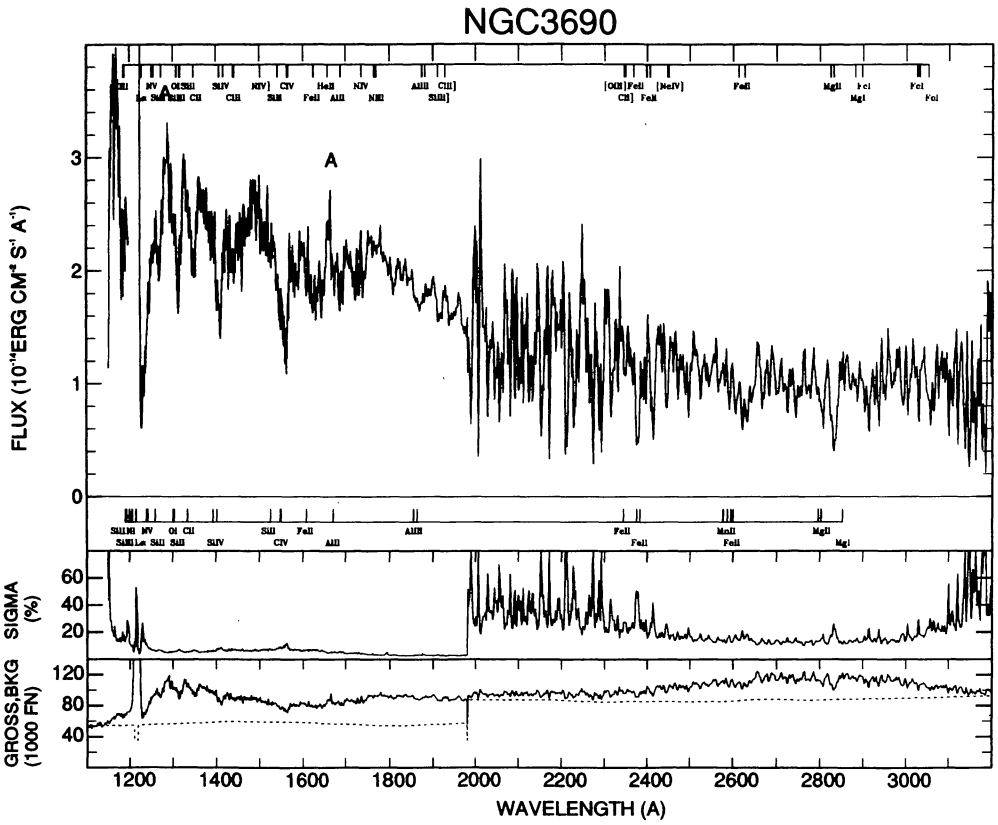


FIG. 54

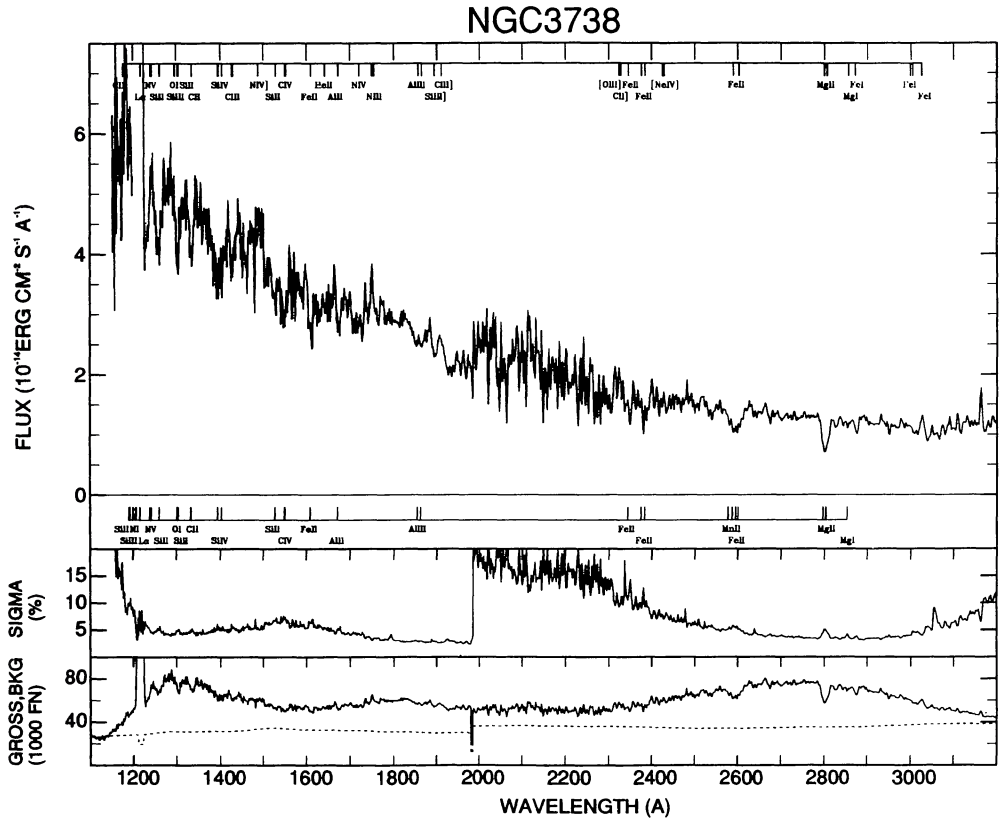


FIG. 55

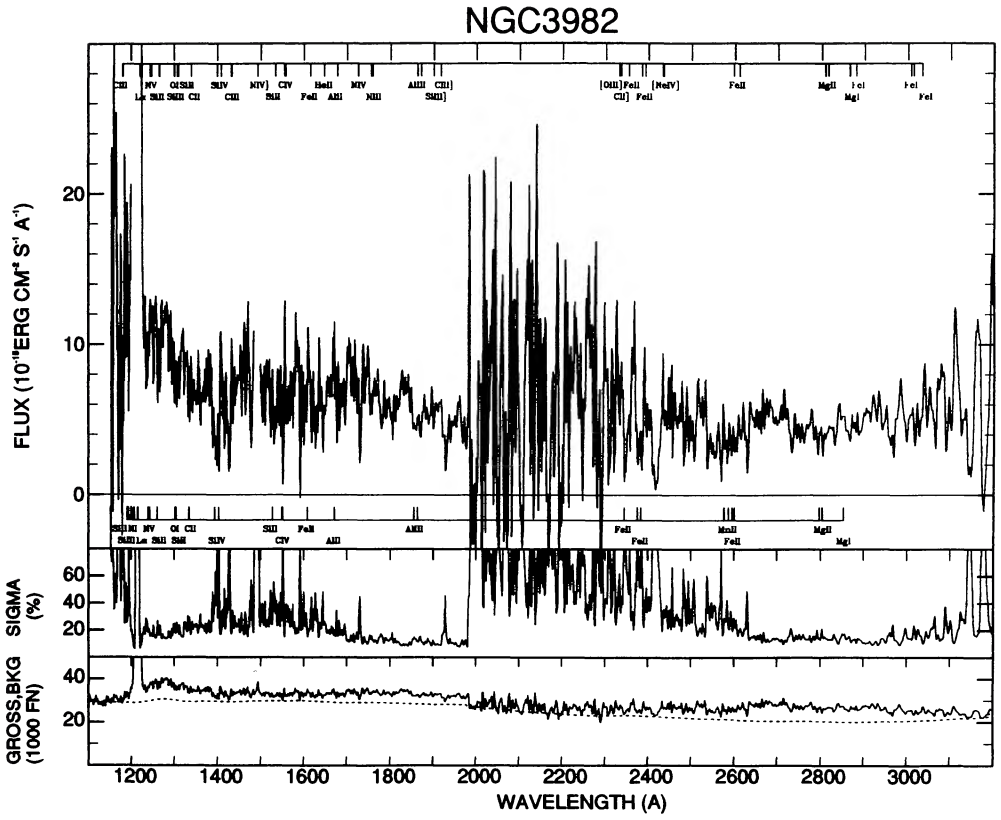


FIG. 56

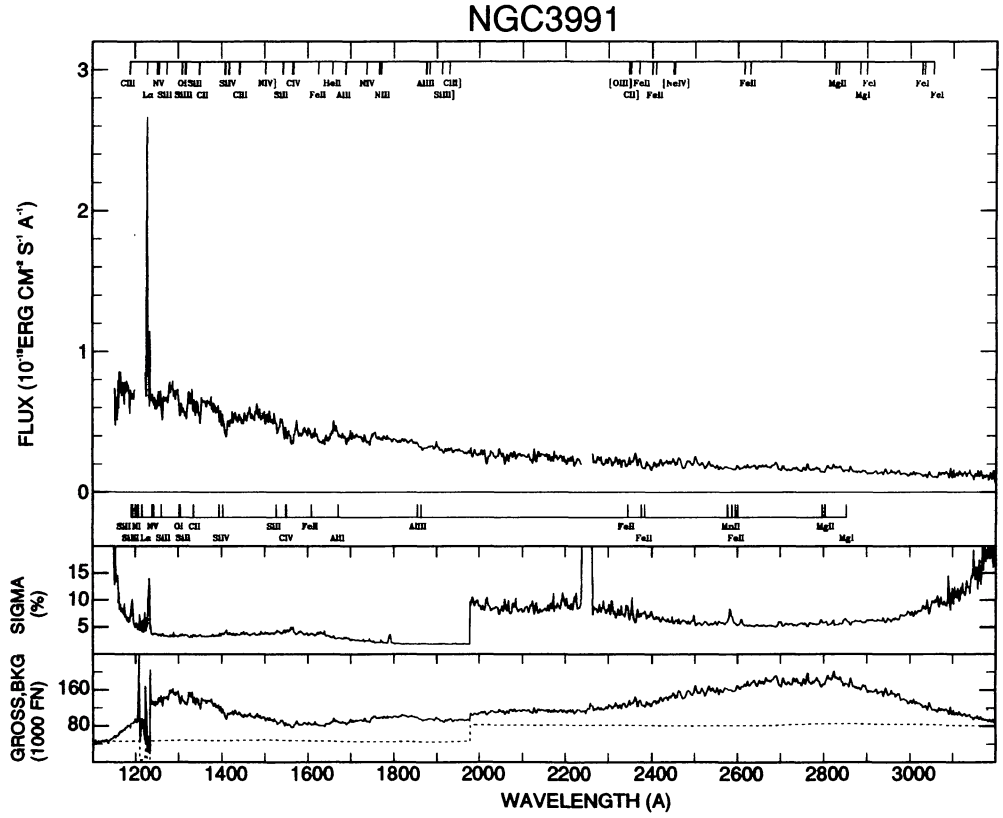


FIG. 57

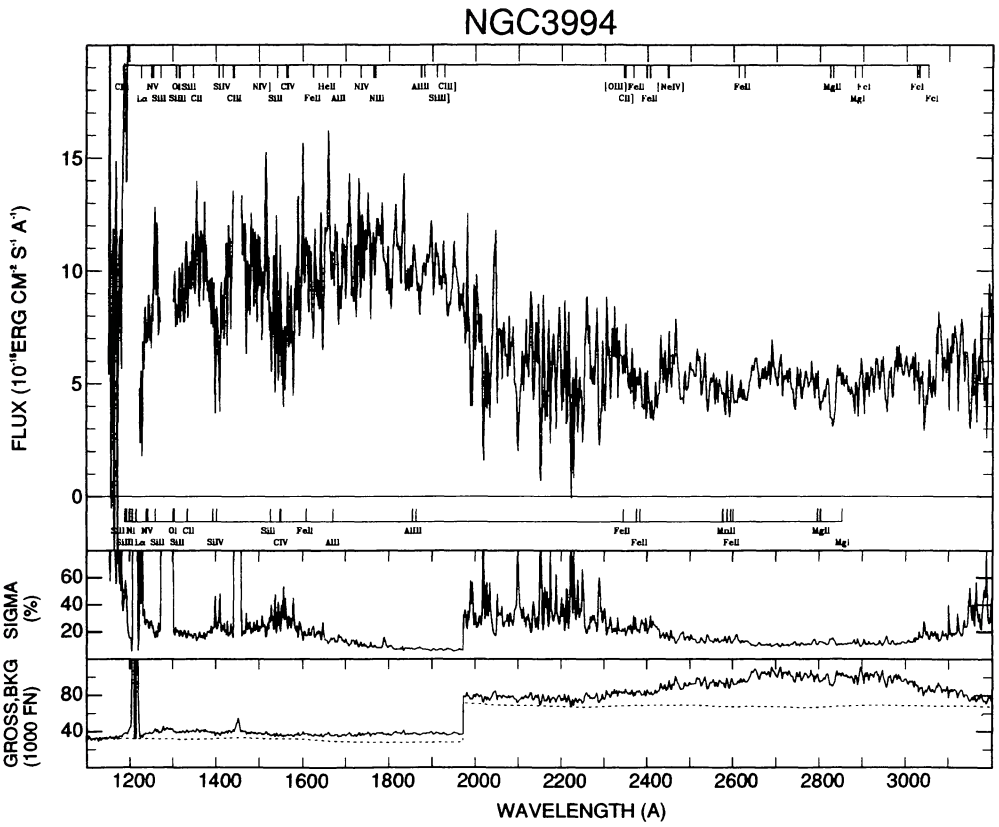


FIG. 58

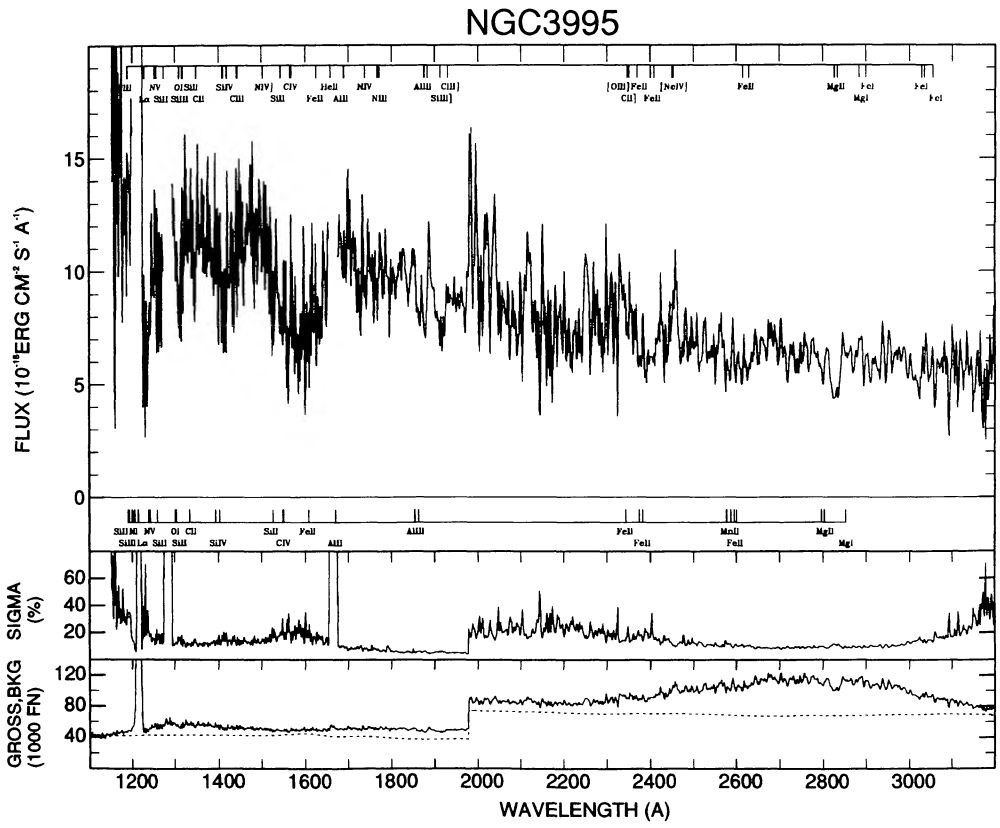


FIG. 59

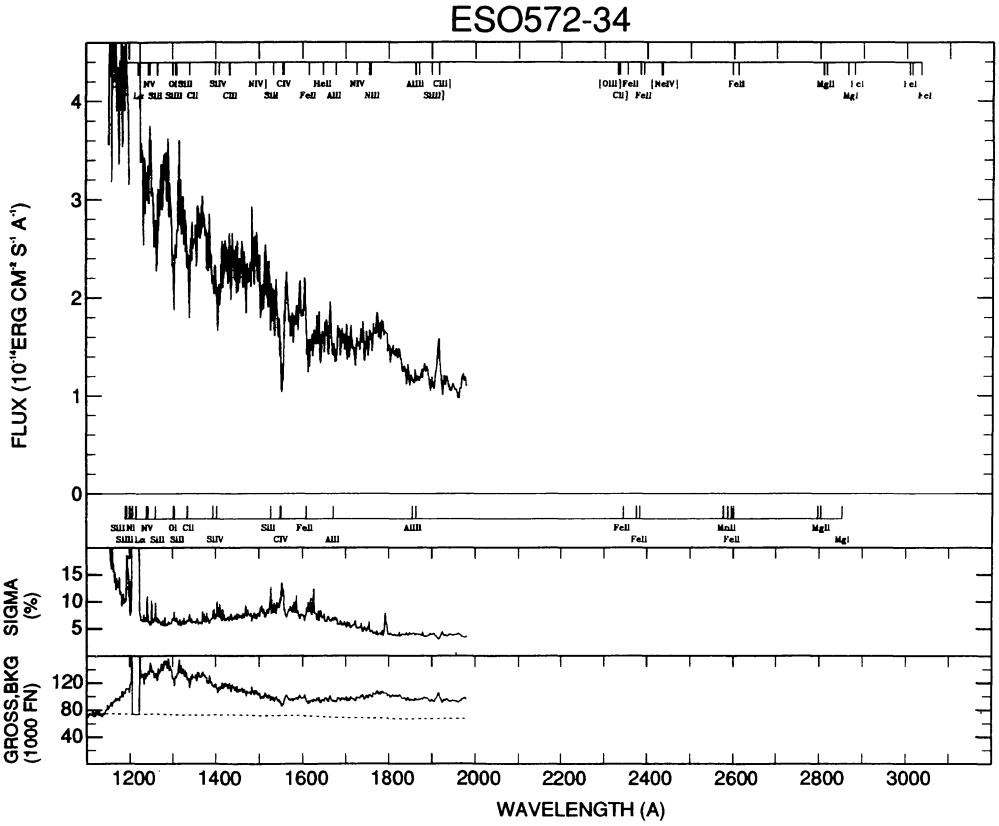


FIG. 60

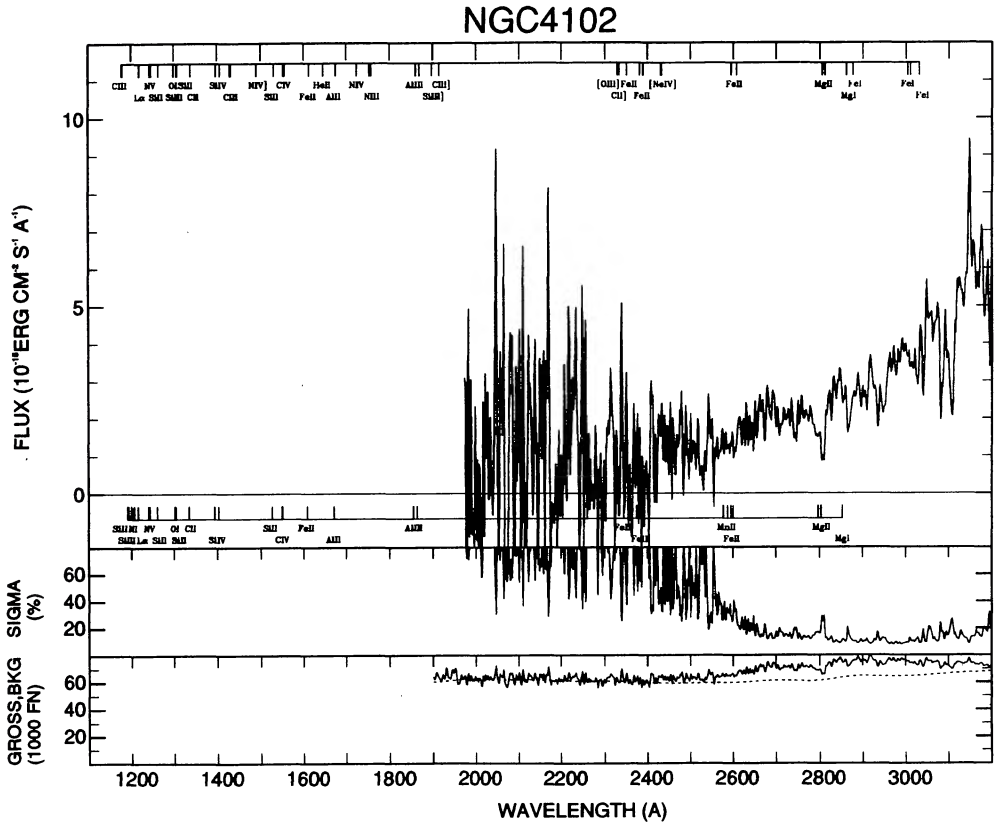


FIG. 61

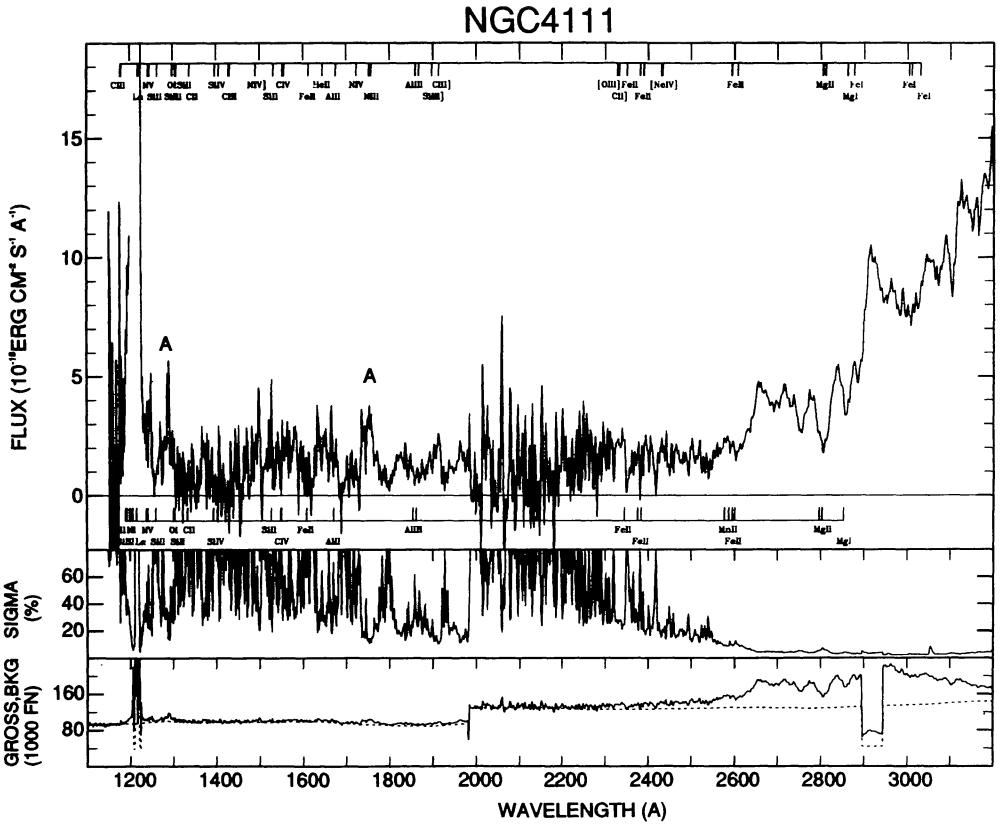


FIG. 62

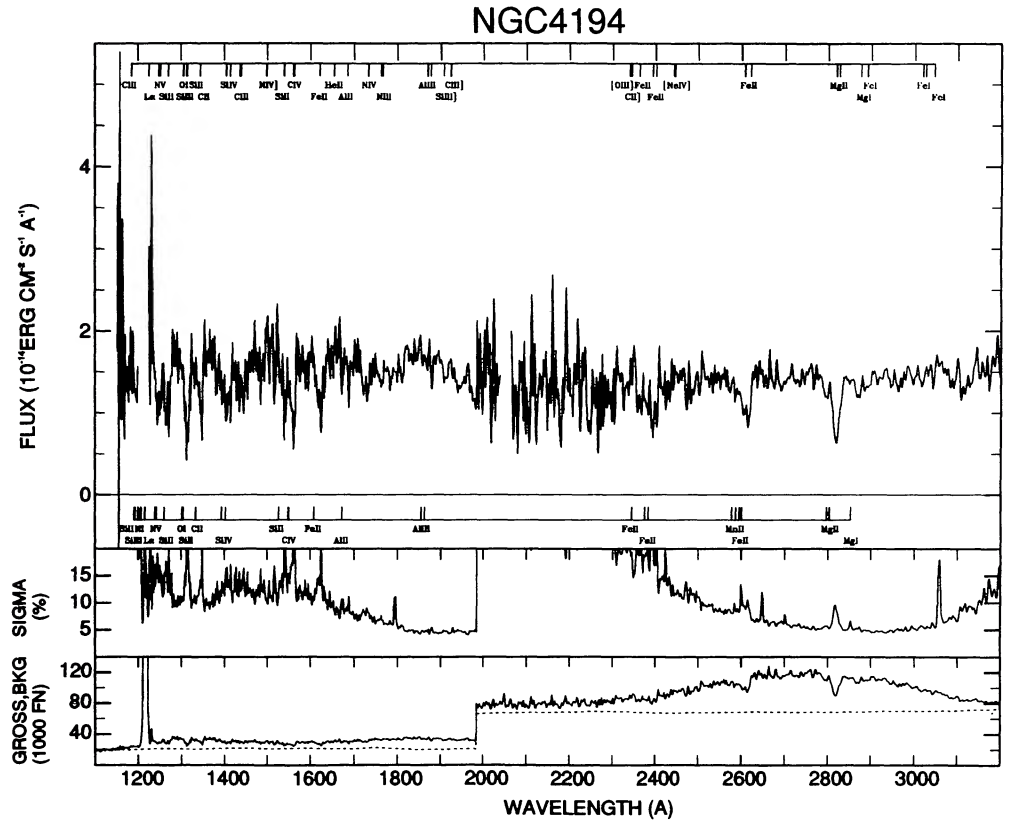


FIG. 63

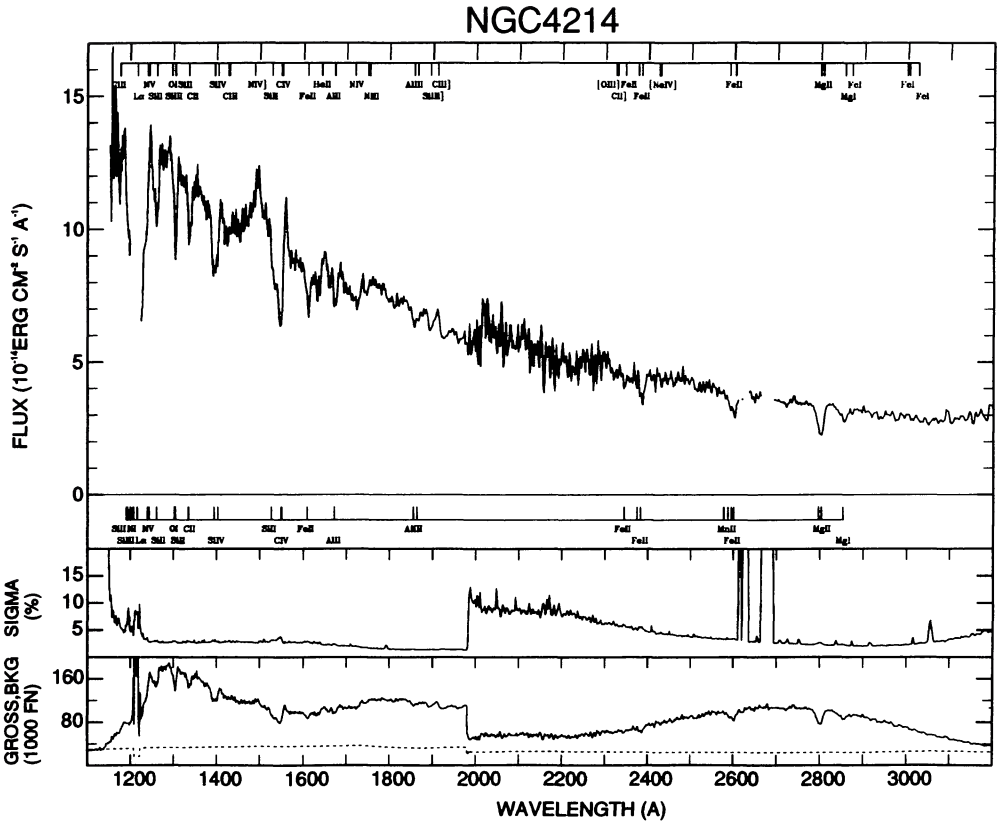


FIG. 64

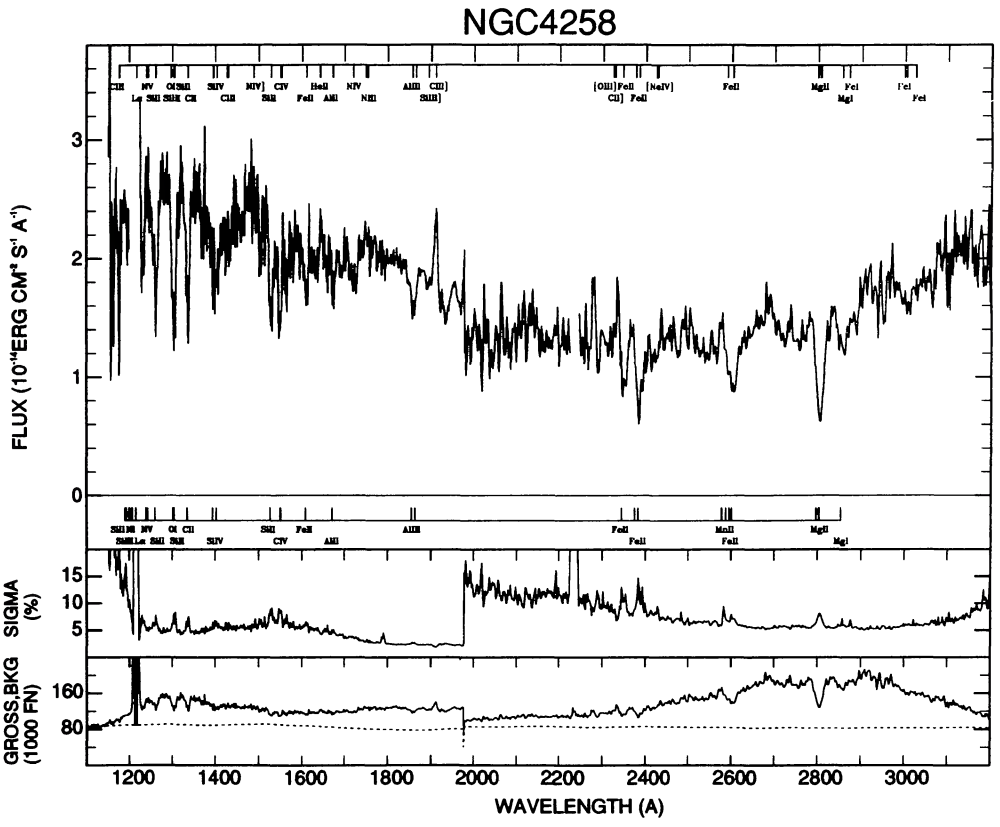


FIG. 65

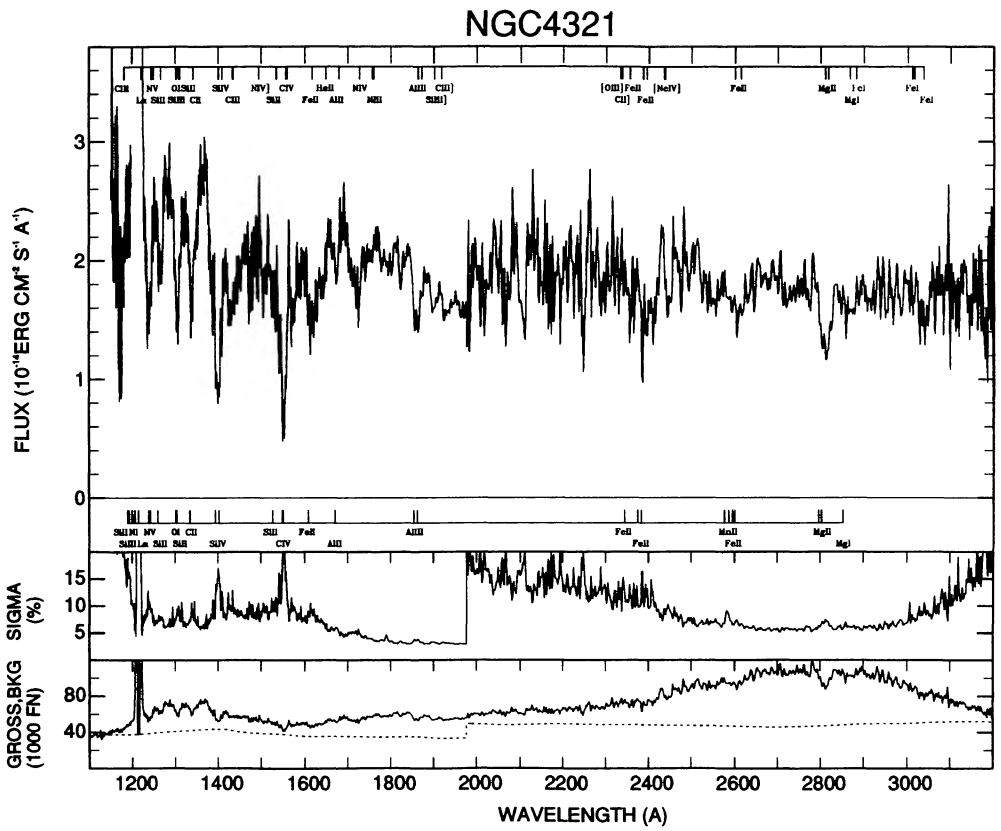


FIG. 66

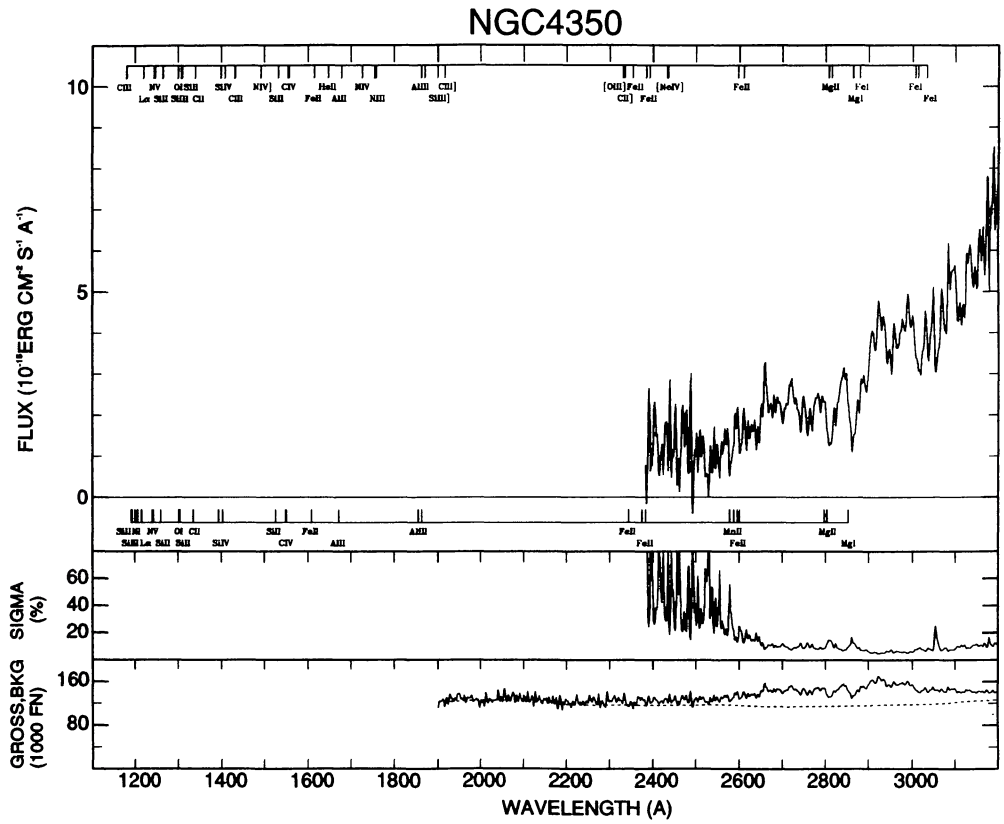


FIG. 67

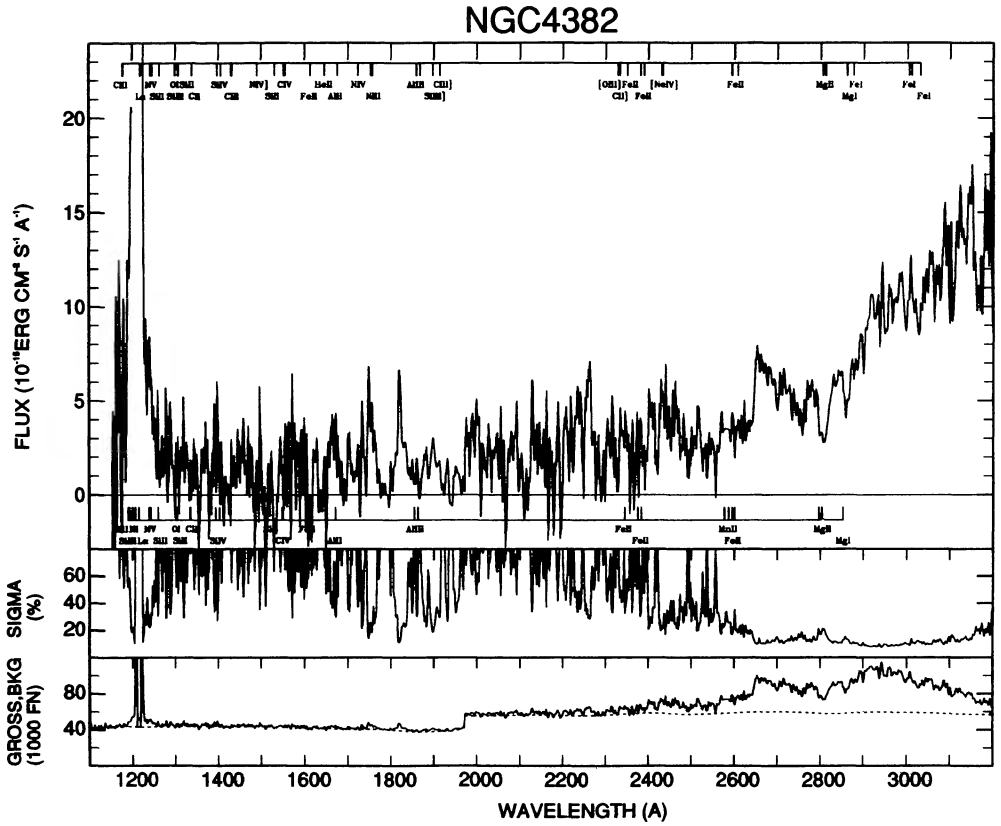


FIG. 68

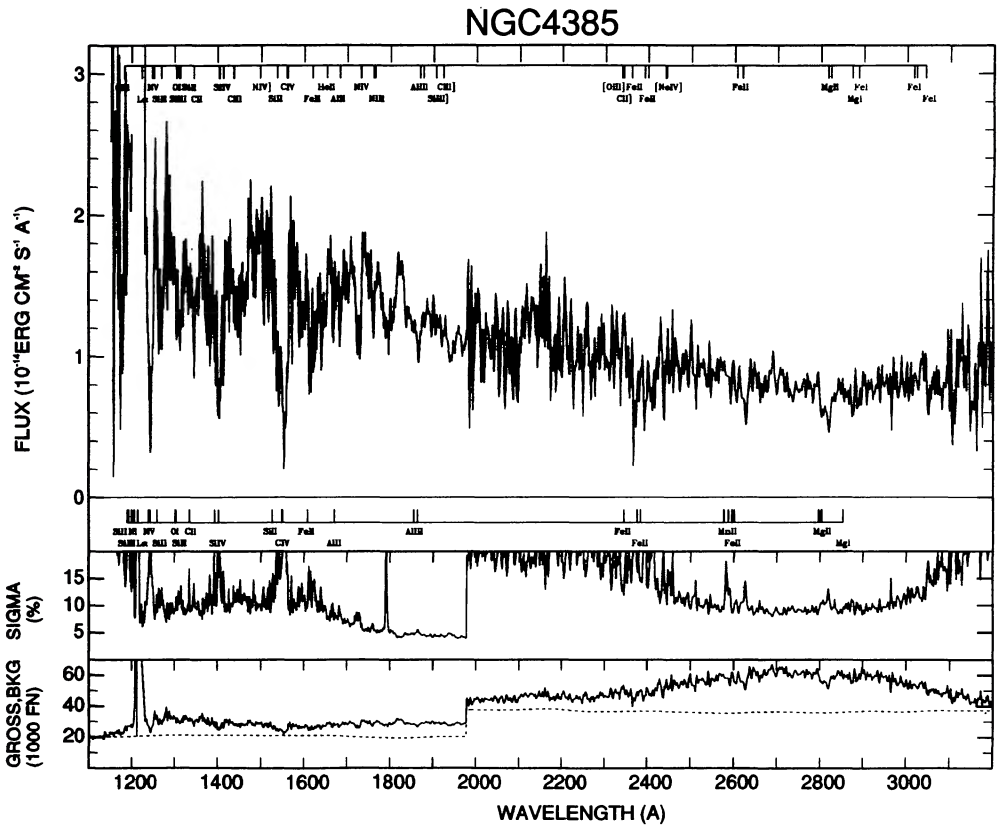


FIG. 69

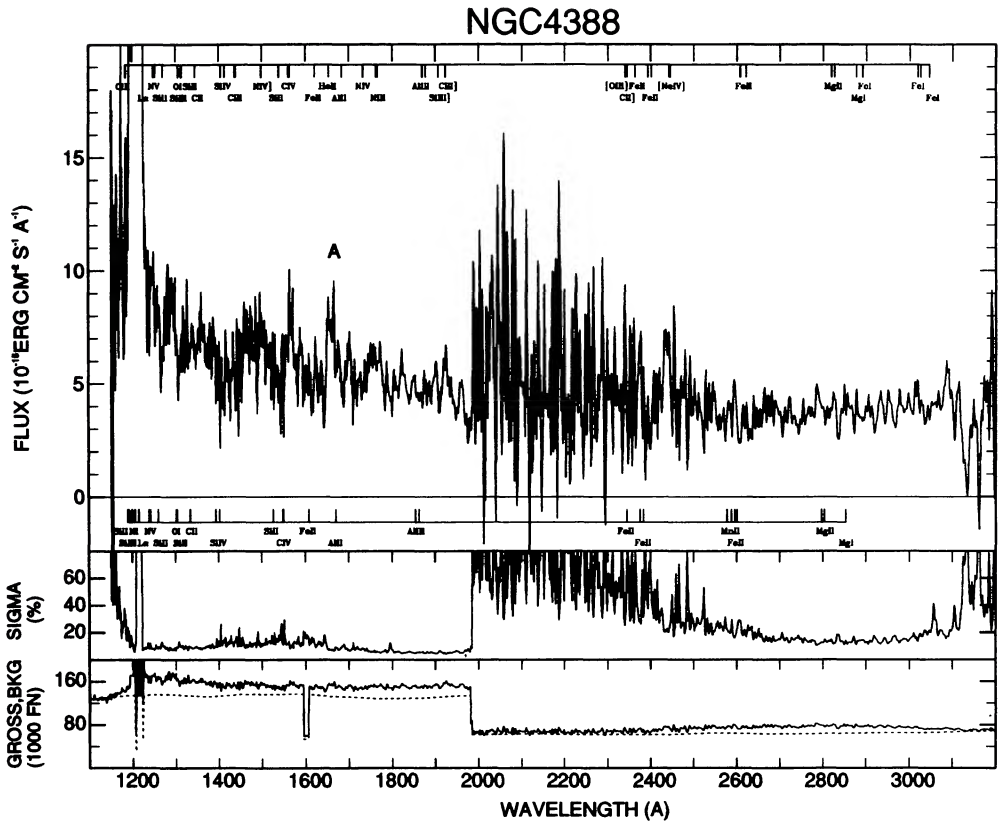


FIG. 70

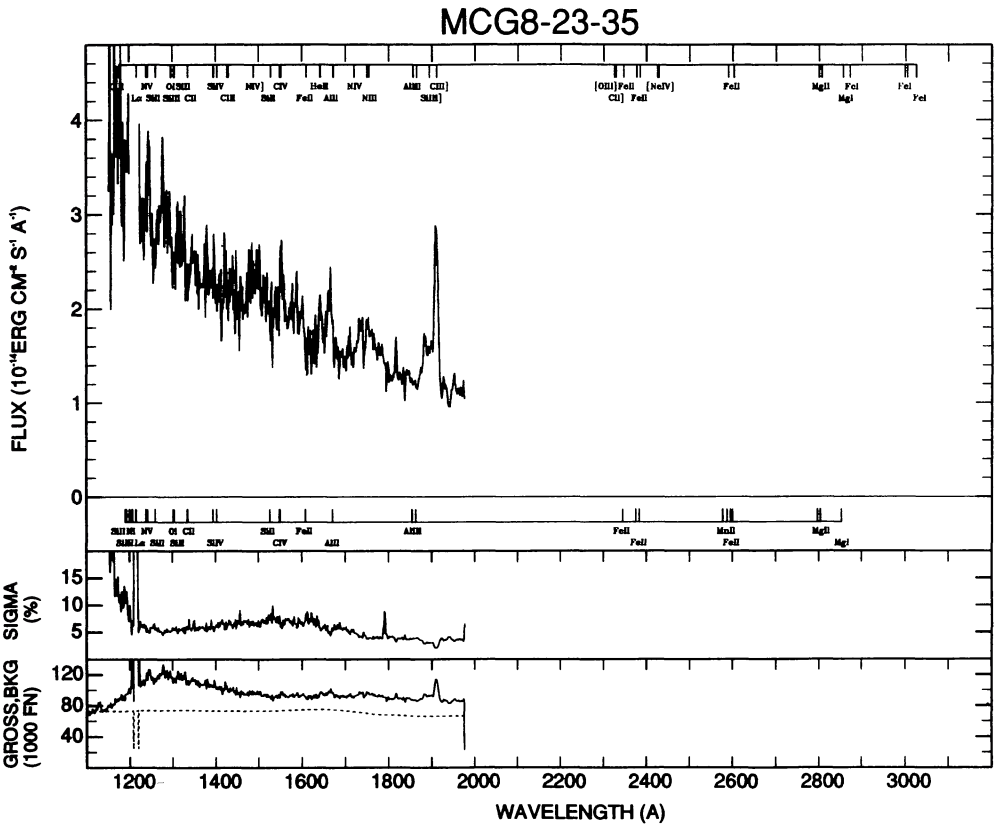


FIG. 71

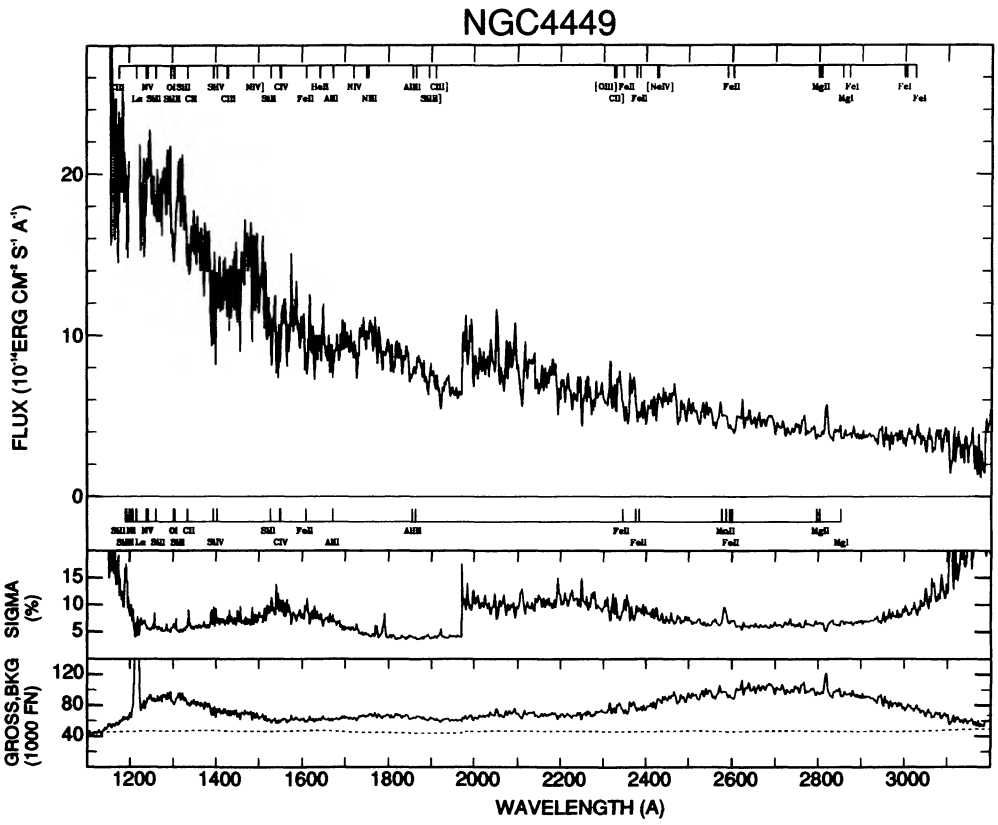


FIG. 72

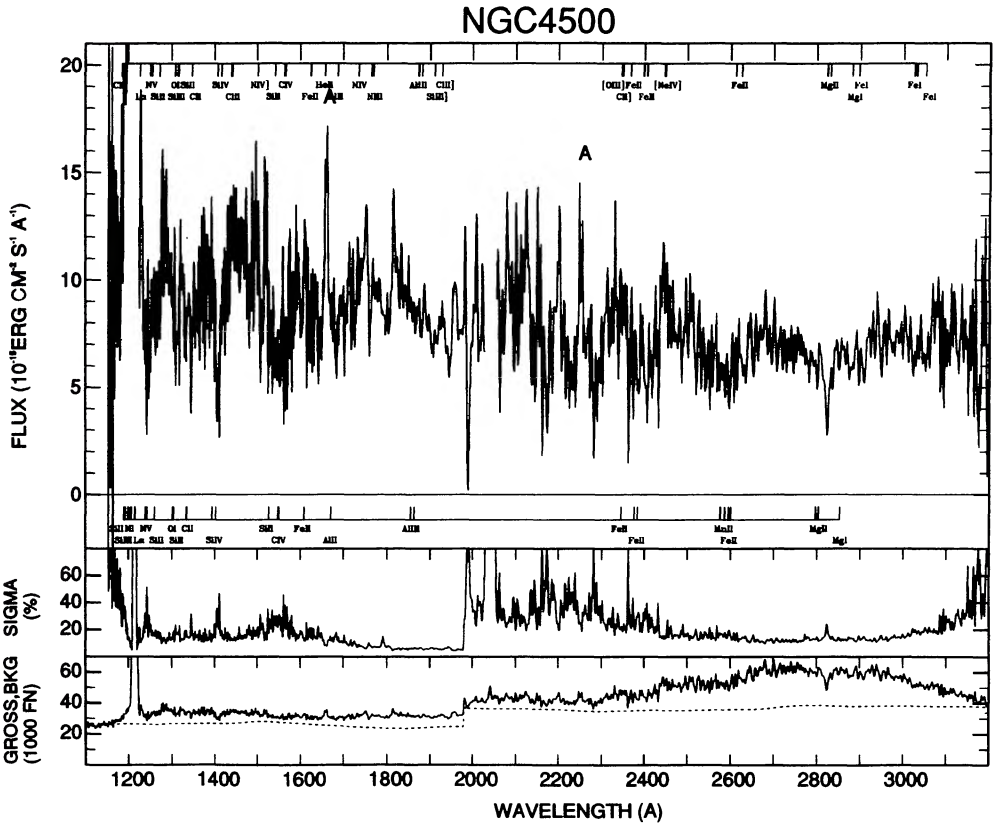


FIG. 73

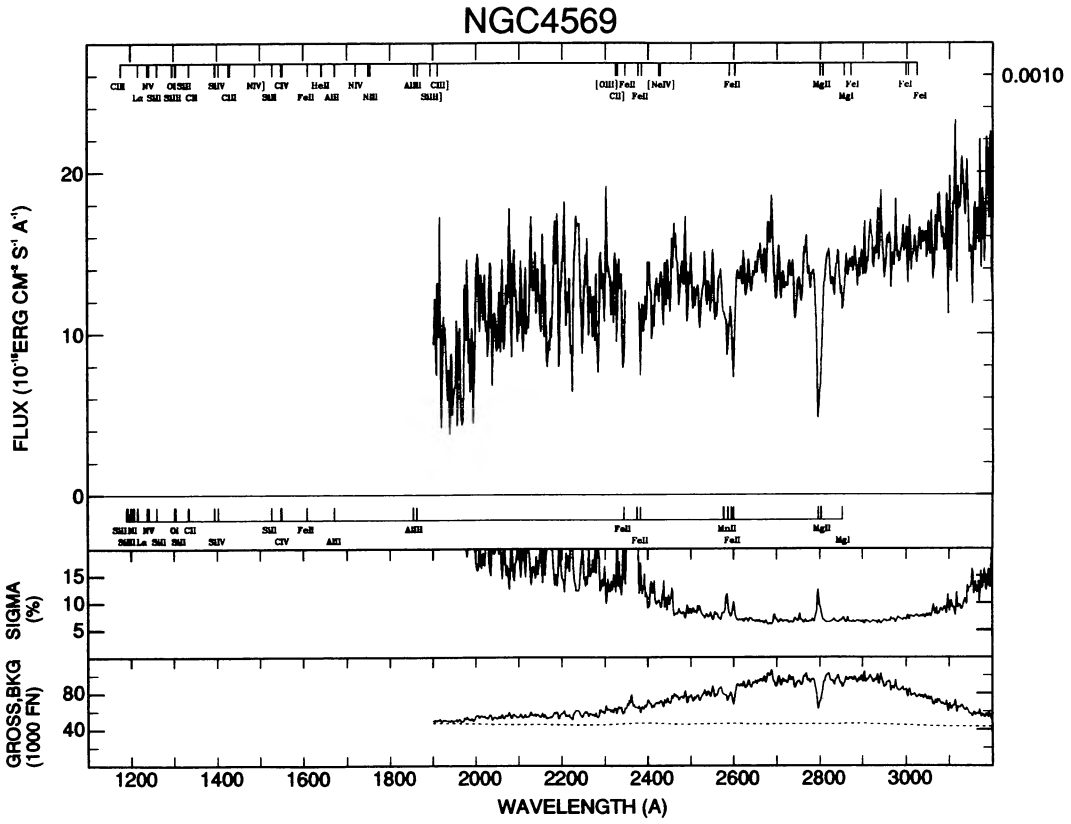


FIG. 74

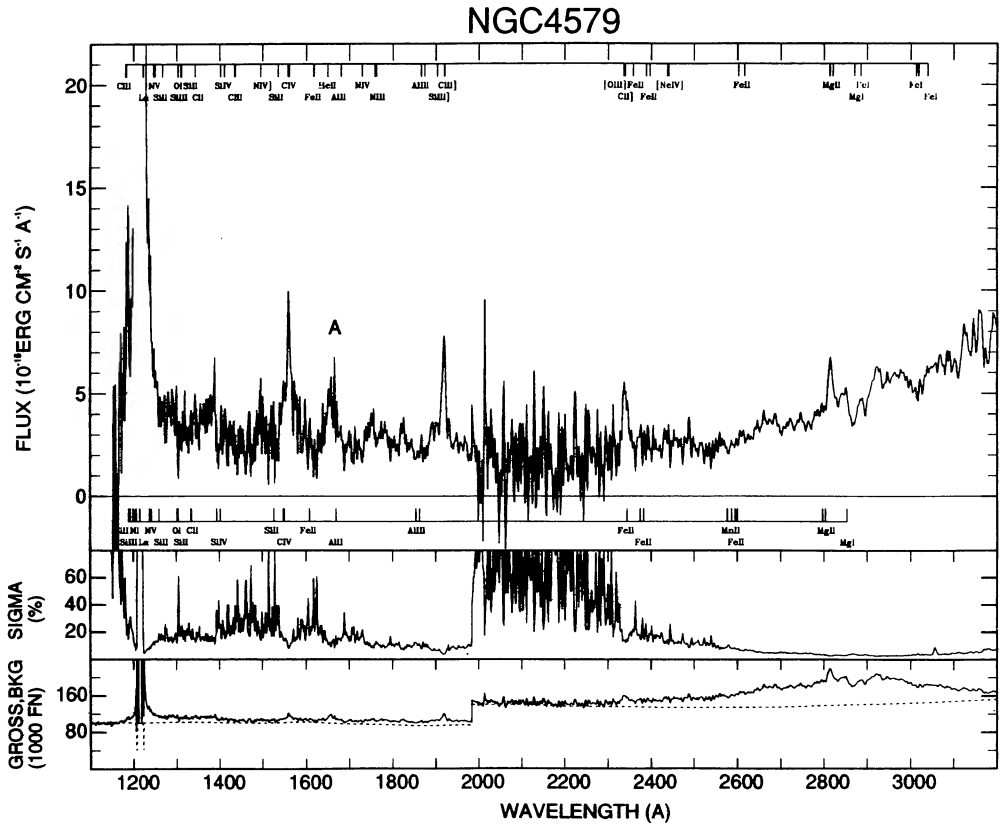


FIG. 75

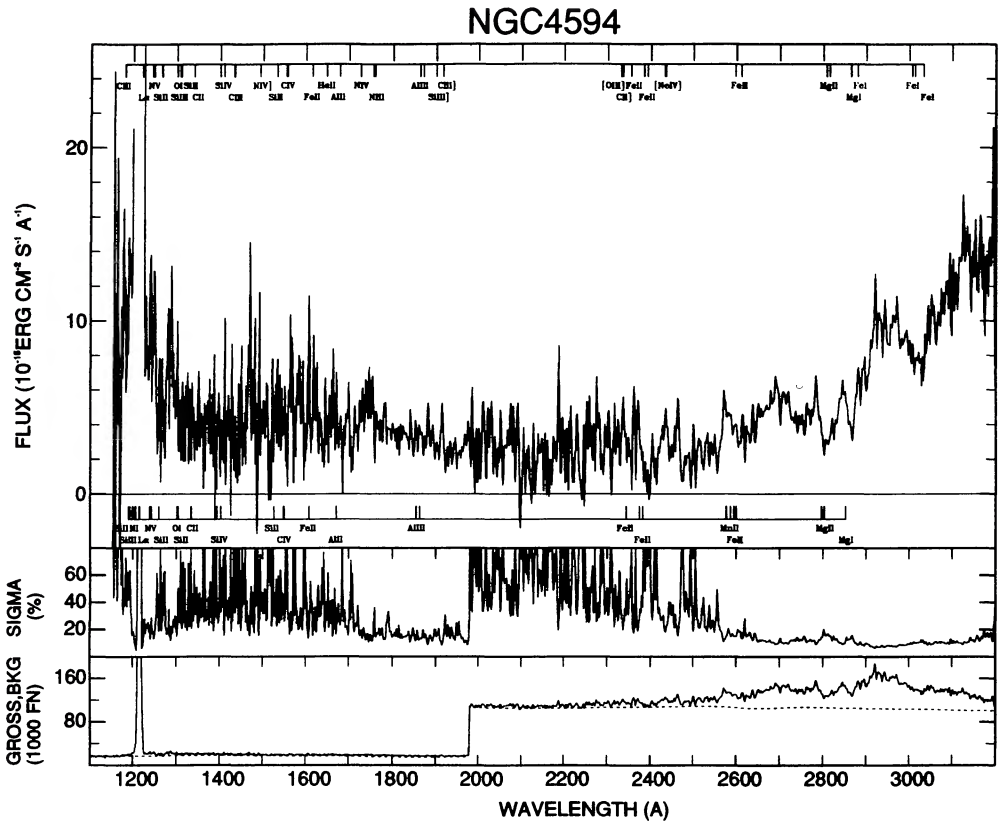


FIG. 76

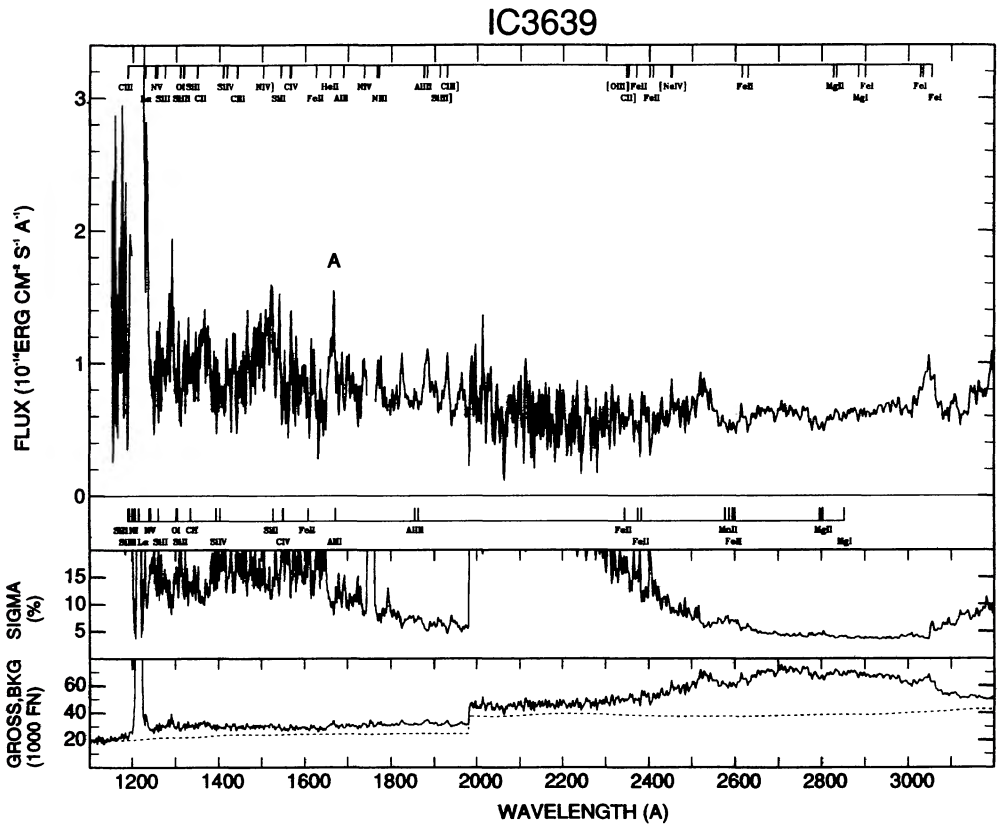


FIG. 77

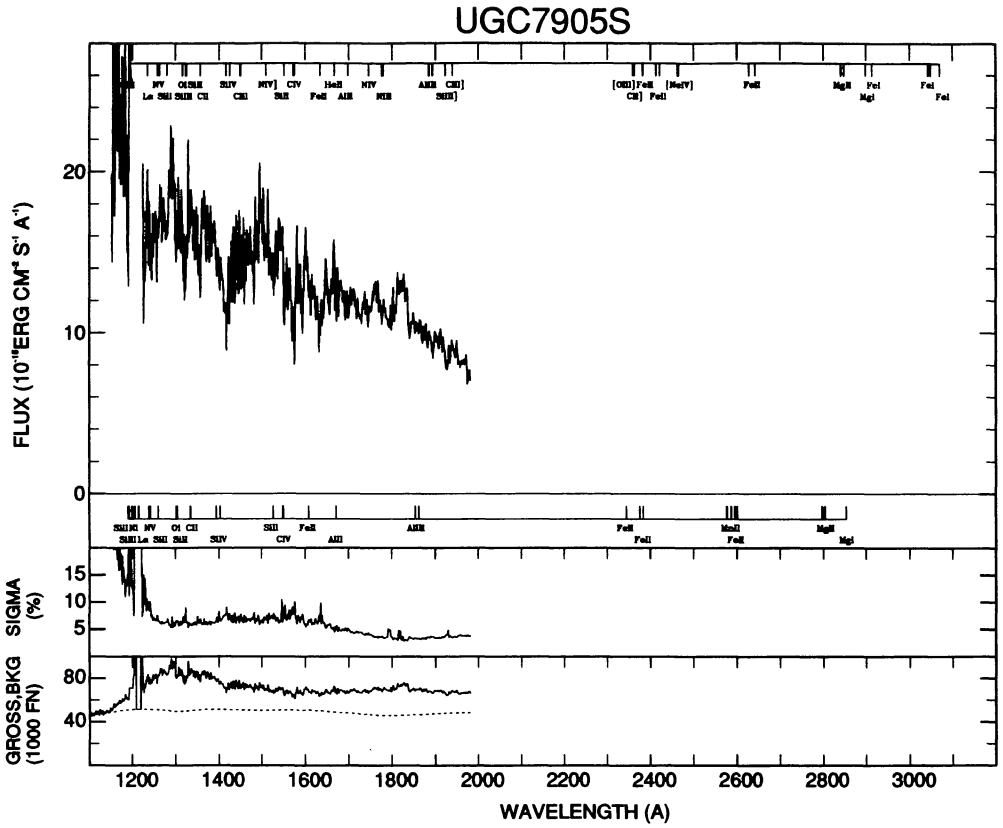


FIG. 78

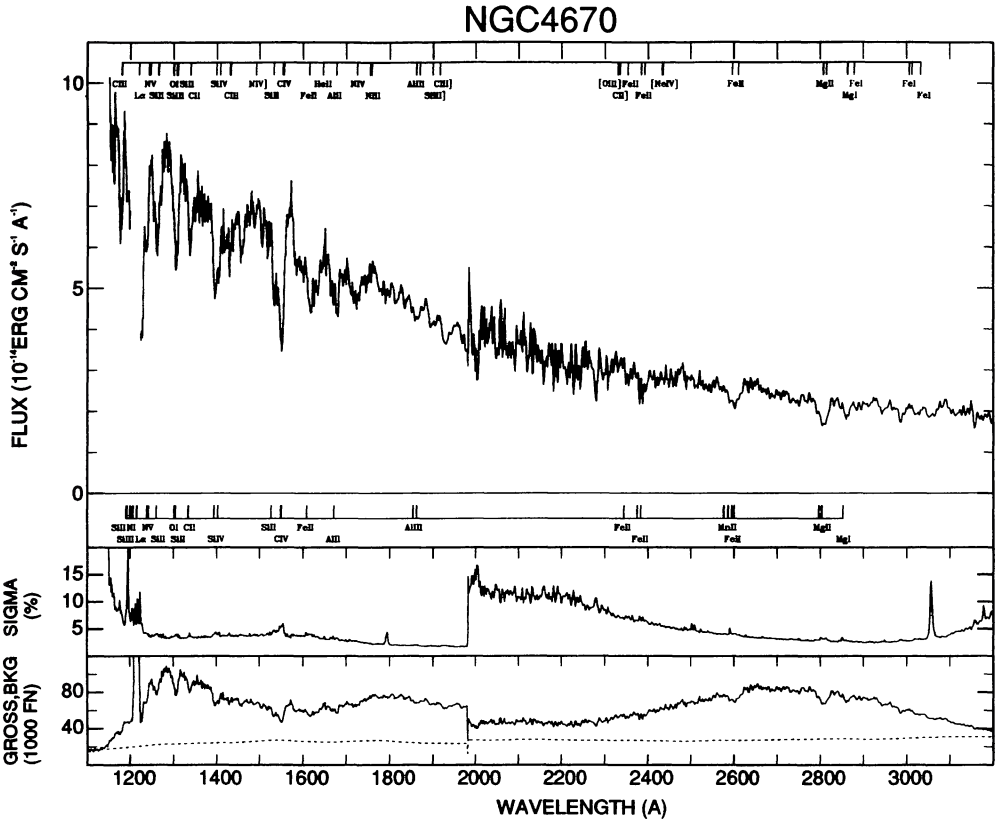


FIG. 79

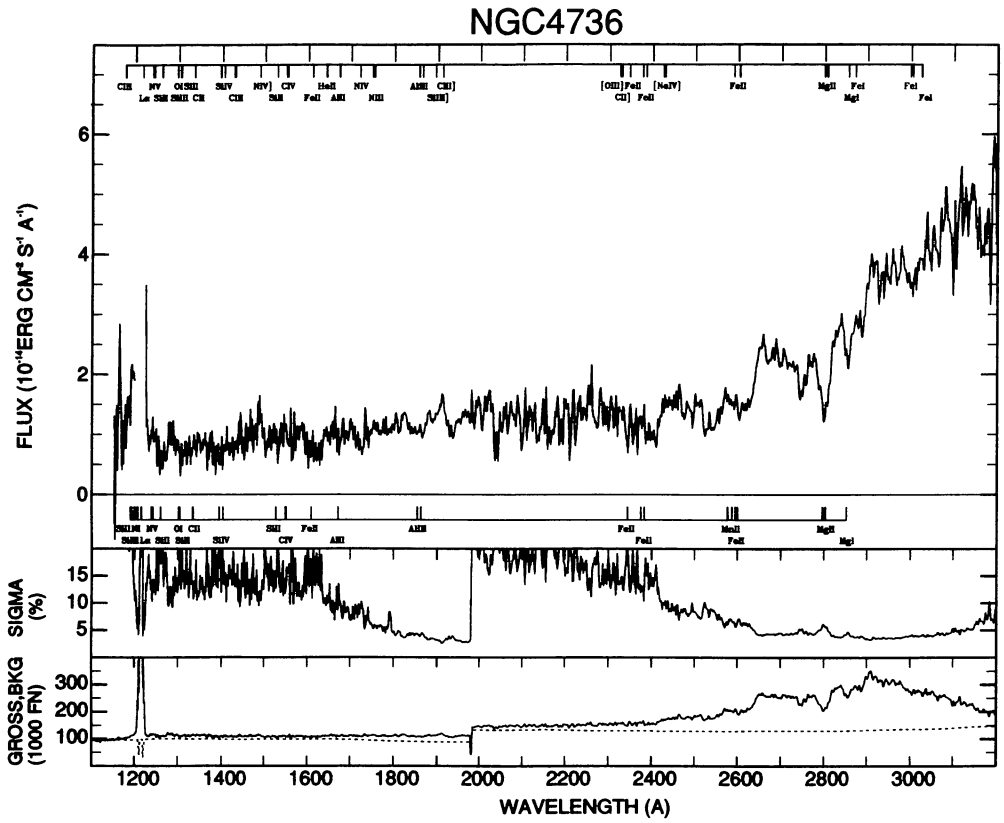


FIG. 80

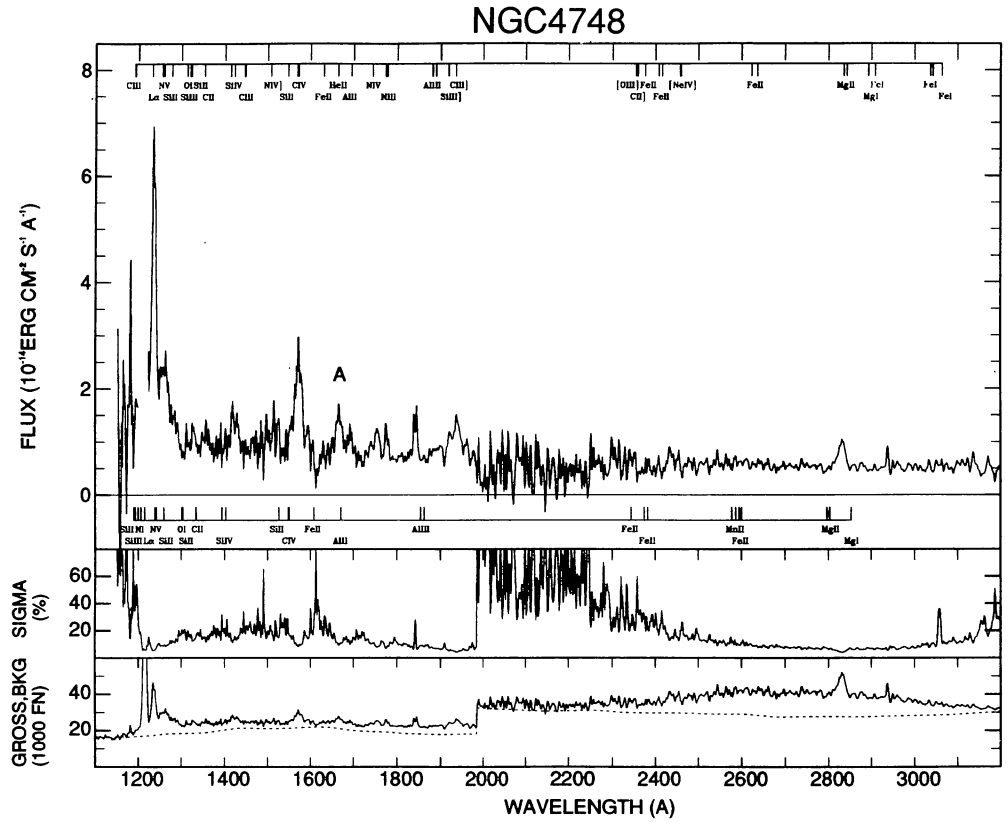


FIG. 81

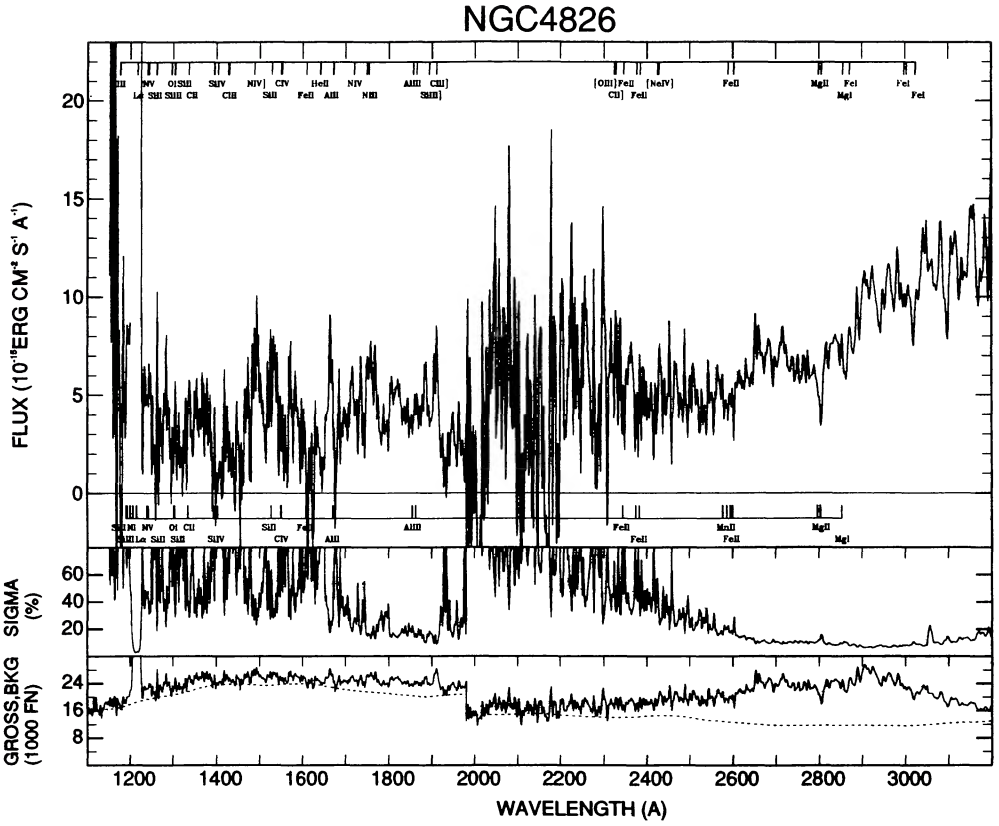


FIG. 82

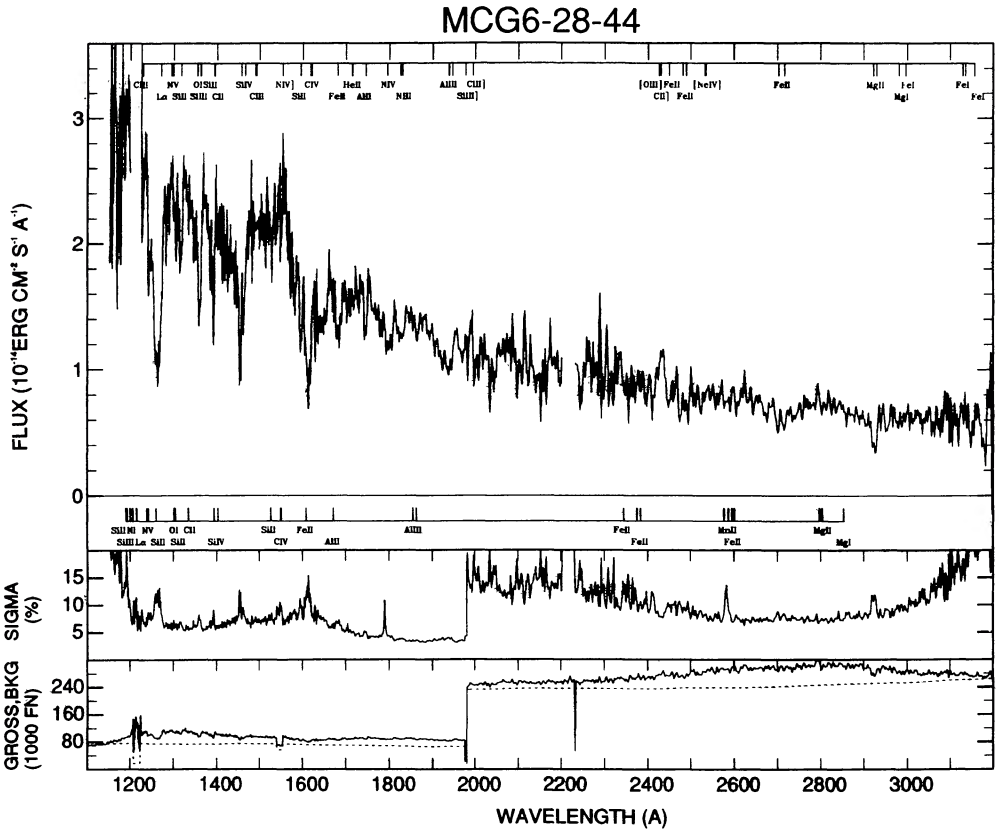


FIG. 83

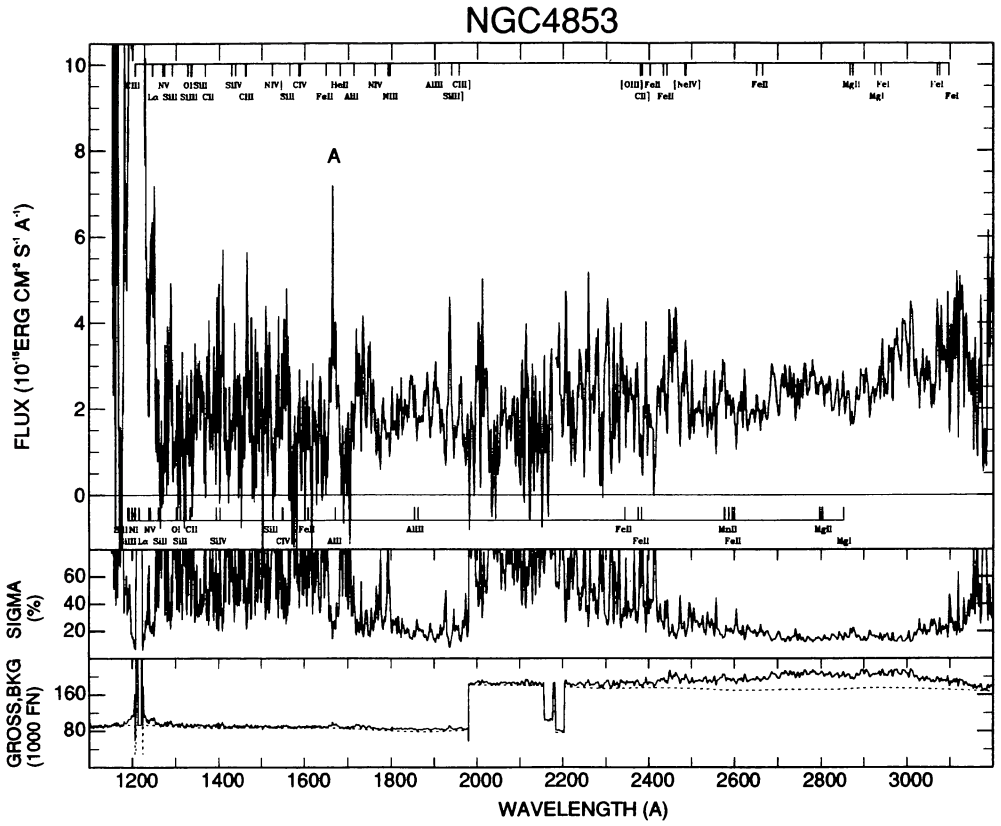


FIG. 84

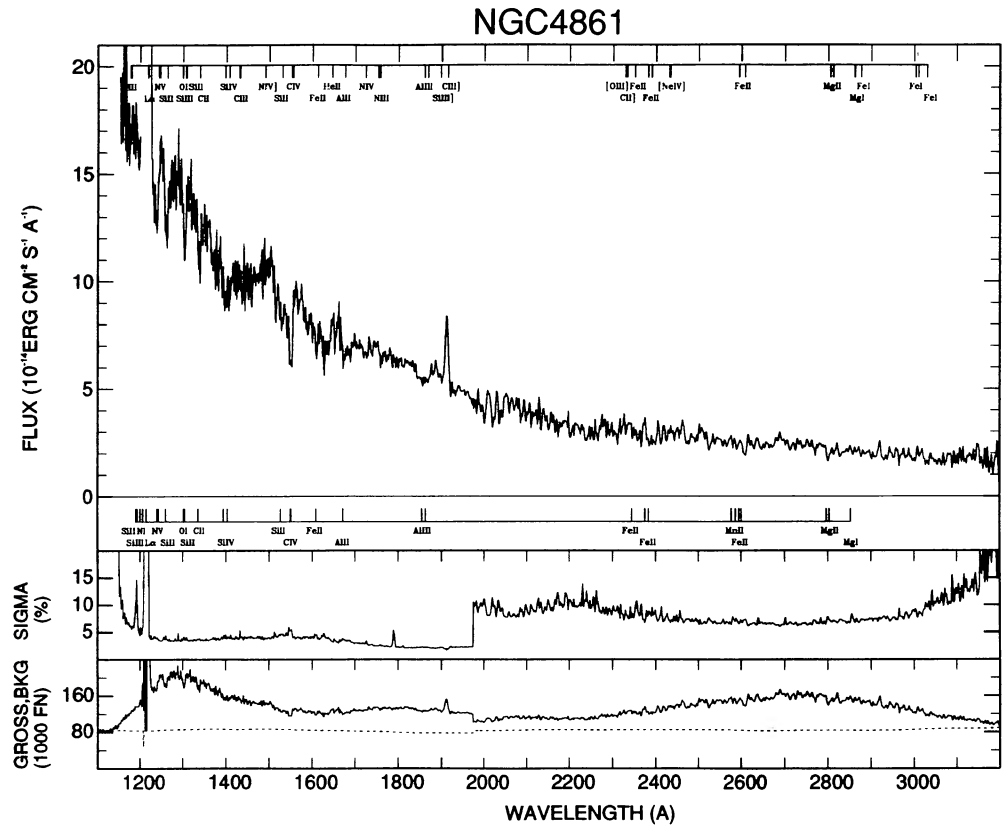


FIG. 85

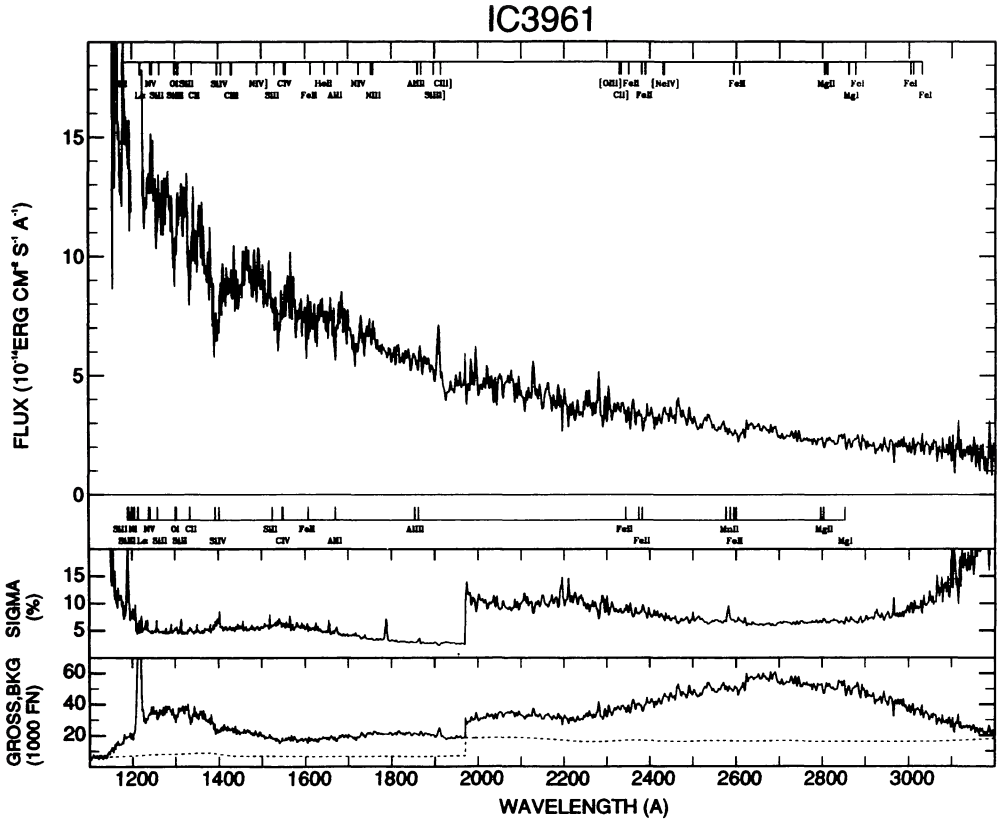


FIG. 86

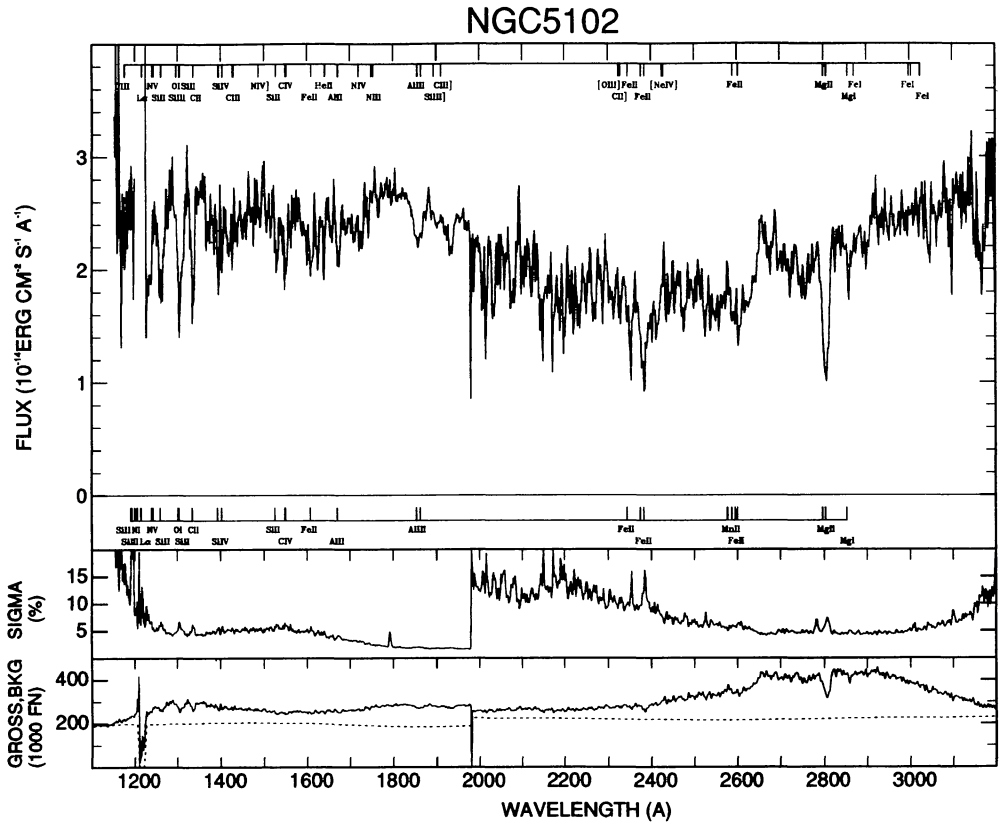


FIG. 87

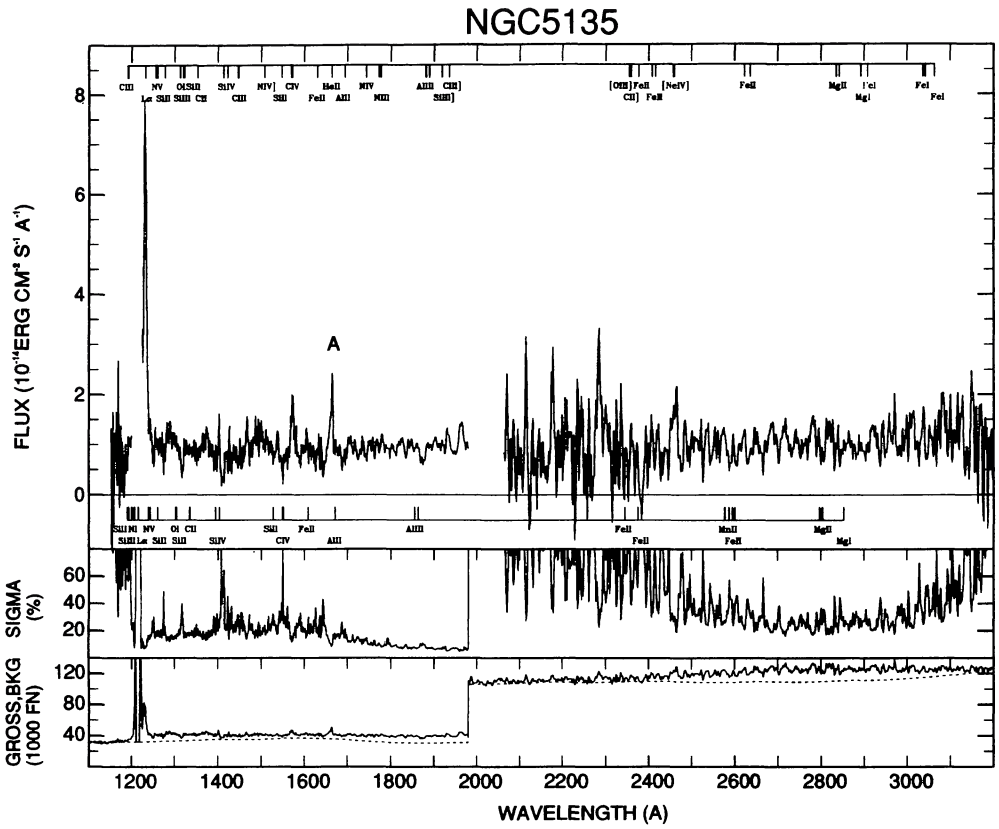


FIG. 88

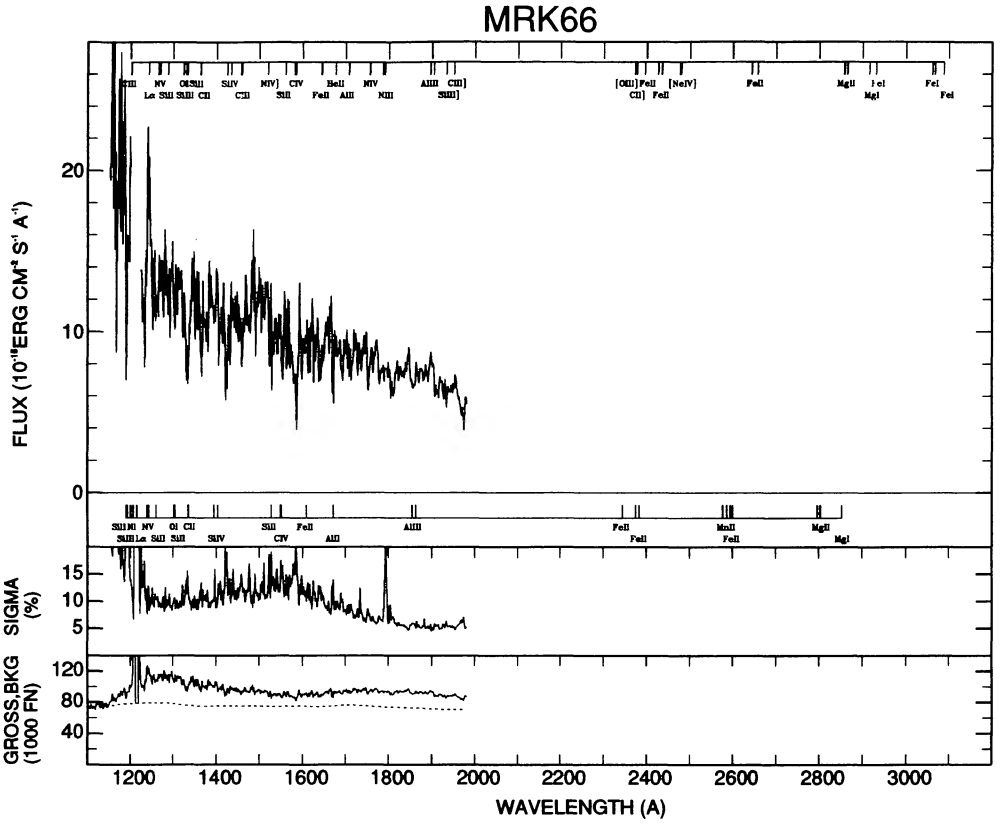


FIG. 89

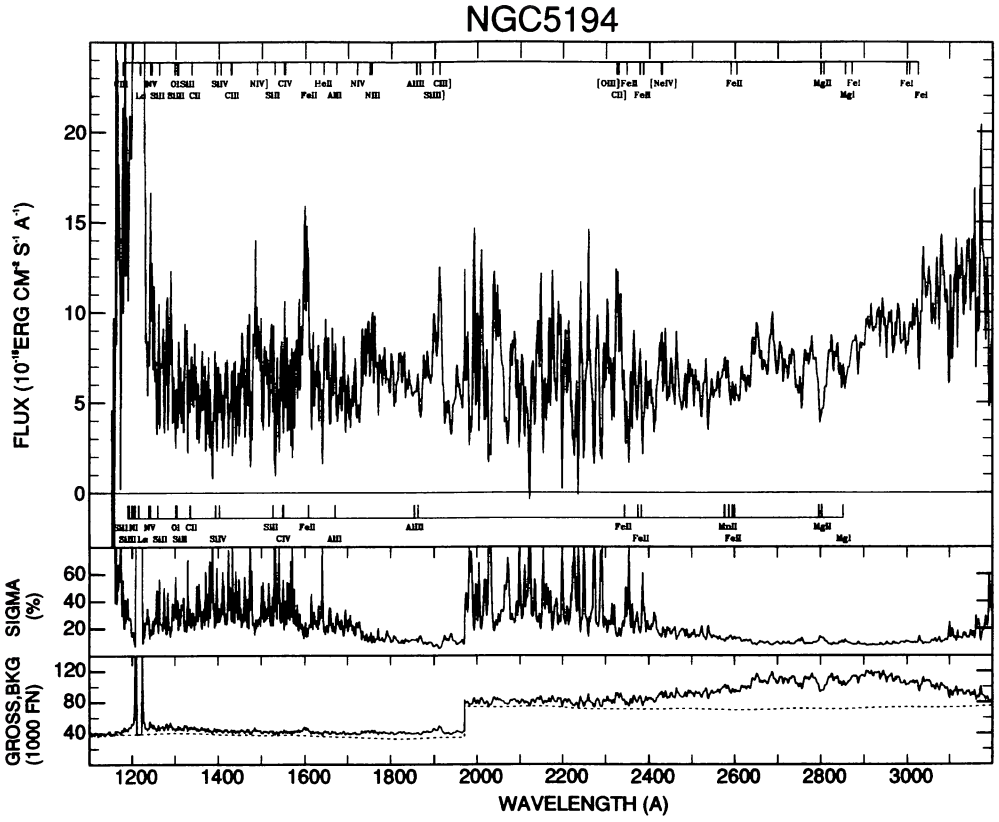


FIG. 90

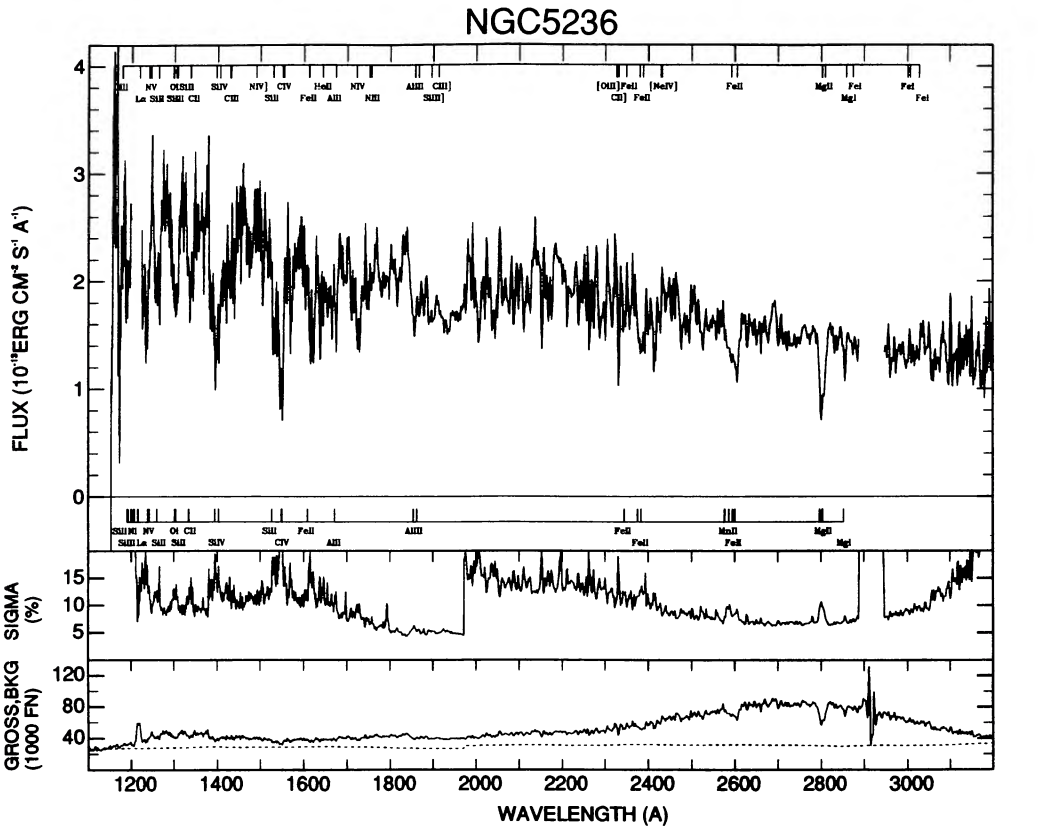


FIG. 91

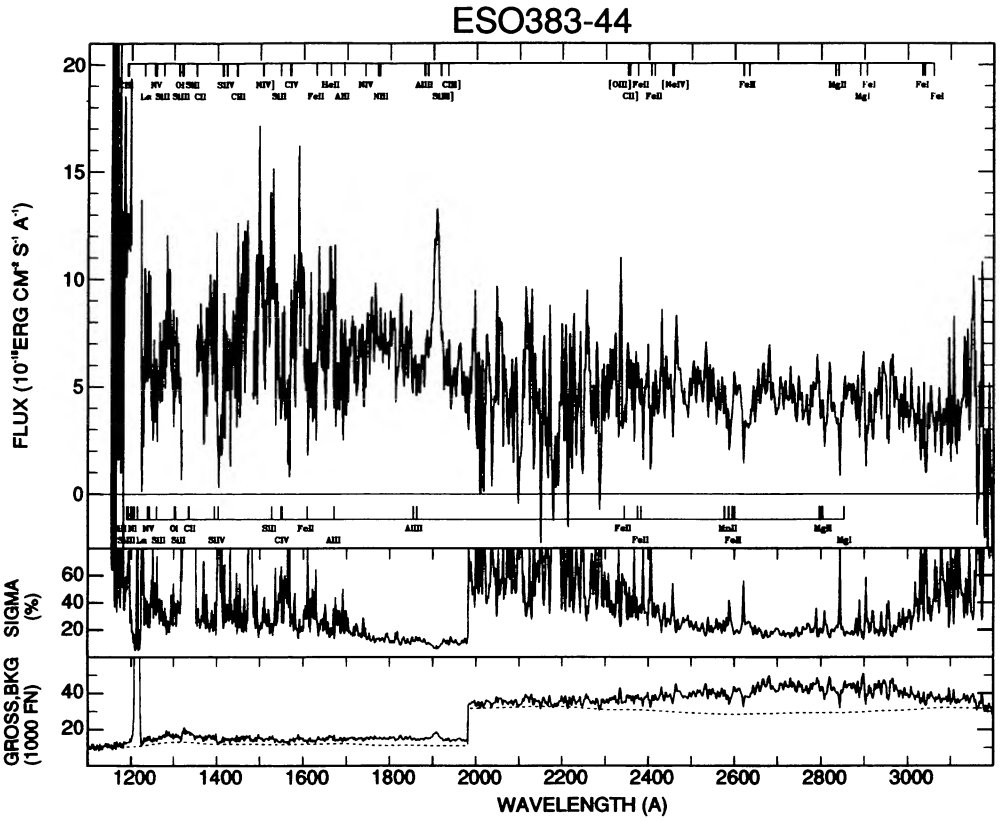


FIG. 92

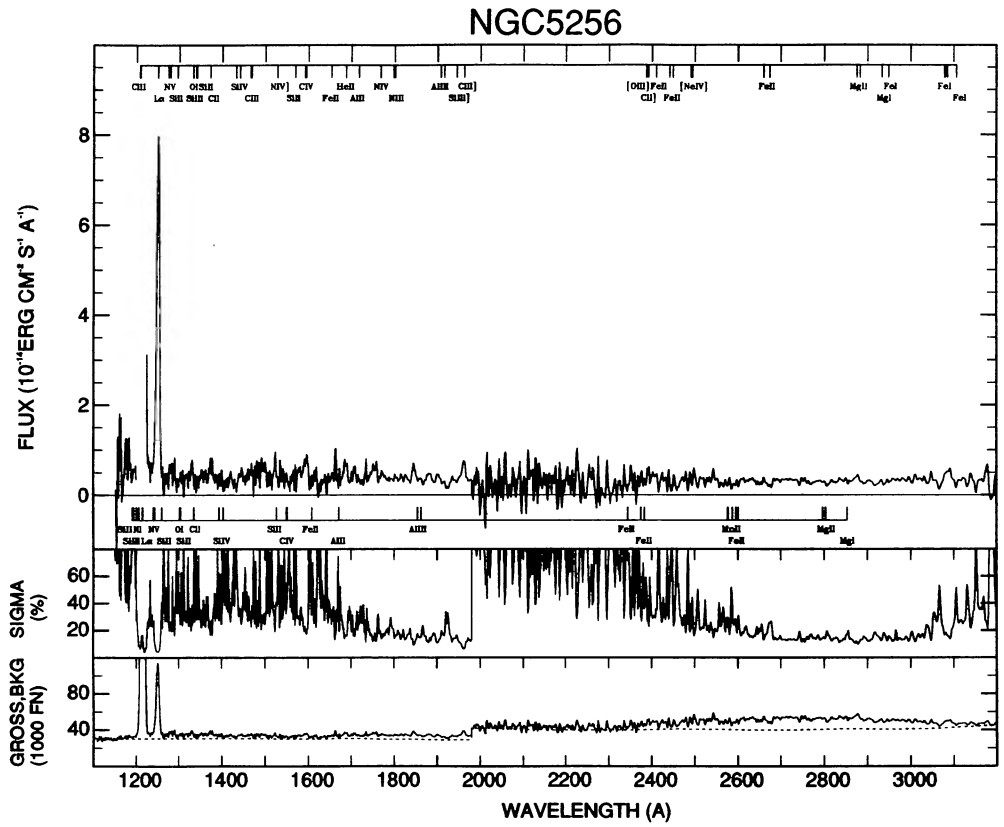


FIG. 93

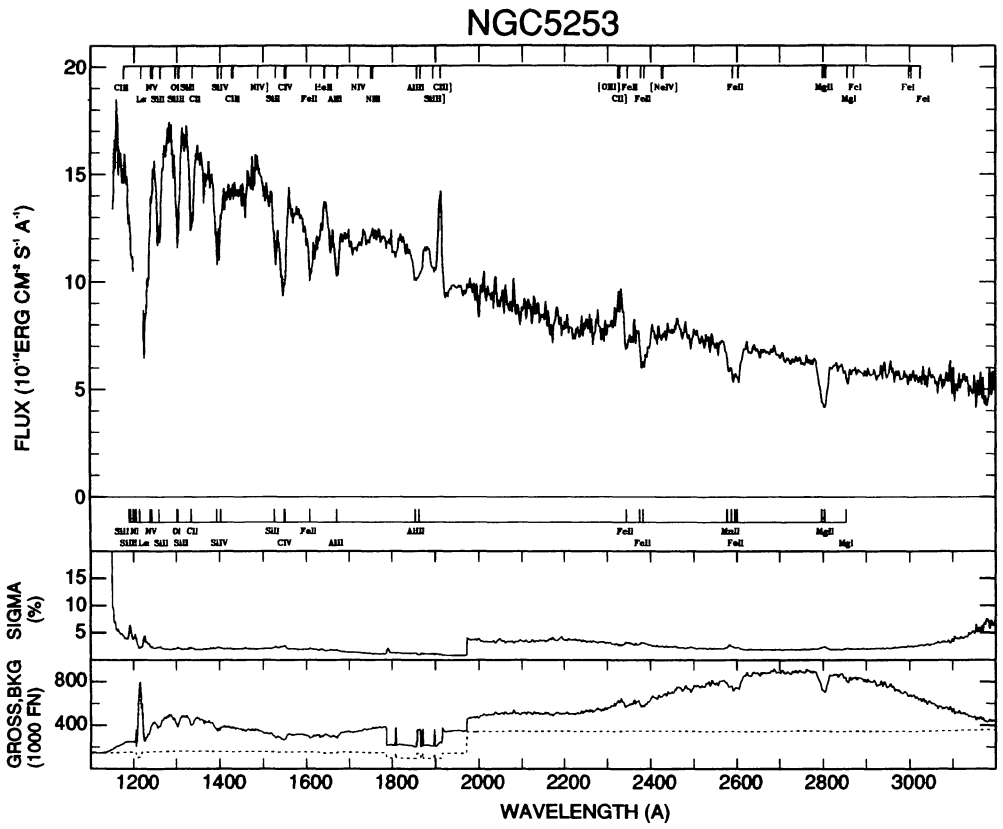


FIG. 94

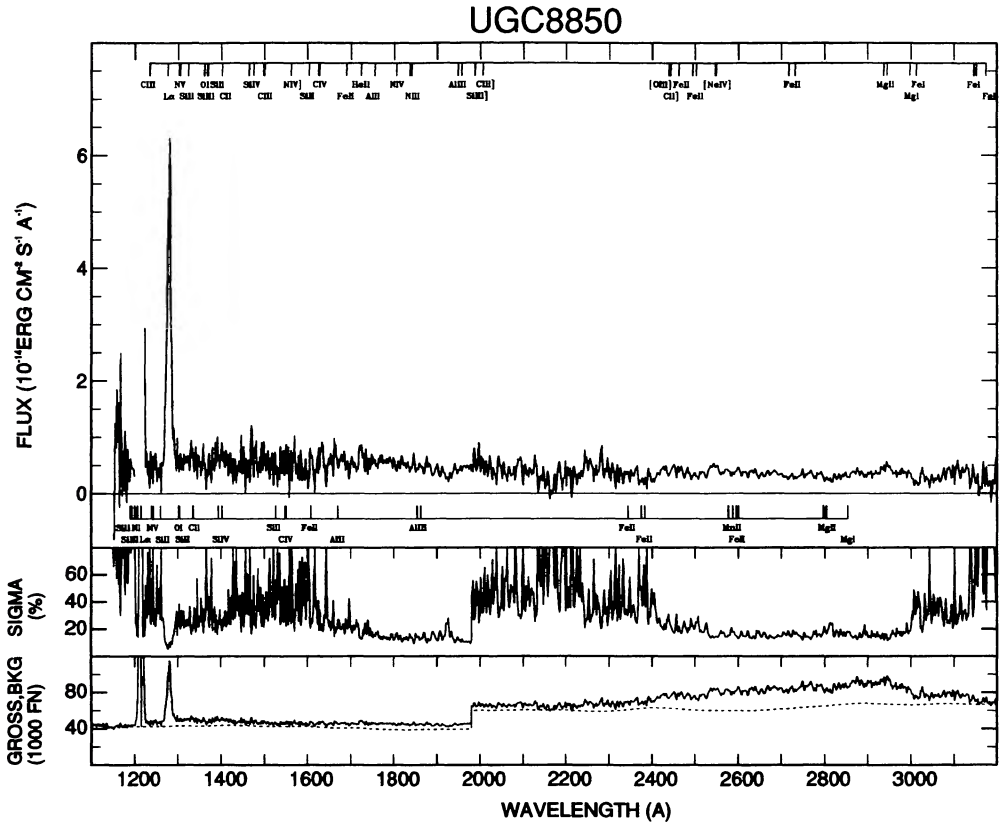


FIG. 95

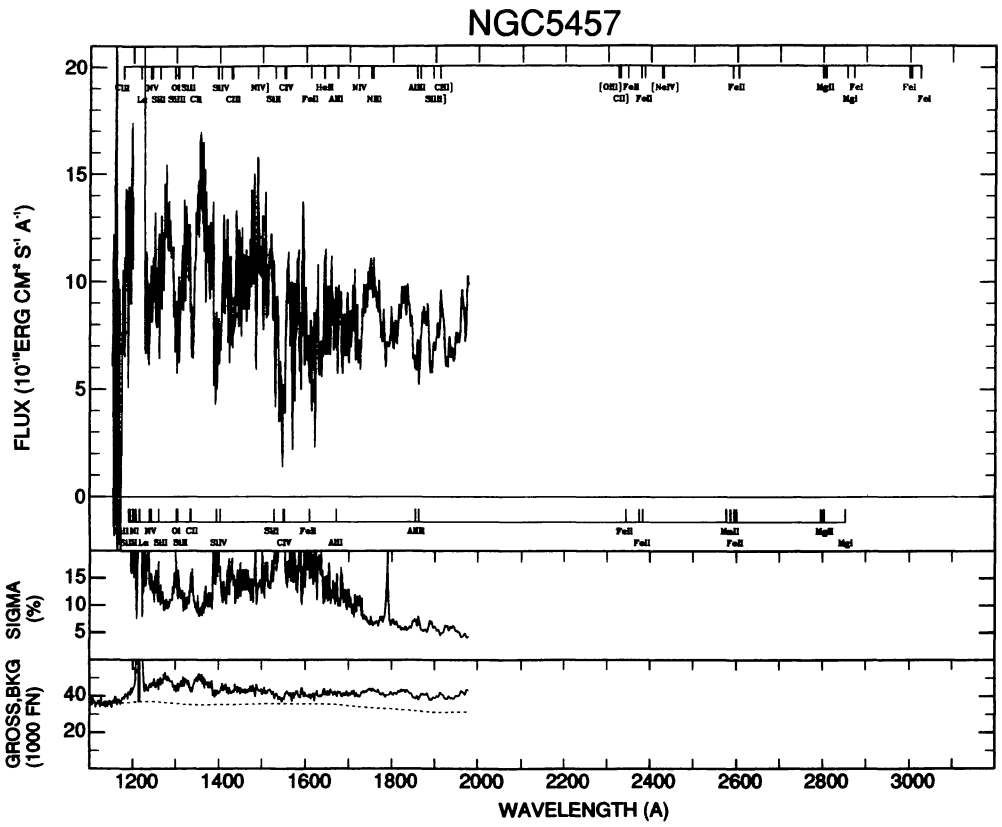


FIG. 96

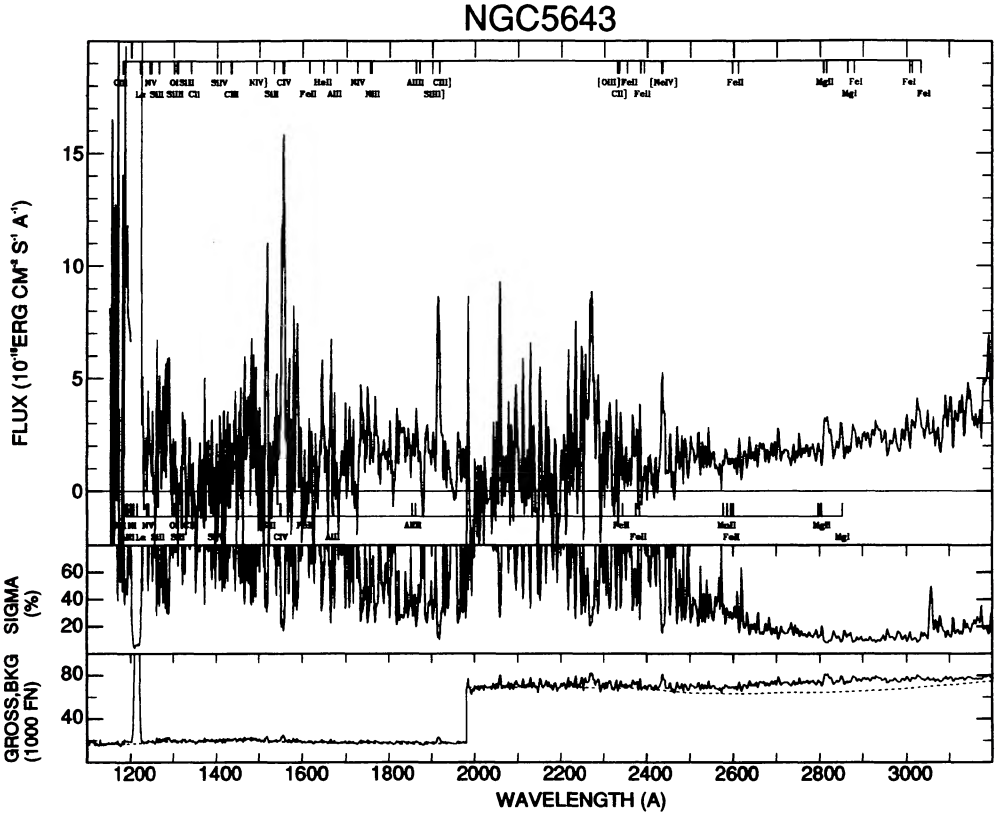


FIG. 97

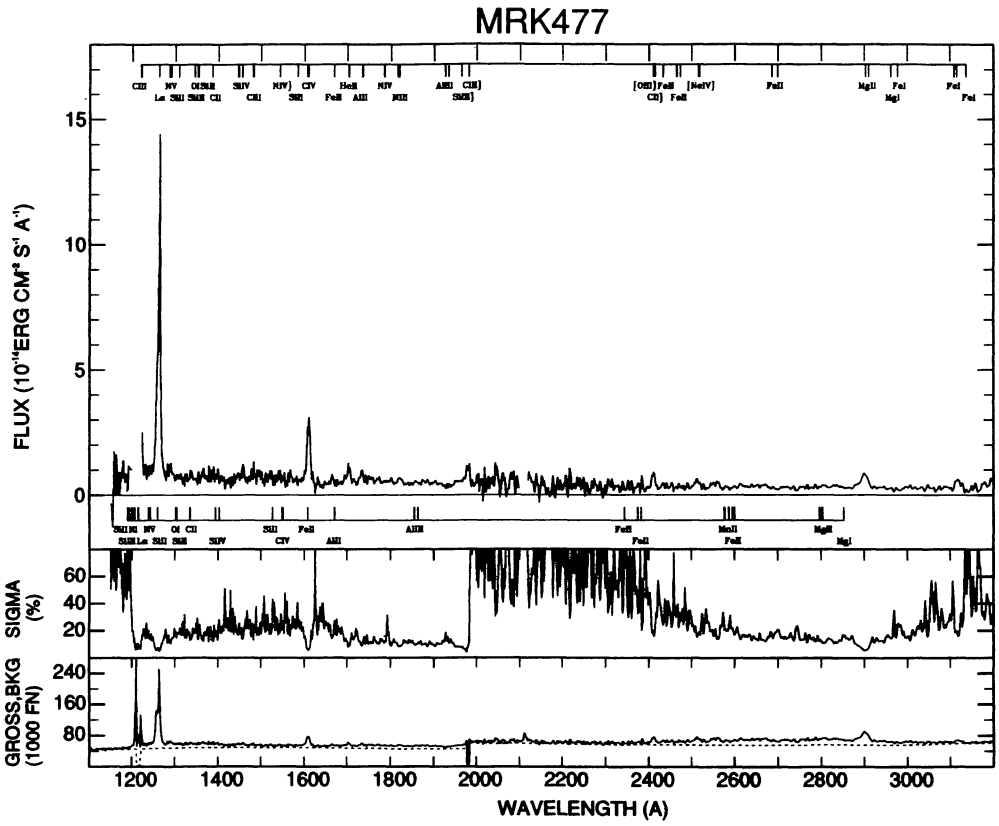


FIG. 98

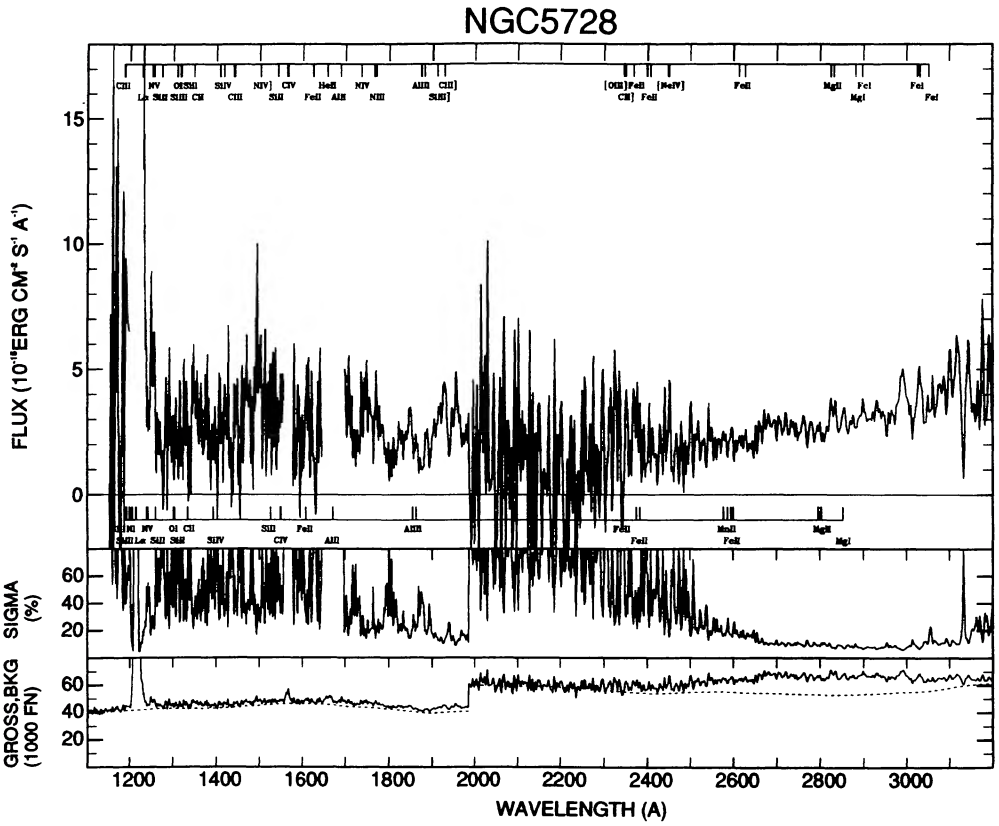


FIG. 99

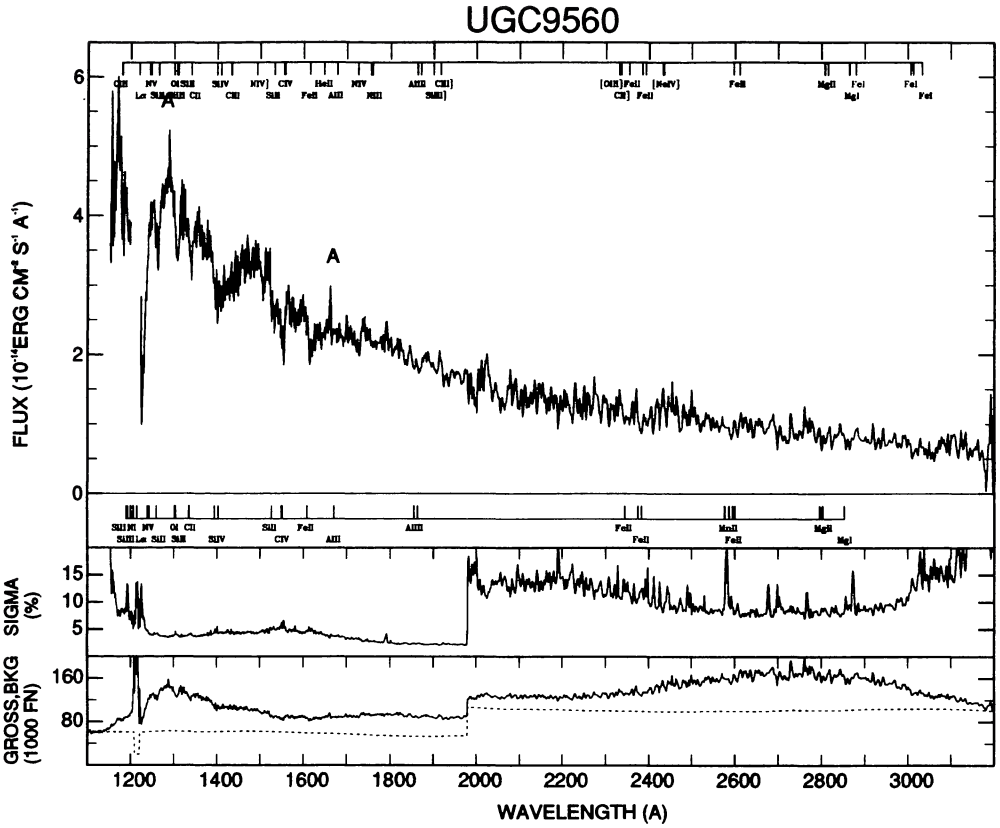


FIG. 100

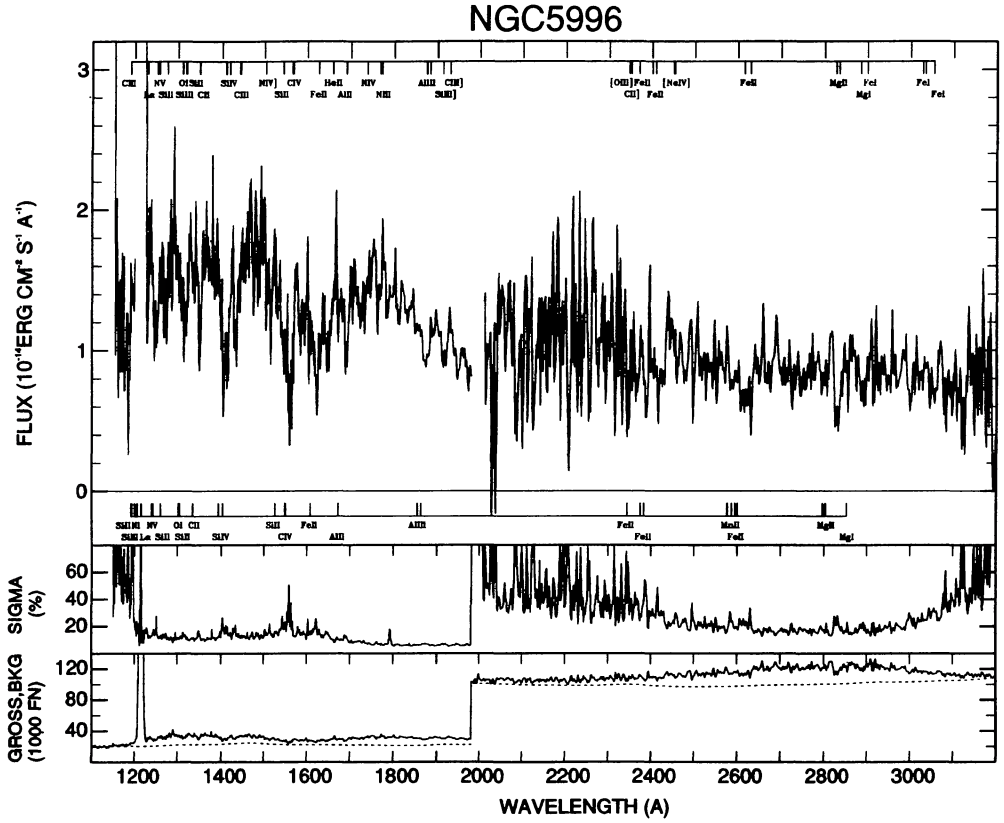


FIG. 101

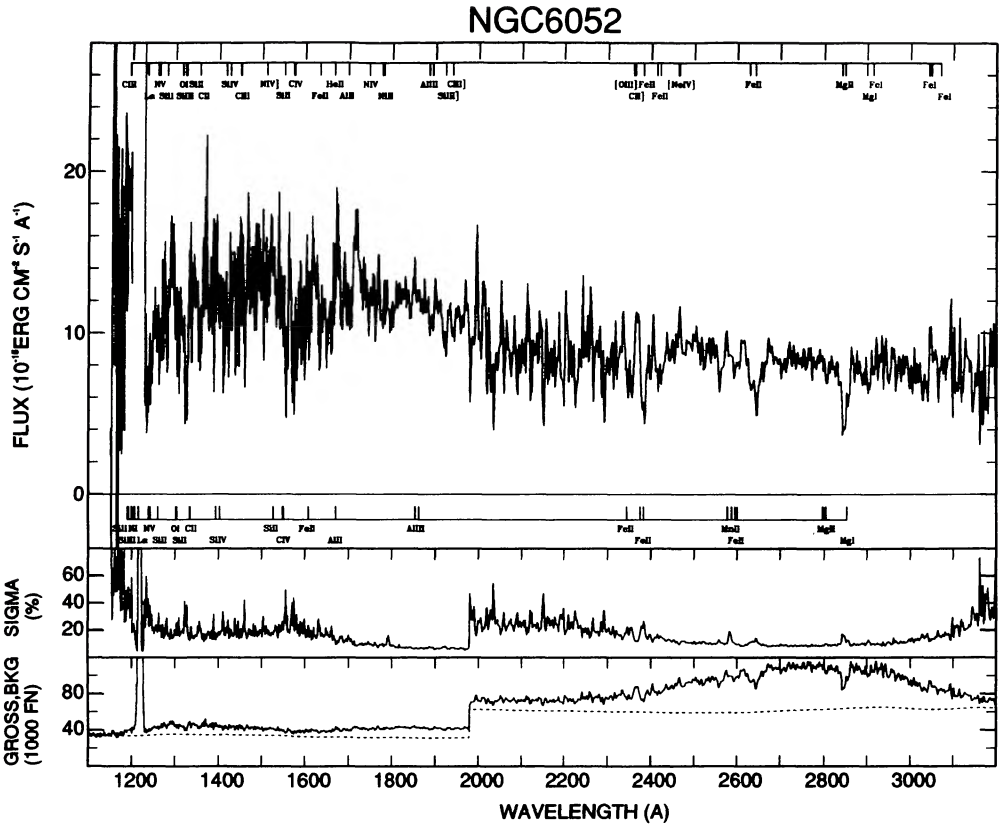


FIG. 102

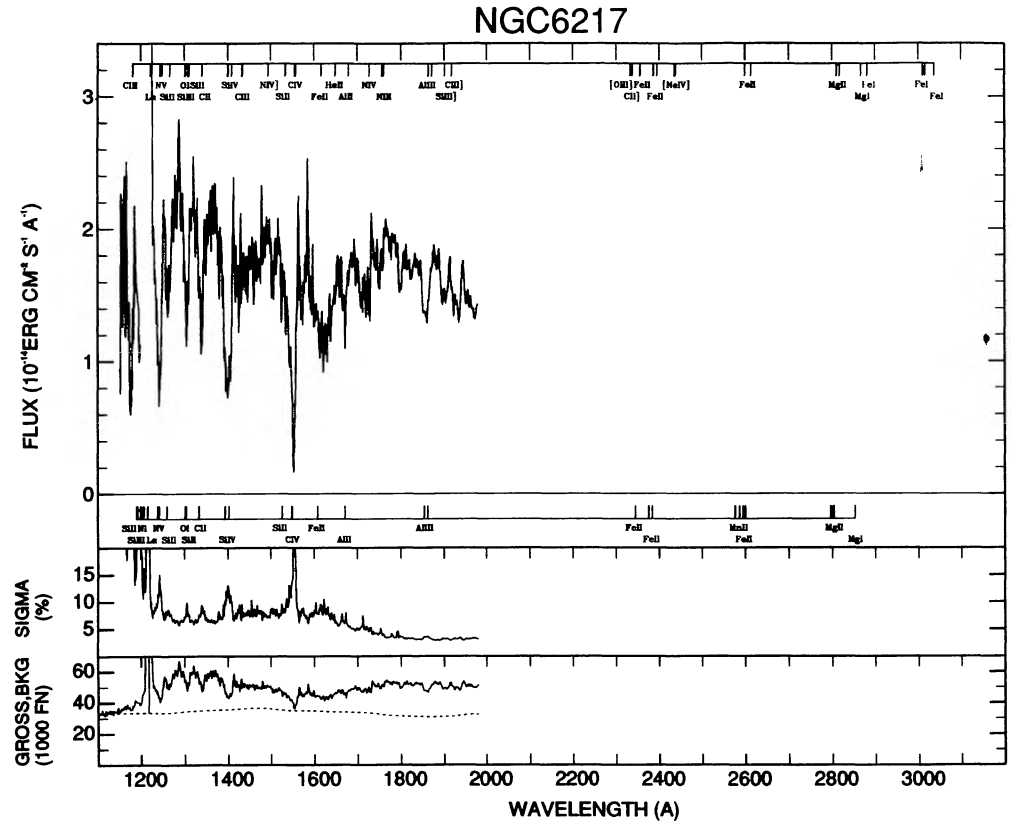


FIG. 103

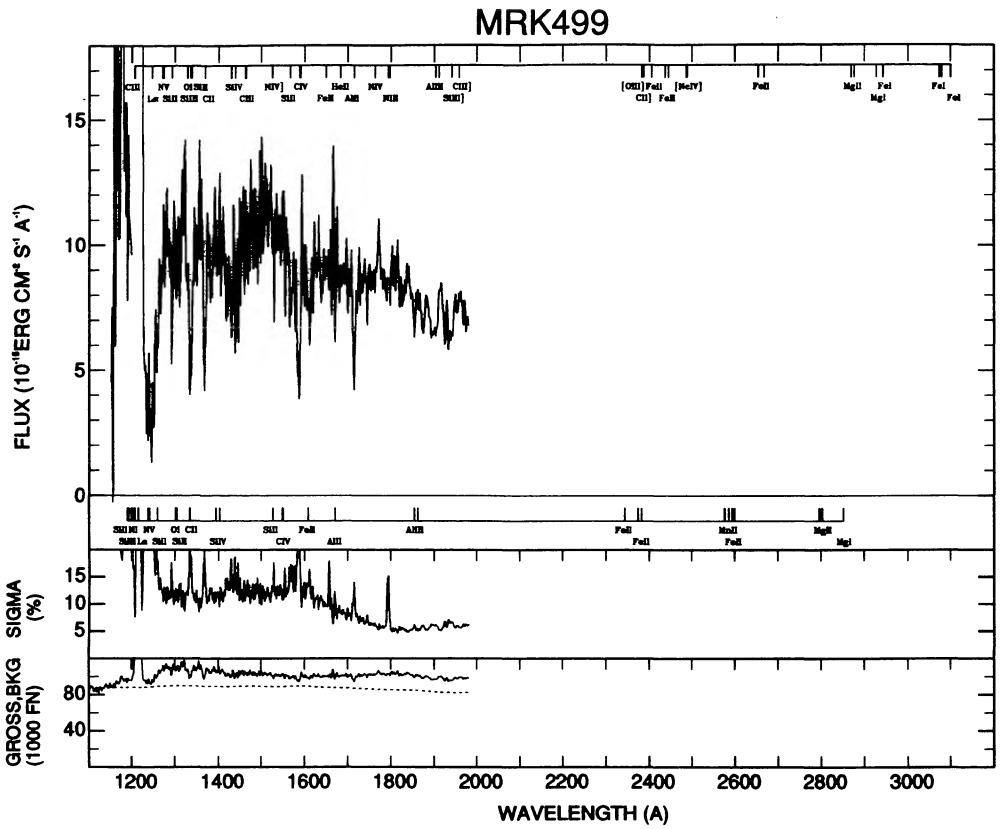


FIG. 104

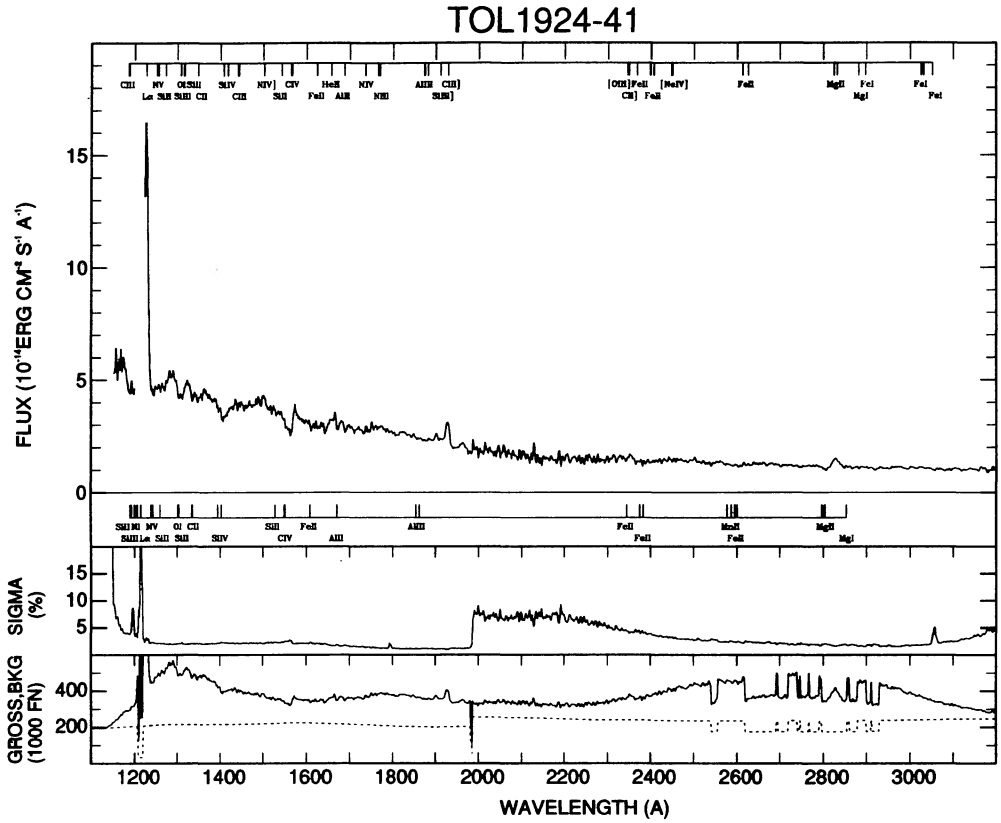


FIG. 105

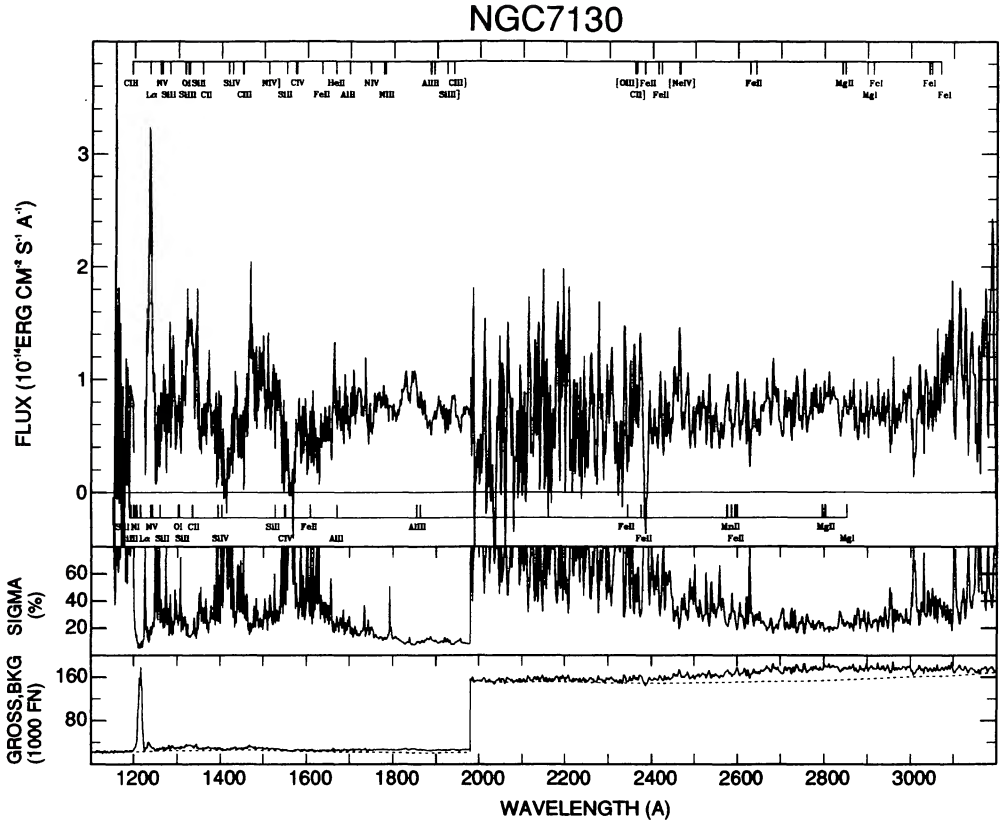


FIG. 106

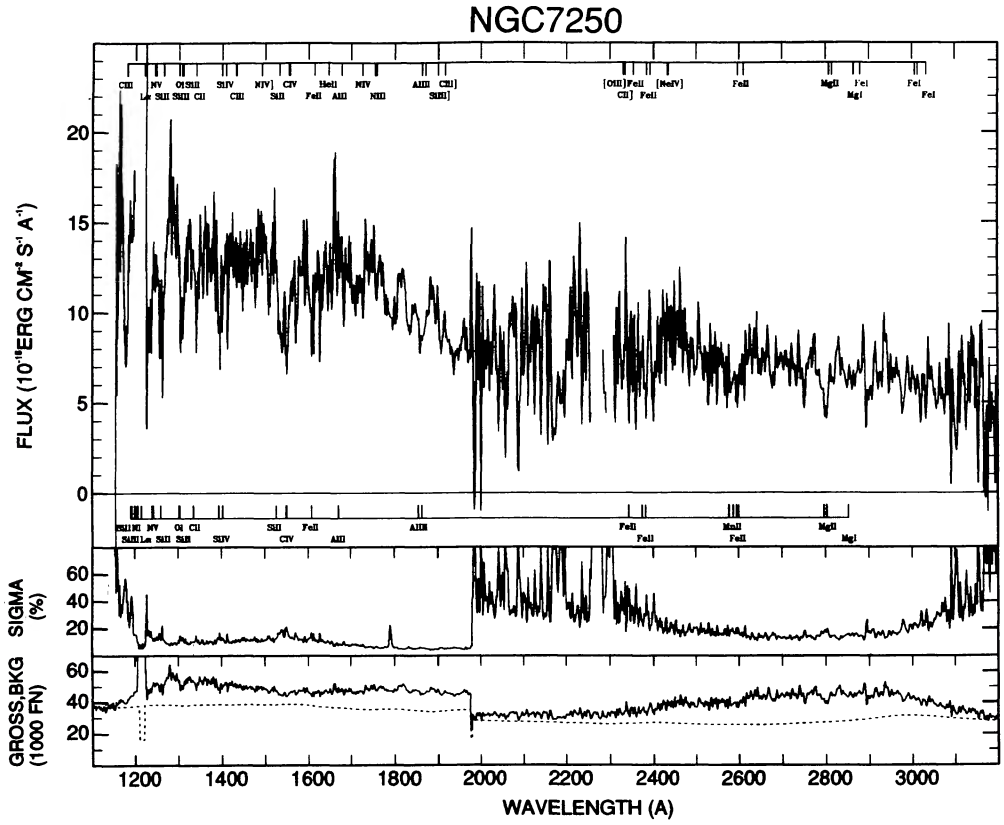


FIG. 107

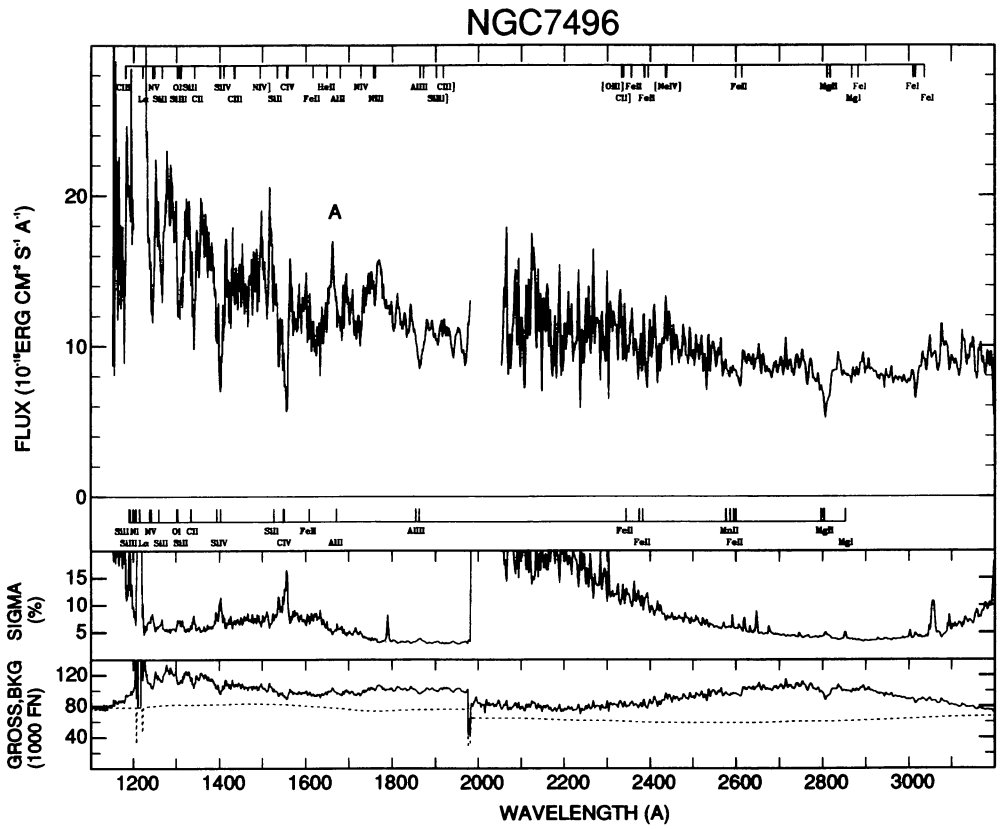


FIG. 108

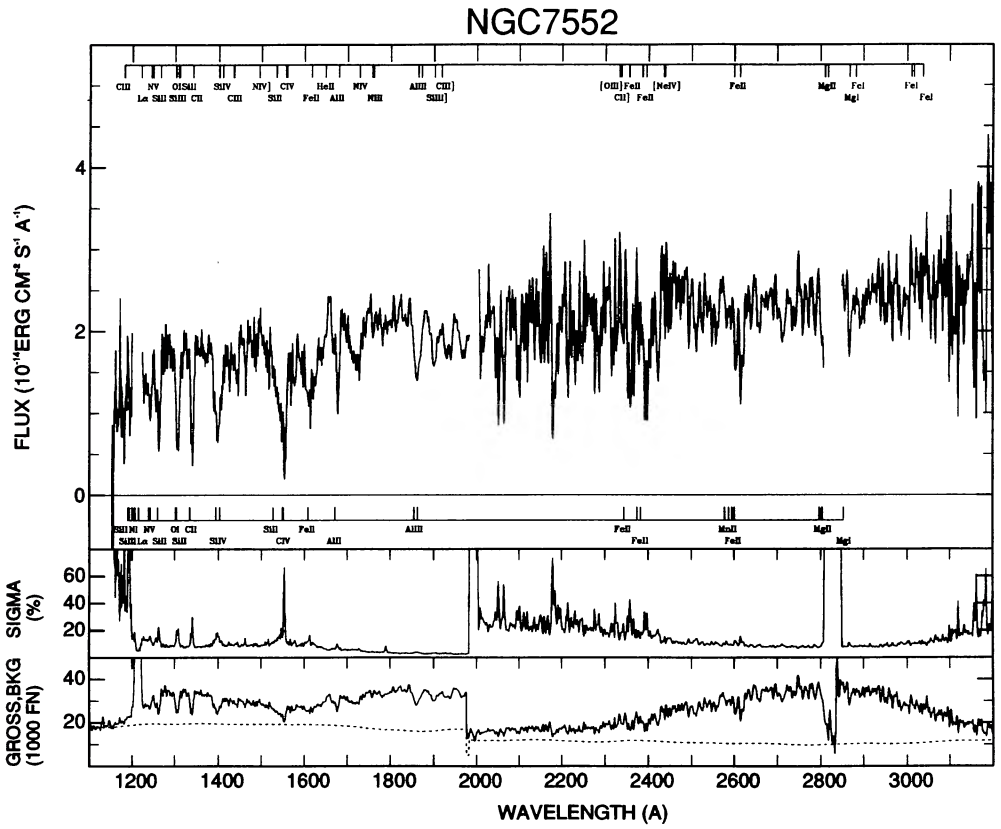


FIG. 109

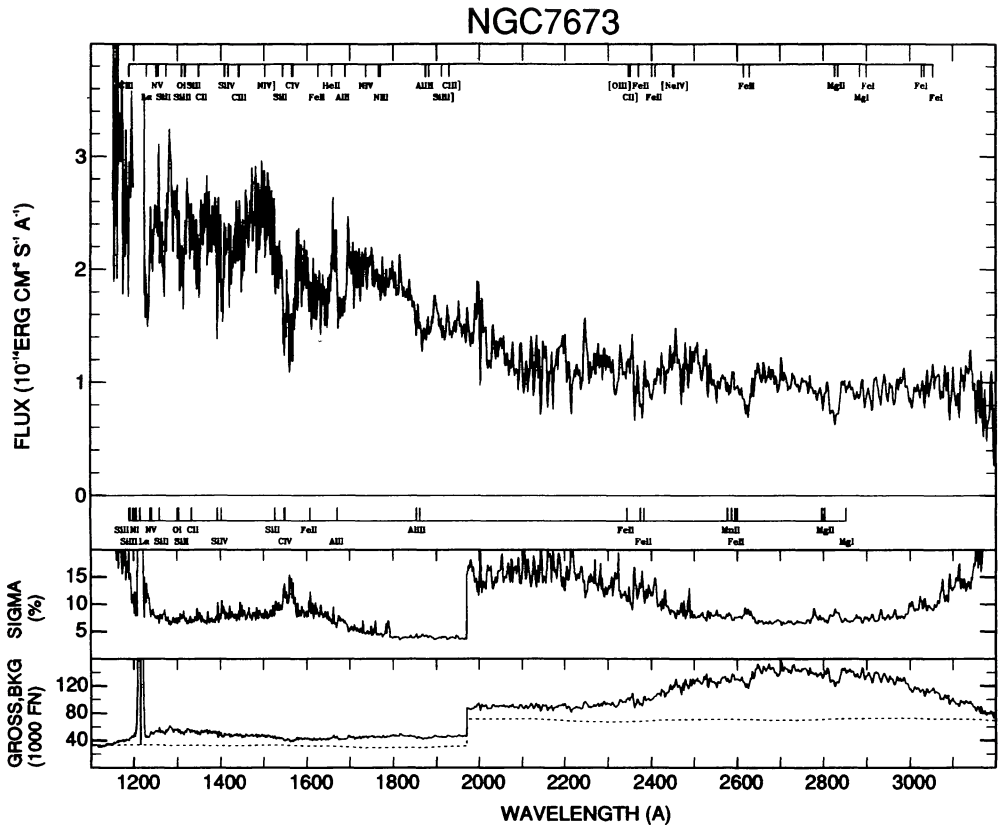


FIG. 110

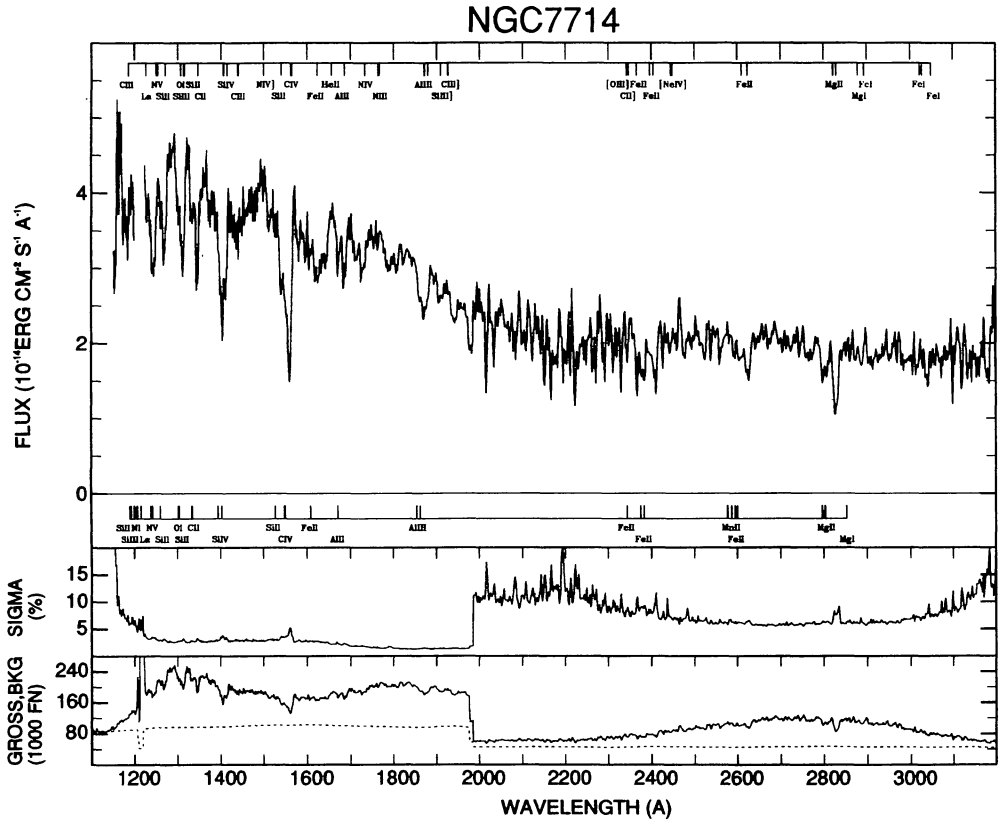


FIG. 111

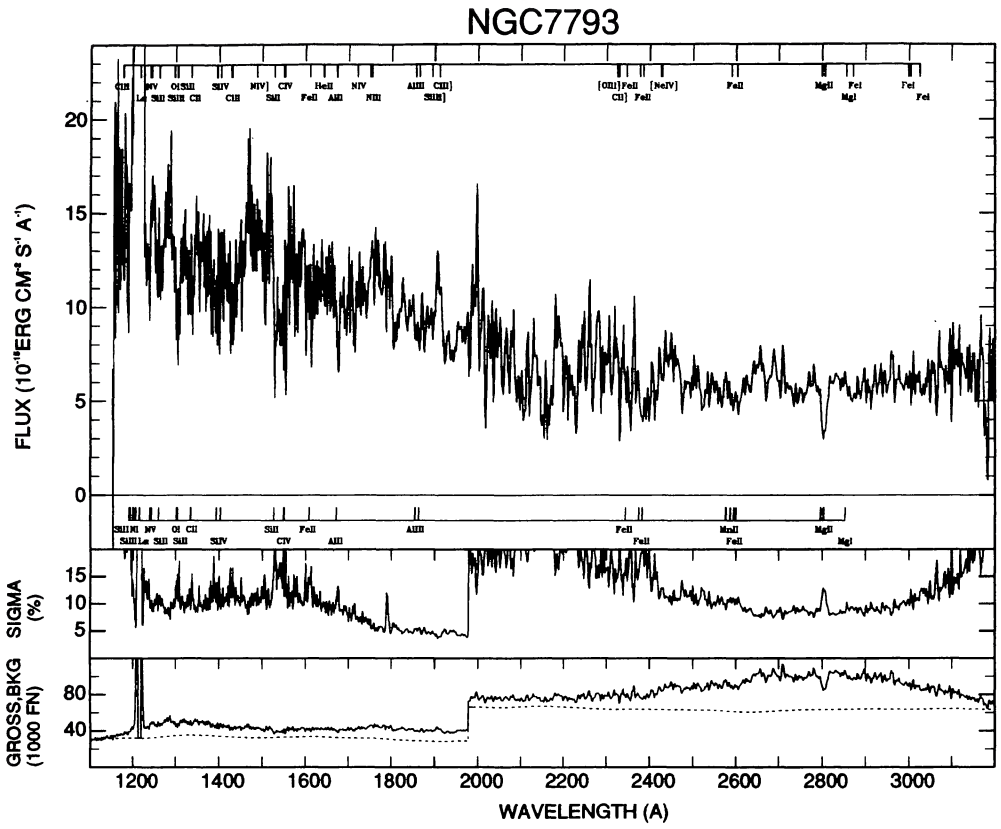


FIG. 112